

Mechanochromic Luminescent Properties of Difluoroboron β -Diketonate Dyes

William Alexander Morris
Wilmington, North Carolina

Bachelor of Science, University of North Carolina Wilmington, 2011

A Dissertation presented to the Graduate Faculty
of the University of Virginia in Candidacy for the Degree of
Doctor of Philosophy

Department of Chemistry

University of Virginia
May, 2016

Abstract

Difluoroboron β -diketonates (BF₂bdk) exhibit unique solid-state photoluminescent properties. Among these is reversible mechanochromic luminescence (ML), where the color of emission can be changed by shear force. Halide-substituted BF₂bdk also show mechanochromic luminescent quenching (MLQ) where mechanical force quenches emission by generating low energy singlet excited states closer in energy to the dark triplet excited state that is quenched at room temperature under air. Crossover to the excited triplet state is responsible for this quenching and halides make this effect more pronounced. These phenomena and other solid-state emission properties can be tuned by changes to the molecular structure. The effects of varying halides, alkoxy chain lengths, heterocycles, and substitution at the α -position of the dioxaborine core were explored. Both halide and alkoxy chain substitution have a significant impact on ML and MLQ properties, with heavier halides and longer chain lengths correlating to stronger MLQ. Substitution with a furan heterocycle brings about emission switchable by different methods of heating while thiophene heterocycle substitution creates high-contrast, highly reversible ML behavior. Solid state emission color, dye morphology, and reversibility of ML are also modulated by halide substituents. Furthermore, density functional theory (DFT) calculations were performed to understand structure/property relationships associated with luminescent properties of these dyes both as solvated molecules and polymeric materials and to begin modeling aggregate emission similar to what would be observed in the solid state. Intermolecular distance between BF₂dbm(OMe)₂ monomers was found to affect the position of a dark singlet excited state relatively close in energy to the strongest observed singlet excited state.

Table of Contents

Chapter 1: Introduction to Luminescence and Mechanochromic Luminescence	
1.1 Introduction to Photoluminescence in the Solution and Solid-State	2
<i>1.1.1 Luminescence and Luminescence Spectroscopy</i>	2
<i>1.1.2 Luminescence of Organic Fluorophores in Solution</i>	8
<i>1.1.3 Luminescence of Organic Fluorophores in the Solid State</i>	12
1.2 Introduction to the Mechanochromic Luminescent Properties of Difluoroboron β-Diketonate Compounds	14
<i>1.2.1 Introduction to Mechanochromic Luminescence</i>	14
<i>1.2.2 Mechanochromic Luminescent Difluoroboron β-Diketonates</i>	16
1.3 References	23
Chapter 2: Mechanochromic Luminescence of Halide-Substituted Difluoroboron β- Diketonate Dyes	
2.1 Introduction	28
2.2 Experimental	29
<i>2.2.1 Materials</i>	29
<i>2.2.2 Methods</i>	29
2.3 Results and Discussion	32
<i>2.3.1 Optical Properties of Dyes in Solution</i>	32
<i>2.3.2 Mechanochromic Luminescence on Paper</i>	33
<i>2.3.3 Mechanochromic Luminescence on Glass</i>	40
<i>2.3.4 Mechanochromic Luminescence of Bulk Powder</i>	46

2.3.5 <i>Differential Scanning Calorimetry of Powders</i>	49
2.4 Conclusions	50
2.5 Acknowledgements	51
2.6 References	51

Chapter 3: Mechanochromic Luminescence Triplet Modulation in Difluoroboron

Dibenzoylmethane Complexes

3.1 Introduction	54
3.2 Experimental	55
3.2.1 <i>Materials</i>	55
3.2.2 <i>Methods</i>	56
3.3 Results and Discussion	59
3.3.1 <i>Optical Properties of Dyes in Solution</i>	59
3.3.2 <i>Mechanochromic Luminescence on Paper</i>	62
3.3.3 <i>Mechanochromic Luminescence on Glass</i>	68
3.3.4 <i>X-ray Diffraction (XRD) of Pristine Powders and Drop-Cast Film</i>	76
3.3.5 <i>Single Crystal XRD</i>	76
3.3.6 <i>Differential Scanning Calorimetry of Dye Powders</i>	80
3.4 Conclusions	81
3.5 Acknowledgements	82
3.6 References	83

Chapter 4: Mechanochromic and Thermally Responsive Emission Properties of Furan and Thiophene Substituted Difluoroboron β -Diketonate Complexes with Short and Long Alkyl Chains

	v
4.1 Introduction	86
4.2 Experimental	88
4.2.1 <i>Materials</i>	88
4.2.2 <i>Methods</i>	88
4.3 Results and Discussion	90
4.3.1 <i>Optical Properties of Solution</i>	90
4.3.2 <i>Pristine Powder</i>	92
4.3.3 <i>Thermally Responsive Emission</i>	94
4.3.4 <i>Differential Scanning Calorimetry</i>	99
4.3.5 <i>Mechanochromic Luminescence</i>	102
4.3.6 <i>X-ray Diffraction of Films</i>	104
4.4 Conclusion	106
4.5 Acknowledgements	107
4.6 References	108

Chapter 5: Effects of α -Substitution on the Mechanochromic Luminescence and Aggregation-Induced Emission of Difluoroboron β -Diketonate Dyes

5.1 Introduction	111
5.2 Experimental	113
5.2.1 <i>Materials</i>	113
5.2.2 <i>Methods</i>	113
5.3 Results and Discussion	116
5.3.1 <i>Optical Properties of Dyes in Solution</i>	116

5.3.2 <i>Aggregation-Induced Enhanced Emission</i>	123
5.3.3 <i>Mechanochromic Luminescent Properties</i>	127
5.3.4 <i>Structural and Morphological Studies</i>	131
5.3.5 <i>Differential Scanning Calorimetry of Dye Powders</i>	134
5.4 Conclusions	134
5.5 Acknowledgements	136
5.6 References	136

Chapter 6: Modeling The Electronic and Optical Properties of Difluoroboron β -Diketonate Dyes Using Density Functional Theory

6.1 Introduction	140
6.2 Results and Discussion	141
6.2.1 <i>Modeling Molecular Orbitals and Absorption Spectra of Naphthyl-Phenyl β-Diketonate Polymer Initiator</i>	141
6.2.2 <i>Computational Investigations into the Solution Optical Properties of Dinaphthoyl β-Diketonates and Their Boronated Counterparts</i>	146
6.2.3 <i>Computational Investigations into the Solution Optical Properties of Thienyl Difluoroboron β-Diketonates</i>	152
6.2.4 <i>Toward Computational Modeling of the Solid-State Emission Properties of Difluoroboron β-Diketonates</i>	158
6.3 Conclusions	163
6.4 Acknowledgements	164
6.5 References	165

Chapter 7: Conclusions and Future Directions

7.1 Conclusions	168
7.2 References	173

Supporting Information

Appendix A: Supporting Information for Chapter 2	176
Appendix B: Supporting Information for Chapter 3	194
Appendix C: Supporting Information for Chapter 4	221
Appendix D: Supporting Information for Chapter 5	234
Appendix E: Supporting Information for Chapter 6	259

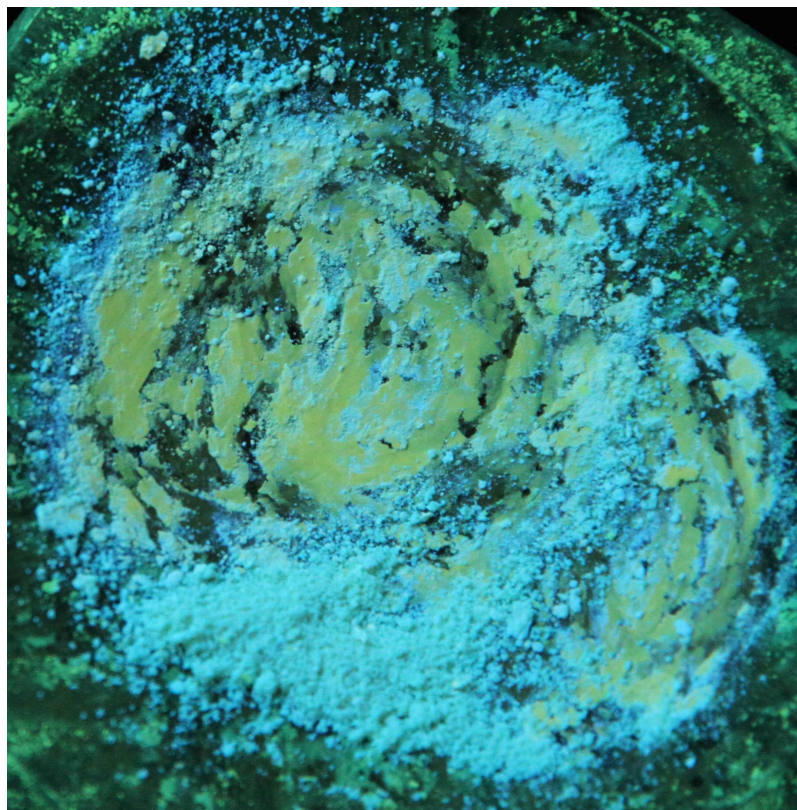
Dedication

I dedicate this dissertation first and foremost to my mother, Susan, my stepfather, Drew, and my grandmother, Ava, who have provided me with loving support throughout my entire graduate school experience. I also dedicate this to my lab group; Liu for getting me started and teaching me all of the basics; Chris and Tristan for providing helpful discussions and moral support. I also thank Professor Carl O. Trindle for being an invaluable resource for theoretical discussions and considerations. Furthermore, I thank Mary Rad, for lovingly cheering me on and providing helpful insight throughout the process of writing this dissertation.

Finally, I dedicate this thesis to Professor Cassandra L. Fraser who provided the scholarly guidance, support, and encouragement necessary to complete such an undertaking.

Chapter 1

Introduction to Luminescence and Mechanochromic Luminescence



1.1 Introduction to Photoluminescence in Solution and the Solid-State

1.1.1 Luminescence and Luminescence Spectroscopy

Luminescence may be defined as the emission of light from a substance that is not the result of heating. This can arise from many different processes. Among them are chemical reactions (chemiluminescence), electrical current passing through a substance (electroluminescence), and as a result of biochemical reactions within a living organism (bioluminescence). However, the remainder of this work will focus on molecular luminescence that results when a chemical species absorbs photons, i.e. photoluminescence.¹ When a photon of sufficient energy is absorbed by a molecule in its ground state with all electrons paired, an electron will be excited from the singlet ground state (S_0) to an excited state of the same spin multiplicity. This first singlet excited state shall be referred to as S_1 . Free radicals may give rise to species with doublet ground and excited states, but those will not be considered here.² Relaxation from S_1 back to S_0 causes a photon to be emitted and this process is known as fluorescence. Since electronic energy transitions resulting in fluorescence do not involve a change in spin multiplicity, fluorescence excited state lifetimes (τ) tend to be brief ($<10^{-5}$ seconds).¹ In most cases, fluorescence emission occurs at a longer wavelength than excitation. This is referred to as the Stokes shift and occurs because decay to the lowest vibrational state of S_1 (internal conversion) is rapid and occurs prior to fluorescence (Figure 1.1). Also, many fluorescent molecules will decay to higher vibrational levels in S_0 .³

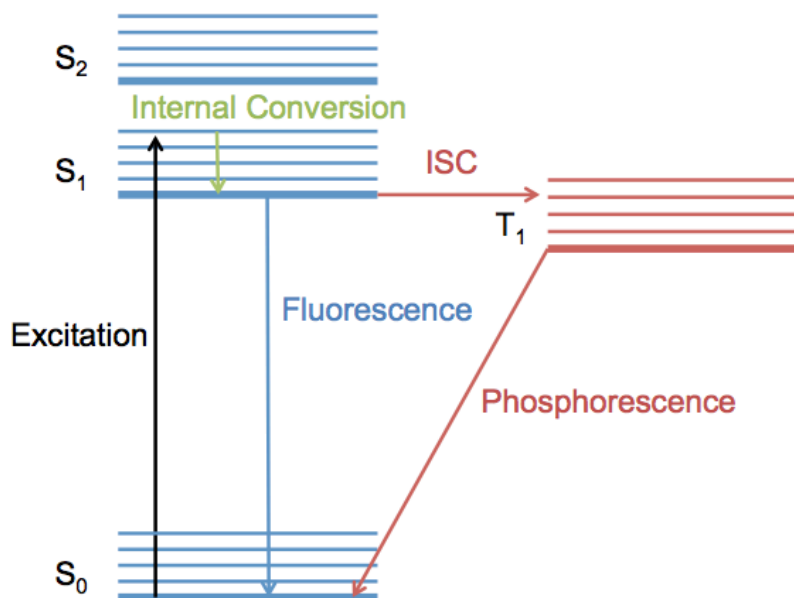


Figure 1.1 Jablonski diagram showing excitation of an electron by absorption of a photon from a singlet ground state (S_0) to a singlet excited state (S_1 or S_2) followed by internal conversion and then either emission of a photon from S_1 (fluorescence) or intersystem crossing (ISC) to the first triplet excited state (T_1). Emission from the T_1 excited state is shown as phosphorescence.

Sometimes, when a species is excited by photon absorption, the electron can undergo a process called intersystem crossing (ISC) wherein the excited electron experiences a spin flip and creates a triplet excited state (T_1). Emission from this T_1 state is known as phosphorescence. Due to the change in spin multiplicity required to return to the ground state (a forbidden transition), triplet excited states exist on a much longer timescale. On the shorter end, these lifetimes can be microseconds, but lifetimes of seconds or even minutes are possible.^{1,4} Phosphorescence does not necessarily have to result from decay from an excited triplet state to a ground singlet state. As long as the transition involves a spin-flip (i.e. is forbidden), a long excited state lifetime and delayed emission will result. In fact, phosphorescence has been observed from organic, aromatic

radicals arising from a quartet excited state to doublet ground state transition.⁵ For many luminescent species, phosphorescence is quenched under ambient conditions and not observed. This quenching typically occurs either by non-radiative decay pathways (i.e. emission of heat) or by collisional quenching with ground state, triplet diatomic oxygen.⁶ This problem can be alleviated by putting the fluorophore in an oxygen poor environment and/or in a rigid matrix to protect the fluorophore from collisions with oxygen and reduce the contributions of non-radiative decay pathways. This has been accomplished by putting fluorophores in a polymer matrix or into a crystalline state.^{7,8} Many luminescent materials will exhibit phosphorescence at low-temperature due to the shutting down of thermally activated non-radiative decay pathways.⁶ Furthermore, the introduction of heavy atoms, such as iodine, either covalently attached to or in close proximity to the fluorophore of interest can greatly enhance phosphorescence *via* a phenomenon known as the heavy atom effect. This occurs because the presence of a heavy atom enhances spin-orbit coupling and thereby increases intersystem crossing between excited states of differing spin multiplicity.⁹

Along with the characteristic emission, excitation, and excited state lifetime, the quantum yield (Φ) of a fluorophore is one of its most significant characteristics. Quantum yield is essentially a measure of emission efficiency and is defined as the ratio of emitted photons to absorbed photons.³

Spectrofluorometers are often employed to measure and quantify luminescence phenomena. These instruments typically consist of a light source (usually a xenon arc lamp), an excitation monochromator, a sample chamber, an emission monochromator, a detector (e.g. photomultiplier tube), a monochromator controller (e.g. computer), and a

display (e.g. computer monitor) (Figure 1.2). Spectrofluorometers are typically capable of recording both excitation and emission spectra, the former being the wavelength distribution of emission over a fixed excitation wavelength and the latter being the dependence of emission intensity at a single wavelength while scanning excitation wavelengths (Figure 1.3).³

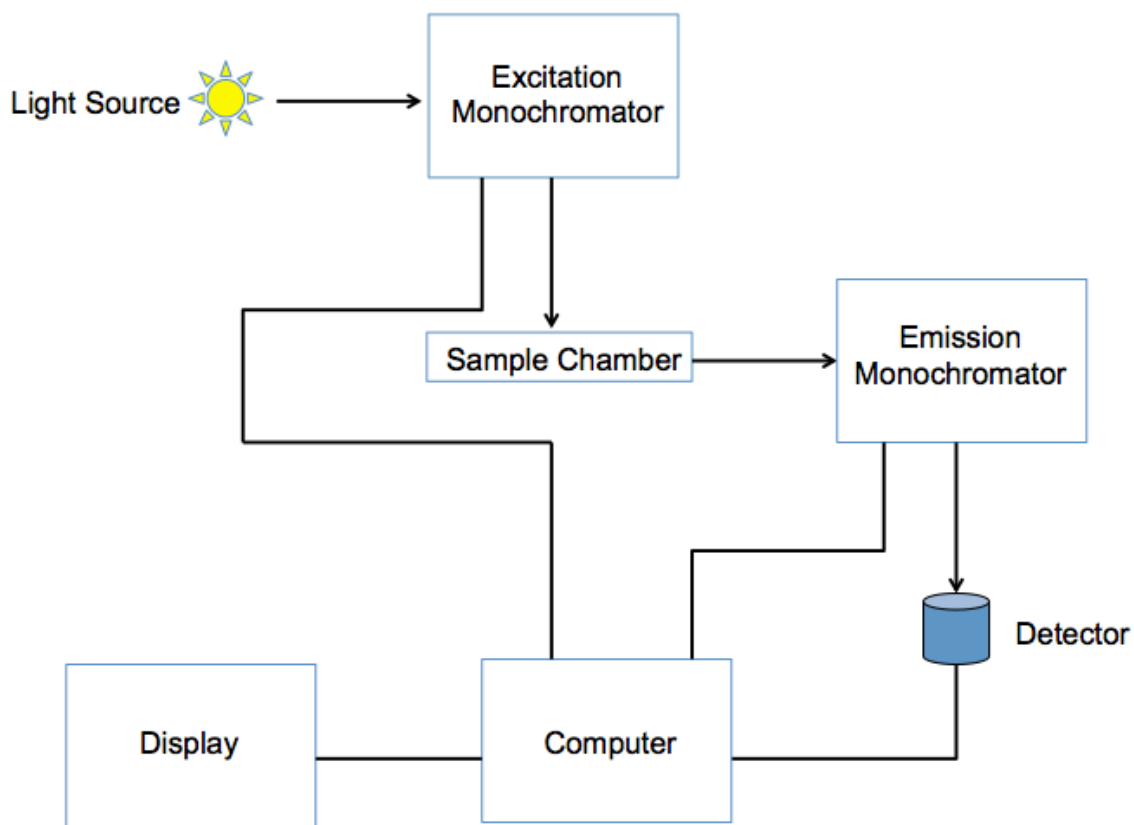


Figure 1.2 Basic block diagram of a spectrofluorometer.

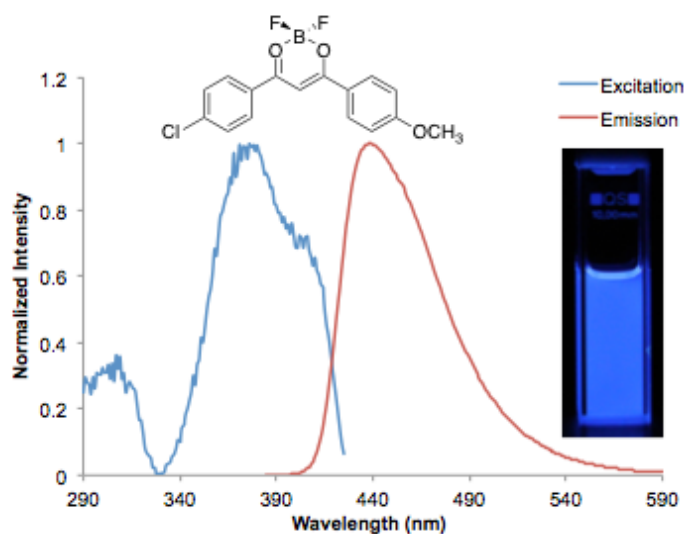


Figure 1.3 Example of excitation and emission spectra of a boron β -diketonate dye, $\text{BF}_2\text{dbm}(\text{Cl})\text{OMe}$ in CH_2Cl_2 . The photo shows the emission under UV excitation.

In addition to emission and excitation spectra, many more sophisticated spectrofluorometers are capable of measuring additional luminescence properties. Among these are emission lifetimes as well as quantum yields both in solution and the solid state. Emission lifetime is defined as the average amount of time a fluorophore remains in the excited state following excitation.³ In many set ups, lifetimes are measured using time-correlated single photon counting (TCSPC). This method involves exciting the sample of interest with a pulse of light. Conditions in the instrument are adjusted so that less than one photon is detected per laser pulse (typically 1 photon per 100 excitation pulses). Measuring the time between the excitation pulse and detection of the photon generates a histogram representing the decay profile of the species being analyzed.³ This data can be fit to an exponential decay function from which the emission lifetime of the sample can be extracted (Figure 1.4).

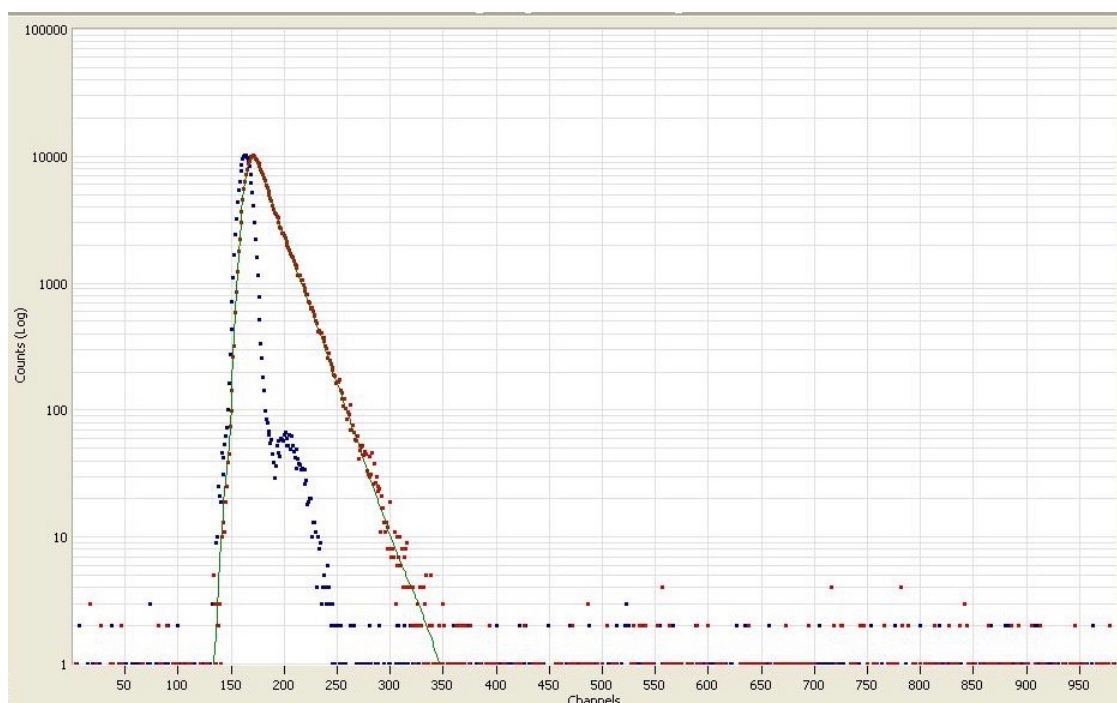


Figure 1.4 Example of time correlated single photon counting (TCSPC) data for $\text{BF}_2\text{dbm}(\text{Cl})\text{OMe}$ in CH_2Cl_2 . The blue points represent a prompt of colloidal silica in water while the red points represent the decay of the sample. In this case, the data was fit to single exponential decay and the lifetime (τ) was found to be 2.03 ns.

Commonly, quantum yields are calculated *versus* a standard of known quantum yield. This is accomplished by comparing the wavelength integrated intensity of the sample in question to a standard using equation (1.1).

$$\Phi = \Phi_R \frac{I}{I_R} \frac{OD}{OD_R} \frac{\eta^2}{\eta_R^2} \quad (1.1)$$

In equation (1.1), Φ is the quantum yield of the sample, Φ_R is the quantum yield of the standard, I is the integrated intensity of the sample emission profile, I_R is the integrated intensity of the standard emission profile, OD is the optical density (i.e. absorption intensity) of the unknown, OD_R is the optical density of the standard, η is the refractive index of the sample solvent, and η_R is the refractive index of the standard solvent.³

In most cases, determining quantum yield *versus* a standard is both convenient and appropriate. However, in some cases, such as determining the quantum yield of a solid-state sample, absolute quantum yield measurements are required and are often performed with the aid of an integrating sphere. In this method, the sample is placed in a sphere of diffuse reflecting interior walls and excited with a monochromatic wavelength source. A blank is also recorded and the absolute Φ is determined according to equation (1.2), where E_c is the integrated luminescence of the sample due to indirect illumination from the film, E_a is the integrated luminescence from an empty integrating sphere (i.e. blank), L_a is the integrated excitation spectrum from an empty integrating sphere, and L_c is the integrated excitation spectrum of the sample directly excited by the incident beam.¹⁰

$$\Phi = \frac{E_c - E_a}{L_a - L_c} \quad (1.2)$$

1.1.2 Luminescence of Organic Fluorophores in Solution

It is common for the luminescence properties of organic fluorophores to be studied in dilute solution. This is primarily due to the ease with which these measurements can be made and interpreted. Various solvent effects can be used to glean important information about the chemical species being studied. Also, many applications in luminescence require emission from solvated molecules.

Typically, organic fluorophores are highly conjugated, aromatic molecules. Not only do high degrees of conjugation result in absorption and emission wavelengths in the visible region of the spectrum (~400-700 nm) but also the high degree of planarity exhibited by such species minimizes contributions from non-radiative decay pathways. These non-radiative pathways often involve molecular rotations that are restricted by a

conjugated, planar structure. This results in more intense, visible emissions. The extent of π conjugation also has profound effects on the characteristic emissions of organic fluorophores, with a general trend of increasing absorption and emission wavelength corresponding to greater degrees of π conjugation. This is due to the presence of more nodes in the molecular orbitals resulting in a smaller energy gap between the highest occupied molecular orbital (HOMO) and the lowest unoccupied molecular orbital (LUMO). A smaller HOMO-LUMO gap produces lower energy, red-shifted absorption and emission. It has also been demonstrated that designing fluorophores around donor/acceptor motifs (Figure 1.5) is an effective strategy for producing more red-shifted emissions. In addition to this, donor/acceptor motifs also tend to lead to high quantum yields in solution.¹¹

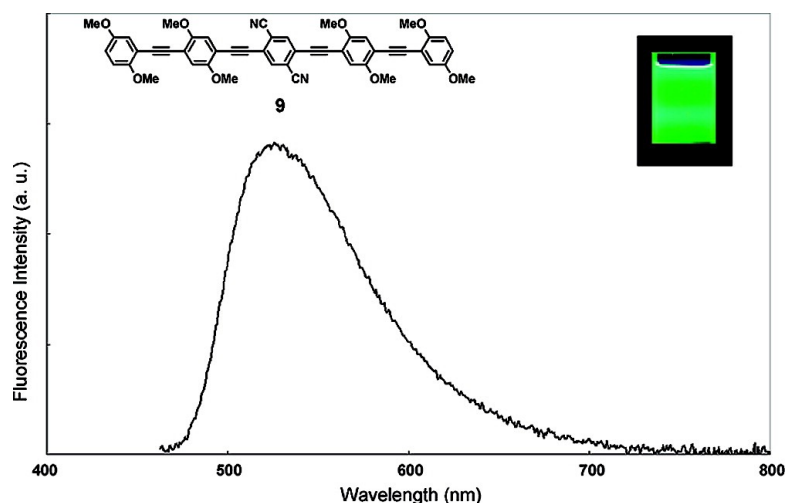


Figure 1.5 An example of a π -conjugated, long wavelength emitting, high quantum yield dye ($\Phi_f = 88\%$ and $\lambda_{em} = 527$ nm in CHCl_3) built upon a donor (OMe) and acceptor (CN) design strategy. (Adapted from reference 11).

Solvents, themselves, can have profound effects on the luminescence properties of organic fluorophores and, collectively, solvent effects on both electronic absorption and emission spectra of fluorophores are known as solvatochromism.² In fact, when a

molecule is excited to S_1 the rapid loss of vibrational energy to solvent molecules is partly responsible for the observed Stokes shift. This is due to the fact that fluorescence lifetimes (τ_F) occur on a time scale much longer than that of solvent relaxation (10-100 ps). Therefore, emission from a species in solution arises from a solvent relaxed, vibrational excited state. Polar fluorophores in polar solvents can result in even larger Stokes shifts due to a stabilization of the excited state by solvent molecules. This occurs because most polar fluorophores will exhibit a larger dipole moment (μ) in the excited state compared to the ground state. The dipoles of polar solvent molecules will relax around the dipole moment of the excited state molecule and lower the energy of the excited state.³ Solvents of greater polarity can heighten this effect and the increase in emission wavelength in response to dissolution in solvents of increasing polarity is referred to as a solvatochromic shift.² Polar solvents can also induce shifts to longer wavelength emissions in species that experience what is called intramolecular charge transfer (ICT) in the excited state (Figure 1.6).¹² These fluorophores are developed not by designing species which will have large excited state dipole moments, but by designing the fluorophore with donor/acceptor pairs attached.³ Charge transfer will proceed from the donor in the HOMO to the acceptor in the LUMO when the fluorophore is excited.¹² Absorption spectra are much less sensitive to solvatochromic shifts than emission spectra due to the speed at which absorption of light occurs ($\sim 10^{-15}$ s).³ Solvatochromic shifts are well understood and documented and serve as an excellent example of how a fluorophore can be used to probe its environment.^{12,13}

Different solvents can also either quench or enhance the fluorescence of their solutes and these phenomena most often must be evaluated on a case-by-case basis. In

many cases, polar aprotic solvents may quench the emission of fluorophores with strong excited state dipoles. In general, this is believed to be due to the aforementioned lowering in energy of S_1 making the non-radiative decay to S_0 more rapid. This, in turn, makes radiative transitions slow and provides greater opportunity for quenching. Protic solvents can also quench luminescence by protonation of the fluorophore in the excited state. Conversely, polar solvents can also enhance the emission of some fluorophores by causing a dark (not luminescent) $n-\pi^*$ state to cross an emissive $\pi-\pi^*$ state.²

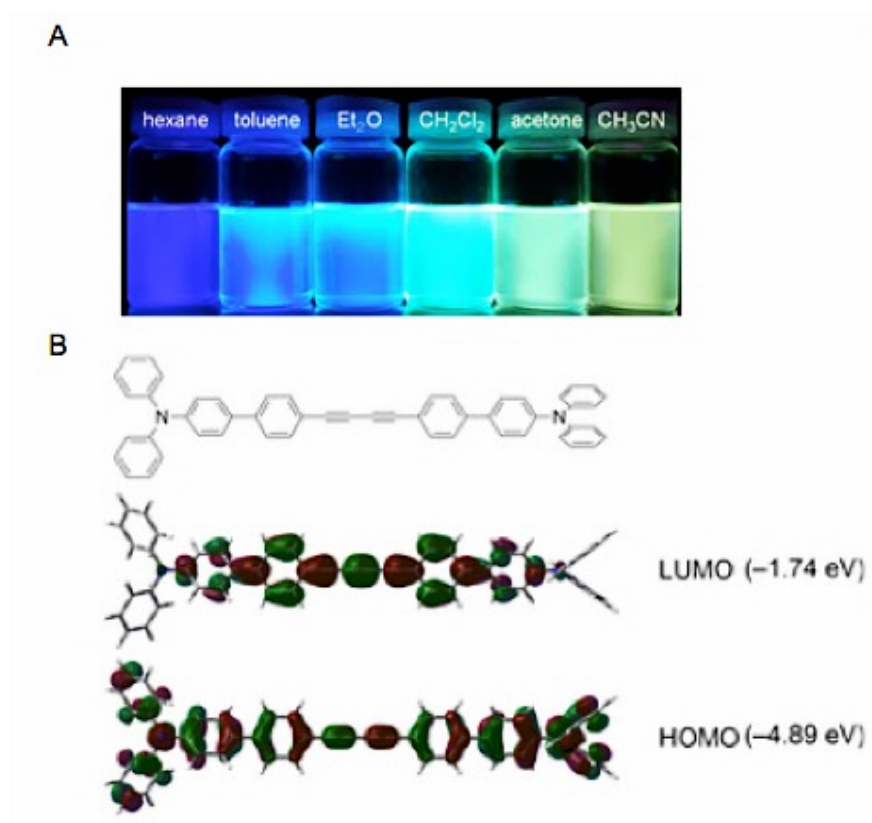


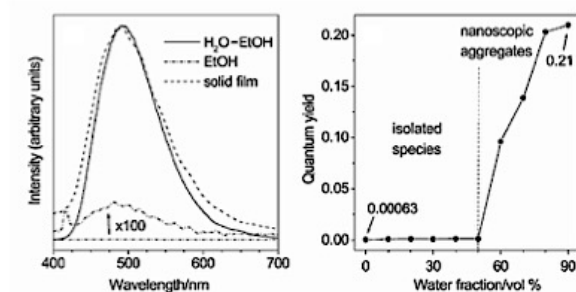
Figure 1.6 The fluorescence solvatochromic shift in solvents of increasing polarity (A) of a 1,4-bis(diaryl)-1,3-butadiyne (B). Molecular orbital (MO) diagrams show charge transfer from donor to acceptor subunits. (Adapted from reference 12).

1.1.3 Luminescence of Organic Fluorophores in the Solid State

In dilute solution, it is assumed that emission is observed from a single molecule absent interactions with other solute molecules. However, quite different luminescent properties can arise from concentrated solutions or even the solid state as powders or thin films. In order to achieve these properties the problem of aggregation-caused quenching (ACQ) must be circumvented.¹⁴ In ACQ emissions of conjugated, aromatic fluorophores are quenched by the formation of “sandwich-shaped” excimers and exciplexes, which are only weakly emissive if emissive at all. This is problematic for many applications of fluorescent probes. Emission from fluorophores in dilute solution can be too weak for fluorescent sensory systems and the inability to increase intensity by increasing fluorophore concentration limits the usefulness of luminescent probes in many applications.¹⁵ Furthermore, solid-state emitting organic materials are desirable for applications such as organic light emitting diodes (OLEDs)¹⁶ and designing dyes responsive to mechanical force.¹⁷ Ben Zhong Tang and coworkers have found a solution to this problem by designing aggregation-induced emission (AIE) fluorophores specifically engineered to exhibit enhanced emission in concentrated solutions or the solid state. Their first achievement on this front was the compound 1-methyl-1,2,3,4,5-pentaphenylsilole which was virtually non-emissive in solution but displayed bright fluorescence in the solid state and as nanoscopic aggregates in water-ethanol mixtures (Figure 1.7). From their studies, they concluded that the reason for this unique behavior can be linked to the compound existing as a non-planar rotamer in dilute solution. According to calculations, in the absence of other intermolecular interactions, the phenyl rings attached to the silole core are twisted almost 90° in relation to the core. This

twisting out of planarity places the degree of conjugation in this species to a minimum, thus substantially reducing emission efficiency. However, aggregation in very concentrated solutions or in the solid state as a film would restrict these rotations and result in highly planar, conjugated, and emissive aggregates.¹⁸ Since this initial report, many AIE fluorophores have been designed using this strategy^{15,19,20} and these dyes have been adapted to many applications including explosives sensing,^{21,22} immunoassay markers²³, monitoring of layer-by-layer assemblies²⁴, and drug delivery,²⁵ to name a few.

A



B

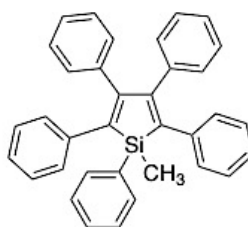


Figure 1.7 A) The spectroscopic properties of 1-methyl-1,2,3,4,5-pentaphenylsilole (B) under various conditions (left) and the dependence of quantum yield on the percent water in EtOH-H₂O mixtures (right). In this case, EtOH is considered to be a solvent for the compound while water is a non-solvent. (Adapted from reference 18).

1.2 Introduction to the Mechanochromic Luminescent Properties of Difluoroboron β -Diketonate Compounds

1.2.1 Introduction to Mechanochromic Luminescence

Materials that are responsive to external force stimuli are of interest to the scientific and technological communities due to their potential for use in sensors, memory storage, security inks, and other applications.²⁶⁻³⁰ However, developing reliable design strategies for fabricating mechanofunctional materials is challenging and a cutting edge area of materials science research.^{26,27} Mechanochromic luminescent (ML) materials are so named because a change in their luminescence colors can be caused by mechanical stimuli. There are many classes of ML materials including, but certainly not limited to, inorganic and organic molecular solids,^{31,32} polymers,^{28,33,34} liquid crystals,^{35,36} and micelles.³⁷ Recently, many researchers have made great strides in not only the synthesis of such materials but also in understanding the mechanisms and applications of ML. In 2008, Sagara *et al.* reported pyrene-based liquid crystals that exhibit ML *via* a shear force-induced phase transition from a micellar cubic phase (yellow) to a columnar phase (green) (Figure 1.8). Furthermore, this process is completely reversible, meaning the two phases of the materials can be switched back and forth.³⁵ This is an important feature of ML materials both in application and concept. Obviously, reversible ML materials are desired due their reusability. The reason many ML materials display this property reversibly is, like the example from Sagara *et al.*, due to the fact that the change elicited by heat and mechanical force is physical and not chemical. For this reason, materials showing ML more often than not must be chemically stable under air and at relatively high temperatures. Another example of an ML material comes from Qingkai *et*

al. They have reported that the molecule, tetrakis(4-(dimethylamino)phenyl)ethylene (TDMAPE), which has a natural propeller structure, displays a red-shift in emission due to a change in intramolecular conformation when powders of the material are ground. The blue-shifted emission of the pristine powders can be fully recovered by fuming with solvent or partially recovered by annealing. They reason that the red-shift in emission upon grinding is caused by a mechanically induced planarization of the propeller-like molecular structure.³⁸

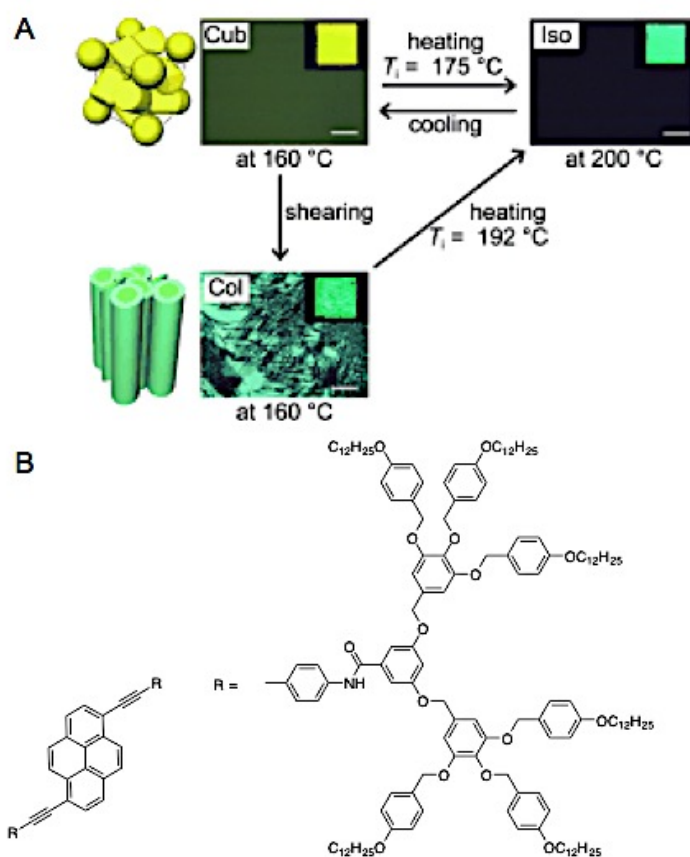


Figure 1.8 A) The mechanochromic luminescence (ML) behavior of pyrene based liquid crystals. B) Molecular structure of the liquid crystals. (Adapted from reference 35).

1.2.2 Mechanochromic Luminescent Difluoroboron β -Diketonates

Difluoroboron β -diketonates,^{7,39,40} β -diiminates,^{41,42} and β -ketoiminates,⁴² are known for their unique optical properties, among which include reversible ML. In particular, difluoroboron β -diketonates, which shall be referred to as BF₂bdk, have received much attention in recent years for their impressive optical properties. These include efficient quantum yields,⁴³⁻⁴⁵ high extinction coefficients,⁴³⁻⁴⁵ two-photon absorption cross-sections,^{43,46} tunable absorption in the near-UV range,^{43,45} a range of emission colors in the solid state,^{40,45} intramolecular charge transfer (ICT) character,^{44,47} oxygen-sensitive room temperature phosphorescence in rigid media such as polymers,⁴⁸⁻⁵⁰ organic vapor sensitivity,^{51,52} and ML. In 2010, Fraser and coworkers reported a sunscreen derivative difluoroboron avobenzene (BF₂AVB) exhibiting unique polymorphism and ML behavior (Figure 1.9). When films of the dye were annealed, they exhibited a green emission with a narrow spectral profile. Upon smearing the annealed films, the emission turned yellow and a much broader spectral profile was observed. Furthermore, it was discovered that smeared films could at least partially recover the annealed emission profile under ambient conditions, but annealing was required for a full recovery. Images of spin-cast films on glass collected by atomic force microscopy (AFM) revealed an ordered, crystalline morphology in the annealed films and an amorphous morphology in the as-spun films (approximating smeared films).³⁹ The transient nature of the amorphous emissive state is revealing about the nature of the ML in these dyes. It shows that the annealed, bluer form represents a thermodynamically stable state for the materials while the smeared, redder form represents a kinetically accessible metastable state. It has been since discovered that certain BF₂bdk compounds are capable of making

a complete recovery under ambient conditions without heating. By substituting only one phenyl ring of difluoroboron dibenzoylmethane (BF₂dbm) at the 4-position with alkoxy chains of varying length, the recovery ability of the ML dye under ambient conditions could be tuned. In general, dyes bearing shorter chains were able to make more complete recoveries to the ordered emissive state after smearing while dyes with longer chains did not recover as fully (Figure 1.10).⁵³ This shows that the ML properties of these dyes are, in fact, tunable by alterations to the diketonate structure. If recovery times of the dyes can be tuned, other properties can also be tuned. Studies toward understanding and predicting how these properties can be tuned would prove to be invaluable moving toward rational material design.

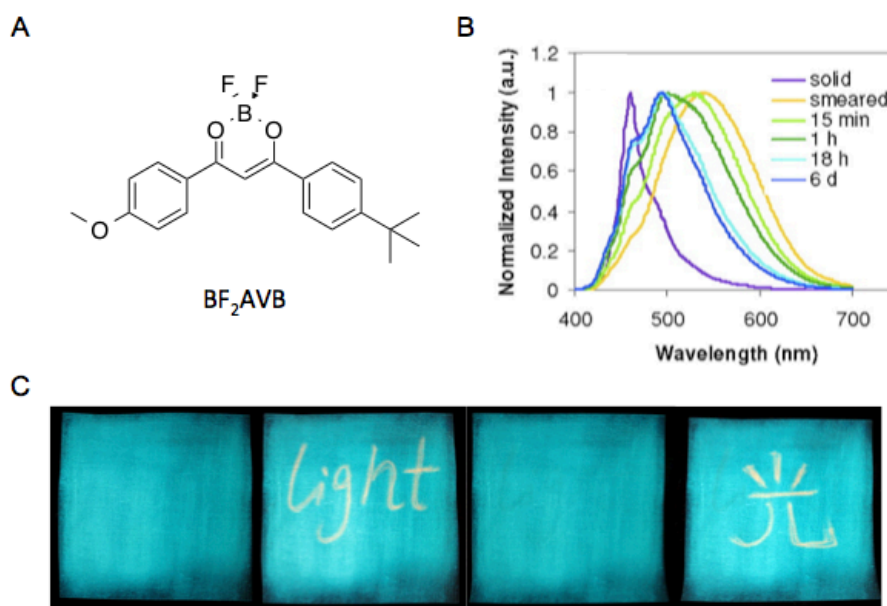


Figure 1.9 A) Chemical structure of BF₂AVB. B) Spectra of BF₂avb films on weighing paper demonstrating ML and spontaneous recovery at room temperature. C) Photographs of BF₂AVB demonstrating reversible ML as a film on weighing paper. (Adapted from reference 39).

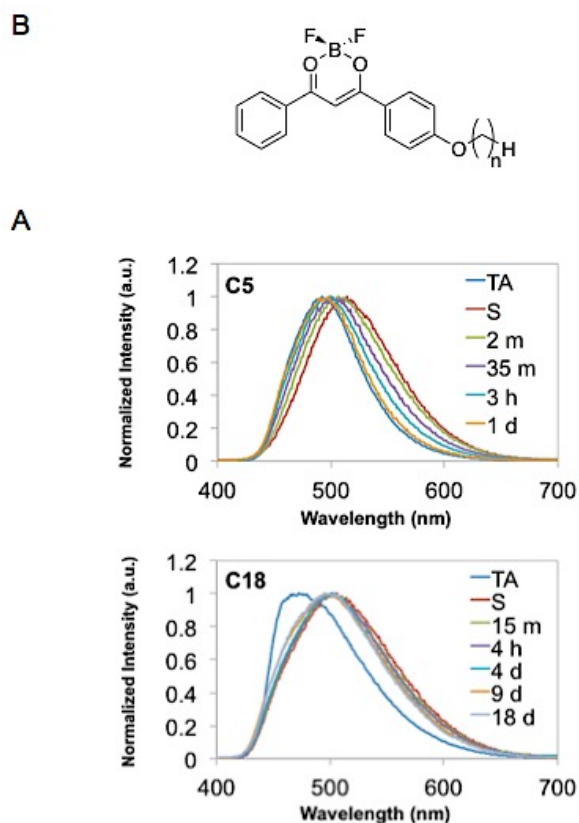


Figure 1.10 A) Structure of BF₂dbm dyes with varying alkoxy chain lengths (C2 = OC₂H₅, C3 = OC₃H₆, C5 = OC₅H₁₁, C6 = OC₆H₁₃, C12 = OC₁₂H₂₅, C18 = C₁₈H₃₇) B) Spontaneous recovery of the annealed emissions of BF₂dbm dyes with varying alkoxy chain lengths monitored over time. (Adapted from reference 53).

The nature of ML in BF₂bdk dyes can also be exploited to create other interesting and potentially applicable phenomena. For example, introduction of an iodine heavy atom into the diketone ligand scaffold of the dye can facilitate mechanically induced luminescence quenching (MLQ). This is the processes by which fluorescence intensity of solid-state emission is diminished by mechanically-induced enhanced crossover to the triplet state, which is sensitive to, and thus quenched, by oxygen. Specifically, BF₂dbm(I)OC₁₂H₂₅, a lipid derivative of difluoroboron iodo-dibenzoylmethane, exhibited green fluorescence in the solid state under UV light after annealing. Upon application of

shear force, the emission from the dye became noticeably less intense at room temperature under air. The dye also exhibited both fluorescence and phosphorescence (dual emission) at 77K in liquid N₂ and smearing greatly altered the fluorescence to phosphorescence ratio (F/P) in favor of the more red-shifted phosphorescence, presumably by creating aggregates with S₁ excited states that are closer in energy to the aggregate T₁ state (Figure 1.11).⁶

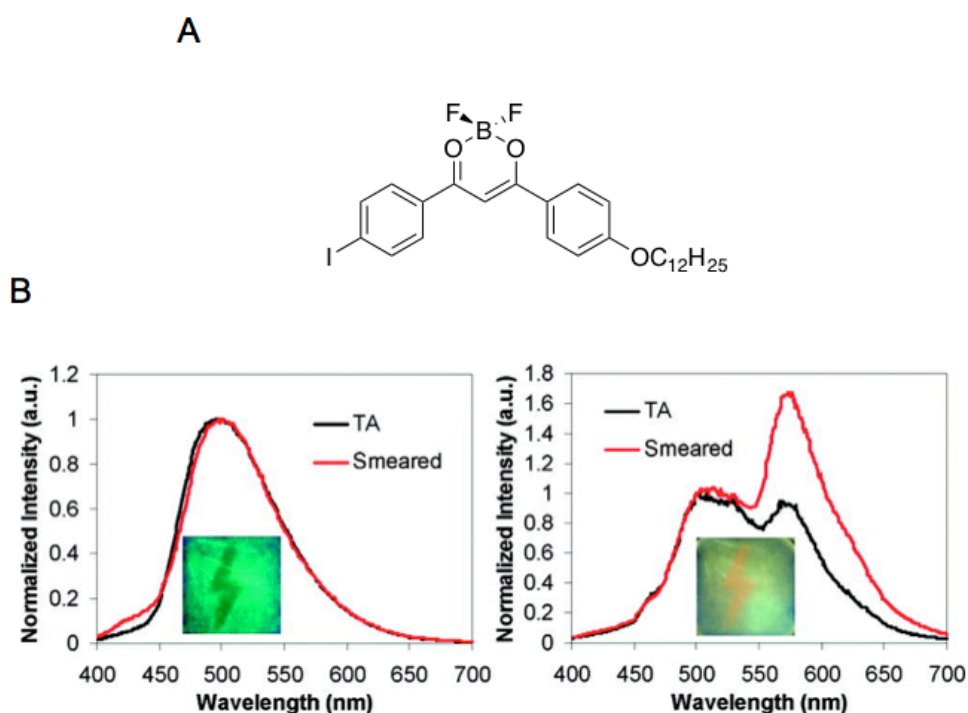


Figure 1.11 A) Chemical structure of the lipid derived BF₂dbm(I)OC₁₂H₂₅. B) A dye film showing the annealed and smeared emission profiles under ambient conditions (left) and submerged in liquid N₂ (right). (Adapted from reference 6).

Since these seminal studies, many other groups have performed studies on the ML and morphological dependent emissions of BF₂bdks. Recently, a mechanism was proposed for ML in BF₂bdk dyes. Sun *et al.* postulated that smearing of similar annealed BF₂bdk dyes leads to the formation of ground state and excimeric aggregate species.

Among these were ground-state H-aggregates in which the BF₂bdk molecules adopt a face-to-face arrangement and exhibit red-shifted emissions. As a result of their cofacial configuration, H-aggregates also have blue-shifted absorption spectra and can form excited state dimers (excimers) with lower energy singlet excited states compared to the more ordered polymorphs and could serve as acceptors for migrating excitons (an electron-hole pair) (Figure 1.12).^{54,55} Therefore, even if all molecules in the system do not adopt the lower energy conformation, the overall emission from the perturbed region of the material can be red-shifted. The authors deduced this mechanism by using covalently linked dimers and dye molecules covalently linked to polymers to spatially confine two or more fluorophores in dilute solution. In so doing, they were able to observe aggregate emission absent the typical complications brought about by self-absorption and light scattering. They found covalently linked dimers in solvents of decreasing polarity formed aggregates with blue shifted absorptions (H-aggregates) and red-shifted emissions, thus proving their proposed mechanism.⁵⁴

Sket and coworkers recently reported a BF₂bdk system (difluoroboron 1-phenyl-3-(3,5-dimethoxyphenyl)-propane-1,3-dione) demonstrating polymorphism and ML (Figure 1.13). The compound formed two distinct emissive polymorphs differing in orientation of the methoxy groups. One mode of packing exhibited distinct ML behavior as well as crystallization induced emission enhancement (CIEE). Furthermore, the ML was reversible either by applying CH₂Cl₂ dropwise, heating, or allowing the sample to sit for a period of time at room temperature. They also found it was possible to switch between the two polymorphs by heating and also by evaporation from various solvents.⁵⁶

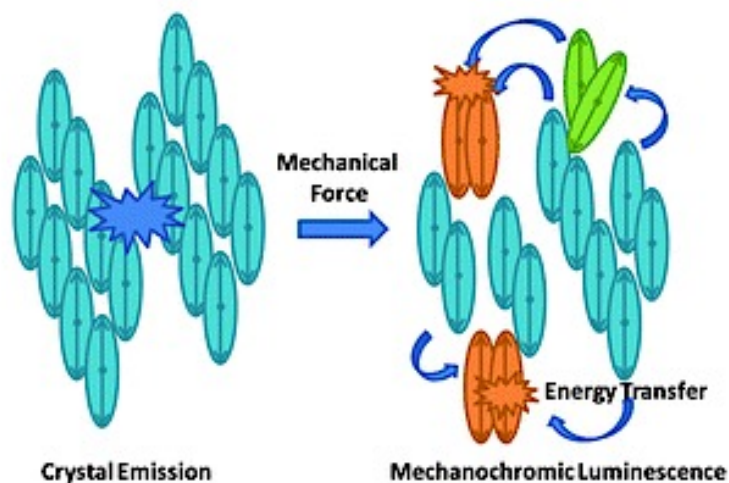


Figure 1.12 Illustration showing how the crystalline blue emission of BF_2bdks can be altered to a red-shifted emission *via* energy transfer in the presence of H-aggregates. (adapted from reference 54).

Chujo and coworkers have demonstrated many examples of organoboron compounds with highly tunable emission properties.⁵⁷⁻⁵⁹ Among them is the recent discovery of boron ketoiminates exhibiting AIE as well as ML. They found that the reversible ML properties could be tuned by altering end functional groups. Furthermore, substitution with halogens afforded much more dramatic ML than dyes without such substituents. This was attributed to intermolecular interactions, such as halogen-halogen bonding, not present in non-halogen substituted dyes.⁶⁰

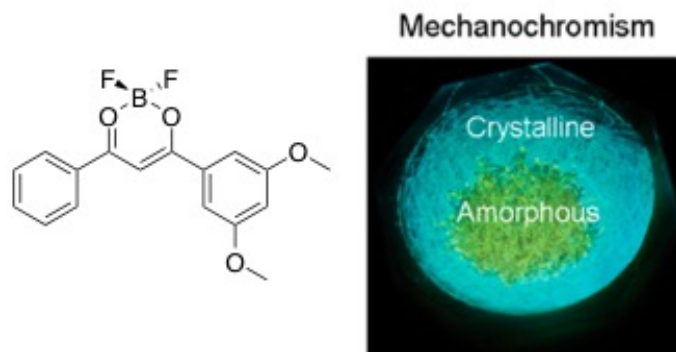


Figure 1.13 Mechanochromic luminescence of difluoroboron 1-phenyl-3-(3,5-dimethoxyphenyl)-propane-1,3-dione. (adapted from reference 56).

Despite the great strides that have been made in understanding these materials, many questions still remain unanswered. It is important from both fundamental and materials science points of view to understand how functional properties of dyes can be obtained. A promising avenue for tuning dye properties involves modifications to the the β-diketonate structure with substituents. Because synthesis of these ligands is quite straightforward, involving Claisen condensations between commercially available ketone and ester pairs, myriad such structures can be synthesized and tested.⁶¹ Findings presented in this thesis arise from the study of newly synthesized BF₂bdk dyes with various substituents on the β-diketonate ligands. These BF₂bdk are tested for their mechanoresponsiveness as well as other functional properties. In chapters 2, 3, 4, and 5, halide substitutions, varying alkoxy chain lengths, heterocycle substitutions, and substitutions at the α carbon of the dioxaborine core are all explored, respectively. Varying material processing methods including spin casting, making films on weighing paper, and bulk powders are examined for all of these materials. Finally, in chapter 6,

density functional theory is employed to model the emissive properties of BF₂bdk dyes in solution. Early work toward modeling the solid-state emissions of BF₂bdk using DFT is also presented.

1.3 References

- (1) Skoog, D. A.; Holler, F. J.; Crouch, S. R. *Principles of Instrumental Analysis*; Brooks/Cole : Thomson Learning: Australia, 2007.
- (2) Suppan, P.; Ghoneim, N. *Solvatochromism*; Royal Society of Chemistry, 1997.
- (3) Lakowicz, J. R. *Principles of Fluorescence Spectroscopy*; Springer: New York, Ny, 2007.
- (4) An, Z.; Zheng, C.; Tao, Y.; Chen, R.; Shi, H.; Chen, T.; Wang, Z.; Li, H.; Deng, R.; Liu, X.; Huang, W. *Nat. Mater.* **2015**, *14*, 685.
- (5) Brugman, C. J. M.; Rettschnick, R. P. H.; Hoytink, G. J. *Chem. Phys. Lett.* **1971**, *8*, 263.
- (6) Zhang, G.; Lu, J.; Fraser, C. L. *Inorg. Chem.* **2010**, *49*, 10747.
- (7) Zhang, G.; Palmer, G. M.; Dewhirst, M. W.; Fraser, C. L. *Nat. Mater.* **2009**, *8*, 747.
- (8) Yuan, W. Z.; Shen, X. Y.; Zhao, H.; Lam, J. W. Y.; Tang, L.; Lu, P.; Wang, C.; Liu, Y.; Wang, Z.; Zheng, Q.; Sun, J. Z.; Ma, Y.; Tang, B. Z. *J. Phys. Chem. C* **2010**, *114*, 6090.
- (9) Lower, S. K. E.-S., M.A. *Chem. Rev.* **1966**, 199.
- (10) Horiba Jobin Yvon Inc.: Edison, NJ, 2010.
- (11) Yamaguchi, Y.; Matsubara, Y.; Ochi, T.; Wakamiya, T.; Yoshida, Z.-i. *J. Am. Chem. Soc.* **2008**, *130*, 13867.
- (12) Kamimoto, N.; Nakamura, N.; Tsutsumi, A.; Mandai, H.; Mitsudo, K.; Wakamiya, A.; Murata, Y.; Hasegawa, J.-y.; Suga, S. *Asian J. Org. Chem.* **2016**, 373.
- (13) Tong, J.; Wang, Y.; Mei, J.; Wang, J.; Qin, A.; Sun, J. Z.; Tang, B. Z. *Chem. Eur. J.* **2014**, *20*, 4661.
- (14) Ma, X.; Sun, R.; Cheng, J.; Liu, J.; Gou, F.; Xiang, H.; Zhou, X. *J. Chem. Educ.* **2015**.

- (15) Hong, Y.; Lam, J. W. Y.; Tang, B. Z. *Chem. Commun.* **2009**, 4332.
- (16) Huang, J.; Sun, N.; Chen, P.; Tang, R.; Li, Q.; Ma, D.; Li, Z. *Chem. Commun.* **2014**, 50, 2136.
- (17) Chi, J. X. a. *Z. Mechanochromic Fluorescent Materials*; 1st ed.; The Royal Society of Chemistry: Cambridge, UK, 2014.
- (18) Luo, J.; Xie, Z.; Lam, J. W. Y.; Cheng, L.; Chen, H.; Qiu, C.; Kwok, H. S.; Zhan, X.; Liu, Y.; Zhu, D.; Tang, B. Z. *Chem. Commun.* **2001**, 1740.
- (19) Hu, J.; He, Z.; Wang, Z.; Li, X.; You, J.; Gao, G. *Tetrahedron Lett.* **2013**, 54, 4167.
- (20) Jia, W.-b.; Wang, H.-w.; Yang, L.-m.; Lu, H.-b.; Kong, L.; Tian, Y.-p.; Tao, X.-t.; Yang, J.-x. *J. Mater. Chem. C* **2013**, 1, 7092.
- (21) Li, Z.; Dong, Y.; Mi, B.; Tang, Y.; Häußler, M.; Tong, H.; Dong, Y.; Lam, J. W.; Ren, Y.; Sung, H. H. *J. Phys. Chem. B* **2005**, 109, 10061.
- (22) Dong, Y.; Lam, J. W.; Qin, A.; Li, Z.; Liu, J.; Sun, J.; Dong, Y.; Tang, B. Z. *Chem. Phys. Lett.* **2007**, 446, 124.
- (23) Chan, C. P.-y.; Haeussler, M.; Tang, B. Z.; Dong, Y.; Sin, K.-k.; Mak, W.-c.; Trau, D.; Seydack, M.; Renneberg, R. *J. Immunol. Methods* **2004**, 295, 111.
- (24) Jin, J.-K.; Sun, J.-Z.; Dong, Y.-Q.; Xu, H.-P.; Yuan, W.-Z.; Tang, B. Z. *J. Luminesc.* **2009**, 129, 19.
- (25) Li, D.; Liang, Z.; Chen, J.; Yu, J.; Xu, R. *Dalton Trans.* **2013**, 42, 9877.
- (26) Chi, Z.; Zhang, X.; Xu, B.; Zhou, X.; Ma, C.; Zhang, Y.; Liu, S.; Xu, J. *Chem. Soc. Rev.* **2012**, 41, 3878.
- (27) Yoshimitsu, S.; Takashi, K. *Nat. Chem.* **2009**, 1, 605.
- (28) Kinami, M.; Crenshaw, B. R.; Weder, C. *Chem. Mater.* **2006**, 18, 946.
- (29) Black, A. L.; Lenhardt, J. M.; Craig, S. L. *J. Mater. Chem.* **2011**, 21, 1655.
- (30) Davis, D. A.; Hamilton, A.; Yang, J.; Cremar, L. D.; Van Gough, D.; Potisek, S. L.; Ong, M. T.; Braun, P. V.; Martínez, T. J.; White, S. R.; Moore, J. S.; Sottos, N. R. *Nature* **2009**, 459, 68.

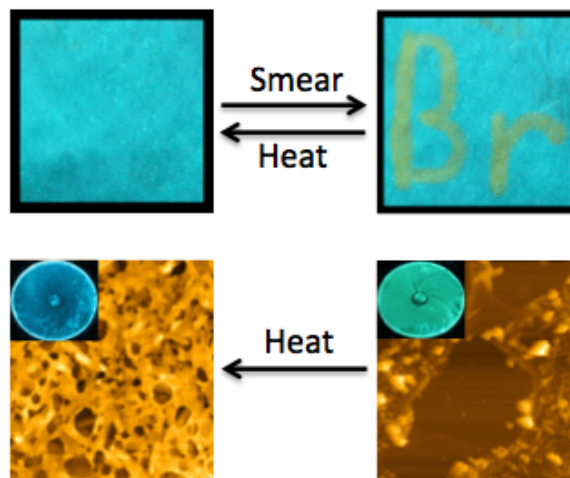
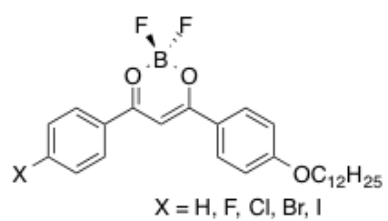
- (31) Ito, H.; Saito, T.; Oshima, N.; Kitamura, N.; Ishizaka, S.; Hinatsu, Y.; Wakeshima, M.; Kato, M.; Tsuge, K.; Sawamura, M. *J. Am. Chem. Soc.* **2008**, *130*, 10044.
- (32) Ni, J.; Zhang, X.; Qiu, N.; Wu, Y.-H.; Zhang, L.-Y.; Zhang, J.; Chen, Z.-N. *Inorg. Chem.* **2011**, *50*, 9090.
- (33) Löwe, C.; Weder, C. *Adv. Mater.* **2002**, *14*, 1625.
- (34) Crenshaw, B. R.; Weder, C. *Chem. Mater.* **2003**, *15*, 4717.
- (35) Sagara, Y.; Kato, T. *Angew. Chem. Int. Ed.* **2008**, *47*, 5175.
- (36) Sagara, Y.; Yamane, S.; Mutai, T.; Araki, K.; Kato, T. *Adv. Funct. Mater.* **2009**, *19*, 1869.
- (37) Sagara, Y.; Komatsu, T.; Ueno, T.; Hanaoka, K.; Kato, T.; Nagano, T. *J. Am. Chem. Soc.* **2014**, *136*, 4273.
- (38) Qi, Q.; Zhang, J.; Xu, B.; Li, B.; Zhang, S. X.-A.; Tian, W. *J. Phys. Chem. C* **2013**, *117*, 24997.
- (39) Zhang, G.; Lu, J.; Sabat, M.; Fraser, C. L. *J. Am. Chem. Soc.* **2010**, *132*, 2160.
- (40) Liu, T.; Chien, A. D.; Lu, J.; Zhang, G.; Fraser, C. L. *J. Mater. Chem.* **2011**, *21*, 8401.
- (41) Yoshii, R.; Hirose, A.; Tanaka, K.; Chujo, Y. *J. Am. Chem. Soc.* **2014**, *136*, 18131.
- (42) Yoshii, R.; Hirose, A.; Tanaka, K.; Chujo, Y. *Chem. Eur. J.* **2014**, *20*, 8320.
- (43) Cogné-Laage, E.; Allemand, J.-F.; Ruel, O.; Baudin, J.-B.; Croquette, V.; Blanchard-Desce, M.; Jullien, L. *Chem. Eur. J.* **2004**, *10*, 1445.
- (44) Chow, Y. L.; Johansson, C. I.; Zhang, Y.-H.; Gautron, R.; Yang, L.; Rassat, A.; Yang, S.-Z. *J. Phys. Org. Chem.* **1996**, *9*, 7.
- (45) Ono, K.; Yoshikawa, K.; Tsuji, Y.; Yamaguchi, H.; Uozumi, R.; Tomura, M.; Taga, K.; Saito, K. *Tetrahedron* **2007**, *63*, 9354.
- (46) Halik, M.; Wenseleers, W.; Grasso, C.; Stellacci, F.; Zojer, E.; Barlow, S.; Bredas, J.-L.; Perry, J. W.; Marder, S. R. *Chem. Commun.* **2003**, *0*, 1490.
- (47) Xu, S.; Evans, R. E.; Liu, T.; Zhang, G.; Demas, J. N.; Trindle, C. O.; Fraser, C. L. *Inorg. Chem.* **2013**, *52*, 3597.

- (48) DeRosa, C. A.; Kerr, C.; Fan, Z.; Kolpaczynska, M.; Mathew, A. S.; Evans, R. E.; Zhang, G.; Fraser, C. L. *ACS Appl. Mater. Interfaces* **2015**, *7*, 23633.
- (49) DeRosa, C. A.; Samonina-Kosicka, J.; Fan, Z.; Hendargo, H. C.; Weitzel, D. H.; Palmer, G. M.; Fraser, C. L. *Macromolecules* **2015**, *48*, 2967.
- (50) Samonina-Kosicka, J.; DeRosa, C. A.; Morris, W. A.; Fan, Z.; Fraser, C. L. *Macromolecules* **2014**, *47*, 3736.
- (51) Zhang, X.; Liu, X.; Lu, R.; Zhang, H.; Gong, P. *J. Mater. Chem.* **2012**, *22*, 1167.
- (52) Liu, X.; Zhang, X.; Lu, R.; Xue, P.; Xu, D.; Zhou, H. *J. Mater. Chem.* **2011**, *21*, 8756.
- (53) Nguyen, N. D.; Zhang, G.; Lu, J.; Sherman, A. E.; Fraser, C. L. *J. Mater. Chem.* **2011**, *21*, 8409.
- (54) Sun, X.; Zhang, X.; Li, X.; Liu, S.; Zhang, G. *J. Mater. Chem.* **2012**, *22*, 17332.
- (55) Liang, W. Y. *Phys. Educ.* **1970**, *5*, 226.
- (56) Galer, P.; Korošec, R. C.; Vidmar, M.; Šket, B. *J. Am. Chem. Soc.* **2014**, *136*, 7383.
- (57) Matsumi, N.; Naka, K.; Chujo, Y. *J. Am. Chem. Soc.* **1998**, *120*, 5112.
- (58) Nagai, A.; Kokado, K.; Nagata, Y.; Arita, M.; Chujo, Y. *J. Org. Chem.* **2008**, *73*, 8605.
- (59) Yoshii, R.; Nagai, A.; Tanaka, K.; Chujo, Y. *Chem. Eur. J.* **2013**, *19*, 4506.
- (60) Yoshii, R.; Suenaga, K.; Tanaka, K.; Chujo, Y. *Chem. Eur. J.* **2015**, 7231.
- (61) Zhang, G.; Fiore, G. L.; St. Clair, T. L.; Fraser, C. L. *Macromolecules* **2009**, *42*, 3162.

Chapter 2

Mechanochromic Luminescence of Halide-Substituted Difluoroboron β -Diketonate

Dyes



2.1 Introduction

As was mentioned in the preceding chapter, many questions about BF₂bdks and their unique luminescent properties remain unanswered, especially concerning mechanically induced luminescence quenching (MLQ) and heavy atoms. To what extent does the heavy atom dictate whether or not a dye will show MLQ? How does the presence of a heavy atom affect the formation of the ordered emissive state as well as the amorphous state brought about by smearing? How do different halide substituents influence spontaneous recovery of the dye at room temperature after smearing?

To begin to address some of these questions, a series of dyes of the form BF₂dbm(X)OC₁₂H₂₅, where X = H, F, Cl, Br, or I (Figure 2.1) were synthesized. By altering the halide substituent the effect of varying the weight of the substituent on ML and MLQ was explored. The dyes were studied in CH₂Cl₂ solution, as films on both weighing paper and glass substrates, and as bulk powders. The weighing paper substrate was utilized to study MLQ properties of the dyes at room and low temperature. Spin-cast films of the dyes on glass were used to monitor spontaneous recovery of the dyes at room temperature, and for solid-state quantum yield measurements, and atomic force microscopy (AFM) imaging, and X-ray diffraction (XRD) characterization. Dyes as bulk powders were studied by XRD to find structural differences between as-isolated (AI) powders, thermally annealed (TA) powders, and powders ground (GR) using a mortar and pestle.

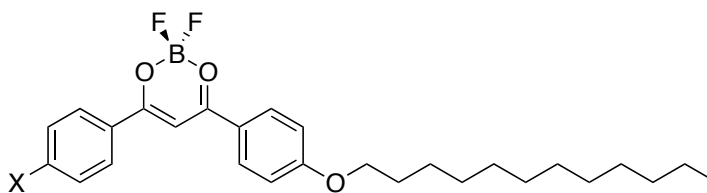


Figure 2.1 Chemical structure of $\text{BF}_2\text{dbm}(\text{X})\text{OC}_{12}\text{H}_{25}$ dyes ($\text{X} = \text{H}, \text{F}, \text{Cl}, \text{Br}, \text{or I}$).

2.2 Experimental

2.2.1 Materials

4-Dodecyloxyacetophenone was synthesized *via* a Williamson ether synthesis as previously reported.¹ Solvents CH_2Cl_2 and THF were either dried and purified by passage through alumina columns or dried over 3 Å molecular sieves according to a previously reported method.² All other chemicals were reagent grade from Sigma Aldrich and were used without further purification.

2.2.2 Methods

^1H NMR (300 MHz) spectra were recorded on a UnityInova 300/51 instrument in CDCl_3 . ^1H NMR spectra were referenced to the signal for the chloroform residual proton at 7.26 ppm and coupling constants are given in Hertz. Mass spectra were recorded using an Applied Biosystems 4800 spectrometer with a MALDI TOF/TOF analyzer. Melting points were recorded on a Mel-Temp II by Laboratory Devices, USA. UV/vis spectra were recorded on a Hewlett-Packard 8452A diode-array spectrophotometer. Steady-state fluorescence emission spectra were recorded on a Horiba Fluorolog-3 Model FL3-22 spectrofluorometer (double-grating excitation and double-grating emission monochromator). A 2 ms delay was used when recording the delayed emission spectra. Time-correlated single-photon counting (TCSPC) fluorescence lifetime measurements were performed with a NanoLED-370 ($\lambda_{\text{ex}} = 369$ nm) excitation source and a Datastation

Hub as the SPC controller. Phosphorescence lifetimes were measured with a 1 ms multi-channel scalar (MCS) excited with a pulsed xenon lamp ($\lambda_{\text{ex}} = 369$ nm; duration < 1 ms). Lifetime data were analyzed with DataStation version 2.6 software from Horiba Jobin Yvon. Fluorescence quantum yields (Φ_{F}) in CH_2Cl_2 solution were referenced *versus* quinine sulfate in 0.1 M H_2SO_4 as a standard according to a previously described method.³ The following values were used: Φ_{F} quinine sulfate = 0.54⁴, n_{D}^{20} 0.1 M H_2SO_4 = 1.33, n_{D}^{20} CH_2Cl_2 = 1.424. Quantum yields for $\text{BF}_2\text{dbm}(\text{I})\text{OC}_{12}\text{H}_{25}$ and $\text{BF}_2\text{dbm}(\text{H})\text{OC}_{12}\text{H}_{25}$ were previously reported.^{5,6} Optically dilute CH_2Cl_2 solutions of the dyes were prepared in 1 cm path length quartz cuvettes with absorbance < 0.1 (a.u.). Solid-state quantum yields of spin-cast films were measured using a Quanta- Φ F-3029 Integrating Sphere from Horiba Jobin Yvon. The Data was analyzed using FlourEssence software V 2.1 also from Horiba Jobin Yvon.

Films on weighing paper were fabricated by smearing a small amount of dye onto 5×5 cm² pieces of weighing paper with nitrile examination gloves. After this, the samples were weighed to ensure a dye mass of ~ 1 -3.5 mg spread out over the entire 5×5 cm² area. The films were annealed for 10 min in a Thermo Heratherm oven according to the respective optimum annealing temperatures (determined experimentally) (H = 110 °C, F = 142 °C, Cl = 150 °C, Br = 140 °C, I = 110 °C).⁷ A Laurel Technologies WS-650S spin-coater was used to make the spin-cast films. The films were fabricated by preparing 10^{-2} M solutions of each dye and applying ~ 5 drops of these solutions to circular microscope cover glass slides 25 mm in diameter rotating at 3,000 rpm. The films were dried *in vacuo* for 15 min before further processing and were annealed in the same way as the films on weighing paper. Films for solid-state quantum yield measurements were

made in the same way, except they were cast onto circular cover glass slips 13 mm in diameter. The sample morphologies of spin-cast films were characterized by Atomic Force Microscopy (AFM) (Digital Image, DI 3000) in tapping mode. The scan area was $20 \times 20 \mu\text{m}^2$ with a scan rate of 1.00 Hz. The resulting images were processed using Gwyddion software version 2.31.

Samples for X-ray diffraction (XRD) analysis were prepared as follows. The as-isolated (AI) powders were obtained by recrystallization from hexanes/acetone. The AI powders were heated at their predetermined optimum annealing temperatures for 3 h to obtain the thermally annealed (TA) powders. The AI powders were ground in a mortar and pestle for ~ 30 min to obtain the ground (GR) powders. Spin-cast films subjected to XRD analysis were made from 10^{-2} M dye solutions on 25 mm diameter glass slides as follows: H: ~ 30 drops, 2,000 rpm; F: ~ 50 drops, 2,000 rpm; Cl and Br: ~ 40 drops, 4,000 rpm; I: ~ 40 drops, 3,000 rpm. XRD patterns for both powders and films were collected using a Panalytical X'Pert Pro MPD diffractometer. The diffractograms were collected as follows: start angle: 10° , step size: 0.01° , time/step: 60 s, end angle: 60° .

Differential scanning calorimetry (DSC) was performed on the as-isolated powders using a TA Instruments DSC 2920 Modulated DSC. The thermograms were recorded using the standard mode. The temperature of the sample chamber was increased at a rate of $5^\circ\text{C}/\text{min}$ from 0 to 200°C and held isothermic for 10 min. The sample chamber was then cooled at the same rate to 0°C and held isothermic for 10 min. After the conditioning run, the same protocol was repeated to generate the reported thermograms. Thermograms were analyzed using the Universal Analysis software V 2.3 from TA Instruments.

2.3 Results and Discussion

2.3.1 Optical Properties of Dyes in Solution

The BF₂dbm(X)OC₁₂H₂₅ dyes were synthesized via Claisen condensation of 4-dodecyloxyacetophenone with the appropriate halo-ester, followed by boronation in CH₂Cl₂. Purification by recrystallization from hexanes/acetone yielded emissive yellow powders. The absorption and emission properties of the compounds were studied in dilute CH₂Cl₂ solution (Table 2.1). All dyes exhibited high extinction coefficients (>50,000 M⁻¹ cm⁻¹) that increased along with the molecular weight of the halogen. There was also a red-shift in absorbance maxima from H to I. The dyes have quantum yields near unity, with the exception of BF₂dbm(I)OC₁₂H₂₅,⁵ which can be easily explained by the heavy atom effect increasing spin-orbit coupling and thereby decreasing the S₁ population and increasing species population in T₁.⁸ All dyes have fluorescence lifetimes between 1.22 and 2.02 ns, fit to single exponential decay. There is a slight red shift in fluorescence maxima as the weight of the heavy atom increases.

Table 2.1 Absorption and Emission Properties of Boron Dyes in CH₂Cl₂ Solution.^a

Dye	$\lambda_{\text{abs}}^{\text{b}}$	ϵ	$\lambda_{\text{em}}^{\text{c}}$	Φ_{F}	τ
BF ₂ dbm(X)OC ₁₂ H ₂₅	[nm]	[M ⁻¹ cm ⁻¹]	[nm]	[%]	[ns]
[X=]					
H	399 ^d	51,600 ^d	439 ^d	100 ^d	2.02 ^d
F	400	55,000	435	99	1.77
Cl	404	58,000	441	99	1.22
Br	406	61,000	442	95	1.95
I	409	63,000	444	67 ^e	1.50 ^e

^a 369 nm; room temperature, air.

^b Absorbance maximum.

^c Emission maximum; fluorescence.

^d Values taken from reference 6.

^e Values taken from reference 5.

2.3.2 Mechanochromic Luminescence on Paper

Weighing paper was used as the substrate for dye films to visualize effects with photographs and take measurements at room temperature in air and at 77K in liquid N₂.⁵ Previously BF₂dbk dyes were annealed at 110 °C for ML studies.^{1,5,6} While the I and H dyes achieved their most blue-shifted emissions and narrowest full widths at half maxima (FWHM) at 110 °C (Figure 2.2),^{1,5,7} this temperature was found to be insufficient to anneal the F, Cl and Br dyes in this study. For these dyes, different temperatures were tested until a stable maximal blue shifted emission was found (Figure 2.2). Higher temperatures (140 – 150 °C) at or near the melting points for the dyes (Table S2.1 Appendix A) were required, suggesting that the dyes may be melting and then crystallizing as they cool to form the ordered emissive states. Smear spectra are essentially the same regardless of annealing temperature. An exemplary smeared emission spectrum is provided for each dye (Figure 2.2).

As annealed films on weighing paper, the F dye exhibited the most blue-shifted emission ($\lambda_{em} = 467$ nm), followed by the H dye ($\lambda_{em} = 475$ nm) and more red-shifted heavier halides (Cl and Br: $\lambda_{em} = 483$ nm; I: $\lambda_{em} = 502$ nm) (Table 2.2). All dyes exhibited ML at room temperature in air. When the annealed films were smeared with a cotton swab, their emissions red-shifted (Figure 2.3, Table 2.2). Furthermore, all dyes showed perturbations in their pre-exponential weighted lifetimes (τ_{pw0}) after smearing and emission bands broadened (i.e. increased full widths at half maxima (FWHM)).³ All lifetimes were fit to multi-exponential decays as is typical for this family of solid-state dyes.^{1,6,9} Such behavior is indicative of either excimer or ground state dimer formation, perhaps H-aggregates as proposed by Zhang *et al.*¹⁰⁻¹³ The H, F, Cl, and Br dyes all showed substantial increases in their pre-exponential weighted lifetimes (Table S2.2 Appendix A) after smearing while the I dye actually showed a slight decrease in this value. This may be attributed to increased intersystem crossing from S_1 to T_1 .⁵ As with most BF₂bdk dyes exhibiting ML, the blue-shifted emissions and narrower full widths at half maxima can be recovered by re-annealing with the only visible difference in the materials being mechanical damage and thinning caused by repeated smearing over time (Figure 2.3, Figure S2.5 Appendix A). The extent of these changes is force and substrate dependent.

The dyes were also tested to see how they responded to multiple cycles of heating and annealing by monitoring their full widths at half maxima. As can be seen in Figure S2.5 in Appendix A, the F and Cl dyes showed a gradually diminishing ability to respond to mechanical force after consecutive cycles of annealing and smearing. For reasons unclear at this time, repeatedly heating and perturbing the dyes seem to give them a

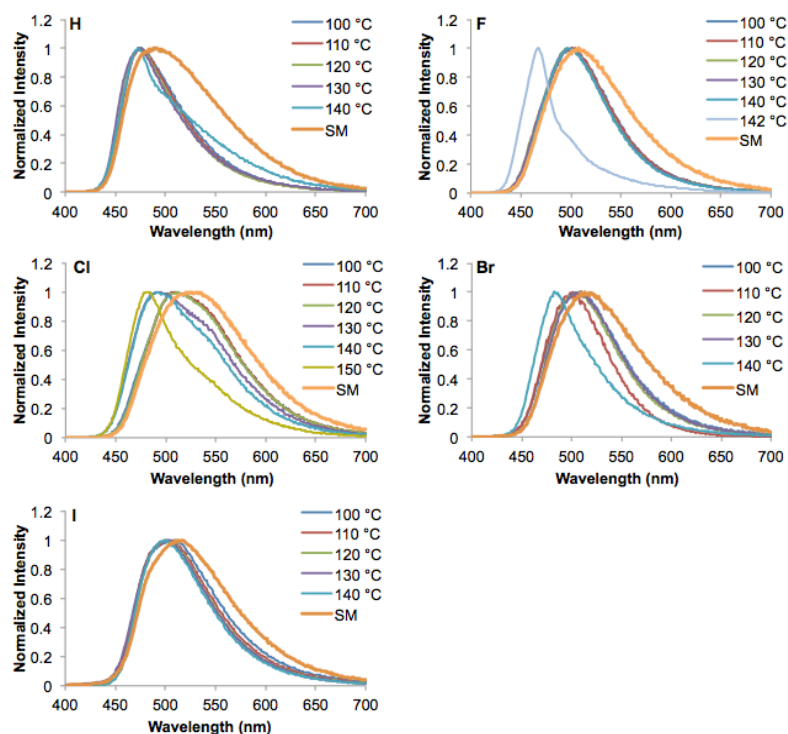


Figure 2.2 Emission spectra of $\text{BF}_2\text{dbm}(\text{X})\text{OC}_{12}\text{H}_{25}$ dyes as films on weighing paper after annealing for ten minutes at the indicated temperatures ($\lambda_{\text{ex}} = 369$ nm) (room temperature, air). Note: SM = an exemplary spectrum of the smeared dye film.

Table 2.2 Luminescence Properties of Dye Films on Weighing Paper.^a

Dye	Thermally Annealed			Smeared		
	$\lambda_{\text{em}}^{\text{b}}$	$\tau_{\text{pw0}}^{\text{c}}$	FWHM ^d	λ_{em}	$\tau_{\text{pw0}}^{\text{c}}$	FWHM ^d
[X=]	[nm]	[ns]	[nm]	[nm]	[ns]	[nm]
H	475	7.40	65	487	16.0	108
F	467	2.83	36	507	20.0	121
Cl	483	5.13	66	514	13.4	125
Br	483	1.40	63	519	6.66	111
I	502	1.29	87	513	1.01	95

^a $\lambda_{\text{ex}} = 369$ nm; room temperature, air.

^b Emission maximum; fluorescence.

^c Pre-exponential weighted fluorescence lifetime.³

^d Full Width at Half Maximum.

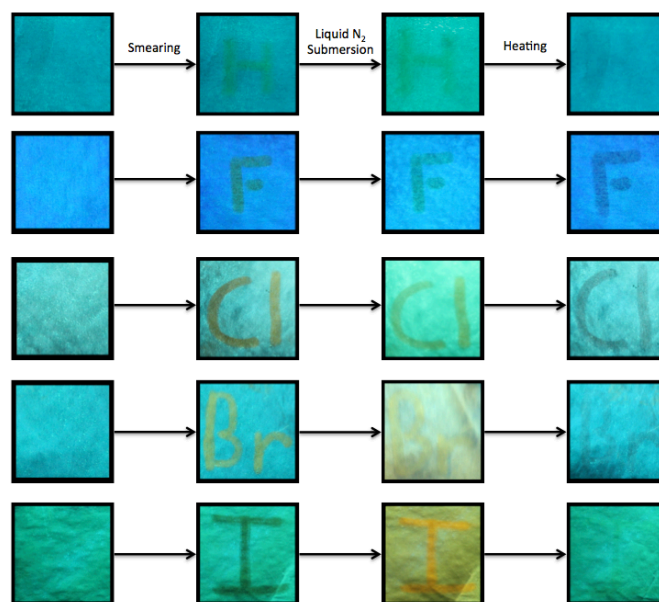


Figure 2.3 The $\text{BF}_2\text{dbm}(\text{X})\text{OC}_{12}\text{H}_{25}$ dyes as films on weighing paper. Thermally annealed films are smeared, showing mechanochromic luminescence and mechanochromic luminescence quenching (e.g. I). Cooling in liquid nitrogen inhibits oxygen quenching, making phosphorescence visible (e.g. I). Heating facilitates erasure.

greater affinity for the ordered emissive state. The H and Br dyes, on the other hand, continued to respond to mechanical force through seven cycles. The I dye did not show a particularly large bathochromic shift or increase in FWHM after smearing on weighing paper and showed only a slight decrease in its ability to respond to smearing over time. As previously described for $\text{BF}_2\text{dbm}(\text{I})\text{OC}_{12}\text{H}_{25}$, all of the dyes showed a decrease in fluorescence intensity after smearing at room temperature under air (the emission and excitation slit widths were kept the same for the TA and SM spectra of each dye, respectively) suggesting that mechanical force leads to fluorescence quenching to some extent, likely through mechanically induced changes in dye aggregation that lower the energy of S_1 and enhance intersystem crossing to the triplet excited state.⁵ At first glance, this drop in intensity could be attributed to simply removing emissive material with

smearing. However, because the intensities increased again after re-annealing (Figure S2.4 Appendix A), there must be more to this phenomenon.

The luminescence properties of the dyes were also examined at 77K in liquid N₂. This was necessary to study the effect of mechanical perturbation on triplet emission because, at room temperature under air, the phosphorescence of these dyes is diminished by a combination of collisional O₂ quenching and non-radiative decay from the triplet state.⁵ As can be seen in Figure 2.3, the smeared portion of the I dye undergoes a marked change from dim to bright orange when submerged in liquid N₂. When examining the total emission spectra of the I and Br dyes at 77K in liquid N₂, blue-shifted peaks corresponding to fluorescence and red-shifted peaks corresponding to phosphorescence are observed (Figure 2.4; λ_{em} fluorescence: I dye, annealed: ~490 nm, smeared: ~500 nm; Br dye, annealed: ~500 nm, smeared: ~530 nm. λ_{em} phosphorescence = ~560-580 nm when annealed or smeared for both dyes). To clarify, the H, F, and Cl dyes also exhibit phosphorescence under these conditions, evidenced by delayed emission spectra (Figure S2.6 Appendix A), but the fluorescence signal is too strong relative to phosphorescence for it to be observed in a total emission scan. As can be seen in Figure 2.4, smearing the annealed films of the Br and I dyes produces the aforementioned red-shift in fluorescence as well as a change in F/P that can be observed in liquid N₂.

Interestingly, the intensities of the phosphorescence peaks increase for every dye studied when the thermally annealed sample is smeared (Figure 2.5). The emission and excitation slit widths were kept the same for the TA and SM spectra for each dye, making this comparison possible. Changes in F/P intensity ratios could only be observed in total emission scans at 77K in liquid N₂ for the Br and I dyes, respectively. The expected trend

was noted in the phosphorescence lifetimes of the annealed films. As the weight of the heavy atom substituent increased, the phosphorescence lifetimes decreased (i.e. H = 463 ms, F = 244 ms, Cl = 208 ms, Br = 42.6 ms, and I = 14.4 ms) (Table S2.4 Appendix A). This trend is commonly observed for halide substituted luminescent, aromatic organic compounds.^{14,15} In Table S2.4 (Appendix A) and Figure 2.5, the delayed emission maxima of all dyes change very little in response to mechanical force, while their pre-exponential weighted phosphorescence lifetimes increase dramatically. This shows that the energy of the aggregate T_1 excited state is not changing in a significant way but the population of excited-state species in T_1 is increasing in response to mechanical force. Fraser *et al.* have put forth that a lowering of the energy of the aggregate S_1 excited state in response to mechanical force could increase intersystem crossing between S_1 and T_1 in the presence of a heavy atom, and that this is a possible explanation for the mechanism of MLQ.^{5,16} These data strongly support that claim. Furthermore, these data show that MLQ is a phenomenon not limited to the iodine substituted $\text{BF}_2\text{dbm(I)OC}_{12}\text{H}_{25}$, but extends to dyes with lighter halogen substituents and, surprisingly, even to a dye without any heavy atom at all. The iodine substituent simply makes this effect visible to the unaided eye at both room temperature in air and at 77K in liquid N_2 .

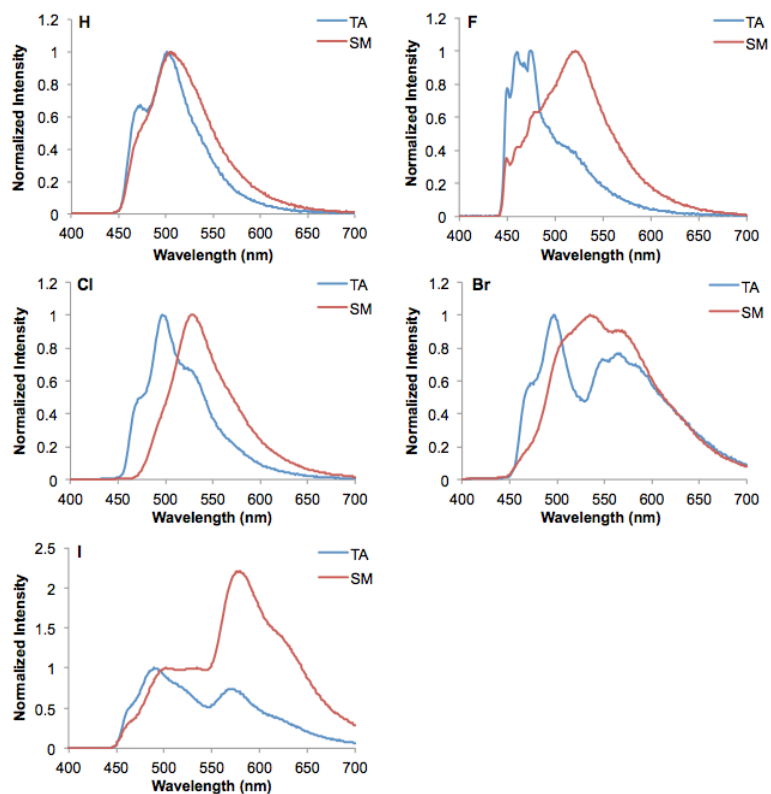


Figure 2.4 Normalized total emission spectra of boron dyes on weighing paper in both thermally annealed (TA) and smeared (SM) states ($\lambda_{\text{ex}} = 369$ nm) (77K, liquid N₂). Spectra are normalized to their corresponding fluorescence maxima (i.e. singlet emission).

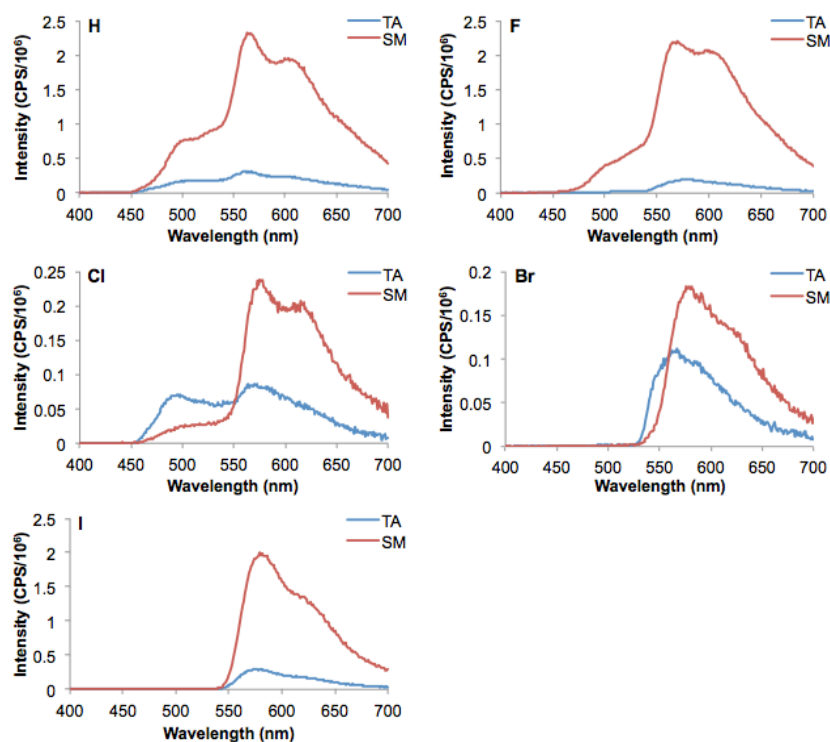


Figure 2.5 Delayed emission spectra of boron dyes on weighing paper in both thermally annealed (TA) and smeared (SM) states ($\lambda_{\text{ex}} = 369$ nm) (77K, liquid N₂). The intensities were recorded in photon counts per second (CPS) and shown as CPS/10⁶.

2.3.3 Mechanochromic Luminescence on Glass

In order to study substrate effects, the spontaneous recovery of the dye materials after smearing, and to acquire images of the materials in various states using atomic force microscopy (AFM), thin spin-cast films on microscope cover glass were utilized. Fluorescence spectra of the films were recorded and a blue-shift, narrowing of the full widths at half maxima, and shortening of the pre-exponential weighted lifetimes (with the exception of the I dye for which the lifetime actually increased) were observed upon annealing the as-spun films, suggesting that the as-spun films represent a more amorphous emissive material (Figure 2.6, Table S2.5 Appendix A). Also, all dyes had

more blue-shifted fluorescence maxima in the thermally annealed (TA) state as spin-cast films than they did as films on weighing paper, which is an interesting processing effect.

Perhaps the dye molecules show a greater propensity to adhere to each other and form

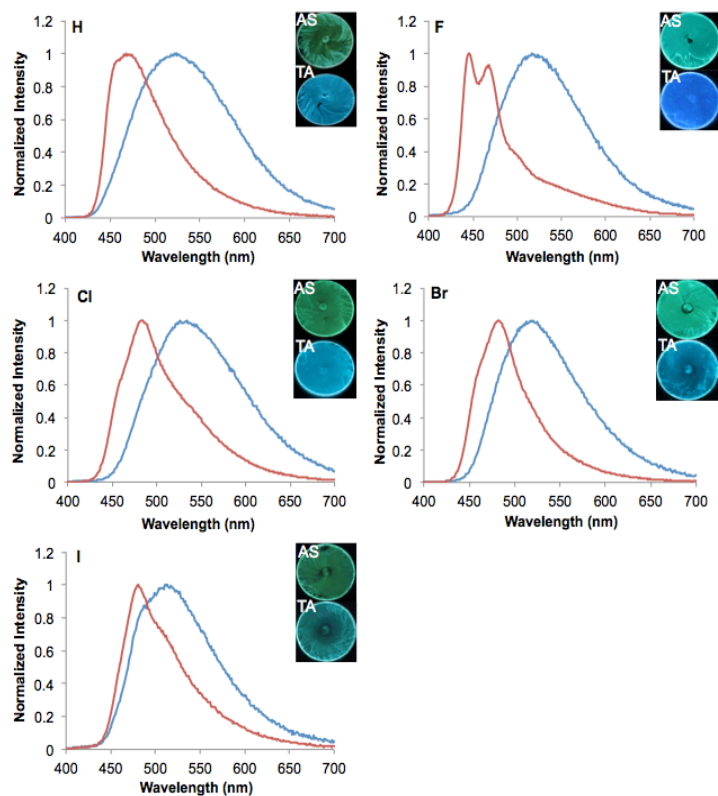


Figure 2.6 Normalized emission spectra of boron dyes as spin-cast films on microscope cover glass in both as-spun (AS) and thermally annealed (TA) states ($\lambda_{\text{ex}} = 369$ nm) (room temperature, air).

crystallites when on glass substrates, compared to paper where there may be stronger interactions with the fibrous cellulose substrate. The annealed F dye on glass exhibits the same peak at ~ 467 nm as on weighing paper. However, a more blue-shifted peak at 445 nm is also present in the spectrum. This may be a thickness effect due to increased self-absorption causing the loss of the blue-shifted peak in the thicker film on weighing paper.⁶

Solid-state quantum yields were collected for the spin-cast films. The values were measured after annealing and then again after smearing the films (Table 2.3). Both annealed and smeared films exhibited trends typically associated with the heavy atom effect. Films of the H dye had the highest quantum yields (~50-68%), F and Cl films had intermediate values (~34-46%), and films of Br and I dyes had the lowest quantum yields (~2-13%). As was expected, the H, F, Cl, and I dyes all experienced a decrease in quantum yield corresponding to smearing, consistent with MLQ. Curiously, the Br dye showed anomalous behavior compared to the others in the set, exhibiting a slight increase (~3%) in its quantum yield corresponding to smearing. In all experiments except for this one, this dye demonstrates MLQ. Perhaps for some structural reason unknown to us at this time, the amorphous state exhibits both enhanced crossover to the triplet state and more efficient singlet emission at room temperature under air.

Table 2.3 Solid State Luminescence Quantum Yields for the Dyes as Spin-Cast Films on Glass at Room Temperature Under Air.^a

Dye BF ₂ dbm(X)OC ₁₂ H ₂₅ [X=]	Thermally Annealed Φ^b [%]	Smeared Φ [%]
H	67.66	49.53
F	38.33	35.80
Cl	46.06	33.93
Br	9.71	13.23
I	8.10	2.37

^a $\lambda_{\text{ex}} = 369$ nm.
^b Solid state luminescence quantum yield.

Just as has been previously observed with BF₂bdk dyes exhibiting ML, the transition from as-spun to thermally annealed films seems to correspond to a change from a relatively amorphous material to a more ordered material.¹ This was confirmed by

analyzing spin-cast films of the dyes using atomic force microscopy (AFM) (Figure 2.7). As can be seen from the AFM images, all dyes show a significant growth of crystallites after annealing. The F and Cl dyes form rather large, lamellar crystallites by comparison to the other dyes, which form smaller, needle-like crystallites. A possible explanation for this could be that the smaller, more electronegative halogen substituents provide greater stability for more highly organized dye aggregates via halogen-hydrogen and halogen-halogen interactions. In fact, $\text{BF}_2\text{dbm}(\text{H})\text{OC}_{12}\text{H}_{25}$ molecules are already known to exhibit $\text{C-H}\cdots\text{F}$ bonding between the ortho carbon of the phenyl ring on one molecule and the BF_2 moiety on another in the solid state resulting in the observation of lamellar structures when studied using scanning tunneling microscopy (STM).¹⁷ Furthermore, Saccone *et al.* have reported crystal structures of azobenzene compounds that exhibit intermolecular $\text{F}\cdots\text{F}$ bonding and bifurcated $\text{H}\cdots\text{F}\cdots\text{H}$ bonds.¹⁸

Boron dyes of this type are known to possess the ability to spontaneously return to more blue-shifted emissive states after smearing at room temperature.^{1,9} Furthermore, $\text{BF}_2\text{dbm}(\text{H})\text{OC}_{12}\text{H}_{25}$ and BF_2AVB have been shown to recover spontaneously at room temperature as thin films on paper and on glass.^{6,9} For this study, the spontaneous recovery of the dyes was studied as spin-cast films on glass. The dyes were annealed at their predetermined optimum temperatures and then their recovery was monitored for a period of three weeks after which they were annealed a second time. It was found that all of the dyes were able to spontaneously recover blue-shifted emissive states to some extent (Figure S2.7 Appendix A) Out of all of the dyes studied, the H dye showed the greatest ability to recover spontaneously, reaching an emission maximum within 10 nm

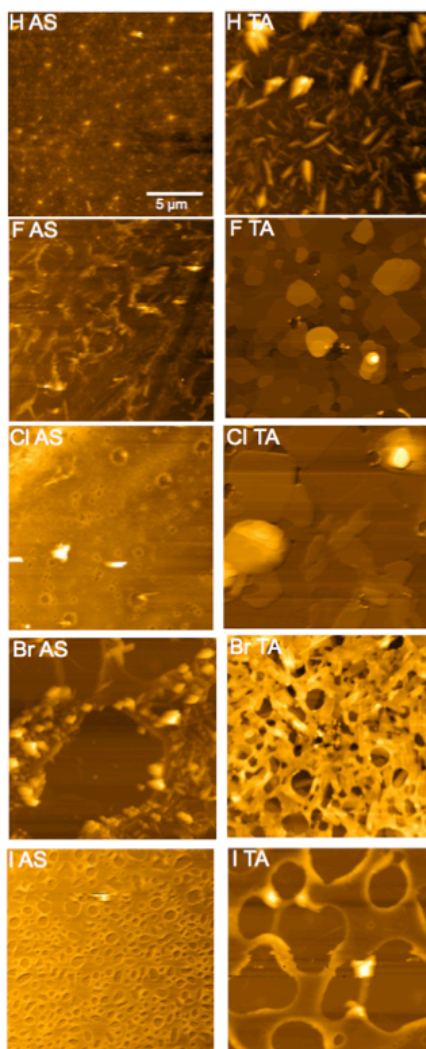


Figure 2.7 AFM images of boron dyes as spin-cast films on glass in both as-spun (AS) and thermally annealed (TA) states.

of that of the TA state after 16 days. The dyes with halogen substituents showed a much more limited ability to recover, with the Cl, Br, and I dyes ceasing to recover after one week and only getting to within ~25 nm of the TA emissions. The F dye also ceased to recover further after one week and only got to within 53 nm of the TA emission wavelength. When re-annealed after three weeks, all of the dyes recovered their ordered emissive states with the exception of the I dye. This dye seemed to lose its ability to

recover. This could be due to its decreased affinity for forming the more organized lamellar crystallites compared to the other dyes, as evidenced by the AFM images (Figure 2.7). Once again, this suggests that these dyes have a greater affinity for the ordered emissive state after re-annealing. The fact that these dyes either don't fully recover at room temperature or do so very slowly could potentially make them useful for applications where a longer lasting inscription is desirable. For example, a billboard in a restaurant or café could be inscribed with the specials of the day and then heated at the end of the day to erase.

X-ray Diffraction (XRD) techniques were also used to study the dyes as spin-cast films on glass. In order to obtain sufficient signal strength using this technique, it was necessary to make thicker films of the dyes than those used for studying the optical properties. The optimal method for producing such films was determined empirically and varied on a case-by-case basis. These differences may be attributed to observed variations in solubility and aggregation tendencies among the dyes. As expected, the films were most crystalline after annealing and most amorphous after smearing. The F dye showed the most drastic change going from as-spun to thermally annealed and then to smeared (Figure 2.8). When this dye was annealed, a strong peak arose at $\sim 12.6^\circ$ and a much weaker yet clearly distinguishable peak appeared at $\sim 18.8^\circ$. When the thermally annealed sample was smeared, these peaks disappeared. The I dye also showed clear signs of crystallinity in both the AS and TA films (Figure 2.8). In the as-spun film, there are three intense peaks at $\sim 13.9^\circ$, $\sim 10.4^\circ$ and $\sim 27.8^\circ$. When this sample is annealed, these peaks become more intense and their relative ratios change. Again, when the

sample is smeared it becomes amorphous and no peaks are evident. XRD data for H, Cl, and Br are provided in Figure S2.9 (Appendix A).

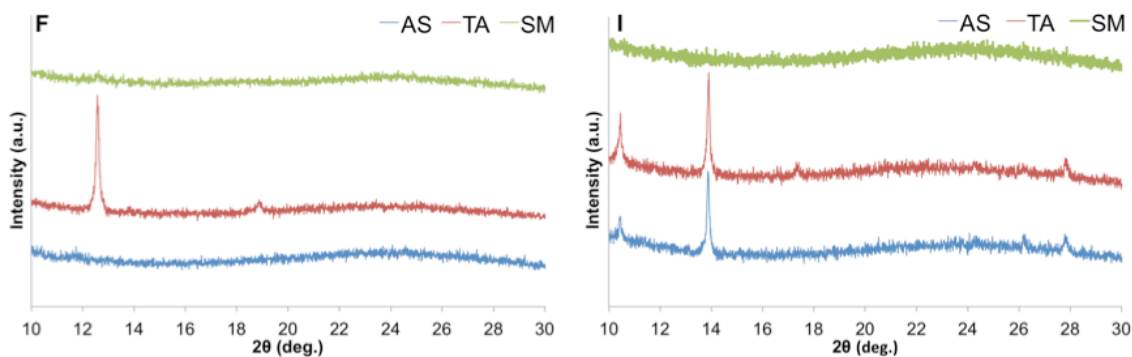


Figure 2.8 X-ray diffraction (XRD) patterns of the F and I dyes as-spun (AS), thermally annealed (TA), and smeared (SM).

2.3.4 Mechanochromic Luminescence of Bulk Powders

Just like the films on weighing paper and glass substrates, the emissions of the bulk powders also responded to annealing and mechanical stress to varying degrees (Table S2.6, Figure S2.8, and Figure S2.10 Appendix A). However, more drastic thermal and mechanical conditions were required to induce emission changes in powders. Compared to films, bulk powders required longer annealing times (i.e. 3 hours) in order to achieve stable, maximal blue-shifts in emission. Typical trends are observed upon annealing (blue-shift) and smearing (red-shift) (Figure 2.9). Powders also required vigorous grinding with a mortar and pestle for ~30 minutes to achieve typical red-shifts in emission. The same emissions were observed whether as-isolated or thermally annealed powders were ground. Powder samples were also subjected to XRD analysis to assess structural factors. To prepare as-isolated and thermally annealed samples for XRD

analysis it was necessary to lightly chop the powders with a razor blade for ~ 1 min. Importantly, this did not produce the red-shifts in emission observed for the ground

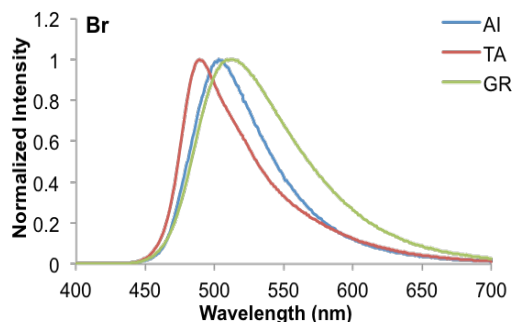


Figure 2.9 Emission spectra of the Br dye as a bulk powder ($\lambda_{\text{ex}} = 369$ nm) (room temperature, air). As-isolated (AI), thermally annealed (TA), and ground (GR) powders are compared.

samples. The most notable differences for the bulk powders can be observed by comparing the XRD patterns for thermally annealed and as-isolated forms with the ground sample patterns (Figure 2.10). In general, the as-isolated and thermally annealed diffractograms have many more distinct, strong peaks suggesting crystallinity. The diffractograms of the ground samples, on the other hand, show fewer peaks and a general decrease in diffraction intensity. This suggests that the ground samples are more amorphous, as expected.

From analyzing the XRD diffractograms of the dyes in all three forms, it was concluded that the as-isolated samples represent a mixture of both amorphous and ordered emissive species. In almost every case, peaks unique to thermally annealed or ground samples are both present in the diffractograms of the as-isolated samples. Using the diffractograms of the Br dye as an example, a distinctly structured peak is present at

$\sim 14.5^\circ$ in both the AI and GR samples, but this peak is absent from the diffractogram of the TA sample (Figure 2.10). In addition to this, there is a distinctly structured peak at $\sim 18.4^\circ$ in the AI diffractogram that becomes more intense in the TA diffractogram, but is absent from the GR diffractogram. Credence is also lent to this idea by studying the emission spectra of the Br bulk powder sample in all three forms; the AI emission spectrum is intermediate in relation to the other two and overlaps considerably with both of them (Figure 2.9). The H dye bulk powder is anomalous in that it shows very little change in its emission spectrum in response to both heating and mechanical force. This is reflected in the XRD patterns where the AI, TA, and GR diffractograms are practically identical, barring changes in overall intensity. The only significant difference between the patterns is seen in the GR sample where the peak at $\sim 19.1^\circ$ increases in relative intensity. The I dye is unique as well because it shows very little change in its emission or XRD diffractograms when the AI powder is annealed. Once again, this correlates with the AFM data to suggest that the I dye has less affinity for forming a crystalline, ordered emissive state upon annealing. However, the GR emission spectrum is red-shifted and the XRD pattern suggests a significant decrease in crystallinity.

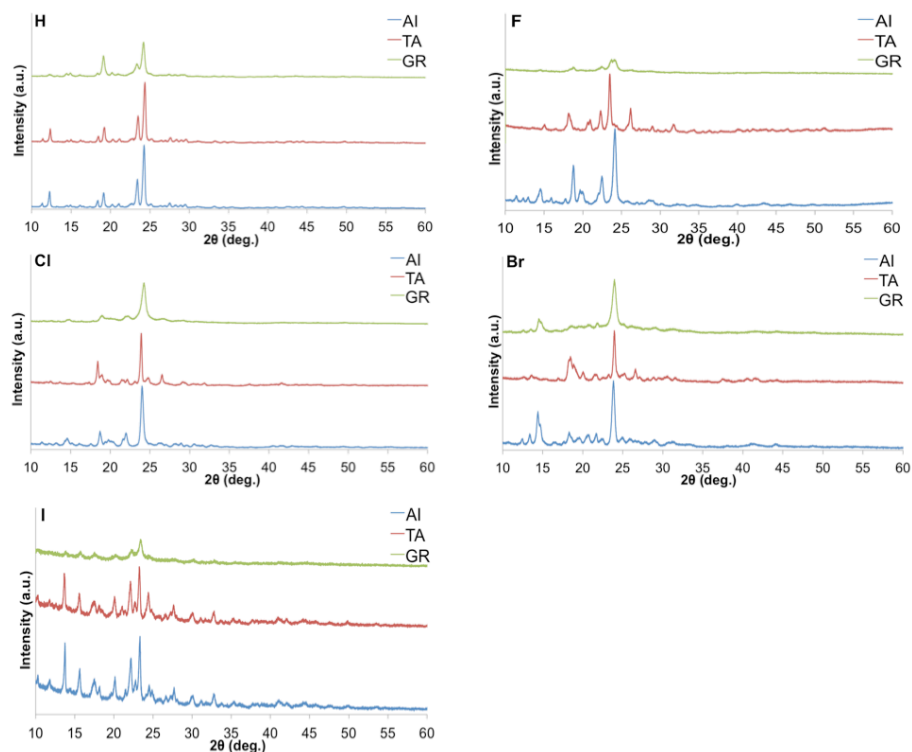


Figure 2.10 Powder X-ray diffraction (XRD) patterns of the boron dyes as bulk powders in their as-isolated (AI), thermally annealed (TA), and ground (GR) states.

2.3.5 Differential Scanning Calorimetry of Powders

In order to gain a greater understanding of the thermal properties of the dyes, differential scanning calorimetry (DSC) measurements were carried out on the bulk, AI powders. TA and GR powders were also studied, but showed no significant differences. The results are summarized in Table 2.4 and the thermograms are displayed in the supporting information (Figure S2.11 Appendix A). All dyes showed melting points (T_m) in the range of ~ 135 - 156 °C and crystallization temperatures (T_c) between ~ 110 - 144 °C. Interestingly, strong transitions can be observed in the 2nd cycles of the F and I samples in addition to their melting and crystallization. The exact nature of these transitions is

difficult to decipher, but they are most likely not transitions to liquid crystalline states because their respective enthalpies are much too large.¹⁹

Table 2.4 Differential Scanning Calorimetry (DSC) Data for As-Isolated Dyes.^a

Dye BF ₂ dbm(X)OC ₁₂ H ₂₅ [X=]	T _m ^b (ΔH ^c)	T _c ^d (ΔH ^c)
H	134.66 (560.0)	109.81 (573.7)
F	145.47 (314.9)	140.45 (308.4)
Cl	156.05 (432.3)	143.82 (414.3)
Br	153.76 (375.3)	136.89 (386.5)
I	151.87 (289.9)	141.91 (266.8)

^a All data was taken from the 2nd cycle.
^b Melting point given in °C as the peak of the major endothermic transition.
^c Enthalpy of the transition given in kJ/mol.
^d Crystallization point given in °C as the peak of the major exothermic transition.

2.4 Conclusion

In conclusion, a series of lipid derivative BF₂bdk dyes with and without halide substituents were synthesized and all were found to exhibit MLQ, demonstrating that the effect is not limited to BF₂dbm(I)OC₁₂H₂₅.⁵ In fact, it may be universal to all BF₂bdk dyes exhibiting ML due to mechanical force creating aggregates with lower energy S₁ excited states while the energy of the aggregate T₁ excited states remain, by and large, unchanged.¹² A trend of decreasing emission intensity was observed as the weight of the halogen substituent was increased due to an increasing heavy atom effect. Furthermore, it was found that films on weighing paper of the dyes with F, Cl, and Br substituents required higher temperatures to anneal than those with H or I substituents. Annealed spin-cast films on microscope cover glass of the F and Cl dyes also exhibited relatively large and organized lamellar crystallites by comparison to their H, Br, and I counterparts when examined by AFM. Along with a highly organized morphology, films of the F dye

showed the most blueshifted and structured emissions after annealing. This may be attributed to the aforementioned presence of stronger intermolecular interactions. Spin-cast films of the dyes with halogen substituents showed a slower recovery of their ordered emissive states after smearing under ambient conditions compared to the hydrogen analogue. This ability to tune fading time could make them useful for applications in which a more permanent inscription is desirable. Finally, XRD data collected for both bulk powders and spin-cast films on glass revealed a transition from a relatively amorphous state to a state with a higher degree of crystallinity after thermally annealing the AI powders and films. The crystallinity of the samples was further reduced after the AI powders were ground using a mortar and pestle. In many cases, the AI powder samples contained both ordered and amorphous features in XRD patterns and emission spectra.

2.5 Acknowledgements

Tiandong Liu is acknowledged for help with designing and performing syntheses of these dyes. This work has been published in the *Journal of Materials Chemistry C*.²⁰

2.6 References

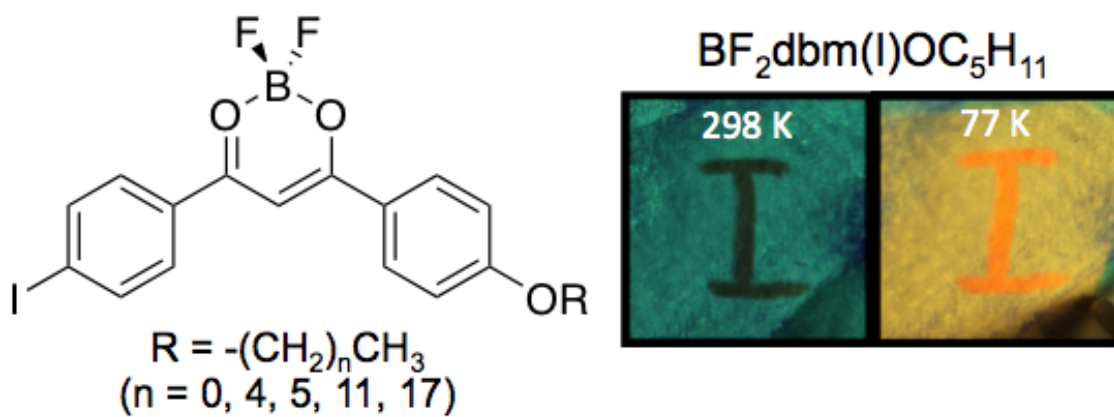
- (1) Nguyen, N. D.; Zhang, G.; Lu, J.; Sherman, A. E.; Fraser, C. L. *J. Mater. Chem.* **2011**, *21*, 8409.
- (2) Williams, D. B. G.; Lawton, M. *J. Org. Chem.* **2010**, *75*, 8351.
- (3) Carraway, E. R.; Demas, J. N.; DeGraff, B. A.; Bacon, J. R. *Anal. Chem.* **1991**, *63*, 337.
- (4) Zhu, H.; Wang, X.; Li, Y.; Wang, Z.; Yang, F.; Yang, X. *Chem. Commun.* **2009**, *0*, 5118.
- (5) Zhang, G.; Lu, J.; Fraser, C. L. *Inorg. Chem.* **2010**, *49*, 10747.

- (6) Zhang, G.; Singer, J. P.; Kooi, S. E.; Evans, R. E.; Thomas, E. L.; Fraser, C. L. *J. Mater. Chem.* **2011**, *21*, 8295.
- (7) Liu, T.; Chien, A. D.; Lu, J.; Zhang, G.; Fraser, C. L. *J. Mater. Chem.* **2011**, *21*, 8401.
- (8) Lower, S. K. E.-S., M.A. *Chem. Rev.* **1966**, 199.
- (9) Zhang, G.; Lu, J.; Sabat, M.; Fraser, C. L. *J. Am. Chem. Soc.* **2010**, *132*, 2160.
- (10) Mirochnik, A. G.; Bukvetskii, B. V.; Fedorenko, E. V.; Karasev, V. E. *Russ. Chem. Bull.* **2004**, *53*, 291.
- (11) Lakowicz, J. R. *Principles of Fluorescence Spectroscopy*; Springer: New York, NY, 2007.
- (12) Sun, X.; Zhang, X.; Li, X.; Liu, S.; Zhang, G. *J. Mater. Chem.* **2012**, *22*, 17332.
- (13) Sagara, Y.; Kato, T. *Angew. Chem. Int. Ed.* **2008**, *47*, 5175.
- (14) McClure, D. S. *J. Chem. Phys.* **1949**, *17*, 905.
- (15) Ventura, B.; Bertocco, A.; Braga, D.; Catalano, L.; d'Agostino, S.; Grepioni, F.; Taddei, P. *J. Phys. Chem. C* **2014**, *118*, 18646.
- (16) Zhang, G.; Palmer, G. M.; Dewhurst, M. W.; Fraser, C. L. *Nat. Mater.* **2009**, *8*, 747.
- (17) Zhang, X.; Yan, C.-J.; Pan, G.-B.; Zhang, R.-Q.; Wan, L.-J. *J. Phys. Chem. C* **2007**, *111*, 13851.
- (18) Saccone, M.; Terraneo, G.; Pilati, T.; Cavallo, G.; Priimagi, A.; Metrangolo, P.; Resnati, G. *Acta Crystallogr. Sect. B* **2014**, *70*, 149.
- (19) Singh, S. *Phys. Rep.* **2000**, *324*, 107.
- (20) Morris, W.A.; Liu, T.; Fraser, C.L. *J. Mater. Chem. C* **2015**, 352.

Chapter 3

Mechanochromic Luminescence Triplet Modulation in Difluoroboron

Dibenzoylmethane Complexes



3.1 Introduction

In the preceding chapter, it was demonstrated how changing a single substituent, from F to Cl, Br or I, can alter film morphology, solid-state fluorescence wavelength, phosphorescence intensity, and the ability of BF₂bdk dye materials to recover their ordered emissive states after smearing. Utilizing both fluorescence lifetime measurements under ambient conditions and phosphorescence lifetime measurements at low temperature, the proposed MLQ mechanism was substantiated. Enhancement of the triplet excited state population may be a phenomenon common to all BF₂bdk dyes exhibiting ML. Heavy atoms such as iodide simply make the effect much more obvious.^{1,2}

All of the dyes in the aforementioned halide study bore C₁₂H₂₅ alkyl chain substituents and all of their singlet excited state energies were found to be alterable by mechanical perturbation. However, their triplet states were relatively insensitive to this stimulus. Therefore, we were curious to see if we could synthesize materials with triplet states that could be perturbed by mechanical force. Given solid state fluorescence properties can be tuned by alkyl chain length³, we wanted to test whether varying the chain length might lead to mechanoresponsiveness of the triplet state as well as probe what other effects chain length might have on MLQ and triplet emission enhancement. Thus, we performed a study wherein the halide substituent remains static and the alkyl chain length is modulated. Since the iodine substituent yielded the most prominent MLQ and phosphorescence enhancement in a previous study,¹ it seemed the most promising substituent for probing the effects of mechanical perturbation on the triplet state. Six dyes of the form BF₂dbm(I)R, where R = H (**H**), OCH₃ (**C1**), OC₅H₁₁ (**C5**), OC₆H₁₃ (**C6**),

OC₁₂H₂₅ (**C12**), OC₁₈H₃₇ (**C18**) were synthesized (Figure 3.1). Both short and long chain derivatives were targeted. Additionally, **C5** and **C6** were chosen to probe for the presence of even/odd effects as it has previously been reported that these effects play an important role in the self-assembly of alkyl chain molecules.⁴ The dyes were studied in CH₂Cl₂ solution and as films on both weighing paper and glass substrates. Density Functional Theory (DFT) calculations were performed on the **H**, **C1**, and **C5** dyes in order to optimize ground state geometries, generate HOMO and LUMO molecular orbital (MO) diagrams, and to simulate absorption and emission spectra. Films on glass and pristine (i.e. as-isolated) dye powders were subjected to powder X-ray diffraction (XRD) analysis to reveal crystalline or amorphous character. Films on glass were also studied using atomic force microscopy (AFM) to investigate morphologies. Solid-state quantum yield measurements were performed. Single crystals of the **H** and **C5** dyes were grown and studied by single crystal XRD. Differential Scanning Calorimetry (DSC) was also utilized to detect thermal transitions in the pristine dye powders.

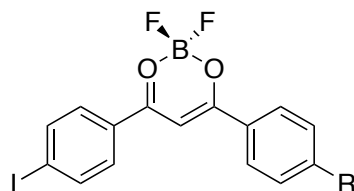


Figure 3.1 Chemical structure of BF₂dbm(I)R dyes (R = H (**H**), OCH₃ (**C1**), OC₅H₁₁ (**C5**), OC₆H₁₃ (**C6**), OC₁₂H₂₅ (**C12**), OC₁₈H₃₇ (**C18**)).

3.2 Experimental

3.2.1 Materials

4-Methoxyacetophenone, 4-pentyloxyacetophenone, 4-hexyloxyacetophenone, 4-dodecyloxyacetophenone, and 4-octadecyloxyacetophenone were synthesized *via* a

Williamson ether synthesis as previously reported.³ Solvents CH₂Cl₂ and THF were dried over 3 Å molecular sieves according to a previously reported method.⁵ All other chemicals were purchased from Sigma Aldrich and used without further purification. Synthetic procedures for the dyes are provided in the Supporting Information.

3.2.2 Methods

¹H NMR spectra were recorded on Varian UnityInova 300/51 (300 MHz) or Varian VMRS/600 (600 MHz) instruments in CDCl₃. ¹H NMR spectra were referenced to the signal for the chloroform residual proton at 7.26 ppm and coupling constants are given in Hertz. Mass spectra were recorded using either an Applied Biosystems 4800 spectrometer with a MALDI TOF/TOF analyzer or with a Micromass Q-TOF Ultima spectrometer using electrospray ionization (ESI) MS techniques. Melting points were recorded on a Mel-Temp II by Laboratory Devices, USA. UV/vis spectra were recorded on a Hewlett-Packard 8452A diode-array spectrophotometer. Steady-state fluorescence emission spectra were recorded on a Horiba Fluorolog-3 Model FL3-22 spectrofluorometer (double-grating excitation and double-grating emission monochromator). A 2 ms delay was used in recording delayed emission spectra. Time-correlated single-photon counting (TCSPC) fluorescence lifetime measurements were performed with a NanoLED-370 ($\lambda_{\text{ex}} = 369$ nm; duration <1 ms) excitation source and a Datastation Hub as the SPC controller. Lifetime data were analyzed with Datastation version 2.6 software from Horiba Jobin Yvon. Fluorescence quantum yields (Φ_{F}) in CH₂Cl₂ solution were referenced *versus* quinine sulfate in 0.1 M H₂SO₄ as a standard according to a previously described method.⁶ The following values were used: Φ_{F} quinine sulfate = 0.54,⁷ n_{D}^{20} 0.1 M H₂SO₄ = 1.33, n_{D}^{20} CH₂Cl₂ = 1.424. The quantum yield for

$\text{BF}_2\text{dbm}(\text{I})\text{OC}_{12}\text{H}_{25}$ has been previously reported.² Optically dilute CH_2Cl_2 solutions of the dyes were prepared in 1 cm path length quartz cuvettes with absorbance <0.1 (a.u.). Solid-state quantum yields of spin-cast films were measured using a Quanta- Φ F-3029 integrating sphere from Horiba Jobin Yvon. The data was analyzed using the FlourEssence software V 2.1 also from Horiba Jobin Yvon.

Films on weighing paper were created by smearing a small amount of dye onto $5 \times 5 \text{ cm}^2$ pieces of weighing paper with nitrile examination gloves. After this, the samples were weighed to ensure a dye mass of $\sim 1\text{-}3.5$ mg spread out over the entire $5 \times 5 \text{ cm}^2$ area. The films were annealed for 10 min in a Thermo Heratherm oven according to the respective optimum annealing temperatures (determined experimentally) (**H** = 110 °C, **C1** = 110 °C, **C5** = 150 °C, **C6** = 120 °C, **C12** = 110 °C, **C18** = 120 °C). A Laurel Technologies WS-650S spin-coater was used to make the spin-cast films. The films were fabricated by preparing 10^{-2} M solutions of each dye and applying ~ 5 drops of these solutions to circular microscope cover glass slides 25 mm in diameter rotating at 3000 rpm. The films were dried *in vacuo* for 15 min before further processing and were annealed in the same way as the films on weighing paper. Films for solid-state quantum yield measurements were made in the same way, except they were cast onto circular glass cover slips 13 mm in diameter. The sample morphologies of spin-cast films were characterized by atomic force microscopy (AFM) (Digital Image, DI 3000) in tapping mode. The scan areas were $10 \times 10 \mu\text{m}^2$ and $2 \times 2 \mu\text{m}^2$ with a scan rate of 0.50 Hz. The resulting images were processed using Gwyddion software version 2.31.

Samples for powder X-ray diffraction (XRD) analysis were prepared as follows. The pristine powders were analyzed as isolated by recrystallization. Films were

prepared by “drop-casting”. That is, 10^{-2} M solutions of each dye were prepared and ~20 drops of the respective solution were applied to circular microscope cover glass slides 25 mm in diameter. The films were allowed to dry under ambient conditions and then further dried *in vacuo* for 15 min before further processing and analysis. XRD patterns for both powders and films were collected using a Panalytical X’Pert Pro MPD diffractometer. The diffractograms were recorded as follows: start angle: 10° , step size: 0.01° , time per step: 60 s, end angle: 60° .

Differential scanning calorimetry (DSC) was performed on the as-isolated powders using a TA instruments DSC 2920 Modulated DSC. The thermograms were recorded using the standard mode. The temperature of the sample chamber was increased at a rate of 5°C min^{-1} until a temperature $\sim 20^\circ\text{C}$ hotter than the predetermined melting point of the given dye was reached and held isothermic for 10 min. The sample chamber was then cooled at the same rate to 0°C and held isothermic for 10 min. After the conditioning run, the same protocol was repeated to generate the reported thermograms. Thermograms were analyzed using the Universal Analysis software V 2.3 from TA Instruments.

The **H**, **C1**, and **C5** dyes were computationally modeled using the Gaussian 09⁸ suite of programs using density functional theory (DFT). B3LYP/6-311+G(d) was utilized for ground state and singlet (S_1) excited state geometry optimization with a Tomasi polarized continuum for dichloromethane solvent.⁹ The vibrational frequencies for the optimized geometries were all positive, assuring that the optimized geometries were at least a local minimum. Single point energy calculations were used to generate the molecular orbital diagrams using B3LYP-6-31G(d). Time-dependent density functional

theory, TD-B3LYP/6-311+G(d), was employed for estimates of the absorption and emission spectra.^{10,11} The first three excited states were computed for each compound. In all calculations, B3LYP/SDD was used to simulate the iodine atom with the exception of the S₁ geometry optimization of the C5 dye, for which B3LYP/6-311G was used.

Crystals for single crystal XRD were grown by slow evaporation from acetone/hexanes. Data collections for the **H** and **C5** derivatives were carried out on a Bruker Kappa Duo CCD diffractometer at -120 °C using MoK α radiation. Crystal data for **H**: monoclinic space group P2₁/c, a = 7.4702(4), b = 13.1831(6), c = 14.4768(7)Å, β = 99.941(1)°, Z = 4, V = 1404.3(1) Å³. The structure was solved by the charge flipping method of the Bruker SHELXTL program¹² and refined to an R = 0.0197 using 2791 reflections with I > 2 σ (I). **C5**: monoclinic space group P2₁/c, a = 19.482(6), b = 7.190(2), c = 14.609(5)Å, β = 105.384(5)°, Z = 4, V = 1973(2) Å³. The structure was solved by the direct methods of the Bruker SHELXTL program and refined to an R = 0.0559 using 3316 reflections with I > 2 σ (I).

3.3 Results and Discussion

3.3.1 Optical Properties of Dyes in Solution

Synthesis of the BF₂dbm(I)R dyes *via* Claisen condensation of methyl 4-iodobenzoate with the appropriate 4-alkoxyacetophenone followed by boronation, purification by passage through a silica column with CH₂Cl₂, and then recrystallization yielded yellow, emissive powders. The optical properties were studied in dilute solution (Table 3.1 and Figure 3.2). With the exception of the **H** dye (i.e. without an alkoxy tail), all dyes exhibited extinction coefficients >50,000 M⁻¹ cm⁻¹. The **H** dye was also, by far, the most blue-shifted of the dyes with respect to both absorption and emission. The

presence of an electron-donating alkoxy group has the effect of red-shifting the absorption by ~ 20 nm and the emission by ~ 30 nm. This is presumably due to the π donating lone pairs on the oxygen atom having a similar effect to increasing conjugation (i.e. raising the energy of the HOMO). The alkoxy substituent also affects a dramatic increase in both fluorescence quantum yield and lifetime; the **H** dye has a quantum yield of only 9% and a lifetime of 0.2 ns while all other dyes have quantum yields $>25\%$ and lifetimes >1 ns. There is also a rather large increase in quantum yield when the tail length is increased from **C1** to **C5** and a substantial decrease in quantum yield when the chain length is increased from **C12** to **C18**. In solution, the longer alkyl chains would possess a large range of motion. Perhaps this gives the compounds more ways to dissipate energy non-radiatively remote to the BF_2dbm fluorophore itself, resulting in an increase in quantum yield. A similar increase in quantum yield has been previously observed for BF_2dbm complexes when alkyl chain length is increased from **C1** to **C5**.³

In order to gain further insight into the optical properties in solution, density functional theory (DFT) calculations were performed on the **H**, **C1**, and **C5** compounds. Computational limitations prevented analysis of the longer chain dyes using the same method. The computed absorption and emission maxima for all three dyes are in good agreement with the results obtained experimentally (Table S3.2, Table S3.3, Table S3.5, and Table S3.6 Appendix B). The HOMO and LUMO diagrams show a transition mostly π to π^* in character with only a slight shift in amplitude from the arene rings to the BF_2 diketone moiety when going from HOMO to LUMO (Figure 3.3). A difference in amplitude distribution was observed when comparing the generated molecular orbital diagram images for the three compounds. For the **H** dye there is, qualitatively, more

amplitude concentrated on the iodine heavy atom in the HOMO when compared to the **C1** and **C5** dyes. This means that the **H** dye should experience a more pronounced heavy atom effect in which enhanced spin-orbit coupling increases crossover from the S_1 excited state to the “dark” T_1 excited state, thus decreasing fluorescence lifetime and quantum yield. This prediction is confirmed by the experimental results wherein the **C1** dye has a quantum yield of 55% and a fluorescence lifetime of 2.0 ns and these same values for the **C5** dye are 70% and 1.2 ns, respectively. The **H** dye has corresponding values of only 9% and 0.2 ns. Looking at the MOs of the **C5** dye, it can be seen that the length of the alkyl chain beyond **C1** has no effect on the distribution of amplitude in the HOMO or LUMO. This is demonstrated experimentally, in that solution absorption and emission maxima of the dyes bearing chains differ very little from each other.

Table 3.1 Absorption and Emission Properties of Boron Dyes (Figure 3.1) in CH_2Cl_2 .^a

Dye BFdbm(I)R [R=]	λ_{abs}^b [nm]	ϵ [$\text{M}^{-1} \text{cm}^{-1}$]	λ_{em}^c [nm]	Φ_{F} [%]	τ [ns]
H	390 ^e	45,000 ^e	412 ^e	9 ^e	0.2 ^e
C1	411	56,000	439	55	2.0
C5	409	61,000	444	70	1.2
C6	409	62,000	445	64	1.2
C12	409	63,000	444	67 ^e	1.5 ^e
C18	408	58,000	443	29	1.2

^a $\lambda_{\text{ex}} = 369$ nm; room temperature, air.
^b Absorbance maximum.
^c Emission maximum; fluorescence.
^e Values taken from ref. 2.

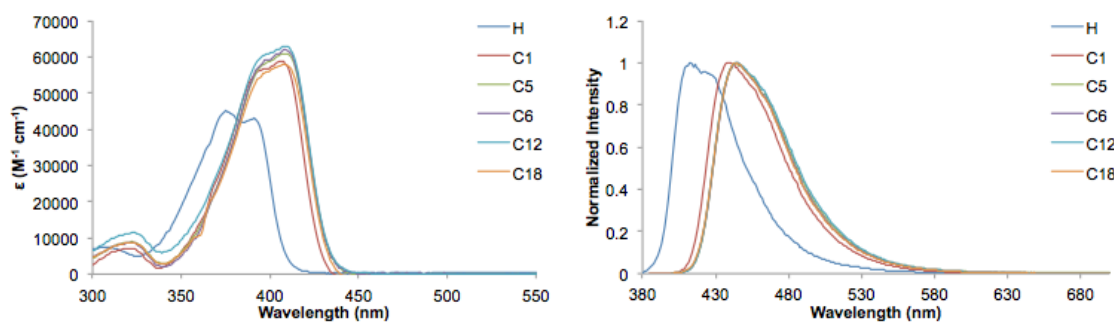


Figure 3.2 UV/vis absorption spectra (left) and steady-state fluorescence spectra (right) of BF₂dbm(I)R (R = H (**H**), OCH₃ (**C1**), OC₅H₁₁ (**C5**), OC₆H₁₃ (**C6**), OC₁₂H₂₅ (**C12**), OC₁₈H₃₇ (**C18**)) dyes in CH₂Cl₂ solution (5 × 10⁻⁶ M; λ_{ex} = 369 nm; room temperature, air).

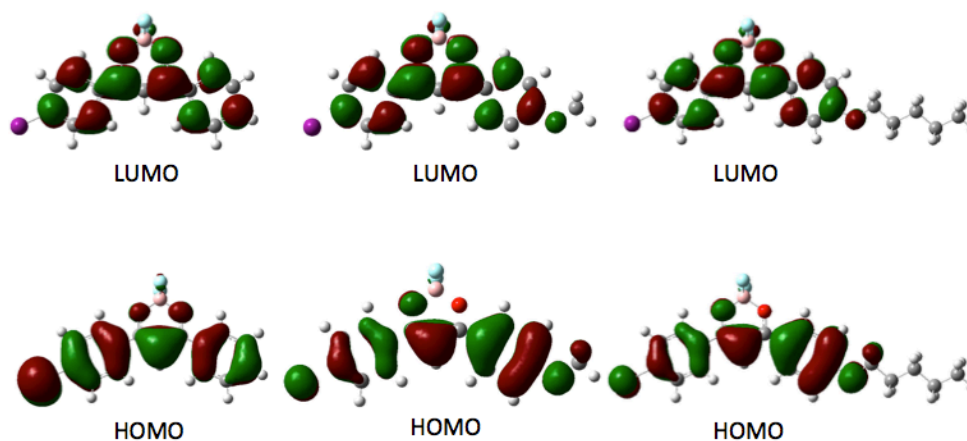


Figure 3.3 Highest occupied molecular orbital (HOMO) and lowest unoccupied molecular orbital (LUMO) diagrams of the **H**, **C1**, and **C5** dyes (left to right).

3.3.2 Mechanochromic Luminescence on Paper

For ready comparison with previous reports, weighing paper was used as a substrate for visualizing optical phenomena and taking measurements at 77K submerged in liquid N₂.^{1,2} First, it was necessary to determine the optimum annealing temperature for each dye as this can vary on a case-by-case basis.¹ Different temperatures were tested for each dye until a stable maximal blue shift was achieved (Figure S3.1 Appendix B). As with previous systems, 110 °C was sufficient for annealing the **H**, **C1**, and **C12** dyes.^{1-3,13}

However, the **C5**, **C6**, and **C18** dyes required slightly higher temperatures to achieve the same blue-shifted maxima and narrow full widths at half maxima (FWHM). These temperatures were 150 °C for **C5** and **C6** and 120 °C for **C18**. Just as in solution, the **H** dye had the most blue-shifted emission as a film on weighing paper ($\lambda_{em} = 451$ nm). However, emission from this dye is quite dim at room temperature under air even when annealed, suggesting a high degree of quenching. In addition, the **H** dye did not show the typical red-shifting in emission upon smearing the annealed material (Table 3.2, Figure 3.4). The **C1** dye also did not show a red-shift in peak emission, however, it did show a broadening of the FWHM, an increase in intensity of a red-shifted shoulder at ~510 nm, and a decrease in overall emission intensity suggesting the formation of lower energy emitting aggregates.

The **C5**, **C6**, and **C12** dyes show only slight red-shifts in emission after smearing (i.e. only ~10 nm) along with, once again, a broadening of the peaks and a decrease in emission intensity. Carrying the **C1**, **C5**, **C6**, and **C12** dye films through seven cycles of annealing followed by smearing, it was found that the emission intensity was recoverable by re-annealing (Figure S3.2 Appendix B). All of these dyes also show perturbations in their pre-exponential weighted lifetimes (τ_{pw0}) after smearing. The **C18** dye showed ML behavior typical of most other BF₂dbm derived materials, with a more dramatic red-shift upon smearing the annealed material (i.e. ~30 nm), and an increase in both τ_{pw0} and FWHM.^{3,14} The **C18** dye was unique in the set because, instead of the usual decrease in emission intensity, this dye actually showed a slight increase in emission intensity when smeared, suggesting the formation of unique aggregate species (Figure S3.3 Appendix B).

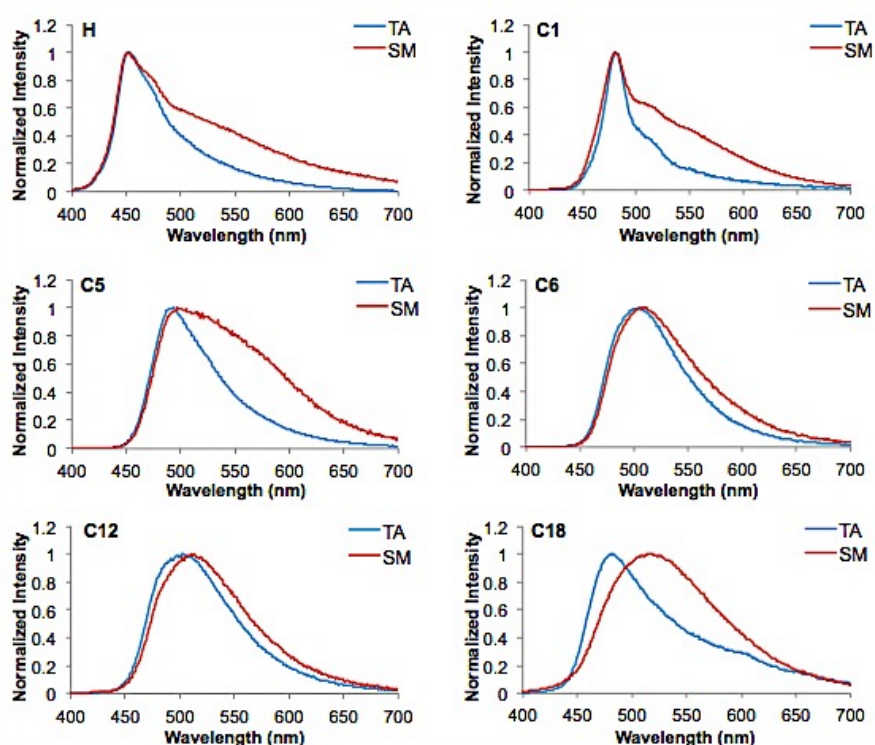


Figure 3.4 Emission spectra of BF₂dbm(I)OR dyes as films on weighing paper in both thermally annealed (TA) and smeared (SM) forms. ($\lambda_{\text{ex}} = 369$ nm; room temperature, air).

In order to observe the effects of mechanical perturbation on triplet emission (i.e. phosphorescence), measurements were performed on the films submerged in liquid N₂. This was necessary because triplet emission of small molecules is often quenched under air either by non-radiative relaxation or collisional quenching with O₂. The **C1**, **C5**, **C6**, and **C12** dyes all showed typical MLQ behavior, manifesting as a decrease in emission intensity at room temperature under air along with an increase in phosphorescence intensity at 77K in liquid N₂ (Figures 3.5 and 3.6).^{1,2} Once again, the **H** dye was unique among the set in that it showed very little mechanical responsiveness; only a slight increase in phosphorescence lifetime and FWHM were observed after smearing the

annealed dye (Table 3.3). Unlike the other dyes, the phosphorescence intensity actually decreased upon smearing. Both this and the decrease in fluorescence emission intensity at room temperature in air are most likely due to the simple removal of dye material caused by smearing.

Table 3.2 Luminescence Properties of Dye Films on Weighing Paper^a

Dye	Thermally Annealed			Smearred		
	λ_{em}^b [nm]	τ_{pw0}^c [ns]	FWHM ^d [nm]	λ_{em} [nm]	τ_{pw0}^c [ns]	FWHM ^d [nm]
BF ₂ dbm(I)R [R=]						
H	451	0.37	74	457	0.83	117
C1	481	0.04	28	480	0.06	68
C5	493	1.05	67	497	0.69	123
C6	504	2.42	78	511	0.45	90
C12	502	1.29	87	513	1.01	95
C18	480	0.16	83	518	0.98	122

^a λ_{ex} = 369 nm; room temperature, air.
^b Emission maximum; fluorescence.
^c Pre-exponential weighted fluorescence lifetime.⁶
^d Full Width at Half Maximum.

As we have asserted before, the MLQ phenomenon is most likely due to a lowering in energy of the S₁ excited state, leading to increased intersystem crossing to the T₁ excited state.^{1,2} However, the extent to which triplet emission is enhanced varies. In order to more easily gauge the extent of phosphorescence enhancement, we have defined a phosphorescence enhancement parameter (I_{SM}/I_{TA}) as the peak intensity of phosphorescence for the smeared sample divided by the peak intensity of phosphorescence for the annealed sample at 77K in liquid N₂. This is displayed in Table 3.4 along with the difference in the fluorescence and phosphorescence peak maxima calculated from the total emission spectra at 77K in liquid N₂ (Figure S3.4 Appendix B).

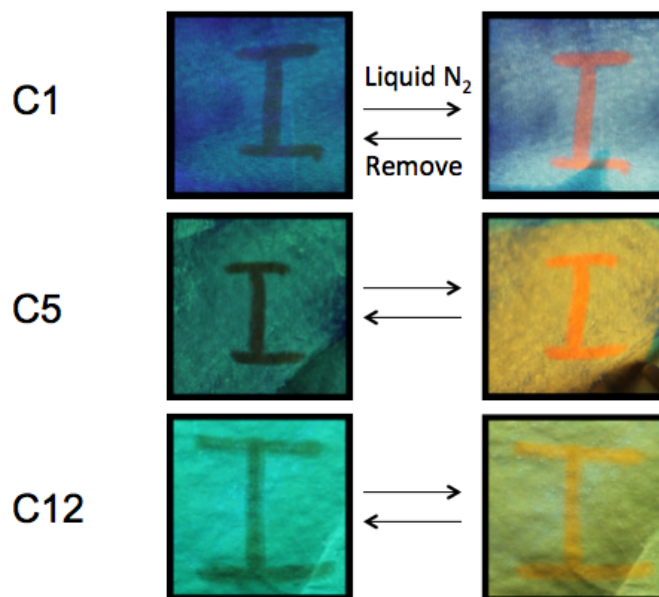


Figure 3.5 Photographs of the MLQ effect using the **C1**, **C5**, and **C12** dyes as examples. Samples were photographed under ambient conditions (left) and then immediately after removal from liquid N_2 (right).

It can be clearly seen that a wider gap between fluorescence and phosphorescence peak emissions corresponds to lower phosphorescence enhancement parameters (Table 3.4). In previous studies we have put forth, and demonstrated compelling evidence for, the idea that the formation of aggregates with lower S_1 excited states in response to mechanical force could enhance phosphorescence by increasing intersystem crossing between the S_1 and T_1 excited states in the presence of a heavy atom.^{1,2} However, in all of these earlier studies, mechanical force only perturbed the S_1 excited state, not the T_1 excited state. As can be seen in Table 3.3 and Figure 3.6, the shorter-chain **C1** and **C5** dyes experience a significant red-shifting of phosphorescence in response to smearing compared to the other dyes bearing alkyl chains. The reason for this is unclear at this time. Furthermore, the **C1** and **C5** dyes have the lowest I_{SM}/I_{TA} values. If the T_1 excited

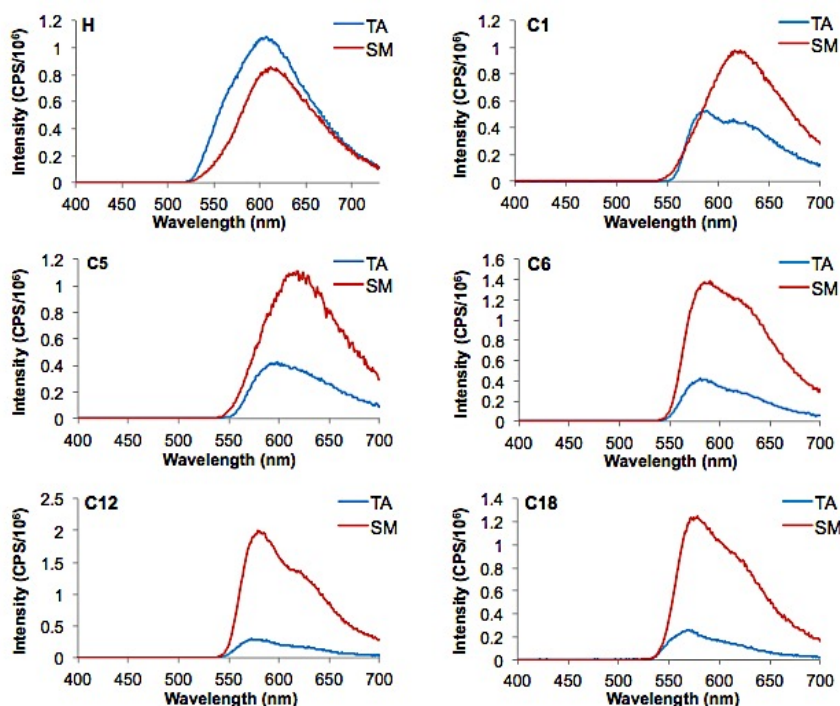


Figure 3.6 Delayed emission spectra of boron dyes on weighing paper in both thermally annealed (TA) and smeared (SM) states ($\lambda_{\text{ex}} = 369 \text{ nm}$; 77K, liquid N_2). The intensities were recorded as photon counts per second (CPS) and shown as $\text{CPS}/10^6$.

Table 3.3 Delayed Emission Properties of Dye Films on Weighing Paper.^a

Dye	Thermally Annealed			Smeared		
	$\lambda_{\text{em}}^{\text{b}}$	$\tau_{\text{pw0}}^{\text{c}}$	FWHM ^d	$\lambda_{\text{em}}^{\text{b}}$	$\tau_{\text{pw0}}^{\text{c}}$	FWHM ^d
[R=]	[nm]	[ms]	[nm]	[nm]	[ms]	[nm]
H	607	0.06	106	611	0.05	95
C1	581	16.6	92	621	9.8	90
C5	598	10.3	89	618	8.6	95
C6	580	11.4	81	590	11.5	95
C12	573	14.4	78	580	35.2	81
C18	567	3.6	72	578	8.2	85

^a $\lambda_{\text{ex}} = 369 \text{ nm}$; 77K, Liquid N_2 .

^b Emission maximum; phosphorescence.

^c Pre-exponential weighted phosphorescence lifetime.⁶

^d Full Width at Half Maximum.

state energy is lowered as well as the S_1 energy upon application of mechanical force, the two states will not be as close to one another as they would be if only the S_1 energy was

lowered. This results in a larger singlet-triplet energy gap, less intersystem-crossing enhancement, and less enhancement of phosphorescence. Therefore, the extent of phosphorescence enhancement after smearing is tunable by the singlet-triplet energy gap after smearing which is tunable by alkyl chain length.

Table 3.4 Triplet-Singlet Energy Gaps and Phosphorescence Enhancement Parameters

Dye BF ₂ dbm(I)R [R=]	T ₁ – S ₁ ^a [nm]	I _{SM} /I _{TA} ^b
H	151	N/A
C1	135	1.84
C5	~83 ^c	2.62
C6	62	3.30
C12	46	6.74
C18	~78 ^c	4.79

^a T₁ – S₁ = Estimated gap between S₁ and T₁ excited states; 77K, Liquid N₂.
^b I_{SM}/I_{TA} = Phosphorescence enhancement parameter; (intensity of phosphorescence when smeared)/(intensity of phosphorescence when annealed); 77K, Liquid N₂.
^c Fluorescence maximum estimated from blue-shifted shoulder in total emission spectrum.

3.3.3 Mechanochromic Luminescence on Glass

Thin films were fabricated by spin-casting dye solutions onto microscope cover glass slides to study substrate effects, spontaneous recovery at room temperature, and solid-state quantum yields. Atomic force microscopy was also used to gauge sample morphology in both TA and SM states. The **C5**, **C6**, **C12**, and **C18** dyes all exhibit ML behavior when the annealed films are smeared (Table 3.5). In fact, the red-shifting is

much more pronounced in these dyes as thinner spin-cast films on glass than it was when the dyes were smeared as thicker films on weighing paper substrates. This could either be a thickness effect, a substrate effect, or a combination of both. For **C5-C18**, the emission wavelengths of the as-spun (AS) films are intermediate to the annealed and smeared states. This suggests that the AS films may be a mixture of both the ordered and amorphous emissive species. Once annealed, these dyes exhibit the typical blue-shifted

Table 3.5 Emission Properties of Spin-Cast Dye Films on Microscope Cover Glass^a

Dye	As-Spun			Thermally Annealed			Smeared		
	λ_{em}^b [nm]	τ_{pw0}^c [ns]	FWHM ^d [nm]	λ_{em}^b [nm]	τ_{pw0}^c [ns]	FWHM ^d [nm]	λ_{em}^b [nm]	τ_{pw0}^c [ns]	FWHM ^d [nm]
BF ₂ dbm(I)R [R=]									
H	561	2.21	127	565	1.66	112	541	1.24	154
C1	481	0.21	34	480	0.04	30	550	1.35	132
C5	549	1.54	132	488	1.34	76	557	1.84	128
C6	527	0.41	120	490	3.25	79	536	1.40	122
C12	513	0.75	107	479	1.44	68	513	0.15	104
C18	484	0.27	69	478	0.11	69	522	0.79	110

^a $\lambda_{ex} = 369$ nm; room temperature, air.
^b Emission maximum; fluorescence.
^c Pre-exponential weighted fluorescence lifetime.⁶
^d Full Width at Half Maximum.

emissions and narrow FWHMs. However, the **C1** dye shows very little change when the AS film is annealed, indicating that this dye has a strong propensity to form the ordered emissive state similar to iodide-free BF₂dbmOMe.³ The **C1** dye also shows a significant red-shift in emission when smeared, unlike its behavior as a film on weighing paper. Once again, this may be attributed to a thickness or substrate effect. The **H** dye showed very little change when the AS film was annealed, only a slight decrease in FWHM. When smeared, the peak emission actually blue-shifted slightly, but this is probably just a

side effect of the broadening FWHM. Overall, the emission of the **H** dye does not seem to change substantially in response to thermal or mechanical processing. Once again, the presence of the donating alkoxy group seems to be necessary to affect significant mechano-responsiveness in this class of dyes.

Solid-state quantum yields were recorded for the dyes in both annealed and smeared states as spin-cast films on glass (Table 3.6). As expected, based upon their MLQ behavior, the **C1-C12** dyes showed a decrease in fluorescence quantum yield upon smearing of the annealed films. The **C6** and **C12** dyes showed the most substantial decreases in fluorescence quantum yield in response to mechanical force (82% and 70% decreases, respectively). The **H** dye showed only a very slight decrease in quantum yield upon smearing, which is consistent with its lesser degree of mechanical responsiveness. A trend of increasing quantum yield of the annealed dyes is observed moving from **H** to **C6**, with **C6** having the highest quantum yield of the set. At **C12** and **C18**, however, the quantum yield diminishes substantially. It seems that, much like in solution, increasing tail length raises quantum efficiency until a threshold is reached, at which point the quantum yield begins to attenuate. Finally, The **C18** dye showed a slight increase in fluorescence quantum yield upon smearing the annealed film consistent with the previously observed increase in intensity of the weighing paper films when smeared. This could possibly explain why the **C18** dye shows a mitigated increase in phosphorescence intensity at low temperature by comparison to **C12**. The process causing this increase in fluorescence quantum yield might diminish the effects of MLQ and low-temperature phosphorescence enhancement.

To measure spontaneous recovery of thin films at room temperature, the films were fabricated, annealed at the appropriate temperature for 10 minutes, smeared, monitored with steady-state fluorescence spectroscopy for one week, and then re-annealed (Figure 3.7 and Figure 3.8). Alkyl chain length had substantial effects on spontaneous recovery as previously reported for other BF₂dbmOR samples.³ The length

Table 3.6 Solid State Luminescence Quantum Yields for Spin-Cast Dye Films on Glass.^a

Dye BF ₂ dbm(I)R [R=]	Thermally Annealed Φ [%]	Smeared Φ [%]
H	1.94 (\pm 0.284)	1.54 (\pm 0.188)
C1	4.44 (\pm 0.180)	1.81 (\pm 0.165)
C5	14.25 (\pm 0.258)	7.09 (\pm 0.197)
C6	22.80 (\pm 0.332)	4.12 (\pm 0.155)
C12	8.10 (\pm 0.405)	2.37 (\pm 0.111)
C18	1.04 (\pm 0.049)	2.15 (\pm 0.067)

^a $\lambda_{\text{ex}} = 369$ nm; room temperature, air.

of the chain had a direct influence on the ability of the dyes to recover the ordered emissive state. Longer chains hindered recovery after smearing. In fact, the **C12** dye did not recover fully with re-annealing after one week. Bulky substituents, such as long alkyl chains, seem to hinder the recovery of the ordered emissive state. The FWHM is relatively narrow for the **C1** dye in the TA state and this dye, by far, shows the most rapid recovery in the set. Therefore, there seems to be a correlation between the degree of order in the annealed state and the recovery ability of the dye after smearing. The **C1** dye also displays very few peak emissions between the smeared and recovered states while the **C5** dye, for example, recovers much more slowly with many intermediate peak emissions. In

studies concerning the reversible ML behavior of BF₂AVB molecular crystals by Reddy *et al.*, it was discovered that the recovery to the ordered emissive state after mechanical perturbation of more rigid forms of the crystals was more facile compared to more elastic forms.¹⁵ In this study, the narrow FWHM and more structured peak observed for the **C1** dye suggests a more ordered, rigid annealed state. Recovery to such a state should happen more quickly than to a less ordered, more elastic annealed state.

Excitation spectra were recorded of the **C1** and **C5** dyes in their TA and SM states as well as several points during the spontaneous recovery of the materials under ambient conditions to see if emissions were arising from distinct ground-state species (Figure S3.6 Appendix B). After smearing the annealed **C1** dye, the excitation peak red-shifts to a new peak and then rapidly recovers the original peak, just like in the emission spectra. On the other hand, the excitation spectra of the annealed **C5** dye exhibits two peaks, a more intense blue-shifted peak and a less intense red-shifted peak. When the film is smeared, the intensity ratio switches in favor of the red-shifted peak and then the intensity of the blue-shifted peak is slowly recovered. Therefore, each peak emission along the recovery path does not represent a distinct ground-state species; rather, the partially recovered spectra represent unique mixtures of ordered and metastable amorphous emissive species. The emission profiles of both the **C6** and **C18** dyes cease recovery at a certain point after which re-annealing is required to recover the ordered emissive state. The materials may become trapped in a local energy minimum. This is probably also true of the **C12** dye. It seems likely that the longer alkyl chains may create a more elastic environment and promote the formation of a much less rigid ordered emissive state than the shorter chains.

This could be a reason why recovery to the ordered emissive states is much slower in the longer-chain dyes.

In previous studies, annealing the AS films of BF₂dbk dyes has caused a change from an amorphous morphology to a much more ordered morphology.^{1-3,14,16,17} This phenomenon also supports why the TA dye films have blue-shifted emissions and narrow FWHMs when compared to the AS films and why these dyes exhibit ML, since the AS films seem to correlate with the SM state.¹⁴ However, as was mentioned before, the alkyl chain length has a significant effect on tendency to form the crystalline TA form, with shorter-chained dyes having a much greater affinity for this state. These variable tendencies toward the ordered emissive state are further demonstrated utilizing AFM imaging (Figure 3.9). The **H**, **C1**, **C5**, and **C18** dyes were chosen as representative examples. The **H** dye exhibits rod-like crystallites in the AS state which, qualitatively, do not appear to change significantly when the film is annealed. This lack of change correlates to the limited stimuli responsiveness of emission of the **H** dye, given that molecular packing controls solid-state emissions. The **C1** dye film is also comprised of rod-like crystallites that show very little change in size or morphology when annealed. Since this dye does exhibit ML, this seems to be indicative of an affinity for the ordered emissive state and could further help to explain why the emission recovers so rapidly after smearing. On the other hand, the **C5** and **C18** dyes, which both show significant changes in emission between the AS and TA states, experienced substantial morphological changes when the AS films were annealed. The **C5** dye exhibited a change from small, rod-like crystallites to larger block-like crystallites when annealed and the morphology of the **C18** dye was, by and large, amorphous in the AS state. When

annealed, a thick patchwork of lamellar crystallites formed, corresponding to the change in emission for these dyes when annealed.

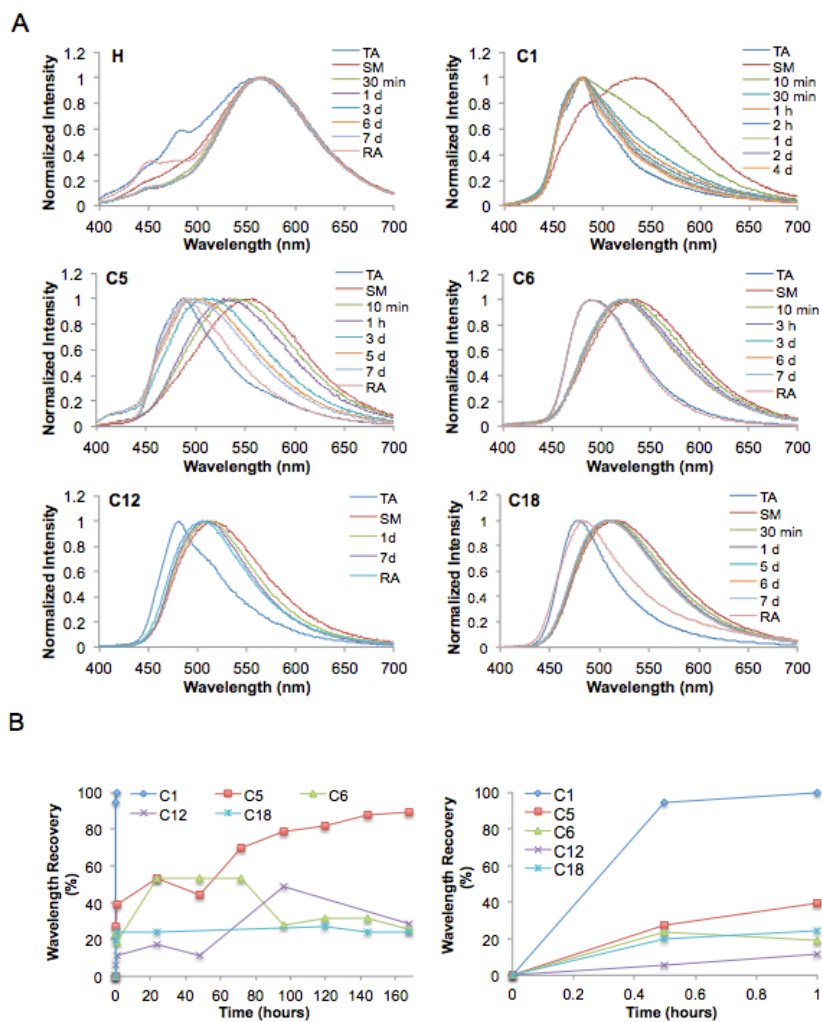


Figure 3.7 A) Emission spectra of boron dyes as spin-cast films on glass ($\lambda_{\text{ex}} = 369$ nm) (room temperature, air). The dyes were thermally annealed (TA), smeared (SM), and then the emission spectra were monitored over time. After one week, the films were re-annealed (RA). Note: min = minutes, d = days. B) Recovery of the **C1-C18** dyes represented as percent recovery of the annealed emission maxima. The graph on the right shows the first hour of recovery for all dyes.

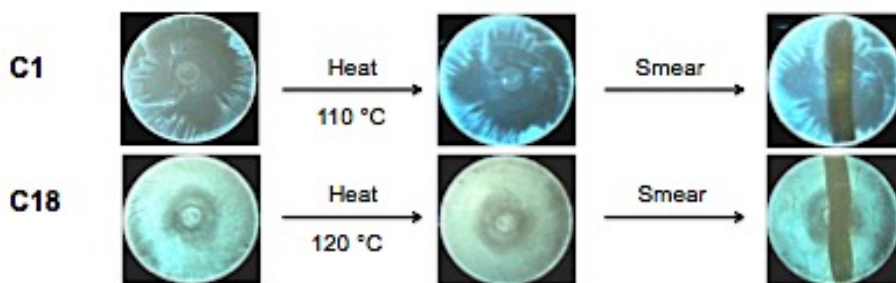


Figure 3.8 Spin-cast films of the **C1** and **C18** dyes going from as-spun (AS) to thermally annealed (TA) to smeared (SM) states (room temperature, air).

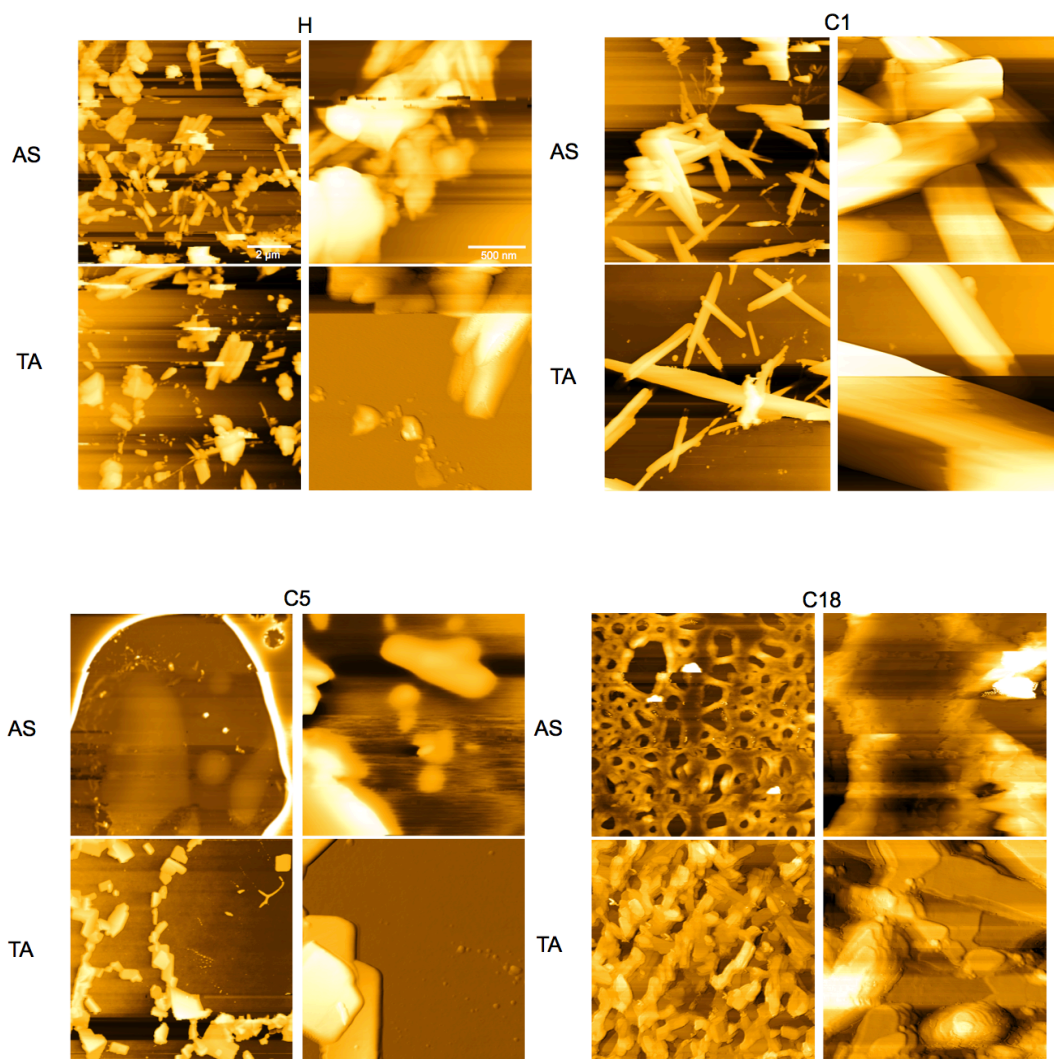


Figure 3.9 AFM images of boron dyes as spin-cast films on glass in both as-spun (AS) and thermally annealed (TA) states. Note: images on the left depict a $10 \times 10 \mu\text{m}^2$ scan area while images on the right depict a $2 \times 2 \mu\text{m}^2$ scan area.

3.3.4 X-ray Diffraction (XRD) of Pristine Powders and Drop-cast Films

X-ray diffraction (XRD) analyses were performed on the dyes as pristine powders and drop-cast films on glass in order to ascertain crystallinity of the samples in various forms (Figure S3.8 Appendix B). Drop-casting was used to fabricate the films because this method produces thicker films than spin-casting, which are more suitable for diffraction. The diffractograms of the pristine powders exhibited many strong peaks, indicating a high degree of crystallinity. In general, the diffractograms of the dye films showed few differences between the as cast (AC) and thermally annealed (TA) states. The AC form may represent a mixture of both ordered and amorphous emissive species that is still at least partly crystalline. All dyes showed a decrease in crystallinity after smearing of the TA film. This manifested as either a decrease in intensity of certain peaks or a diffractogram devoid of peaks. The **C12** dye showed the least change after smearing with only slight decreases in the intensities of a peaks at $\sim 17^\circ$, $\sim 27^\circ$, $\sim 23^\circ$, and $\sim 41^\circ$.

3.3.5 Single Crystal XRD

Crystals suitable for single crystal XRD were grown of the **H** and **C5** dyes by slow evaporation from hexanes/acetone. Crystal growth of the other dyes was attempted using similar methods, but was not successful. The **H** and **C5** crystals exhibited distinct emission properties much like their respective solutions and films on both weighing paper and glass. The **C5** crystals were visibly emissive under UV excitation and appeared green to the eye (506 nm). On the other hand, emission from crystals of the **H** dye was not visible, but fluorescence spectroscopy revealed a broad emission profile with a relatively sharp peak at 479 nm (Figure 3.10).

In addition to differences in emission properties, the **H** and **C5** dye crystals show key differences in crystal packing. Both compounds are highly planar and arrange themselves in offset, J-aggregate type dimer packing (Figures 3.11 and 3.12 A-C). But as can be seen in Figures 3.11 and 3.12 B, the two dyes differ significantly in their dimer π - π stacking. The **H** dye packs with the BF_2 moieties facing in the same direction such that the phenyl ring bearing the iodine substituent is overlapping with the unsubstituted phenyl ring. Conversely, the **C5** dye packs with the BF_2 moieties facing in opposite

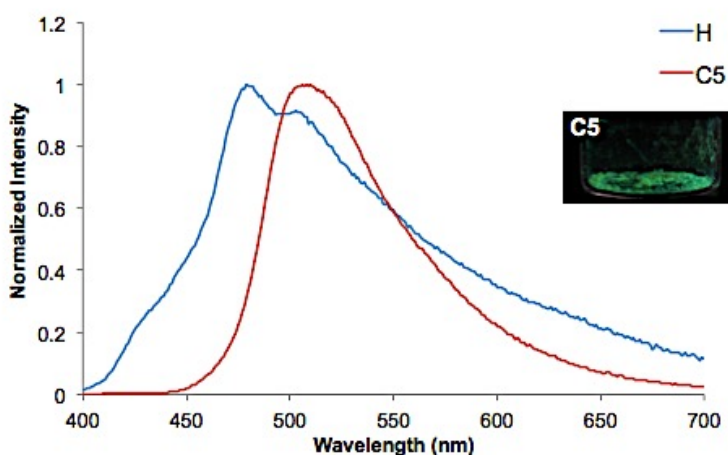


Figure 3.10 Emission spectra ($\lambda_{\text{ex}} = 369$ nm; room temperature, air) of the **C5** and **H** dye crystals used for single crystal XRD analysis under UV light. A photograph of the **C5** crystals under UV light is inset.

directions with the phenyl ring bearing the alkyl chain partially overlapping with both the dioxaborine core of the dye and the chain-bearing phenyl ring of the opposing molecule. This type of stacking with the BF_2 moieties facing in opposite directions is typical for BF_2bdk dyes and, in particular, BF_2bdk dyes known to exhibit ML properties.^{14,15,18-20} With the BF_2 moieties facing in opposite directions, the dye molecules would be free to form the H-aggregates proposed by Zhang *et al.* to be responsible for the red-shifted emission observed upon smearing.¹⁹ However, when the BF_2 moieties are facing in the

same direction, forming the face-to-face H-aggregate would bring the fluorine atoms into direct contact with one-another in a stereoelectronically unfavorable interaction. This may explain why the **C5** dye exhibits strong mechano-responsiveness while the **H** dye does not. This structure is also quite different from what has been reported for the BF₂dbm dye absent I substitution. Mirochnik *et al.* have reported J-aggregate type packing of BF₂dbm with overlap of the phenyl rings and the molecules arranged in an anti-parallel fashion with the BF₂ moieties of adjacent molecules positioned opposite one-another.²¹ BF₂dbm systems with tert-butyl groups and ML display this same anti-parallel arrangement of the BF₂ moieties.^{14,22}

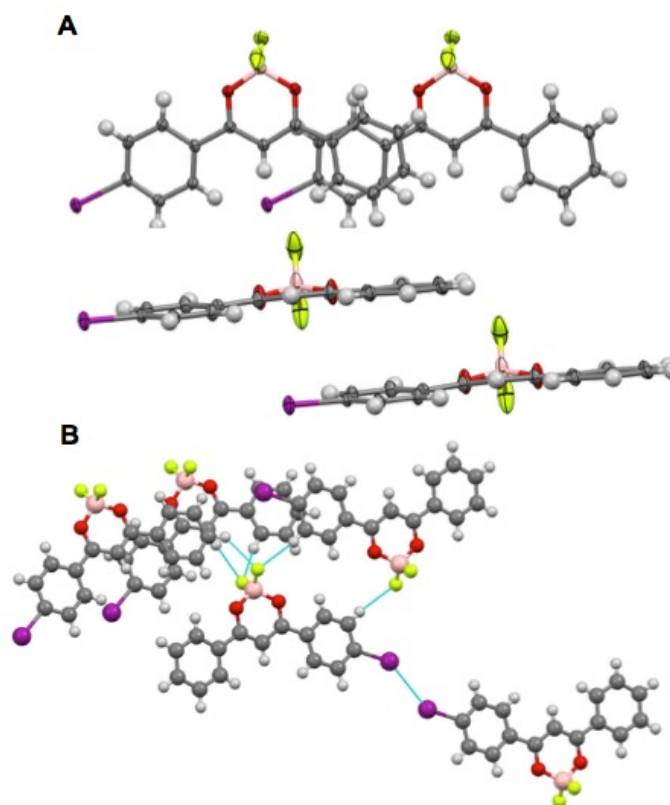


Figure 3.11 Crystal structure and packing of the **H** dye from single crystal XRD analysis. A) Stacked dimer with offset, J-aggregate type π -stacking. The stacking motif overlaps the I-substituted phenyl rings with the non I-substituted phenyl rings. B) View highlighting short atom-atom interactions. Close I-I and F-H interactions are shown.

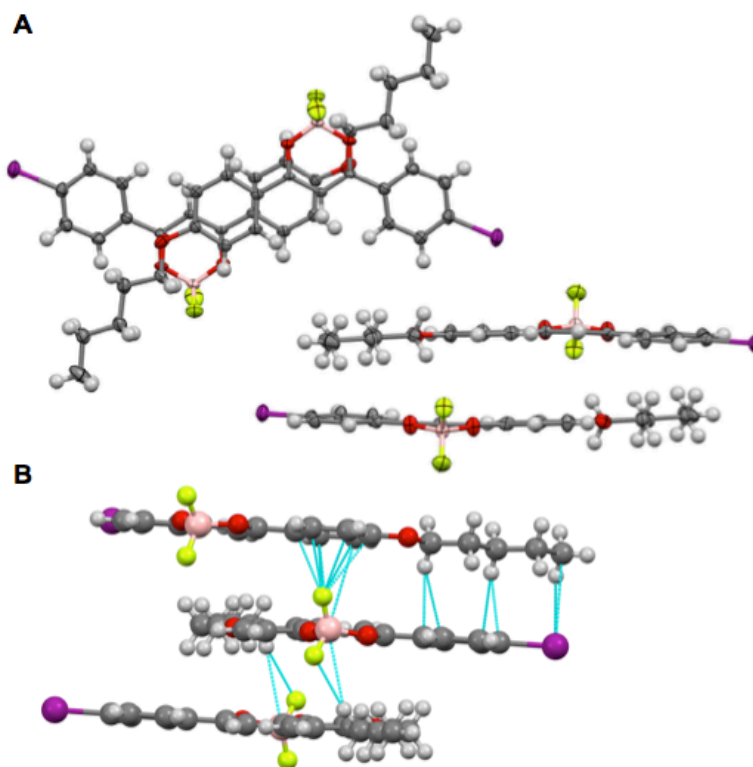


Figure 3.12 Crystal structure and packing of the **C5** dye from single crystal XRD analysis. A) Stacked dimer with offset, J-aggregate type π -stacking. The stacking motif places the alkoxy chain-substituted phenyl C-O-CH₂- over the dioxaborine core α -C=C-O of an adjacent molecule. B) View highlighting short atom-atom interactions. Close F-C, I-H, I-C, F-H, B-H, and B-C interactions are shown.

Figures 3.11C and 3.12C emphasize the short contacts present in the crystal structures. In the **H** dye, short contacts between fluorine and aromatic hydrogen atoms are present as well as a short I-I contact of 3.85 Å (the Van der Waals radius of I-I is 3.96 Å). In comparison, for the **C5** dye, the alkyl chains seem to disrupt short I-I contacts (i.e. contacts within the Van der Waals radius of 3.96 Å), as none are present. There is, however, a unique short F-C contact occurring between the fluorine atoms of the BF₂ moiety and the carbon atoms of the phenyl ring bearing the alkyl chain of an adjacent molecule. The shortest F-C contact is 2.65 Å (the Van der Waals radius of F-C is 3.20 Å). A close F- π contact such as this has been previously reported by Ono *et al.* in the crystal

packing of a difluoroboron perfluorotetracene derivative.²³ The **C5** dye also exhibits intermolecular I-H contacts involving the H atoms of the **C5** tail, F-H and B-H contacts with aromatic H atoms, and close C-H interactions between the C atoms of the iodine-substituted phenyl ring and the H atoms on the alkyl chain of the opposing molecule. There are also B-C interactions between the B atom on one molecule and the phenyl ring bearing the **C5** tail on the other molecule.

The dimer packing of the **H** and **C5** dye crystals may help to explain their differing emissions. Though they are both packed in offset J-aggregate type dimers, the **C5** dye exhibits greater overlap of conjugated π -bonds. When this overlap is maximized in an H-aggregate conformation, emission is much more dramatically red-shifted as demonstrated by Zhang and coworkers,¹⁹ so it stands to reason that greater overlap yields more red-shifted emissions. Mirochnik *et al.* have also demonstrated in crystals of BF₂bdk_s that more efficient π -overlap leads to bathochromic shifts in emission.^{18,21} Finally, the broadness of the emission spectra for both crystals could result from excimer formation.

3.3.6 Differential Scanning Calorimetry of Dye Powders

Differential scanning calorimetry (DSC) analyses were performed on the dyes in pristine powder form in order to gain more insight into their thermal properties. The results of these studies are summarized in Table 3.7 and the thermograms are provided in the ESI (Figure S3.7 Appendix B). As expected, the melting temperatures (T_m) varied as a function of alkyl chain length, with the **H** and **C1** dyes having the highest melting points (~235-250 °C), the **C5** and **C6** dyes having intermediate melting temperatures (~190-200 °C), and the **C12** and **C18** dyes having the lowest melting points (~150 °C).

Crystallization temperatures (T_c) follow a similar trend and fall in the range of ~140-240 °C. The **C12** and **C18** dyes both show broad, lower temperature T_m and T_c transitions in addition to the major peaks. We are unable to determine the exact origin of these transitions other than that they must be inherent to longer-chained dyes and have been observed in other similar studies.^{1,3} We can say with a high degree of certainty that they are not liquid crystal transitions due to their large enthalpy values.²⁴

Table 3.7 Differential scanning calorimetry (DSC) data for pristine dyes.^a

Dye BF ₂ dbm(I)R [R =]	T_m^b (ΔH^c)	T_c^d (ΔH^c)
H	235.48 (268.6)	197.90 (260.6)
C1	251.32 (326.5)	238.51 (306.2)
C5	198.91 (410.9)	182.36 (403.1)
C6	191.51 (345.7)	177.30 (335.5)
C12	151.87 (289.9)	141.91 (266.8)
C18	150.17 (261.8)	144.04 (285.0)

^a All data was taken from the 2nd cycle.
^b Melting point given in °C as the peak of the major endothermic transition.
^c Enthalpy of the transition given in kJ/mol.
^d Crystallization temperature given in °C as the peak of the major exothermic transition.

3.4 Conclusion

In conclusion, the effects of alkyl chain length on ML, MLQ, and phosphorescence enhancement were probed by synthesizing and screening a series of iodine-substituted BF₂dbm dyes. When compared to the **H** dye, dyes bearing alkoxy chains displayed much more impressive optical properties such as high fluorescence quantum yields in solution and ML and MLQ in the solid state. The presence of an alkoxy chain afforded the dyes high quantum yields in solution as well as significant ML

and MLQ behavior as films on both weighing paper and glass. Furthermore, it was found that the length of the chain, itself, had a significant impact on the MLQ and phosphorescence enhancement properties of the dyes. Dyes with shorter chains exhibited smaller phosphorescence enhancement parameters (I_{SM}/I_{TA}) due to a larger gap between the S_1 and T_1 excited states after smearing. This is due to the fact that mechanical perturbation not only lowers the energy of S_1 for dyes bearing shorter chains, but the T_1 energy as well. As spin-cast films on glass, dyes bearing longer alkyl chains recovered more slowly and incompletely after smearing. In general, emission spectra, excitation spectra, and AFM images of spin-cast films suggest that shorter-chain dyes are more crystalline than longer-chain dyes. Powder XRD of drop-cast films revealed changes from crystalline to amorphous states when annealed films were smeared. Single crystal XRD of the **H** and **C5** dyes revealed differences in crystal packing. The alignment of the BF_2 moieties opposite to one-another appears to be key in engineering ML functionality. Also, crystals of the **H** dye revealed unique short I-I contacts while those of the **C5** dye revealed close F- π contacts. Finally, the presence of even/odd effects was probed but no significant impacts on emission properties were identified as the biggest differences were observed for long *versus* short chains. With greater insight into the tunable properties of dyes, systematic design of mechano-responsive materials may be achieved.

3.5 Acknowledgements

Michal Sabat is acknowledged for interpretation and guidance with the single crystal XRD results. Tristan Butler is acknowledged for obtaining the single crystal XRD structures and helping with synthesis. Christopher DeRosa is acknowledged for helping

with synthesis. Professor Carl O. Trindle is acknowledged for helpful discussions and guidance concerning calculations.

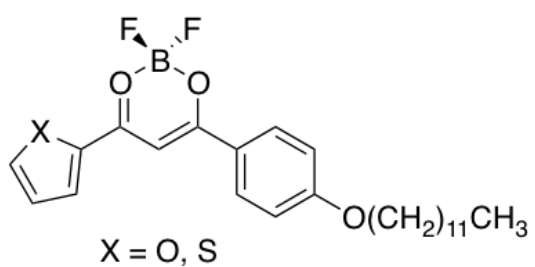
3.6 References

- (1) Morris, W. A.; Liu, T.; Fraser, C. L. *J. Mater. Chem. C* **2015**, 352.
- (2) Zhang, G.; Lu, J.; Fraser, C. L. *Inorg. Chem.* **2010**, 49, 10747.
- (3) Nguyen, N. D.; Zhang, G.; Lu, J.; Sherman, A. E.; Fraser, C. L. *J. Mater. Chem.* **2011**, 21, 8409.
- (4) Hibino, M.; Sumi, A.; Tsuchiya, H.; Hatta, I. *J. Phys. Chem. B* **1998**, 102, 4544.
- (5) Williams, D. B. G.; Lawton, M. *J. Org. Chem.* **2010**, 75, 8351.
- (6) Carraway, E. R.; Demas, J. N.; DeGraff, B. A.; Bacon, J. R. *Anal. Chem.* **1991**, 63, 337.
- (7) Zhu, H.; Wang, X.; Li, Y.; Wang, Z.; Yang, F.; Yang, X. *Chem. Commun.* **2009**, 0, 5118.
- (8) Frisch, M. J.; Trucks, G. W.; Schlegel, H. B.; Scuseria, G. E.; Robb, M. A.; Cheeseman, J. R.; Scalmani, G.; Barone, V.; Mennucci, B.; Petersson, G. A.; Nakatsuji, H.; Caricato, M.; Li, X.; Hratchian, H. P.; Izmaylov, A. F.; Bloino, J.; Zheng, G.; Sonnenberg, J. L.; Hada, M.; Ehara, M.; Toyota, K.; Fukuda, R.; Hasegawa, J.; Ishida, M.; Nakajima, T.; Honda, Y.; Kitao, O.; Nakai, H.; Vreven, T.; Montgomery, J. A.; Peralta, J. E.; Ogliaro, F.; Bearpark, M.; Heyd, J. J.; Brothers, E.; Kudin, K. N.; Staroverov, V. N.; Kobayashi, R.; Normand, J.; Raghavachari, K.; Rendell, A.; Burant, J. C.; Iyengar, S. S.; Tomasi, J.; Cossi, M.; Rega, N.; Millam, J. M.; Klene, M.; Knox, J. E.; Cross, J. B.; Bakken, V.; Adamo, C.; Jaramillo, J.; Gomperts, R.; Stratmann, R. E.; Yazyev, O.; Austin, A. J.; Cammi, R.; Pomelli, C.; Ochterski, J. W.; Martin, R. L.; Morokuma, K.; Zakrzewski, V. G.; Voth, G. A.; Salvador, P.; Dannenberg, J. J.; Dapprich, S.; Daniels, A. D.; Farkas; Foresman, J. B.; Ortiz, J. V.; Cioslowski, J.; Fox, D. J. Wallingford CT, 2009.
- (9) Tomasi, J.; Mennucci, B.; Cammi, R. *Chem. Rev.* **2005**, 105, 2999.
- (10) Samonina-Kosicka, J.; DeRosa, C. A.; Morris, W. A.; Fan, Z.; Fraser, C. L. *Macromolecules* **2014**, 47, 3736.
- (11) Xu, S.; Evans, R. E.; Liu, T.; Zhang, G.; Demas, J. N.; Trindle, C. O.; Fraser, C. L. *Inorg. Chem.* **2013**, 52, 3597.

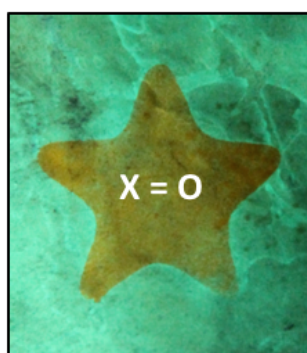
- (12) Sheldrick, G. M. *Bruker AXS, Inc.: Madison, WI* **1997**.
- (13) Zhang, G.; Singer, J. P.; Kooi, S. E.; Evans, R. E.; Thomas, E. L.; Fraser, C. L. *J. Mater. Chem.* **2011**, *21*, 8295.
- (14) Zhang, G.; Lu, J.; Sabat, M.; Fraser, C. L. *J. Am. Chem. Soc.* **2010**, *132*, 2160.
- (15) Krishna, G. R.; Kiran, M. S. R. N.; Fraser, C. L.; Ramamurty, U.; Reddy, C. M. *Adv. Funct. Mater.* **2013**, *23*, 1422.
- (16) Butler, T.; Morris, W. A.; Samonina-Kosicka, J.; Fraser, C. L. *Chem. Commun.* **2015**, *51*, 3359.
- (17) Liu, T.; Chien, A. D.; Lu, J.; Zhang, G.; Fraser, C. L. *J. Mater. Chem.* **2011**, *21*, 8401.
- (18) A.G. Mirochnik, B. V. B., E.V. Fedorenko, and V.E. Karasev *Russ. Chem. Bull.* **2004**, *53*, 291.
- (19) Sun, X.; Zhang, X.; Li, X.; Liu, S.; Zhang, G. *J. Mater. Chem.* **2012**, *22*, 17332.
- (20) Sakai, A.; Ohta, E.; Yoshimoto, Y.; Tanaka, M.; Matsui, Y.; Mizuno, K.; Ikeda, H. *Chem. Eur. J.* **2015**, 18128.
- (21) Mirochnik, A. G.; Bukvetskii, B. V.; Gukhman, E. V.; Zhikhareva, P. A.; Karasev, V. E. *Russ. Chem. Bull.*, *50*, 1612.
- (22) Krishna, G. R.; Devarapalli, R.; Prusty, R.; Liu, T.; Fraser, C. L.; Ramamurty, U.; Reddy, C. M. *IUCrJ* **2015**, *2*.
- (23) Ono, K.; Hashizume, J.; Yamaguchi, H.; Tomura, M.; Nishida, J.-i.; Yamashita, Y. *Org. Lett.* **2009**, *11*, 4326.
- (24) Singh, S. *Phys. Rep.* **2000**, *324*, 107.

Chapter 4

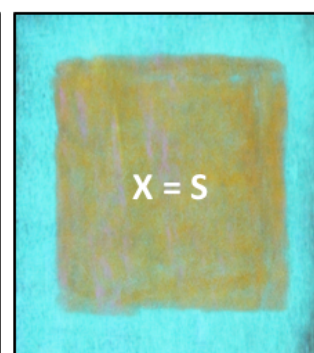
**Mechanochromic and Thermally Responsive Emission Properties of
Furan and Thiophene Substituted Difluoroboron β -Diketonate Complexes with
Short and Long Alkyl Chains**



Thermal Activation



Shear Activation



4.1 Introduction

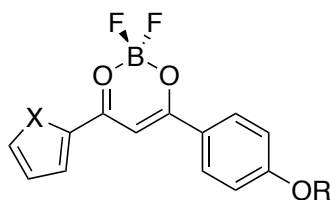
Heteroaromatic systems with impressive optical properties are abundant. As reported by Rasmussen and coworkers, oligothiophene materials have high quantum yields as well as significant solid-state emission.^{1,2} End-capping dithienopyrrole (DTP) oligomers with thienyl groups produced red-shifted absorption and emission maxima in comparison to phenyl end-caps.¹ Yam *et al.* have synthesized a functional material capable of memory storage utilizing a ternary logic state by combining benzothiadiazole and BF₂bdk moieties. This material derives its unique capabilities from charge transfer between the benzothiadiazole and BF₂bdk moieties.³ More recently, Kato and coworkers have demonstrated liquid crystalline materials based on oligothiophenes exhibiting tunable, reversible shear-induced ML.⁴ Oxygen heteroaromatic materials also show responsive behavior. Greco *et al.* have reported reversible temperature dependent emission in solution of furan-containing nucleosides.⁵ Naeem *et al.* have synthesized stimuli-responsive anthracene-benzoxazole (ABO) and anthracene-thiazole (ABT) compounds in which the anthracene acts as an electron donor and the benzoxazole or thiazole moieties act as electron acceptors. The ABO dye exhibited stable ML while the ABT dye recovered mechanically-induced emission changes almost instantly. The differences in behavior were ascribed to the heteroatoms (i.e. oxygen vs sulfur).⁶

Kim and coworkers have recently reported diketopyrrolopyrrole (DPP) derivatives showing mechanical and thermally responsive emissive behavior. They found that the aforementioned properties were also heavily influenced by the length of alkyl chain substituents. In particular, a DPP derivative bearing a C₈H₁₇ chain (DPP8) could access a stable, supercooled liquid state with characteristic low quantum yield red

emission. The reason a C₈H₁₇ chain results in a thermally stable supercooled liquid is thought to be a balancing of aromatic interactions and aliphatic Van Der Waals forces. Once in this state, the material was stable despite subsequent thermal treatment. However, a change to the crystalline, high quantum yield, blue-shifted emissive state could be brought about *via* mechanical shear force creating sufficiently large nucleation sites. They attributed this to an extremely small ΔG between the red emitting, supercooled liquid and the yellow emitting crystalline solid. The C₈H₁₇ substituent afforded this unique functionality while other shorter and longer chains did not. This further demonstrates that the length of an alkyl chain substituent can have substantial effects on thermal properties.⁷

In this study, four compounds were synthesized in order to probe the consequences of replacing one of the aryl moieties in BF₂bdk dyes with either a thiophene or furan heterocycle (Figure 4.1). Based on previous work, we reasoned that thiophene and furan heterocycles might bring about more red-shifted emissions with high quantum yields.¹ In fact, a recent study by Kolpaczynska *et al.* revealed that thiophene-substituted BF₂bdk displayed red-shifted room temperature phosphorescence (RTP) in a polylactic acid (PLA) matrix.⁸ To probe alkyl chain length effects, methoxy and dodecyloxy substituents were attached to the 4-positions of the phenyl rings. The optical properties of the dyes were studied in CH₂Cl₂ solution as well as in the solid state as both films on weighing paper and thinner films on glass substrates. Density Functional Theory (DFT) calculations were performed to model the HOMO and LUMO molecular orbital (MO) diagrams and the absorption spectra in CH₂Cl₂ solution. Specifically, BF₂tbmOMe and BF₂fbmOMe dyes as well as BF₂tbmOC₃H₇ were explored in order to simulate the

effects of chain lengths beyond CH₃ on solution optical properties. As-isolated, pristine powders were studied using differential scanning calorimetry (DSC) to detect thermally induced phase transitions. Powder X-ray diffraction (XRD) analytical techniques were used on both pristine powders and films on glass to gauge the crystallinity of various states. Thermally responsive properties were also investigated.



BF₂tbmOMe: X = S, R = CH₃

BF₂tbmOC12: X = S, R = C₁₂H₂₅

BF₂fbmOMe: X = O, R = CH₃

BF₂fbmOC12: X = O, R = C₁₂H₂₅

Figure 4.1 Chemical structures of thiophene and furan substituted dyes.

4.2 Experimental

4.2.1 Materials

Solvents THF and CH₂Cl₂ were dried over 3 Å molecular sieves activated at 300 °C as previously described.⁹ Reactions were monitored using silica TLC plates. Compounds purchased from Sigma-Aldrich were reagent grade and used without further purification. Methyl 4-dodecyloxybenzoate¹⁰ and thiophene-substituted dyes⁸ were synthesized by a previously reported method. Additional synthetic details are provided in the electronic supporting information (ESI).

4.2.2 Methods

¹H NMR (600 MHz) spectra were recorded in dilute CDCl₃ solvent using a Varian VRMS/600 instrument. Spectra were referenced to the signals for residual protio-

CDCl_3 at 7.26 ppm and coupling constants were reported in Hz. Mass spectra were recorded using a Micromass Q-TOF Ultima spectrometer using electrospray ionization (ESI) MS techniques. UV-vis spectra were collected on a Hewlett-Packard 8452A diode-array spectrophotometer. Steady-state fluorescence emission spectra were obtained on a Horiba Fluorolog-3 Model FL3-22 spectrofluorometer (double-grating excitation and double-grating emission monochromator). Time-correlated single-photon counting (TCSPC) fluorescence lifetime measurements were performed with a NanoLED-370 ($\lambda_{\text{ex}} = 369 \text{ nm}$) excitation source and a DataStation Hub as the SPC controller. Lifetime data were analyzed with DataStation v2.4 software from Horiba Jobin Yvon. Fluorescence quantum yields, Φ_{F} , in CH_2Cl_2 were calculated *versus* a dilute anthracene solution in ethanol as a standard using a previously described method¹¹ and the following values: Φ_{F} anthracene in ethanol = 0.27¹², n_{D} ²⁰ ethanol = 1.36, n_{D} ²⁰ CH_2Cl_2 = 1.424. Optically dilute CH_2Cl_2 solutions of all samples were prepared in 1 cm path length quartz cuvettes with absorbances <0.1 (a.u.). Powder XRD patterns were obtained using a Panalytical X'Pert Pro MPD diffractometer operating at 40kV and 40ma using Cu $\text{K}\alpha$ radiation. DSC was performed on the pristine powders using a TA Instruments DSC 2920 Modulated DSC and data were analyzed using the Universal Analysis software V 2.3 from TA Instruments. Thermograms were recorded using the standard mode and temperature ramp rates of 5 °C/min or 10 °C/min. A conditioning cycle followed by a second heating/cooling cycle was measured for each sample.

Films on weighing paper were created by smearing a small amount of dye onto 5 x 5 cm^2 pieces of weighing paper with nitrile examination gloves. The samples were weighed to ensure a dye mass of ~1-3.5 mg spread out over the entire 5 x 5 cm^2 area. A

Laurel Technologies WS-650S spin-coater was used to make the spin-cast films. The films were fabricated by preparing 10^{-2} M solutions of the dyes and applying ~ 5 drops of these solutions to circular microscope cover glass slides 25 mm in diameter rotating at 3000 rpm. The films were dried *in vacuo* for 15 min before further processing. Thin films for XRD analysis of BF₂fbmOC12 were fabricated by adding 10 drops of a saturated toluene solution to 18 x 18 mm² square microscope cover glass slides and evaporating the solvent in air, yielding films in the green phase. Orange films were produced by heating green BF₂fbmOC12 films above the melting point with a heat gun (i.e. holding the heat source ~ 3 cm from the film for ~ 1 s) followed by rapid cooling in air at room temperature. Drop-cast films of BF₂tbmOC12 were prepared by applying ~ 20 drops of a 10^{-2} M solution to circular microscope cover glass slides 25 mm in diameter. The films were allowed to dry under ambient conditions and then further dried *in vacuo* for 15 min prior to performing measurements.

4.3 Results and Discussion

4.3.1 Optical Properties in Solution

All thiophene and furan compounds showed very similar absorptions and emissions in CH₂Cl₂ solution with peak emissions (λ_{em}) in the range of 437-445 nm and absorbance maxima (λ_{abs}) in the range of 413-418 nm (Table 4.1). Little variation in λ_{abs} , λ_{em} , and fluorescence lifetime (τ_F) was observed despite the difference in alkyl chain length and heteroatom substitution (Table 4.1, Figure S4.1 Appendix C). This is typical for this class of dyes.¹³

Density functional theory (DFT) was used to model the molecular orbital (MO) diagrams and the absorption spectra in CH₂Cl₂ solution of BF₂tbmOMe and BF₂fbmOMe

as well as a compound bearing a C₃H₇ chain (BF₂tbmOC3) to simulate alkyl chain lengths beyond three carbons (Figure 4.2, Table S4.4, Table S4.5 Appendix C). The computed absorption spectra reveal the strongest transitions to be from the highest occupied molecular orbital (HOMO) to the lowest unoccupied molecular orbital (LUMO) for all three dyes. Furthermore, these transitions are predominantly π - π^* in character, as expected from the experimental data. In the past, the solution properties of BF₂bdks have proven to be relatively insensitive to alkyl chain length,¹³ consistent with the fact that amplitude in the HOMOs and LUMOs does not extend past the first carbon in the alkyl chain. With the exception of BF₂tbmOC12 ($\Phi_F = 0.71$), all other derivatives showed modest fluorescent quantum yields (Φ_F) ranging from $\Phi_F = 0.35$ for BF₂fbmOMe, to $\Phi_F = 0.48$ for BF₂fbmOC12.

A trend can be established based on alkyl chain length, as C₁₂H₂₅ derivatives possess higher Φ_F relative to their methoxy-substituted counterparts. An increase in Φ_F when going from methoxy to dodecyloxy chains has been previously observed for BF₂dibenzoylmethane (BF₂dbm) derivatives.¹³

Table 4.1 Optical Properties of Heterocycle-Substituted BF₂bdk_s in CH₂Cl₂.

Dye	$\lambda_{\text{abs}}^{\text{a}}$ (nm)	ϵ^{b} (M ⁻¹ cm ⁻¹)	$\lambda_{\text{em}}^{\text{c}}$ (nm)	$\tau_{\text{F}}^{\text{d}}$ (ns)	$\Phi_{\text{F}}^{\text{e}}$
BF ₂ tbmOMe	417	56,000	445	2.06	0.38
BF ₂ tbmOC12	418	62,000	441	2.08	0.71
BF ₂ fbmOMe	413	28,000	437	1.93	0.35
BF ₂ fbmOC12	415	65,000	439	1.92	0.48

^aAbsorption maxima.

^bExtinction coefficients calculated at the absorption maxima.

^cFluorescence emission maxima excited at 369 nm (except **1** excited at 350 nm).

^dFluorescence lifetime excited with a 369 nm light-emitting diode (LED) monitored at the emission maximum. All fluorescence lifetimes are fitted to single-exponential decay.

^eRelative quantum yield, with anthracene in EtOH as a standard.

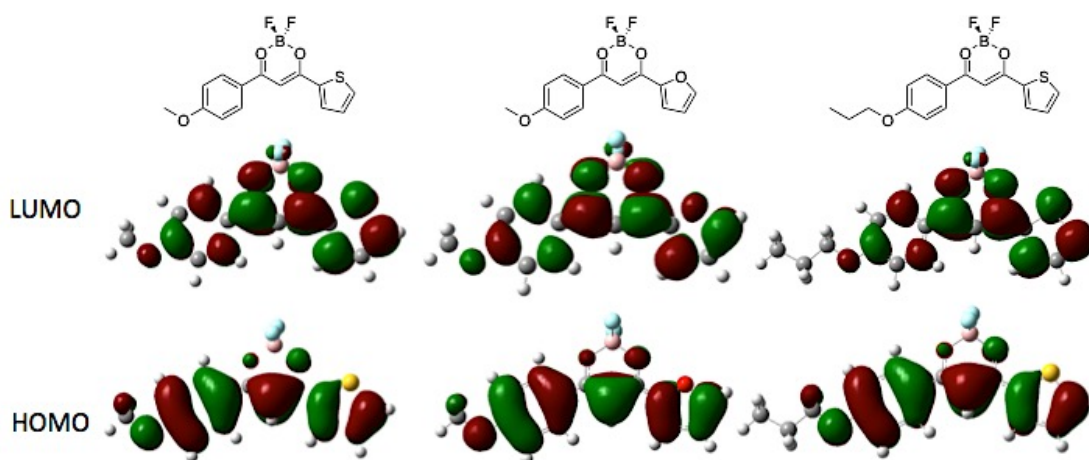


Figure 4.2 Molecular orbital (MO) diagrams of BF₂tbmOMe and BF₂fbmOMe as well as BF₂tbmOC₃H₇ to simulate longer chains. Their respective highest occupied molecular orbitals (HOMO) and lowest unoccupied molecular orbitals (LUMO) are displayed.

4.3.2 Pristine Powders

The emission of dye pristine powders were measured under ambient conditions (Table S4.1 Appendix C, Figure 4.3). The OMe derivatives BF₂tbmOMe and BF₂fbmOMe show very similar broad, red-shifted emission; whereas, the C₁₂H₂₅

derivatives show quite different emission spectra. A single short wavelength emission profile was observed for BF₂tbmOC12, while BF₂fbmOC12 showed a weak, structured, blue-shifted peak similar to the thiophene-substituted counterpart as well as a much more intense, broad, red-shifted peak. Excitation spectra were monitored at the λ_{max} for the blue-shifted and red-shifted transitions. Both excitation spectra were nearly identical from 300-480 nm, suggesting that the two peaks arise from the same ground-state species. This may indicate that the orange emission is due to excimer formation, or energy transfer to other lower energy emitting species in the excited state.¹⁴

These results indicate that the identity of the heteroatom (i.e. S or O) has very little effect on the emission wavelength of pristine powders and that the dominant factor in determining the emission color is the alkyl chain length. The blue-shifted emission observed in C₁₂H₂₅ powders has been previously ascribed to the steric hindrance of the C₁₂H₂₅ chain limiting dye-dye interactions that red shift emission.¹³ In methoxy-substituted analogues, dye-dye interactions such as π -stacking and longer range effects that would red shift emission are more probable since the β -diketonate cores are closer together, undiluted by packed alkyl chain domains.^{13,15} This result is analogous to a study performed by Nguyen *et al.* wherein BF₂dbm derivatives with long alkoxy chains exhibited more blue-shifted solid-state emissions compared to shorter chain derivatives.¹³

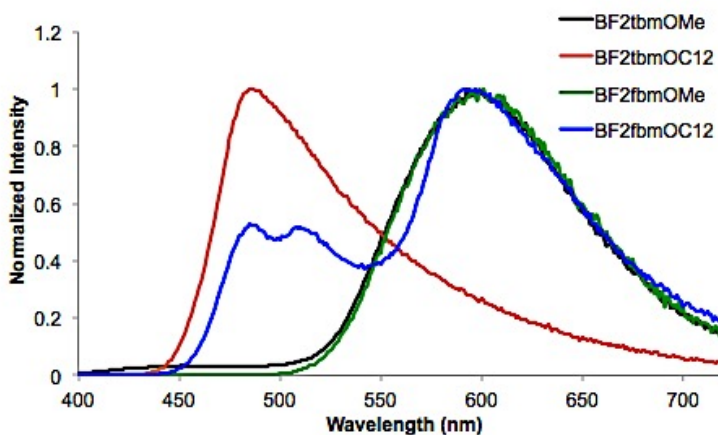


Figure 4.3 Emission spectra of pristine powders ($\lambda_{\text{ex}} = 369$).

4.3.3 Thermally Responsive Emission

In the process of testing these dyes for ML properties, it was discovered that the long chain furan dye BF₂fbmOC12 exhibited highly controllable and reversible changes in emission in response to different methods of heating while the thiophene dye BF₂tbmOC12 did not show this same behavior. The emission spectrum of the melted BF₂fbmOC12 powder was also obtained. The melted phase of BF₂fbmOC12 was accessed by heating the pristine powder above the melting point until melted (~5 seconds) then rapidly removing the heat source and cooling in an ice bath. The resultant melt-quenched material appeared orange to the eye and the emission spectrum showed only a single broad peak at 581 nm corresponding to the red-shifted peak in the spectrum of the dye as a pristine powder (Figure 4.3).

Although, this property could be observed for powders, the effect was much more accessible and reversible with films of the material. When the dye was initially smeared into a film on weighing paper and subjected to UV illumination, it was evident that the film represented a heterogeneous mixture of emissive states, one being blue-shifted (λ_{em}

= ~ 470 nm), and the other being red-shifted ($\lambda_{em} = 587$ nm) and this was corroborated by an emission spectrum of the as-smear (ASM) dye. If the film was gently heated for five seconds (e.g. with a heat gun from approximately one foot away), a homogenous film with green emission ($\lambda_{em} = 519$ nm) could be obtained. Heating for one minute in an oven at 125 °C (just below the melting point of 127 °C) produced the same results. The orange emissive state, on the other hand, was accessible *via* a different method of thermal processing, namely melt quenching. Intense heat sufficient to melt the film was applied (e.g. with a heat gun by holding the heat source approximately one inch from the film). When the heat source was removed rapidly and the film cooled quickly in the air, a homogenous, orange emitting film ($\lambda_{em} = 575$ nm) was obtained. This state is not achieved if the dye is allowed to cool slowly on a heat conductive surface, such as a laboratory bench top. Instead, under these circumstances, the warm surface provides the gentle heating necessary to access the green emissive state. The orange emissive state was also obtained by submersion of the hot film in liquid N_2 which provided sufficiently rapid cooling. Regardless of how the orange state was achieved, the transformation between orange and green emissive states was found to be completely reversible. By cycling back and forth between gentle heating and melt quenching in air, the dye could be carried through seven cycles with no deterioration in responsiveness. Given that a furan functional group is present in this dye, the heat-induced transition could be due to a Diels-Alder cycloaddition.¹⁶ To test this possibility, material from both the orange and green forms were re-dissolved and subjected to UV-Vis (Figure S4.3 Appendix C) and 1H NMR spectral analysis. These analyses suggested that the green and orange-emitting chemical species are of identical chemical composition, inconsistent with formation of a

Diels Alder adduct in one and not the other. Therefore, data are consistent with a thermally induced physical change, not a chemical change.

Like other BF₂bdk dye materials, the relatively blue-shifted BF₂fbmOC12 dye film may represent a thermodynamically stable, ordered emissive state while the more red-shifted film represents a kinetically accessible, metastable, amorphous emissive state. In addition, lifetimes were recorded for films in both orange and green states (Table S4.2 Appendix C). The orange form had a significantly longer τ_{pw0} (7.61 ns) when compared to the green form (τ_{pw0} = 0.80 ns). This behavior is very similar to other BF₂bdk materials exhibiting ML,^{10,17-19} only this time the amorphous, metastable emissive state is accessible *via* heat instead of mechanical perturbation.

Through experimentation, we were able to discover an immediate potential use of this dye for thermal printing.²⁰ By heating a metal object, applying it to the annealed green dye film, removing it and then quickly cooling by submersion in liquid N₂, clear images could be printed (Figure 4.4). Since this transformation is reversible, the process can be repeated many times on a single film. Alternative substrates for thermal printing are desirable because many papers currently used contain bisphenol A (BPA), which is potentially hazardous to human health.²¹ In terms of industrial applications, this material could be used in any process that requires heating to high temperature followed by rapid cooling. Such an example of a potential application could be in the frozen food industry, where many products need to be cooked and then frozen quickly to avoid the formation of large ice crystals, which can damage the product.²² If the dye film were encapsulated in a clear, heat-conductive container attached to the product, it could be used as a quick, easy indicator of quality control.

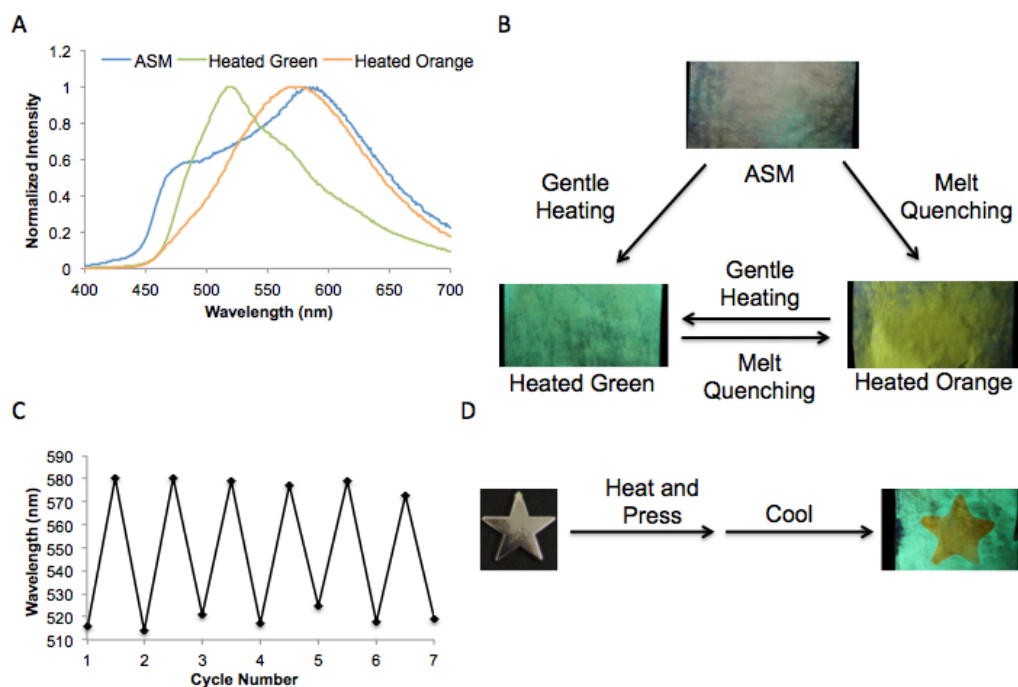


Figure 4.4 Demonstration of the thermally responsive emission for BF₂fbmOC12: A) Spectra of the dye film in the as-smear (ASM), heated green, and heated orange states. B) Photographs of the dye film in all three states. C) Reversibility of the thermally responsive emissive behavior through seven gentle heating and melt quenching cycles. D) Thermal printing. A metal star was heated, pressed onto the green film for ~1 second then removed. The film was then quickly submerged in liquid N₂ to achieve the image.

Interestingly, the BF₂fbmOC12 dye did not exhibit the same thermally responsive, reversible changes in emission properties as a spin-cast film on glass. The AS film was found to have red emission ($\lambda_{em} = 597$ nm) with a long τ_{pw0} under UV illumination (Figure 4.5, Table S4.2 Appendix C). Whether the film was gently heated with a heat gun or annealed in an oven, only a red, long-lifetime emission remained and the green emissive state could not be obtained. Therefore, it appears that spin casting locks this dye into a red-shifted emissive state. This is likely a processing or thickness effect that, at this time, we are unable to explain. However, it was possible to fabricate thermally responsive films of the BF₂fbmOC12 dye on glass by drop-casting from a saturated toluene solution.

Slow evaporation yielded a glass film of BF₂fbmOC12 in the green phase ($\lambda_{em} = 512$ nm) and the orange phase ($\lambda_{em} = 551$ nm) was produced through the melting and room temperature cooling of the green thin films using a heat gun in the same way as the films on weighing paper (Figure 4.5).

Curiously, the C₁₂H₂₅ derivative of the furan-substituted dye exhibited stimuli responsive solid-state emission while the methoxy-substituted counterpart did not have this property. A previous study has shown that incorporation of an alkoxy chain longer than OCH₃ into difluoroboron dibenzoylmethane (dbm) fluorophores can grant ML properties.¹³ Perhaps the ability of the alkoxy chains to break up closer intermolecular π - π interactions creates a greater variety of available states that may be accessed through different processing methods. In this example and others,²³⁻²⁵ the addition of long alkoxy

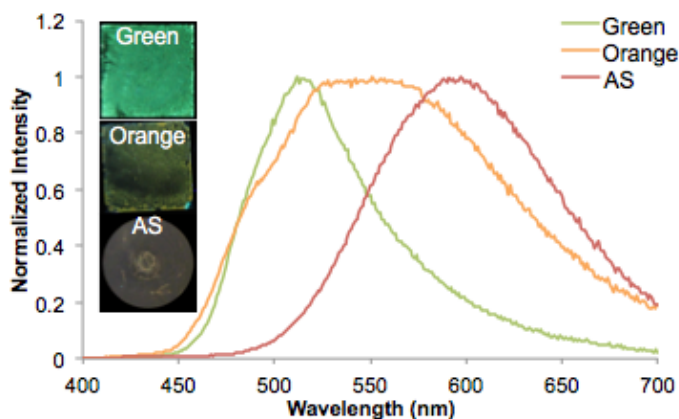


Figure 4.5 Emission of BF₂fbmOC12 as films on glass. Drop-cast films on glass from toluene solutions in both green and orange forms are compared to a spin-cast film from CH₂Cl₂ solution (AS = as spun).

chain substituents to solid-state emitting fluorophores is an effective strategy for imparting switchable luminescence behavior. Both Yang *et al.*²⁵ and Xu *et al.*²⁴ have both reported organic molecules with mechanically switchable emissive behavior in the solid

state brought about by the addition of long aliphatic chains. They proposed, with emission and x-ray diffraction data, that the alkyl chains disrupt close supramolecular interactions such as π - π stacking. They believe this balancing of π - π and aliphatic interactions can create multiple emissive states and thus impart switchable emissive behavior.²⁴

4.3.4 Differential Scanning Calorimetry

The dyes BF₂tbmOC12 and BF₂fbmOC12 show thermally responsive emission whereas their methoxy-substituted counterparts do not. The differences between these samples and the nature of the thermally accessible green and orange states of BF₂fbmOC12 were investigated using differential scanning calorimetry (DSC). Samples were heated above their melting points and cooled to 0 °C at a constant ramp rate (5 °C/min or 10 °C/min).

The thermal properties were reported using thermograms of the second heating/cooling cycle of each compound (Table 4.2, Figure S4.4 Appendix C). The melting points of methoxy-substituted BF₂tbmOMe (265.9 °C) and BF₂fbmOMe (216.5 °C) were higher compared to their alkoxyated counterparts BF₂tbmOC12 (137.0 °C) and BF₂fbmOC12 (127.7 °C). The lower melting points observed in C₁₂H₂₅ samples is further evidence that the alkoxy chains are capable of disrupting stronger intermolecular interactions. In general, thiophene dyes had slightly higher melting points than furan dyes, but the alkoxy chain length, by far, had the greatest effect on melting temperature. In order to investigate transformations in BF₂fbmOC12 brought about by heat, the DSC thermograms of the first heating cycle of both the green and orange powders with a constant ramp rate (10 °C /min) were compared (Figure 4.9). Because BF₂tbmOC12 does

not respond to heat in the same way as BF₂fbmOC12, only the thermal properties of BF₂fbmOC12 were studied in depth. When the green form of BF₂fbmOC12 was heated, only the melting point was observed at 127 °C, but an additional crystallization peak at 56.2 °C was observed when the orange form was heated. Chujo and coworkers have reported similar behavior for powders of difluoroboron β-diiminates in crystalline and amorphous emissive forms.²⁶ This is further evidence that the orange form represents an amorphous, metastable state while the green form represents a thermodynamically stable, crystalline state.

However, one question remains. Why does the furan-substituted derivative exhibit this thermally responsive switchable behavior while the thiophene-substituted dye does not? The answer may be found in comparing π-stacking energies and intermolecular interactions. According to a computational study performed by Huber *et al.*, furan forms

Table 4.2 Differential Scanning Calorimetry (DSC) Data for Pristine Dyes.^a

Dye	T _m ^b (°C)	ΔH ^c (kJ/mol)	T _c ^b (°C)	ΔH ^c (kJ/mol)
BF ₂ tbmOMe	265.9	65.0	197.2	61.3
BF ₂ tbmOC12	137.0	505.7	111.8	515.6
BF ₂ fbmOMe	216.5	142.3	163.0	101.1
BF ₂ fbmOC12	127.7	526.2	103.4	520.9

^a All data was taken from the 2nd cycle.

^b Melting point given in °C as the peak of the major endothermic transition.

^c Enthalpy of the transition given in kJ/mol.

^d Crystallization point given in °C as the peak of the major exothermic transition.

a slightly closer and stronger π-stacking interaction with benzene than thiophene due to the smaller size of the oxygen atom compared to sulfur.²⁷ Furthermore, it stands to reason that the stronger hydrogen bonding affinity afforded by the oxygen atom could also contribute to closer interactions between molecules. If the furan-substituted dye

molecules interact with each other strongly in the H-aggregates present in the amorphous form,¹⁹ a larger energy barrier would have to be overcome to switch from the amorphous to the crystalline emissive form. This could explain why the films and powders of BF₂fbmOC12 become trapped in the amorphous phase when their melts are rapidly quenched. The answer could also lie in the favorability of the ordered emissive state over the amorphous state for the BF₂tbmOC12 dye. The pristine powder of this dye showed preference for the ordered emissive, blue state and could not be easily converted to the amorphous phase like its furan counterpart. Also the melting point of the BF₂tbmOC12 dye pristine powder (always in the blue form) is higher than that of the furan dye, suggesting a greater degree of stability.

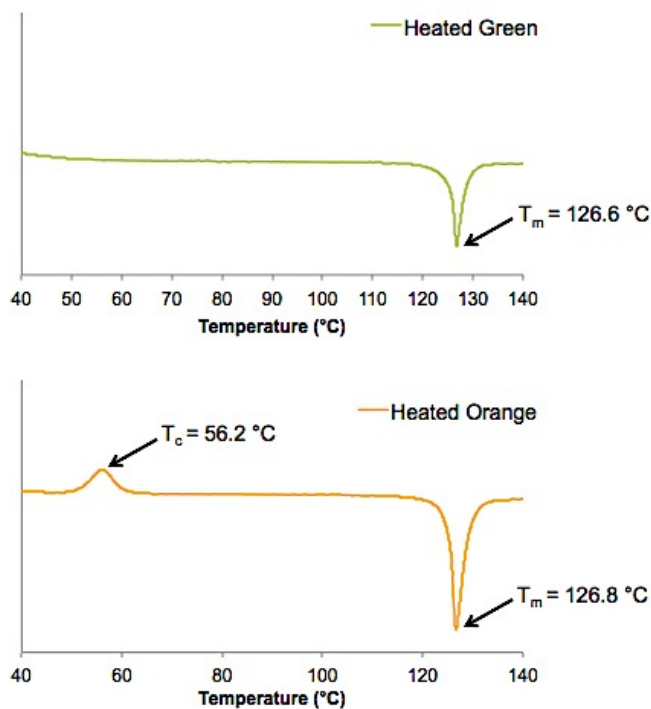


Figure 4.9 DSC thermograms of the first heating cycles of BF₂fbmOC12 powder in both heated green (top) and heated orange (bottom) forms.

4.3.5 Mechanochromic Luminescence

Although BF₂fbmOC12 showed excellent responsiveness to heating, this dye and both methoxy-substituted dyes did not exhibit the ML properties typical for many BF₂bdk. ^{13,18,28} However, BF₂tbmOC12 did possess ML properties. While BF₂bdk exhibit a degree of mechano-responsiveness as bulk powders that can be activated by prolonged grinding, this property is greatly amplified when the dye materials are fabricated as films. ^{10,13,18,28,29} Therefore the dye was fabricated into both thin films on glass substrates and thicker films on weighing paper substrates. When the BF₂tbmOC12 dye weighing paper film is annealed for ten minutes at 130 °C (below the melting temperature of 137 °C), it exhibits blue emission and the spectrum reveals a relatively narrow peak (485 nm) (Figure 4.6). When the thermally annealed (TA) film is smeared with a cotton swab, the emission changes to yellow and the spectrum reveals a much broader red-shifted peak (562 nm). This 77 nm shift in emission after smearing represents a high contrast ML material. Furthermore, the ML property is highly reversible. A process of annealing a film at 130 °C for a minute and then smearing was repeated seven times without any noticeable decline in responsiveness. This excellent reversibility could make this dye useful in many applications in which force responsiveness is required.

To test for thickness and substrate effects, spin-cast films of BF₂tbmOC12 on glass were also fabricated. Immediately after spin-casting, it could be seen that the as-spun (AS) state was unique and unlike what was observed for the both the TA and SM states on weighing paper substrate (Figure 4.7). The AS form seems to represent a combination of the blue and red emissive states, similar to other BF₂bdk dye films exhibiting ML, but here there is a large gap in the peak emissions of the TA and SM

forms.²⁸ Lifetime measurements were also performed on spin-cast films in all three forms (Table S4.2 Appendix C). As is typical for BF₂bdk dyes, the red-shifted, SM emission had a much longer lifetime ($\tau_{\text{pw0}} = 12.12$ ns) than the TA emission ($\tau_{\text{pw0}} = 7.03$ ns). This, along with the broadening of the peak upon smearing, suggests the formation of excimeric or unique ground-state species.^{19,28,29}

Just as with furan derivatives, the thiophene dye substituted with OC₁₂H₂₅ exhibited switchable emissions in the solid state while its methoxy-substituted counterpart did not. This is presumably due to the disruption of close supramolecular interactions.

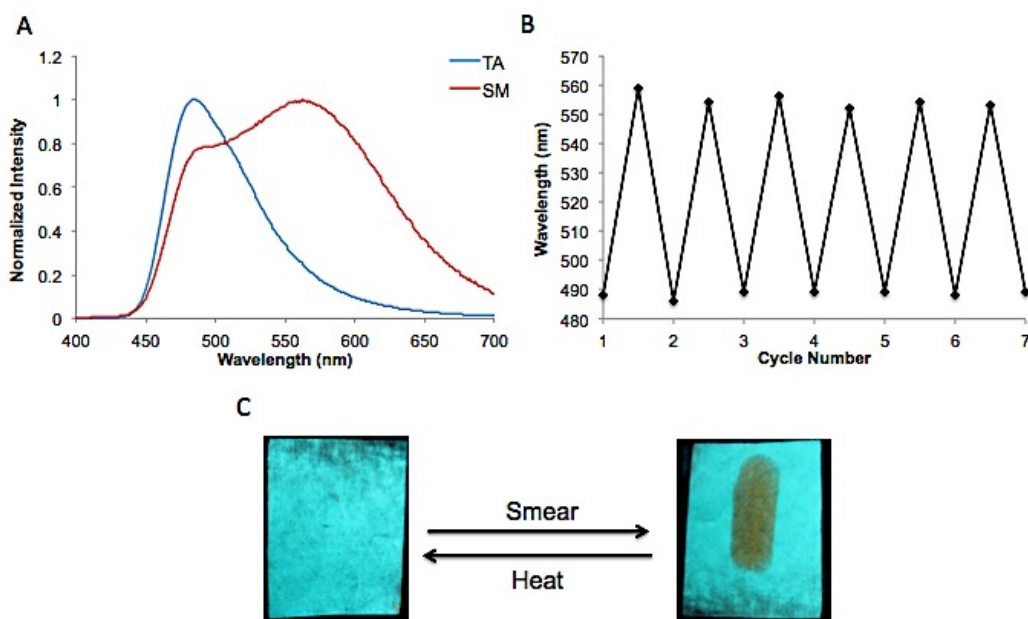


Figure 4.6 Mechanochromic luminescence of BF₂tbmOC12 on weighing paper: A) Emission spectra in thermally annealed (TA) and smeared (SM) states. B) Reversibility of the ML through annealing and smearing cycles. C) Photographs of films after thermal annealing (left) and smearing (right).

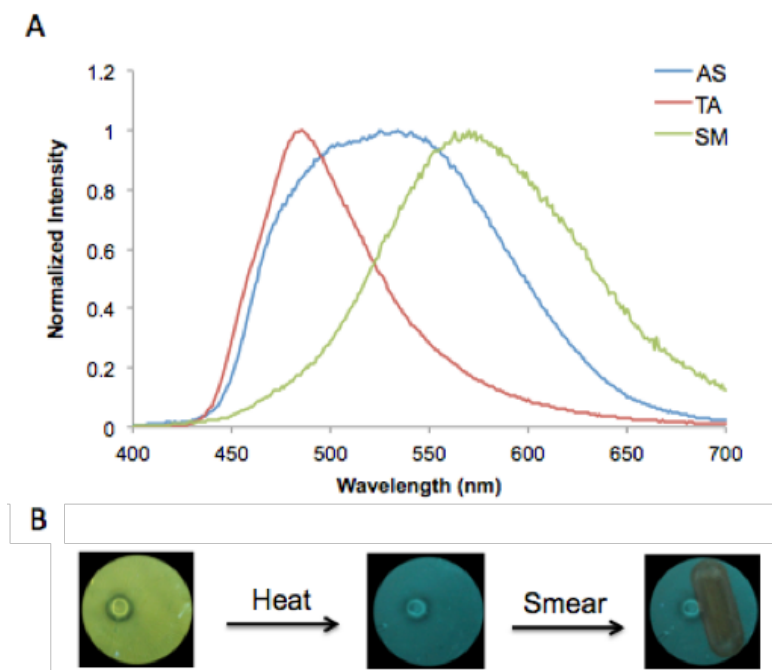


Figure 4.7 Mechanochromic luminescence of BF₂tbmOC12 as spin-cast films on glass. A) Emission spectra of the dye film in the as-spun (AS), thermally annealed (TA), and smeared (SM) states. B) Photographs of a film in AS, TA and SM states.

4.3.6 X-ray Diffraction of Films

X-ray diffraction (XRD) diffractograms were obtained for pristine powders of the BF₂tbmOC12 and BF₂fbmOC12 dyes and compared to those of the drop cast films on microscope cover glass in various forms in order to glean information about the amorphous *versus* crystalline states of these dyes (Figure 4.8). Drop-cast films of the BF₂tbmOC12 dye exhibited behavior typical of ML dye films.^{28,29} There was no change between the as-cast (AC) and thermally annealed (TA) films, with both exhibiting a relatively strong peak at ~10° and a much smaller peak at ~15°. This suggests that the dye film is crystalline both in the AC and TA states. The diffractogram of the smeared film was devoid of peaks, confirming the amorphous nature of the smeared films.

In order to probe the thermally responsive behavior of $\text{BF}_2\text{fbmOC12}$, the powder XRD patterns of orange and green drop-cast films on glass were compared to the diffraction patterns of the pristine powder (Figure 4.8). No peaks were observed in the diffraction pattern of the orange film, whereas sharp peaks at $\sim 24^\circ$ and $\sim 28^\circ$ were detected in the diffraction pattern of the green film. The pattern of the pristine powder also displayed peaks near these same angles. These results indicate that the orange phase generated by melt quenching $\text{BF}_2\text{fbmOC12}$ is amorphous and the green phase produced *via* gentle heating of $\text{BF}_2\text{fbmOC12}$ is crystalline and both are likely to be present in the pristine powder, just as emission spectra and lifetime data suggest.

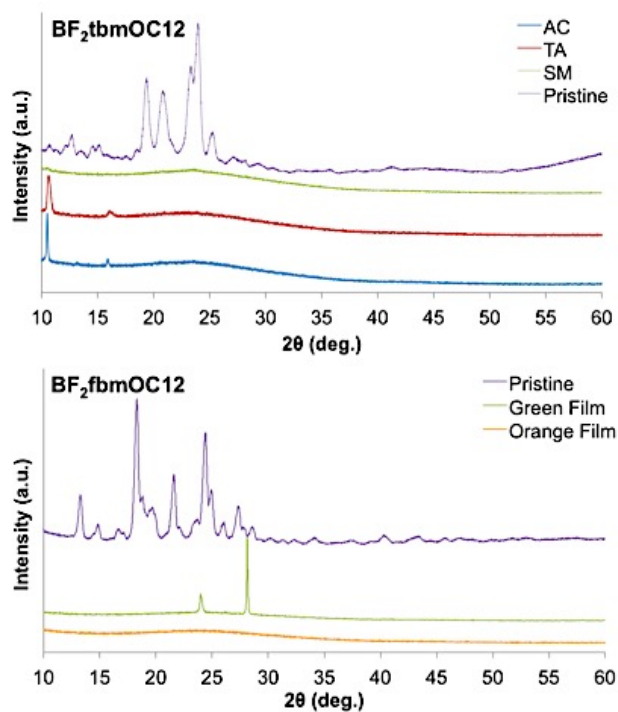


Figure 4.8 Powder XRD diffractograms of mechanochromic luminescent $\text{BF}_2\text{tbmOC12}$ samples (top) and thermally responsive $\text{BF}_2\text{fbmOC12}$ samples (bottom). Note: The pristine powder of $\text{BF}_2\text{tbmOC12}$ is compared to drop-cast films in the as-cast (AC), thermally annealed (TA), and smeared (SM) states. The $\text{BF}_2\text{fbmOC12}$ pristine powder is compared to orange (melt quenched) and green (gentle heated) drop-cast films.

4.4 Conclusion

To summarize, four solid-state emissive difluoroboron β -diketonate dyes bearing thiophene and furan substituents as well as short (OMe) and long (OC₁₂H₂₅) alkoxy chain substituents were synthesized. While the length of the chain had little effect on the optical properties of the dyes in solution, the C₁₂H₂₅ alkoxy chain afforded both the thiophene and furan substituted dyes unique, switchable solid-state luminescence features. The BF₂tbmOC12 dye exhibited high-contrast ($\Delta\lambda_{\text{max}} = 77$ nm) reversible ML as both films on weighing paper and glass substrates. Powder XRD revealed the blue-shifted, thermally annealed (TA) form of the dye to be crystalline in nature while the red-shifted, smeared (SM) form was amorphous. Furthermore, this dye could be carried through at least seven cycles of annealing and smearing without any noticeable deterioration in the dye's responsiveness.

The BF₂fbmOC12 dye showed similar dual emissive behavior as films on glass or weighing paper, but the stimulus required for switching of emission was different. By gently heating the sample a green emissive form could be obtained. An orange emissive form could be obtained *via* melt quenching. This could be achieved by melting the film and then quickly removing the heat source, allowing the film to cool quickly either while held in the air or submerging in liquid N₂. Powder XRD of drop-cast films in both emissive forms revealed the green form to be crystalline with well-defined peaks in the diffractograms while the orange form was amorphous with no peaks. The unique responsiveness could make this dye useful as a quality control indicator for any process requiring intense heating followed by rapid cooling.

Because both dyes bearing OC₁₂H₂₅ alkoxy chains exhibited switchable emissive behavior while their methoxy-substituted counterparts did not, it seems that adding a long alkyl chain substituent to π -stacking, solid-state emitting fluorophores could be an effective strategy for inducing switchable luminescent behavior. Presumably, this is due to the chains disrupting close intermolecular interactions such as π -stacking and thus creating more available molecular configurations. Finally, the difference in thermally responsive emissive behavior between BF₂tbmOC12 and BF₂fbmOC12 may be attributed to closer intermolecular interactions in the H-aggregated furan dye causing the material to become trapped in the amorphous state when it is heated to the melting point and then the melt is rapidly quenched. It may also be attributed to a much more stable ordered emissive state of the BF₂tbmOC12 material strongly driving the transformation to the ordered emissive state.

Although BF₂bdks with only phenyl rings were not considered in this study, we would expect them to have similar functionality to the thiophene derivative given that Huber *et al.* found benzene to have a similar π -stacking interaction energy with other benzene molecules to that of thiophene, only at a larger intermolecular distance.²⁷ However, in future studies, it seems wise to test all BF₂bdk solid state emitting materials for these thermally responsive changes in emission.

4.5 Acknowledgements

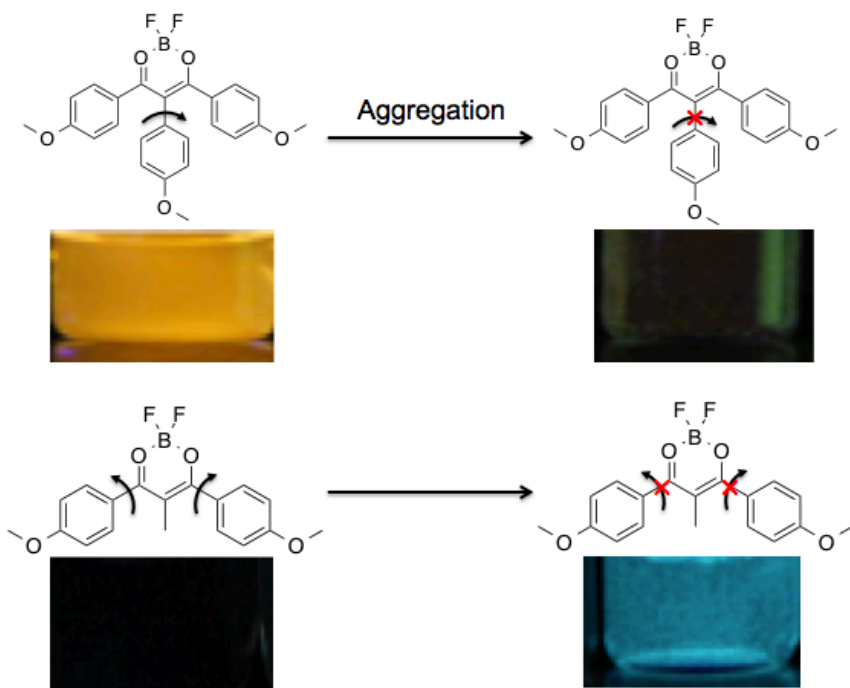
Synthesis and characterization data for the dyes, full computational details, and supporting figures are provided in Appendix C. Milena Kolpaczynska is acknowledged for synthesizing these dyes. Tristan Butler is also acknowledged for help with testing the optical and thermal properties of pristine powders and drop-cast films.

4.6 References

- (1) Evenson, S. J.; Pappenfus, T. M.; Delgado, M. C. R.; Radke-Wohlers, K. R.; Navarrete, J. T. L.; Rasmussen, S. C. *Phys. Chem. Chem. Phys.* **2012**, *14*, 6101.
- (2) Rasmussen, S. C.; Evenson, S. J.; McCausland, C. B. *Chem. Commun.* **2015**, *51*, 4528.
- (3) Poon, C.-T.; Wu, D.; Lam, W. H.; Yam, V. W.-W. *Angew. Chem. Int. Ed.* **2015**, *54*, 10569.
- (4) Mitani, M.; Ogata, S.; Yamane, S.; Yoshio, M.; Hasegawa, M.; Kato, T. *J. Mater. Chem. C* **2015**.
- (5) Greco, N. J.; Tor, Y. *Tetrahedron* **2007**, *63*, 3515.
- (6) Naeem, K. C.; Subhakumari, A.; Varughese, S.; Nair, V. C. *J. Mater. Chem. C* **2015**, *3*, 10225.
- (7) Chung, K.; Kwon, M. S.; Leung, B. M.; Wong-Foy, A. G.; Kim, M. S.; Kim, J.; Takayama, S.; Gierschner, J.; Matzger, A. J.; Kim, J. *ACS Cent. Sci.* **2015**, *1*, 94.
- (8) Kolpaczynska, M.; DeRosa, C. A.; Morris, W. A.; Fraser, C. L. *Aust. J. Chem.* **2016**.
- (9) Williams, D. B. G.; Lawton, M. J. *Org. Chem.* **2010**, *75*, 8351.
- (10) Zhang, G.; Singer, J. P.; Kooi, S. E.; Evans, R. E.; Thomas, E. L.; Fraser, C. L. *J. Mater. Chem.* **2011**, *21*, 8295.
- (11) Carraway, E. R.; Demas, J. N.; DeGraff, B. A.; Bacon, J. R. *Anal. Chem.* **1991**, *63*, 337.
- (12) Heller, C. A.; Henry, R. A.; McLaughlin, B. A.; Bliss, D. E. *J. Chem. Eng. Data* **1974**, *19*, 214.
- (13) Nguyen, N. D.; Zhang, G.; Lu, J.; Sherman, A. E.; Fraser, C. L. *J. Mater. Chem.* **2011**, *21*, 8409.
- (14) Xingxing Sun, X. Z., Xinyang Li, Shiyong Liu, Guoqing Zhang *J. Mater. Chem.* **2012**, *22*, 17332.
- (15) Samonina-Kosicka, J.; DeRosa, C. A.; Morris, W. A.; Fan, Z.; Fraser, C. L. *Macromolecules* **2014**, *47*, 3736.
- (16) Oliver Kappe, C.; Shaun Murphree, S.; Padwa, A. *Tetrahedron* **1997**, *53*, 14179.

- (17) Butler, T.; Morris, W. A.; Samonina-Kosicka, J.; Fraser, C. L. *ACS Appl. Mater. Interfaces* **2016**.
- (18) Zhang, G.; Lu, J.; Sabat, M.; Fraser, C. L. *J. Am. Chem. Soc.* **2010**, *132*, 2160.
- (19) Sun, X.; Zhang, X.; Li, X.; Liu, S.; Zhang, G. *J. Mater. Chem.* **2012**, *22*, 17332.
- (20) Shibata, S.; Murasugi, K.; Kaminishi, K. *IEEE Trans. Parts, Hybrids, Packag.* **1976**, *12*, 223.
- (21) Biedermann, S.; Tschudin, P.; Grob, K. *Anal. Bioanal. Chem.* **2010**, *398*, 571.
- (22) Sun, D.-W. *Advances in Food Refrigeration*; Leatherhead Food RA Pub.: Leatherhead, 2001.
- (23) Sase, M.; Yamaguchi, S.; Sagara, Y.; Yoshikawa, I.; Mutai, T.; Araki, K. *J. Mater. Chem.* **2011**, *21*, 8347.
- (24) Zhang, X.; Chi, Z.; Xu, B.; Jiang, L.; Zhou, X.; Zhang, Y.; Liu, S.; Xu, J. *Chem. Commun.* **2012**, *48*, 10895.
- (25) Liu, W.; Wang, Y.; Bu, L.; Li, J.; Sun, M.; Zhang, D.; Zheng, M.; Yang, C.; Xue, S.; Yang, W. *J. Luminesc.* **2013**, *143*, 50.
- (26) Yoshii, R.; Hirose, A.; Tanaka, K.; Chujo, Y. *Chem. Eur. J.* **2014**, *20*, 8320.
- (27) Huber, R. G.; Margreiter, M. A.; Fuchs, J. E.; von Grafenstein, S.; Tautermann, C. S.; Liedl, K. R.; Fox, T. *J. Chem. Inf. Model.* **2014**, *54*, 1371.
- (28) Morris, W. A.; Liu, T.; Fraser, C. L. *J. of Mater. Chem. C* **2015**, 352.
- (29) Nguyen, N. D.; Zhang, G.-Q.; Lu, J.-W.; Sherman, A. E.; Fraser, C. L. *J. Mater. Chem.* **2011**, *21*, 8409.

Chapter 5

Effects of α -Substitution on the Mechanochromic Luminescence and Aggregation-Induced Emission of Difluoroboron β -Diketonate Dyes

5.1 Introduction

As was mentioned previously, Tang and coworkers addressed the problem of aggregation-caused quenching (ACQ) by developing fluorophores exhibiting aggregation-induced emission (AIE).¹ Soon after the initial discovery of AIE, Park and coworkers reported the compound 1-cyano-*trans*-1,2-bis-(4'-methylbiphenyl)ethylene (CN-MBE) which was only very weakly emissive in dilute solution due to twisting out of plane of the two 4'-methylbiphenyl moieties. Upon aggregating into nanoparticles in THF/water mixtures, planarization of the molecules and subsequent formation of highly emissive J-aggregate species greatly enhanced emission efficiency.² Such behavior is referred to as aggregation-induced enhanced emission (AIEE).^{3,4}

Other groups have investigated α -substitution in similar systems. These groups include Kuimova and coworkers, who reported the viscosity probe 4,4'-difluoro-4-bora-3a,4a-diaza-*s*-indacene. This molecule is a bodipy derivative with a dodecyloxyphenyl moiety attached at the α position of the difluoroboron diiminate core and thus acts as a viscosity-sensitive molecular rotor. In highly viscous media, molecular rotation was restricted, resulting in bright fluorescence and longer fluorescence lifetimes (τ_F). The sensitivity of τ_F to viscosity represents a major advancement over ratiometric sensing methods in terms of ease of calibration, the ability to analyze spatially resolved fluorescence decays, reduced complexity in the sensing system, and highly sensitive detection.⁵ In another example, Qi *et al.* have synthesized and reported a pyrimidine-based difluoroboron compound with a phenyl moiety substituted at the α position of the difluoroboron ketoiminate core. This compound exhibited AIE and reversible ML.⁶

As has been previously mentioned difluoroboron β -diketonate (BF_2bdk) luminescent dyes have unique photo-luminescent properties both in solution and in the solid-state. Among these are intramolecular charge transfer character^{7,8} and mechanochromic luminescence (ML).⁹⁻¹² The cause of ML in this class of dyes has been attributed to the formation of low energy, face-to-face ground-state H-aggregates upon smearing that serve as traps for migrating excitons.¹³ Furthermore, most BF_2bdk compounds exhibit strong fluorescence under UV excitation as both molecular solids and in solution.¹⁰⁻¹² The strongly emissive behavior of these dyes in solution may be attributed to the planar, conjugated nature of the tetra-coordinate dioxaborine core. In this study, planarity is intentionally disrupted by substitution at the alpha position. Three BF_2bdk derivatives, each with groups of varying stereoelectronic demand at the α position of the dioxaborine core, were synthesized. The parent 4,4'-methoxy substituted difluoroboron dibenzoylmethane dye ($\text{BF}_2\text{dbm}(\text{OMe})_2$) was also included as a control. The synthesized compounds and nomenclatures are given in Figure 5.1. The first variation, $\text{BF}_2\text{dbe}(\text{OMe})_2$, is a simple substitution with a methyl group at the α position. This should cause the dye to distort from a planar configuration due to the steric interactions between the H atoms of the sp^3 methyl group and the phenyl rings. The second variation, $\text{BF}_2\text{dbmp}(\text{OMe})_2$, represents a substitution of a much more bulky methoxyphenyl group attached through an sp^2 carbon. This will have the effect of disrupting planarity as well as introducing an electron-donating group attached to the the α position of the electron-accepting dioxaborine core. This is likely to induce significant intramolecular charge transfer (ICT) character. Finally, a “strapped” tetralone derivative was synthesized ($\text{BF}_2\text{bt}(\text{OMe})_2$). This should serve to rigidify the dye and force planarity

on one half of the molecule. The effects of these α -substitutions on the luminescence properties of the dyes were investigated both in solution and in the solid state.

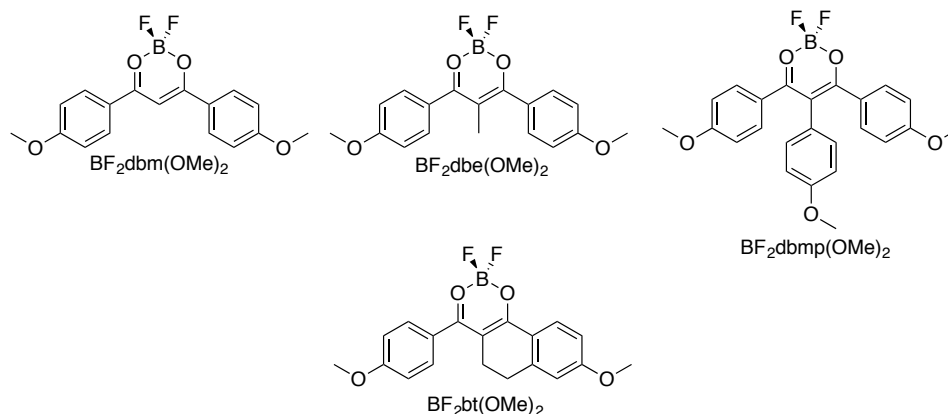


Figure 5.1 Chemical structures of the dimethoxy substituted parent dibenzoylmethane (dbm) dye along with the three α -substituted dyes (dbe = dibenzoyl ethane, dbmp = dibenzoyl methoxyphenyl, bt = β -tetralone).

5.2 Experimental

5.2.1 Materials

Solvents dichloromethane (CH_2Cl_2) and tetrahydrofuran (THF) were dried over 3 Å molecular sieves according to a previously reported method.¹⁴ All other chemicals were reagent grade and purchased from Sigma Aldrich or Alfa Aesar and used without further purification. The dbm(OMe)₂ ligand is commercially available from Sigma Aldrich and the dbe(OMe)₂,¹⁵ dbmp(OMe)₂¹⁶ and bt(OMe)₂¹⁷ ligands and BF₂dbm(OMe)₂ complex⁸ were synthesized by reported methods. Data are in accordance with literature values. (Note: the bt(OMe)₂¹⁷ ligand was reported absent ¹H NMR data so this is included in the supporting information).

5.2.2 Methods

¹H NMR spectra were recorded on a Varian UnityInova 300/51 (300 MHz) or a Varian VMRS/600 (600 MHz) instrument in CDCl₃ or (CD₃)₂SO. ¹H NMR spectra were

referenced to the signal for the chloroform residual proton at 7.26 ppm or the DMSO residual proton at 2.50 ppm. Mass spectra were recorded using a Micromass Q-TOF Ultima spectrometer, using electrospray ionization (ESI) MS/MS techniques. Melting points were recorded on a Mel-Temp II by Laboratory Devices, USA. UV/vis spectra were recorded on a Hewlett-Packard 8452 diode-array spectrophotometer. All steady-state fluorescence emission spectra were recorded on a Horiba Fluorolog-3 Model FL3-22 spectrofluorometer (double-grating excitation and double-grating emission monochromator) except for the spectra for the $\text{BF}_2\text{d}be(\text{OMe})_2$ AIEE experiment with varying water fractions in DMSO, which were recorded on a Horiba Fluoromax-4 spectrofluorometer. Time-correlated single-photon counting (TCSPC) fluorescence lifetime measurements were performed with a NanoLED-370 ($\lambda_{\text{ex}} = 369$) excitation source and a Datastation Hub as the SPC controller. Lifetime data were analyzed with Datastation version 2.6 software from Horiba Jobin Yvon. Fluorescence quantum yields (Φ_{F}) in CH_2Cl_2 solution were calculated *versus* quinine sulfate in 0.1 M H_2SO_4 as a standard according to a previously described method.¹⁸ The following values were used: Φ_{F} quinine sulfate = 0.54¹⁹, n_{D} ²⁰ 0.1 M H_2SO_4 = 1.33, n_{D} ²⁰ CH_2Cl_2 = 1.424. Optically dilute CH_2Cl_2 solutions of the dyes were prepared in 1 cm path length cuvettes with absorbances <0.1 (a.u.). Solid-state quantum yields of spin-cast films were measured using a Quanta- Φ F-3029 Integrating Sphere from Horiba Jobin Yvon. The data was analyzed using FlourEssence software V 2.1 also from Horiba Jobin Yvon.

The AIE experiments were carried out on solutions of the dye in varying water fractions (f_{w}). Water was used as the non-solvent and either DMSO or THF was used as the solvent. Water fractions (f_{w}) of 0%, 10%, 20%, 30%, 40%, 50%, 60%, 70%, 80%,

90%, and 100% were prepared in 10 mL volumetric flasks. Then, a 10^{-3} M DMSO or THF dye stock solution (200 μ L) was added to each water fraction. The flasks were inverted 20 times prior to recording emission and absorption spectra. A blank of each f_w was also recorded and subtracted from the respective spectra.

Differential scanning calorimetry (DSC) thermograms were recorded on a MDSC 2920 from TA Instruments in standard DSC mode. The temperature of the sample chamber was increased at a rate of $5\text{ }^{\circ}\text{C min}^{-1}$ until a temperature $\sim 20\text{ }^{\circ}\text{C}$ hotter than the predetermined melting point of the given dye was reached and held isothermic for 10 min. The sample chamber was then cooled at the same rate to $0\text{ }^{\circ}\text{C}$ and held isothermic for 10 min. After the conditioning run, the same protocol was repeated to generate the reported thermograms. The thermograms were processed and analyzed using Universal Analysis software V 2.3 from TA Instruments.

Films on weighing paper were created by smearing a small amount of dye onto $5 \times 5\text{ cm}^2$ squares of weighing paper with nitrile examination gloves. Samples were weighed to ensure a dye mass of $\sim 1\text{-}3.5\text{ mg}$ spread out over the entire $5 \times 5\text{ cm}^2$ surface. A Laurel Technologies WS-650S spin-coater was used to make spin-cast films. The films were fabricated by preparing 10^{-2} M solutions of each dye and applying ~ 10 drops of these solutions to circular microscope cover glass slides 25 mm in diameter rotating at 3,000 rpm. Films for solid-state quantum yield measurements were made in the same way, except they were cast onto circular cover glass slips 13 mm in diameter. The films were dried *in vacuo* for 15 min before further processing and were annealed at their experimentally determined optimum annealing temperatures in a Thermo Heratherm oven for 5 min.

Samples for powder X-ray diffraction (XRD) analysis were prepared as follows. The pristine powders were analyzed as isolated by either recrystallization or column chromatography. Films were prepared by “drop-casting” ~20 drops of 10^{-2} M dye solutions to 25 mm diameter circular microscope cover glass slides. The films were allowed to dry under ambient conditions and then further dried *in vacuo* for 15 min before further processing and analysis. XRD patterns for both powders and films were collected using a Panalytical X’Pert Pro MPD diffractometer. The diffractograms were recorded as follows: start angle: 10° , step size: 0.01° , time per step: 60 s, end angle: 60° .

The boronated compounds were modeled using the Gaussian 09²⁰ suite of programs with density functional theory (DFT). B3LYP/6-311+G(d) utilized for ground state and singlet excited state geometry optimization with a Tomasi polarized continuum for dichloromethane or dimethyl sulfoxide solvent.²¹ the vibrational frequencies for the optimized geometries were all positive, assuring that the geometries are at least a local minimum. Single point energy calculations were used to generate the molecular orbital diagrams utilizing B3LYP/6-31G(d). Time-dependent density functional theory, TD-B3LYP/6-311+G(d), was employed for estimates of absorption spectra. TD- ω B97XD was also utilized to estimate the absorption spectra of $\text{BF}_2\text{dbmp}(\text{OMe})_2$ in dichloromethane solution.^{8,22}

5.3 Results and Discussion

5.3.1 Optical Properties of Dyes in Solution

Difluoroboron complexes were obtained as yellow emissive powders after synthesis of the β -diketone by Claisen condensation of the appropriate ketone/ester pair followed by boronation and purification either by column chromatography or

recrystallization. Full synthetic details are provided in the supporting information. The optical properties of the boron dyes were first studied in dilute CH_2Cl_2 solution and the α -substitutions were found to have unique effects on the optical properties (Table 5.1, Figure 5.2). Methyl substitution at the α position (i.e. the dibenzoylthane (dbe) variant) resulted in a drastic decrease in extinction coefficient as well as a blue-shift in the absorbance spectrum compared to the parent dye. This is presumably due to a non-planar conformation induced by the steric bulk of the methyl group.

Table 5.1 Absorption and Emission Properties of Boron Dyes in CH_2Cl_2 Solution.^a

Dye	ϵ [$\text{M}^{-1} \text{cm}^{-1}$]	$\lambda_{\text{abs}}^{\text{b}}$ [nm]	$\lambda_{\text{em}}^{\text{c}}$ [nm]	Φ_{F} [%]	Stokes Shift [cm^{-1}]	τ_{F} [ns]	τ_{rad} [ns]
$\text{BF}_2\text{dbm}(\text{OMe})_2$	73,000 ^d	411 ^d	437 ^d	78 ^d	1,450 ^d	1.79 ^d	2.29 ^d
$\text{BF}_2\text{dbe}(\text{OMe})_2$	46,000	395	444	<1%	2,793	1.2	N/A
$\text{BF}_2\text{dbmp}(\text{OMe})_2$	26,000	424	580	16	6,344	2.0	12.5
$\text{BF}_2\text{bt}(\text{OMe})_2$	54,000	420	459	61	2,024	1.9	3.1

^a $\lambda_{\text{ex}} = 369$ nm; room temperature, air.

^b Absorbance maximum.

^c Emission maximum; fluorescence.

^d Values taken from reference 13.

Distortion of the boron dye is supported by computational results obtained using density functional theory (DFT). According to DFT calculations simulating solvation in CH_2Cl_2 , $\text{BF}_2\text{dbe}(\text{OMe})_2$ experiences significant twisting about the C-C-C-C torsion angles starting with the carbon in the six position of either phenyl ring and terminating at the α carbon of the dioxaborine core. The angle in the parent compound is +/- 7° in the

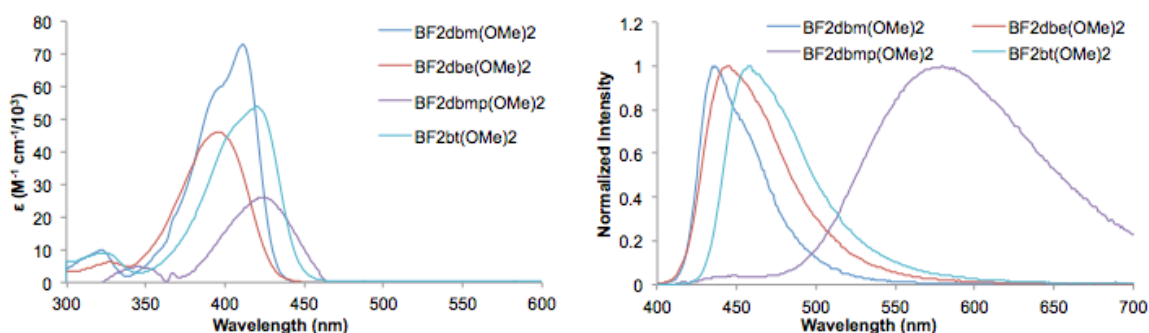


Figure 5.2 UV/vis absorption spectra (left) and steady-state emission spectra (right) of the α -substituted dyes in 5×10^{-6} M CH_2Cl_2 solution ($\lambda_{\text{ex}} = 369$ nm).

ground-state while $\text{BF}_2\text{dbe}(\text{OMe})_2$ experiences a distortion of $\pm 34^\circ$ (Figure 5.3). This twisting also has the effect of drastically decreasing the quantum efficiency of the dye to the point where it would, for all practical purposes, be considered non-emissive in solution (i.e. $<1\%$ quantum yield). While faint, an emission at 444 nm was detected in CH_2Cl_2 solution. The larger Stokes shift exhibited by $\text{BF}_2\text{dbe}(\text{OMe})_2$ ($2,793 \text{ cm}^{-1}$) compared to the parent dye ($1,450 \text{ cm}^{-1}$) is likely due to distortions in this dye causing more drastic geometric rearrangements in the excited state. Interestingly, when dissolved in the more polar DMSO, lifetime data were best fit to multi-exponential decay with a slight contribution from a shorter-lifetime species (Table S5.1 Appendix D). However, emission was still too weak to be visible to the eye. TD-DFT calculations simulating solvation in CH_2Cl_2 determined that the absorption spectrum is dominated by a HOMO to LUMO transition predominantly π to π^* in character with only slight charge transfer from the phenyl rings and the α -methyl moiety to the dioxaborine core (Figure 5.4, Table S5.4, Table S5.5 Appendix D).

The $\text{BF}_2\text{dbmp}(\text{OMe})_2$ dye includes a much bulkier substituent, inducing significant distortions to the planar structure of the parent dye in solution according to DFT calculations. Ground state geometry optimization simulating CH_2Cl_2 solvation revealed, much like in $\text{BF}_2\text{dbe}(\text{OMe})_2$, substantial twisting in the C-C-C-C torsion angles starting with the carbon in the six position of either phenyl ring and terminating at the α carbon of the dioxaborine core. This angle was determined to be $\pm 38^\circ$, which is slightly greater than that of $\text{BF}_2\text{dbe}(\text{OMe})_2$. These calculations also showed the plane of the

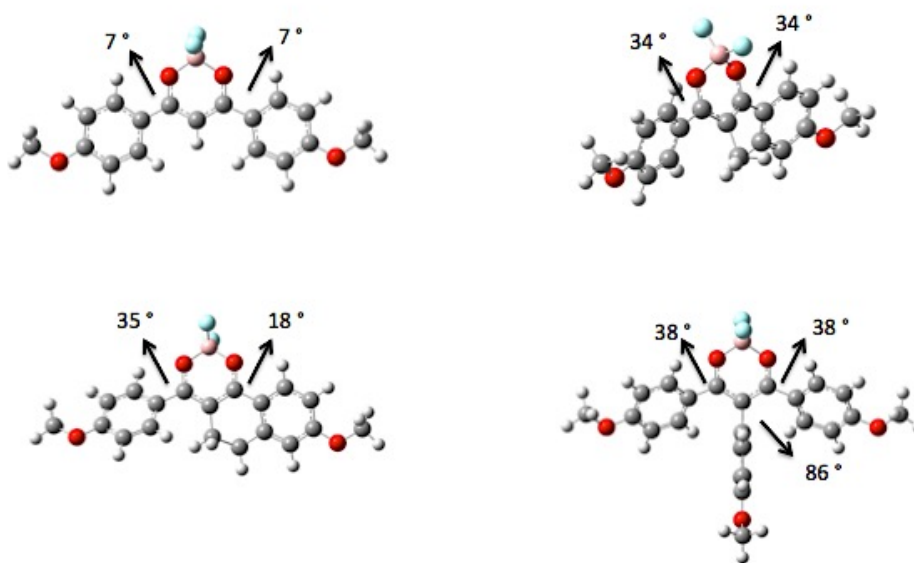


Figure 5.3 Optimized ground state geometries of the dyes showing distortions from planarity as C-C-C-C torsion angles starting with the carbon in the six position of either phenyl ring and terminating at the α carbon of the dioxaborine core.

methoxyphenyl moiety at the α position to be almost completely perpendicular to the planar β -diketonate core with the torsion angle between them being $\pm 86^\circ$. While this dye has a much reduced extinction coefficient compared to the other dyes (Table 5.1), surprisingly, it displays visibly orange emission with $\Phi_F = 16\%$ (Table 5.1, Figure 5.2). Normally, dyes with this degree of distortion are virtually non-emissive in solution,²³

much like $\text{BF}_2\text{dbe}(\text{OMe})_2$, so there must be another explanation for this red-shifted visible emission.

In fact, the red-shifted emission of $\text{BF}_2\text{dbmp}(\text{OMe})_2$ seems to arise from a twisted intramolecular charge transfer (TICT) state.^{8,24,25} Evidence for this is provided by the unusually red and broad emission profile compared to the other dyes in the series. The Stokes shift is quite large ($6,344\text{ cm}^{-1}$), which is typical for TICT emission, and the radiative lifetime (τ_{rad}) is $>10\text{ ns}$, also typical of TICT emissions (Table 5.1).⁸ The emission spectra displayed a very weak blue-shifted shoulder at $\sim 450\text{ nm}$, very close to the emissions of $\text{BF}_2\text{dbe}(\text{OMe})_2$ and $\text{BF}_2\text{dbm}(\text{OMe})_2$. Excitation spectra recorded with the emission monochromator parked at both the peak emission wavelength of 580 nm and the weak shoulder at 450 nm revealed distinct excitation profiles (Figure 5.5). Furthermore, the excitation spectrum recorded at 450 nm closely correlated to the excitation spectrum of the parent dye. The emission from the parent dye is known to arise from a π to π^* transition so it stands to reason that the strongest observed emission from $\text{BF}_2\text{dbmp}(\text{OMe})_2$ arises from a species conducive to TICT while the blue emission arises from a species favoring a π to π^* transition that is weakened by molecular distortions from planarity, similar to $\text{BF}_2\text{dbe}(\text{OMe})_2$.

Further credence is lent to this idea by computationally generated MOs and TD-SCF calculations simulating CH_2Cl_2 solvation. From the generated MOs, the HOMO to LUMO transition appears to be almost entirely ICT with amplitude concentrated on the methoxyphenyl moiety at the α position in the HOMO and on the BF_2dbm portion in the LUMO (Figure 5.4). Qi *et al.* observed a similar transference of electron density from HOMO to LUMO in a α -substituted pyrimidine-based BF_2 dye.⁶ According to the initial

TD-DFT calculation utilizing B3LYP/6-311+G(d), the strongest transition was predicted to be a much more blue-shifted (397.04 nm) HOMO-1 to LUMO π to π^* transition while the red-shifted (424.72 nm) ICT HOMO-LUMO transition was predicted to be much weaker (Table S5.4 and Table S5.5 Appendix D). However, TD-SCF calculations utilizing ω B97XD/6-311+G(d), which contains a full Hartree-Fock exchange at long-range interelectron distance as well as considerations for dispersion interactions gave slightly different results (Table S5.6 and Table S5.7 Appendix D).²⁶ Using this method and calculating 22 excited states produced a much more accurate representation of the excitation where the red-shifted (347.28 nm) ICT HOMO to LUMO transition was dominant and the blue-shifted (320.30 nm) π to π^* HOMO-1 to LUMO transition was barely visible. Although the B3LYP model reproduced the energies (i.e. wavelengths) of transitions more accurately, the long-range ω B97XD model proved much better at predicting the relative strengths of the transitions.

The strapped BF₂bt(OMe) exhibited optical properties in dilute CH₂Cl₂ solution more typical of other BF₂dbm derived dyes, with a high extinction coefficient (54,000 M⁻¹ cm⁻¹), high fluorescence quantum yield ($\Phi_F = 61\%$), and a short radiative lifetime ($\tau_{\text{rad}} = 3.1$ ns).^{11,12,27} Geometry optimizations performed with a B3LYP/6-311+G(d) model simulating solvation in CH₂Cl₂ revealed a distorted structure with the unstrapped phenyl ring twisted out of the plane of the β -diketonate moiety by $\sim 35^\circ$, which is likely the cause of the increase in Stokes shift compared to the parent dye (Table 5.1). In fact, BF₂bt(OMe)₂ shows similar deviations in emission properties to BF₂dbe(OMe)₂, only to a lesser extent. This is no doubt due to the strapped structure limiting distortions from planarity for half of the molecule. The TD-DFT calculation using B3LYP/6-311+G(d)

showed that the dominant transition was HOMO to LUMO and largely π to π^* in character with slight charge transfer from the phenyl rings and the carbon atom attached to the α position to the dioxaborine core, much like $\text{BF}_2\text{dbe}(\text{OMe})_2$.

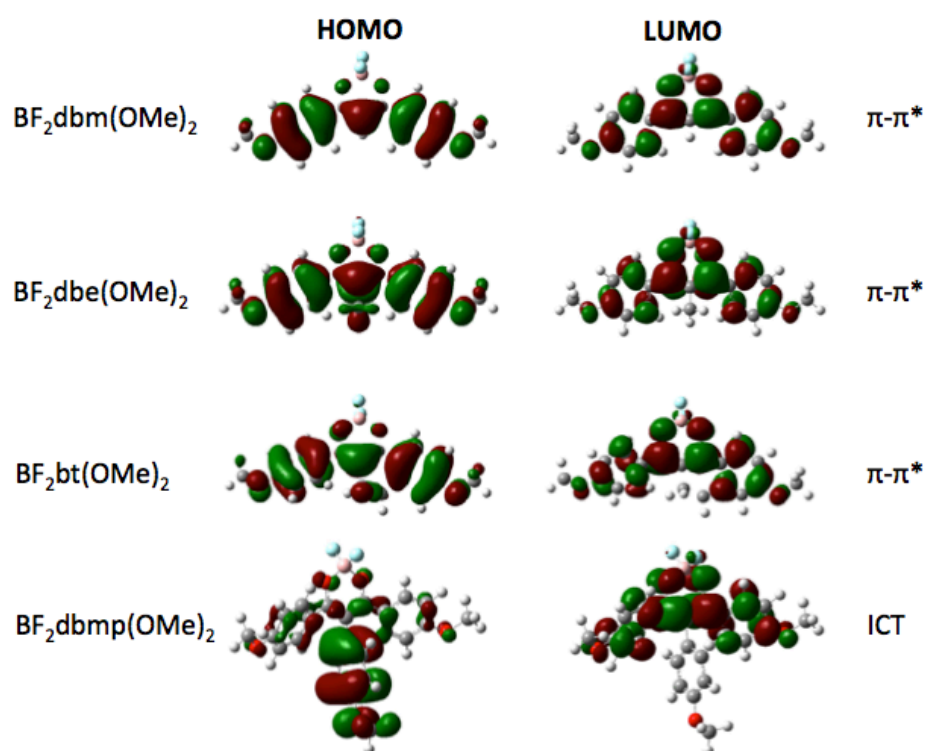


Figure 5.4 Molecular orbitals (MOs) depicting the HOMO and LUMO of each dye and labeling the transition as either π - π^* or intramolecular charge transfer (ICT).

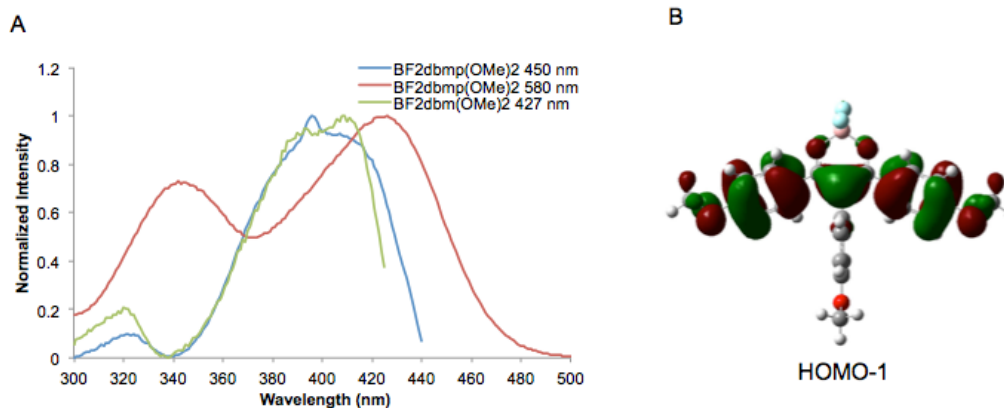


Figure 5.5 A) The excitation spectra of BF₂dbmp(OMe)₂ in dilute (5×10^{-6} M) CH₂Cl₂ solution recorded with emission peaks of 450 nm (blue) and 580 nm (red). The excitation spectrum of BF₂dbm(OMe)₂ recorded with the λ_{max} (437 nm) as the emission peak is also included (green). All spectra were recorded of the dyes in dilute (5×10^{-6} M) CH₂Cl₂ solution. B) Molecular orbital diagram visualizing the HOMO-1 of BF₂dbmp(OMe)₂. The excitation spectra recorded at an emission peak of 450 nm is believed to arise from a π to π^* HOMO-1 to LUMO transition.

5.3.2 Aggregation-Induced Enhanced Emission

Because BF₂dbe(OMe)₂ is practically non-emissive in solution but emitted bright blue as a crystalline solid under UV light, it and other dyes were subjected to typical AIEE experiments using DMSO and THF as solvents and water as the non-solvent (Figure 5.6, Figure S5.1, Figure S5.2, Figure S5.3, Figure S5.4, and Figure S5.5 Appendix D).^{1,2} Using DMSO as the solvent, the parent dye, unsubstituted in the alpha position, showed AIEE up to $f_w = 60\%$, after which the emission red-shifted to resemble the emission from the bulk solid and exhibited attenuation of emission intensity up to $f_w = 100\%$. When this same experiment was performed on the dye using THF as the solvent, the dye exhibited only a decrease in emission intensity as the f_w was increased. It is important to note that all of these dyes are quite emissive in the solid-state and, therefore, do not exhibit true ACQ. On the other hand, the methyl-substituted BF₂dbe(OMe)₂

showed drastic AIEE in DMSO/water mixtures, going from practically non-emissive to bright blue photoluminescence at $f_w = 70\%$, at which point the I/I_0 (intensity/intensity at $f_w = 0\%$) value increased by a factor of seven. The dye exhibited similar AIEE behavior in THF/H₂O mixtures. The BF₂dbmp(OMe)₂ dye shows the most intriguing behavior of all. In $f_w = 0\%$, BF₂dbmp(OMe)₂ has a visibly bright orange emission. As the f_w is increased, the emission attenuates until the dye is practically non-emissive at $f_w = 50\%$. At $f_w = 60\%$, a green emission appears and reaches its maximum intensity at $f_w = 70\%$. At $f_w = 100\%$, a yellow/green emission resembling the emission of the dye as bulk solid was obtained. In THF solution, BF₂dbmp(OMe)₂ only showed AIEE with a drastic increase in emission intensity at $f_w = 100\%$. In both DMSO and THF, BF₂bt(OMe)₂ only showed a decrease in emission intensity as the f_w was increased. It is important to note that at high f_w values (typically $>70\%$), all of the dyes exhibited emission typical of what is observed in the solid state corresponding to a broadening of the absorption spectra and a decrease in absorbance.

The difference in behavior of BF₂dbm(OMe)₂ in DMSO and THF may be attributed to solvent effects. In both CH₂Cl₂ and THF, BF₂dbm(OMe)₂ has high quantum yields ($\Phi_f = 78\%$ in CH₂Cl₂; 100% in THF) (Table 5.1 and Table S5.2 Appendix D). However, the quantum yield is substantially reduced in DMSO with $\Phi_f = 3.7\%$ (Table S5.1). This substantial reduction in Φ_f in DMSO may be due to the highly polar solvent stabilizing a more polar excited state species, leading to internal conversion according to Kasha's rule and subsequent thermal deactivation.^{28,29} Absorption and emission wavelengths increase slightly relative to values in CH₂Cl₂ and the Stokes shift also increases, revealing a mild solvatochromic effect and calculations predict that this dye

should have a larger dipole in the excited state compared to the ground state (8.7422 Debye in the ground state *versus* 9.6716 Debye in the excited state). It seems reasonable to suggest that as the non-solvent (water) is added, the dyes aggregate and this effect of solvation in a polar solvent diminishes. This continues until a certain critical point is reached and emission intensity is attenuated as the bulk solid emission emerges. In the much less polar THF, only decreases in emission intensity are observed as water is added.

For $\text{BF}_2\text{dbe}(\text{OMe})_2$, the story is much simpler. As previously noted, DFT calculations predict a highly twisted, non-planar molecular geometry in the ground state in CH_2Cl_2 solution. As non-solvent is added and the dye molecules aggregate, molecular rotations are restricted, the dyes are forced into a planar conformation, and emission intensity increases. Many AIE luminogens (AIEgens) are quite bulky and have propeller-like molecular structures with many aromatic rings attached to an aromatic core, such as hexaphenylsilole (HPS), for example.³⁰⁻³² However, $\text{BF}_2\text{dbe}(\text{OMe})_2$ is a much simpler, smaller molecule by comparison. By inserting a methyl group at the α position of a BF_2dbm derived core, a fluorophore with stark AIEE behavior results.

Clearly, the behavior of $\text{BF}_2\text{dbmp}(\text{OMe})_2$ in varying DMSO/water mixtures is more than straightforward AIEE. Just as in CH_2Cl_2 , the low energy, structure less, and long τ_{rad} emission in DMSO is indicative of ICT. The moderately larger Stokes shift ($6,697 \text{ M}^{-1} \text{ cm}^{-1}$) and redder emission (600 nm) compared to CH_2Cl_2 is indicative of a modest solvatochromic shift typically associated with ICT emissions.³³ When describing TICT processes, the original hypothesis put forth by Grabowski *et al.* states that a perpendicular conformation between donor (methoxyphenyl) and acceptor (β -diketonate core) allows for a zero or full charge transfer between molecular subunits.²⁵ This could

explain why such strong ICT character is observed for this dye in dilute solution and why the emission is particularly bright. Since an optimum conformation for ICT in the ground state is already favored, little molecular rearrangement in the excited state would be necessary to achieve the charge transfer. This would reduce contributions from non-radiative decay associated with large molecular rearrangement in the excited state.^{24,28} As non-solvent is added and dye molecules are forced to aggregate, the twisting of the methoxyphenyl substituent at the α position to the perpendicular orientation may be restricted and emission from this twisted species weakened, causing the drop in emission intensity up to $f_w = 50\%$. However, this dye is quite emissive in the solid-state and this is why the dye becomes bright again once a critical point of aggregation is reached. The reason for observation of more straightforward AIEE in THF/water mixtures seems to be due to a difference in solubility of the dye in THF *versus* DMSO. BF₂dbmp(OMe)₂ was much less soluble in DMSO than THF. This would make aggregation more facile upon addition of water and could explain the aforementioned behavior.

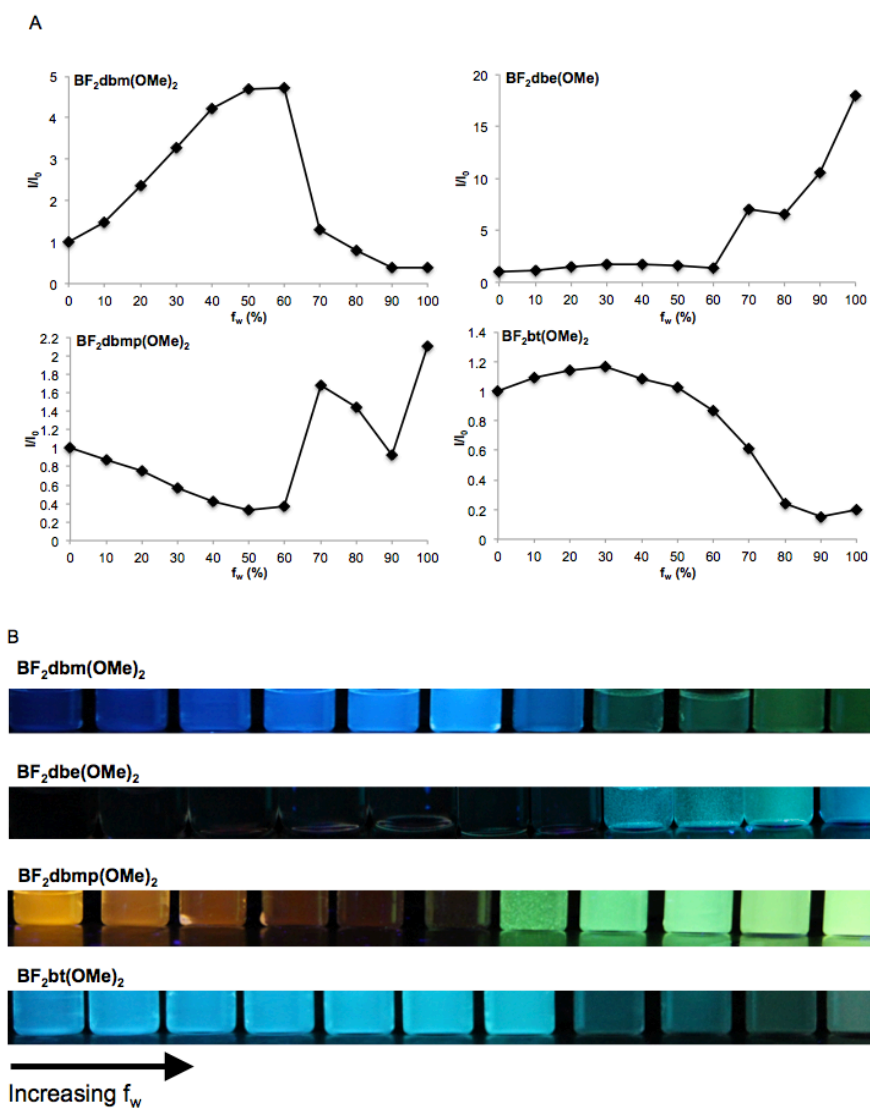


Figure 5.6 AIEE of the dyes in DMSO/water fractions. The water fractions (f_w) were increased from 0 to 100% in increments of 10%. A) The intensity ratio I/I_0 plotted *versus* f_w . B) Photographs of the dyes in varying water fractions.

5.3.3 Mechanochromic Luminescent Properties

It has been demonstrated previously that the BF₂dbm(OMe)₂ parent compound exhibits ML behavior.¹³ These properties were readily reproduced for the dye both as a film on weighing paper and as a spin-cast film on glass (Figures 5.7 and 5.8). While the parent dye showed an observable change from green to yellow when annealed films on

weighing paper were smeared, the annealed α -substituted $\text{BF}_2\text{dbe}(\text{OMe})_2$ films showed no change at all under these same conditions. However, when $\text{BF}_2\text{dbe}(\text{OMe})_2$ was fabricated into much thinner spin-cast films on glass, a mild ML shift from blue to blue/green was observed upon smearing the annealed film. This is indicative of a thickness effect. In the past, more dramatic ML behavior has been observed for spin-cast films of these dyes *versus* weighing paper films.²⁷ The $\text{BF}_2\text{dbmp}(\text{OMe})_2$ dye films exhibited ML both as weighing paper and spin-cast films. Solid-state emission from this dye is more red-shifted by comparison to the others and a change from yellow-green to yellow-orange was observed upon smearing the annealed dye films. In order to test the reversibility of these transformations *via* heating, the parent and $\text{BF}_2\text{dbmp}(\text{OMe})_2$ dye films were carried through five cycles of annealing and smearing (Figure S5.6 Appendix D). The parent dye displayed excellent reversibility with almost no deterioration in response throughout the five cycles. However, $\text{BF}_2\text{dbmp}(\text{OMe})_2$ showed deterioration in its ability to form the amorphous emissive state after just a couple of cycles as the dye seemed to gain more of an affinity for the ordered emissive state.

Because this class of dyes is known to spontaneously recover the ordered emissive state after smearing at room temperature under air, and substituent effects play a role in recovery, the emissions of the dyes were monitored over time after smearing.^{11,12,27} Spin-cast films on glass were used to monitor this change in order to minimize substrate effects on recovery.²⁷ The parent dye exhibited a limited ability to recover. The ordered emissive state was partially recovered after one day after which recovery ceased and re-annealing was required to fully recover the ordered emissive

state. The methyl-substituted dye $\text{BF}_2\text{dbe}(\text{OMe})_2$ was also unable to recover fully under ambient conditions. As usual, when the dye film was smeared, the red-shift corresponded

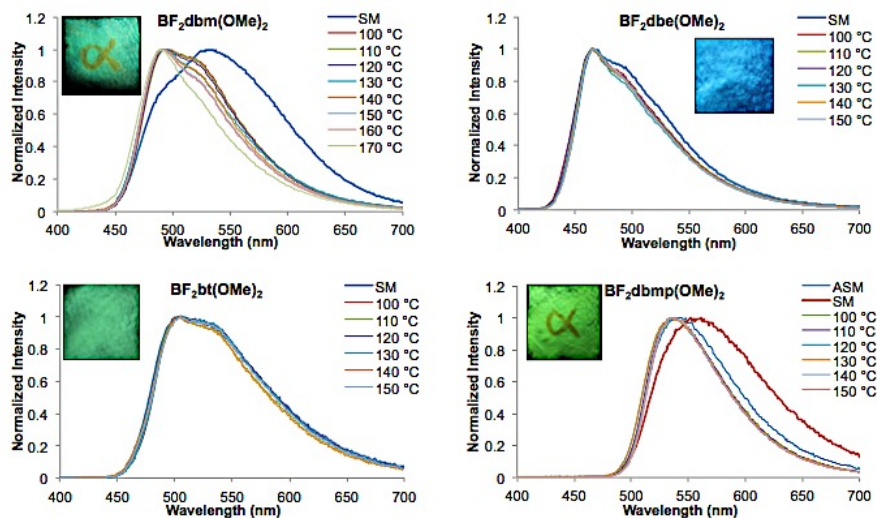


Figure 5.7 Mechanochromic luminescence of the boron dyes as films on weighing paper. The dye films were annealed at their experimentally determined optimum annealing temperatures (indicated in legends) and then smeared with a cotton swab. The spectra of smeared films are labeled as SM in the graphs. The alpha dye recovered so quickly that the as-prepared film (i.e. smeared into a film on weighing paper) resembled the annealed film. For this reason, the unannealed film was labelled as-smeared (ASM).

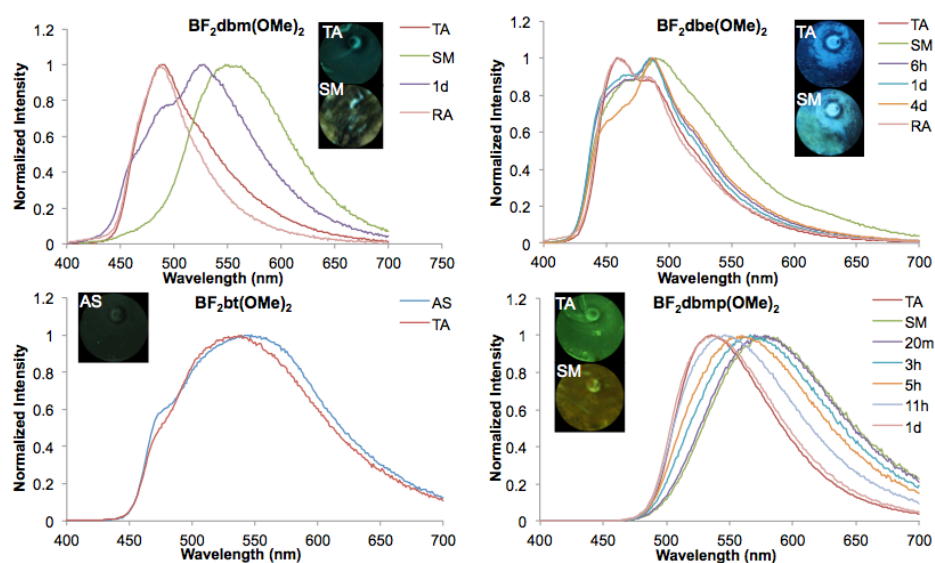


Figure 5.8 Mechanochromic luminescence of the boron dyes as spin-cast films on glass showing their recovery under ambient conditions monitored over time, where TA = thermally annealed and SM = smeared, m = minute(s), h = hour(s), d = day(s).

to a broadening of the FWHM and loss of fine structure in the emission profile.^{13,27} While the peak emission (λ_{max}) never changed, over time the peak became more structured and, after four days, a blue-shifted shoulder at approximately the position of the annealed peak appeared. Spontaneous recovery did not proceed past this point and re-annealing was required to recover the annealed emission profile. By contrast, spin-cast films of the phenyl substituted dye $\text{BF}_2\text{dbmp}(\text{OMe})_2$ dye were able to rapidly recover from the smeared (SM) state at room temperature under air. Just a day after smearing, the annealed emission profile completely recovered. It seems that bulky aromatic substituents at the α position can facilitate both the rapid recovery of the ordered emissive state as spin-cast films and the aforementioned increased affinity for the ordered emissive state through multiple cycles of annealing and smearing as a film on weighing paper. This can be rationalized by invoking steric considerations. The face-to-face H-aggregates of the amorphous emissive state¹³ would be under considerable steric stress as a result of this substitution and this could serve as the driving force to return to the much less sterically-hindered, stable J-aggregate.

Either as a thin, spin-cast film or as a thicker film on weighing paper, the $\text{BF}_2\text{bt}(\text{OMe})_2$ dye exhibited no response either to annealing or mechanical force. Regardless of the processing method used, the dye maintained a green, long-lifetime, broad FWHM emission profile. This suggests inability of the dye to form a more blue-shifted emissive state under these conditions.

Solid-state quantum yields (SSQY) were also recorded for spin-cast dye films on glass in both their thermally annealed (TA) and smeared (SM) states (Table 5.2). All dyes exhibiting ML (i.e. $\text{BF}_2\text{dbm}(\text{OMe})_2$, $\text{BF}_2\text{dbe}(\text{OMe})_2$, and $\text{BF}_2\text{dbmp}(\text{OMe})_2$) showed

decreases in quantum yield >10% after smearing, suggesting the H-aggregates of the amorphous state have less efficient emissions. The BF₂bt(OMe)₂ dye film did not experience this dramatic decrease in quantum yield after smearing, consistent with its lack of ML functionality.

Table 5.2 Solid State Luminescence Quantum Yields for the Dyes as Spin-Cast Films on Glass at Room Temperature Under Air.^a

Dye	Thermally Annealed Φ [%]	Smeared Φ [%]
BF ₂ dbm(OMe) ₂	80	48
BF ₂ dbe(OMe) ₂	82	57
BF ₂ dbmp(OMe) ₂	68	53
BF ₂ bt(OMe) ₂	55	53

^a $\lambda_{\text{ex}} = 369 \text{ nm}$.

5.3.4 Structural and Morphological Studies

Powder XRD analysis was performed on the dyes as pristine powders and drop-cast films on glass after various processing conditions were applied to determine crystallinity of the materials in various states (Figure 5.9). The parent BF₂dbm(OMe)₂ dye exhibited peaks indicative of crystallinity as a pristine powder and in both the as-spun (AS) and thermally annealed (TA) film states. The smeared (SM) film was completely devoid of peaks indicating an amorphous state. Both BF₂dbe(OMe)₂ and BF₂dbmp(OMe)₂ exhibited similar behavior. In particular, when the BF₂dbmp(OMe)₂ film was annealed, an increase in intensity of a sharp peak at ~23° and the disappearance

of a broad peak at $\sim 21^\circ$ was observed. Diffractograms of $\text{BF}_2\text{bt}(\text{OMe})_2$ dye films were without peaks regardless of processing and seem to indicate that this dye is “locked” into an amorphous phase as a film, possibly explaining why this dye does not exhibit ML.

In addition to XRD, atomic force microscopy (AFM) was used to examine the morphology of spin-cast films on glass in as-spun (AS) and thermally annealed (TA) states (Figure 5.10). The parent dye and $\text{BF}_2\text{dbmp}(\text{OMe})_2$ were studied using this technique due to the fact that they showed the most dramatic ML character both as spin-cast films on glass and as films on weighing paper. In the as-spun form, the parent dye was composed of small clusters of serpentine crystallites. When annealed, the film displayed more organized block-like crystallites. Films of $\text{BF}_2\text{dbmp}(\text{OMe})_2$ exhibited very similar morphology in both the as-spun and thermally annealed states, with the emergence of more organized blocky crystallites after annealing. The similarity in morphology between as-spun and thermally annealed films are further evidence that this dye has a strong tendency to form a crystalline, ordered state.

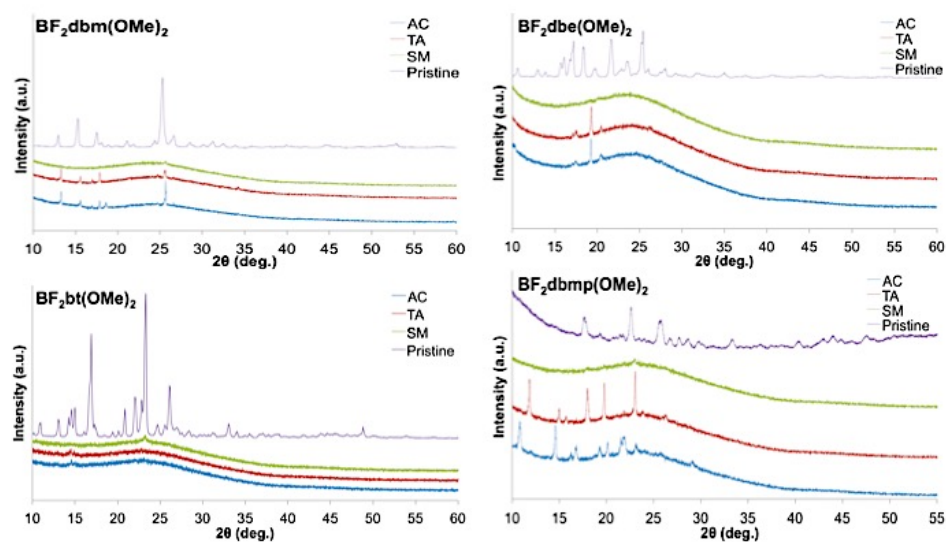


Figure 5.9 X-ray diffraction (XRD) patterns of the parent and α -substituted dyes as pristine powders and drop-cast films in their as-cast (AC), thermally annealed (TA), and smeared (SM) states.

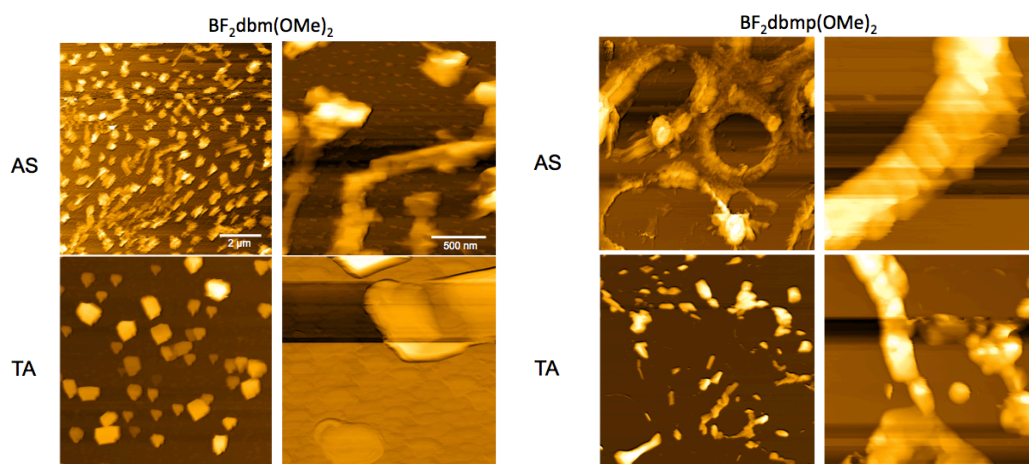


Figure 5.10 AFM images of the $\text{BF}_2\text{dbm}(\text{OMe})_2$ and $\text{BF}_2\text{dbmp}(\text{OMe})_2$ dyes as spin-cast films on glass in both as-spun (AS) and thermally annealed (TA) states. Note: images on the left depict a $10 \times 10 \mu\text{m}^2$ scan area while images on the right depict a $2 \times 2 \mu\text{m}^2$ scan area.

5.3.5 Differential Scanning Calorimetry of Dye Powders

Differential scanning calorimetry (DSC) was performed on the pristine powders in order to characterize their thermal properties. The results are summarized in Table 3 and the thermograms are provided in the supporting information (Figure S5.7 Appendix D). It was noted that the strapped $\text{BF}_2\text{bt}(\text{OMe})_2$ dye had an unusually low crystallization point (T_c) with a relatively small ΔH value compared to the rest of the dyes, which may be indicative of a weaker thermodynamic drive to form the blue-shifted, ordered emissive phase.³⁴ This could explain why annealing films of this dye does not elicit any change in emission.

Table 5.3 Differential Scanning Calorimetry (DSC) Data for Pristine Dyes.^a

Dye	T_m^b (ΔH^c)	T_c^d (ΔH^c)
$\text{BF}_2\text{dbm}(\text{OMe})_2$	236.33 (312.7)	222.74 (300.1)
$\text{BF}_2\text{dbe}(\text{OMe})_2$	203.52 (312.5)	143.20 (268.1)
$\text{BF}_2\text{dbmp}(\text{OMe})_2$	225.09 (263.9)	152.92 (264.3)
$\text{BF}_2\text{bt}(\text{OMe})_2$	229.71 (347.9)	105.27 (91.0)

^a All data was taken from the 2nd cycle.
^b Melting point given in °C as the peak of the major endothermic transition.
^c Enthalpy of the transition given in kJ/mol.
^d Crystallization temperature given in °C as the peak of the major exothermic transition.

5.4 Conclusions

In conclusion, three difluoroboron dibenzoylmethane (BF_2dbm) derivatives with substitutions at the α position of the β -diketonate (BF_2bdk) core ($\text{BF}_2\text{dbe}(\text{OMe})_2$, $\text{BF}_2\text{dbmp}(\text{OMe})_2$, and $\text{BF}_2\text{bt}(\text{OMe})_2$) were synthesized. The α -substitutions were found to

affect significant changes in the optical properties of these dyes in both solution and the solid-state. The methyl-substituted $\text{BF}_2\text{dbe}(\text{OMe})_2$ was practically non-emissive in solution but showed dramatic AIEE behavior, especially for a dye of this size, when dye molecules were forced to aggregate by addition of water to solutions either in THF or DMSO. The $\text{BF}_2\text{dbe}(\text{OMe})_2$ dye films also showed ML behavior heavily dependent on film thickness, with thick films on weighing paper showing no ML behavior, but thinner, spin-cast films on glass exhibited a change from blue to blue-green when annealed films were smeared. Substitution at the α -position with a methoxyphenyl moiety ($\text{BF}_2\text{dbmp}(\text{OMe})_2$) imparted the dye with a broad, red-shifted emission in solution due to emission from a twisted intramolecular charge transfer state. As a result, $\text{BF}_2\text{dbmp}(\text{OMe})_2$ exhibits unique attenuation of emission intensity in DMSO/water up to a water fraction (f_w) of 50% and then AIEE behavior from $f_w = 50\%$ to $f_w = 70\%$. This dye also exhibited rapidly recovering ML behavior, presumably due to steric hindrance driving a return to the ordered emissive state after dye films are smeared. Finally, the strapped $\text{BF}_2\text{bt}(\text{OMe})_2$ dye exhibited fairly typical behavior in solution only with a slightly reduced quantum yield (Φ_f) and slightly larger Stokes shift. The strapped structure seems to limit the effects that molecular distortion caused by α -substitution had on emission. Furthermore, regardless of the applied processing conditions, this dye did not exhibit ML and X-ray diffraction (XRD) revealed the dye to be in amorphous state whether annealed or smeared. The reason for this is unclear but may be due to lower thermodynamic stability in the crystalline phase compared to other dyes. Further study into this matter is required. Insight into how ML properties can be both realized and

tuned is invaluable in moving toward rational design and implementation of such materials for applications.

5.5 Acknowledgements

Milena Kolpaczynska is acknowledged for synthesizing the $\text{BF}_2\text{dbmp}(\text{OMe})_2$ dye. Professor Carl O. Trindle is acknowledged for helpful discussions concerning computational studies.

5.6 References

- (1) Luo, J.; Xie, Z.; Lam, J. W. Y.; Cheng, L.; Chen, H.; Qiu, C.; Kwok, H. S.; Zhan, X.; Liu, Y.; Zhu, D.; Tang, B. Z. *Chem. Commun.* **2001**, 1740.
- (2) An, B.-K.; Kwon, S.-K.; Jung, S.-D.; Park, S. Y. *J. Am. Chem. Soc.* **2002**, *124*, 14410.
- (3) Zhang, X.; Chi, Z.; Xu, B.; Chen, C.; Zhou, X.; Zhang, Y.; Liu, S.; Xu, J. *J. Mater. Chem.* **2012**, *22*, 18505.
- (4) Wu, W.; Ye, S.; Huang, L.; Xiao, L.; Fu, Y.; Huang, Q.; Yu, G.; Liu, Y.; Qin, J.; Li, Q.; Li, Z. *J. Mater. Chem.* **2012**, *22*, 6374.
- (5) Kuimova, M. K.; Yahioğlu, G.; Levitt, J. A.; Suhling, K. *J. Am. Chem. Soc.* **2008**, *130*, 6672.
- (6) Qi, F.; Lin, J.; Wang, X.; Cui, P.; Yan, H.; Gong, S.; Ma, C.; Liu, Z.; Huang, W. *Dalton Trans.* **2016**.
- (7) Chow, Y. L.; Johansson, C. I.; Zhang, Y.-H.; Gautron, R.; Yang, L.; Rassat, A.; Yang, S.-Z. *J. Phys. Org. Chem.* **1996**, *9*, 7.
- (8) Xu, S.; Evans, R. E.; Liu, T.; Zhang, G.; Demas, J. N.; Trindle, C. O.; Fraser, C. L. *Inorg. Chem.* **2013**, *52*, 3597.
- (9) Liu, T.; Chien, A. D.; Lu, J.; Zhang, G.; Fraser, C. L. *J. Mater. Chem.* **2011**, *21*, 8401.
- (10) Zhang, G.; Singer, J. P.; Kooi, S. E.; Evans, R. E.; Thomas, E. L.; Fraser, C. L. *J. Mater. Chem.* **2011**, *21*, 8295.
- (11) Zhang, G.; Lu, J.; Sabat, M.; Fraser, C. L. *J. Am. Chem. Soc.* **2010**, *132*, 2160.

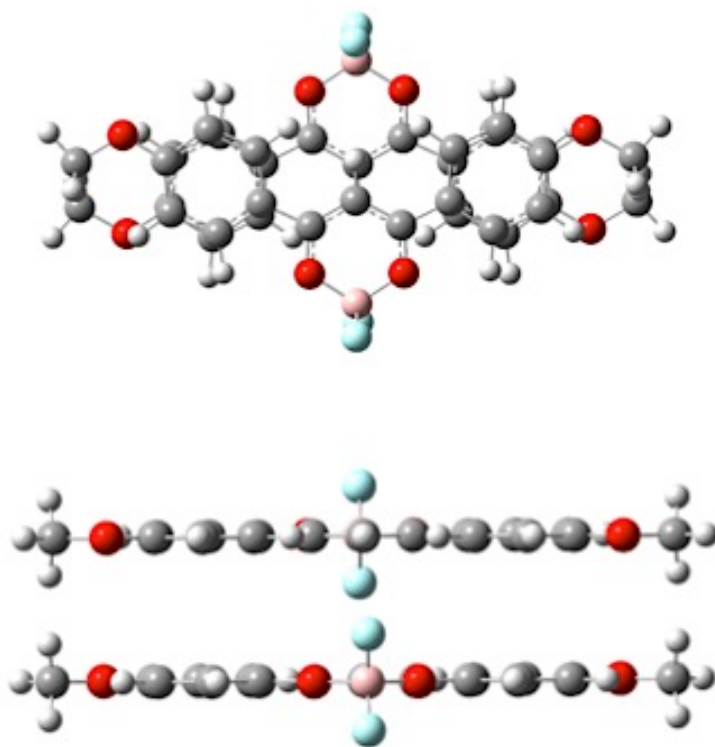
- (12) Nguyen, N. D.; Zhang, G.; Lu, J.; Sherman, A. E.; Fraser, C. L. *J. Mater. Chem.* **2011**, *21*, 8409.
- (13) Sun, X.; Zhang, X.; Li, X.; Liu, S.; Zhang, G. *J. Mater. Chem.* **2012**, *22*, 17332.
- (14) Williams, D. B. G.; Lawton, M. *J. Org. Chem.* **2010**, *75*, 8351.
- (15) Ohtsuka, Y.; Koyasu, K.; Ikeno, T.; Yamada, T. *Org. Lett.* **2001**, *3*, 2543.
- (16) Anstead, G. M.; Altenbach, R. J.; Wilson, S. R.; Katzenellenbogen, J. A. *J. Med. Chem.* **1988**, *31*, 1316.
- (17) Cullinan, G. J.; Eacho, P. I.; Foxworthy-Mason, P. S.; Schelm, J. A.; Eli Lilly and Company, USA . 1999, p 42 pp.
- (18) Carraway, E. R.; Demas, J. N.; DeGraff, B. A.; Bacon, J. R. *Anal. Chem.* **1991**, *63*, 337.
- (19) Zhu, H.; Wang, X.; Li, Y.; Wang, Z.; Yang, F.; Yang, X. *Chem. Commun.* **2009**, *0*, 5118.
- (20) Frisch, M. J.; Trucks, G. W.; Schlegel, H. B.; Scuseria, G. E.; Robb, M. A.; Cheeseman, J. R.; Scalmani, G.; Barone, V.; Mennucci, B.; Petersson, G. A.; Nakatsuji, H.; Caricato, M.; Li, X.; Hratchian, H. P.; Izmaylov, A. F.; Bloino, J.; Zheng, G.; Sonnenberg, J. L.; Hada, M.; Ehara, M.; Toyota, K.; Fukuda, R.; Hasegawa, J.; Ishida, M.; Nakajima, T.; Honda, Y.; Kitao, O.; Nakai, H.; Vreven, T.; Montgomery, J. A.; Peralta, J. E.; Ogliaro, F.; Bearpark, M.; Heyd, J. J.; Brothers, E.; Kudin, K. N.; Staroverov, V. N.; Kobayashi, R.; Normand, J.; Raghavachari, K.; Rendell, A.; Burant, J. C.; Iyengar, S. S.; Tomasi, J.; Cossi, M.; Rega, N.; Millam, J. M.; Klene, M.; Knox, J. E.; Cross, J. B.; Bakken, V.; Adamo, C.; Jaramillo, J.; Gomperts, R.; Stratmann, R. E.; Yazyev, O.; Austin, A. J.; Cammi, R.; Pomelli, C.; Ochterski, J. W.; Martin, R. L.; Morokuma, K.; Zakrzewski, V. G.; Voth, G. A.; Salvador, P.; Dannenberg, J. J.; Dapprich, S.; Daniels, A. D.; Farkas; Foresman, J. B.; Ortiz, J. V.; Cioslowski, J.; Fox, D. J. Wallingford CT, 2009.
- (21) Tomasi, J.; Mennucci, B.; Cammi, R. *Chem. Rev.* **2005**, *105*, 2999.
- (22) Samonina-Kosicka, J.; DeRosa, C. A.; Morris, W. A.; Fan, Z.; Fraser, C. L. *Macromolecules* **2014**, *47*, 3736.
- (23) Hong, Y.; Lam, J. W. Y.; Tang, B. Z. *Chem. Soc. Rev.* **2011**, *40*, 5361.
- (24) Grabowski, Z. R.; Rotkiewicz, K.; Rettig, W. *Chem. Rev.* **2003**, *103*, 3899.

- (25) Zbigniew R. Grabowski, K. R., and Aleksander Siemarczuk *J. Luminesc.* **1979**, 18-19, 420.
- (26) Chai, J.-D.; Head-Gordon, M. *Physical Chem. Chem. Phys.* **2008**, 10, 6615.
- (27) Morris, W. A.; Liu, T.; Fraser, C. L. *J. Mater. Chem. C* **2015**, 352.
- (28) Karpenko, I. A.; Niko, Y.; Yakubovskiy, V. P.; Gerasov, A. O.; Bonnet, D.; Kovtun, Y. P.; Klymchenko, A. S. *J. Mater. Chem. C* **2016**.
- (29) Lakowicz, J. R. *Principles of Fluorescence Spectroscopy*; Springer: New York, Ny, 2007.
- (30) Dong, Y. Q.; Lam, J. W. Y.; Tang, B. Z. *J. Phys. Chem. Lett.* **2015**, 6, 3429.
- (31) Luo, X.; Li, J.; Li, C.; Heng, L.; Dong, Y. Q.; Liu, Z.; Bo, Z.; Tang, B. Z. *Adv. Mater.* **2011**, 23, 3261.
- (32) Yu, G.; Yin, S.; Liu, Y.; Chen, J.; Xu, X.; Sun, X.; Ma, D.; Zhan, X.; Peng, Q.; Shuai, Z.; Tang, B.; Zhu, D.; Fang, W.; Luo, Y. *J. Am. Chem. Soc.* **2005**, 127, 6335.
- (33) Kamimoto, N.; Nakamura, N.; Tsutsumi, A.; Mandai, H.; Mitsudo, K.; Wakamiya, A.; Murata, Y.; Hasegawa, J.-y.; Suga, S. *Asian J. Org. Chem.* **2016**, 373.
- (34) Chung, K.; Kwon, M. S.; Leung, B. M.; Wong-Foy, A. G.; Kim, M. S.; Kim, J.; Takayama, S.; Gierschner, J.; Matzger, A. J.; Kim, J. *ACS Cent. Sci.* **2015**, 1, 94.

Chapter 6

Modeling The Electronic and Optical Properties of Difluoroboron β -Diketonate

Dyes Using Density Functional Theory



6.1 Introduction

Computational chemistry methods can be valuable tools for elucidating information about molecular geometry, optical properties, and electronic transitions in organic fluorophores. The value is considerably greater when these methods can be paired with experimental data to explain phenomena. Previously we used time dependent density functional theory (TD-DFT) calculations to model the absorption spectra and molecular orbitals (MOs) of difluoroboron β -diketonate (BF_2bdk) fluorophores with varying arene substituents.¹ Using computational modeling alongside experimental results in dilute CH_2Cl_2 solution, many unsymmetrical fluorophores displayed complex absorption and emission profiles resulting from species forming red-shifted, twisted intramolecular charge transfer (TICT) states and simpler, blue-shifted π - π^* transitions. A transition from HOMO to LUMO in unsymmetrical dyes often involved a shifting of electron density from the larger arene donor in the HOMO to more even distribution throughout the molecule in the LUMO. Recently, Chibani and coworkers have performed extensive TD-DFT studies on the optical properties of a panel of BF_2bdk fluorophores. They found that replacing the oxygen atoms of the β -diketone with nitrogen induced both bathochromic and hypsochromic spectral shifts in absorption and emission. In the case of a symmetrical 1,3 diketone, replacing OBO with NBN produced a hypsochromic shift in both absorption and emission while this same replacement in an unsymmetric 1,2 diketone produced bathochromic shifts. They also found that increasing π -conjugation length between donor and acceptor groups does not systematically induce charge transfer (CT) character and extending the conjugation around an acceptor OBO unit is the most facile way to red-shift both absorption and emission.² Many experimental results of

BF₂bdk fluorophores in solution and in the solid state are informed by DFT calculations, as this chapter will also demonstrate.

6.2 Results and Discussion

6.2.1 Modeling Molecular Orbitals and Absorption Spectra of Naphthyl-Phenyl β -Diketonate Polymer Initiators

Oxygen sensing is an important application of luminescent materials. Because phosphorescence is often susceptible to collisional quenching by bimolecular oxygen, it can be readily applied to detection methods based on intensity. Such methods are sought after due to their compatibility with common luminescence detection instrumentation.³ Multicomponent systems that combine a phosphor (oxygen sensitive) and fluorophore (oxygen insensitive standard) in an inert matrix processed into nanoparticles or films are common.⁴ Single component, dual emissive BF₂bdk's are unique in that they function as both oxygen sensitive phosphor and oxygen insensitive fluorophore in a polymer matrix. In a seminal study, it was demonstrated that nanoparticles fabricated from BF₂(I)dbmPLA were successful as ratiometric tumor hypoxia imaging agents.⁵ To improve on this method, and attempt to red-shift and enhance phosphorescence intensity for ratiometric oxygen sensing, new materials based on a naphthyl-phenyl motif with and without heavy atom (Br) substituents were investigated. In support of these studies, DFT calculations were performed on the polymer initiators (Figure 6.1) to determine whether their excitations were dominated by ICT or π to π^* transitions, as this is important both in designing dual-emissive organic luminophores and in determining the strength of the heavy-atom effect. Adachi and coworkers have shown how TICT states with substantial geometry changes in S₁ can lead to thermally activated delayed fluorescence (TADF) by

making the energy gap between singlet and triplet excited states small, which is useful for OLED development but detrimental for developing internal standard ratiometric oxygen sensors.⁶ When the energy gap between the S_1 and T_1 excited states is small, intersystem crossing from T_1 back to S_1 can occur and result in delayed fluorescence.⁷ Furthermore, heavy atom effects are greater when more electron density is concentrated on the heavy atom in both the HOMO and LUMO. Electronic transitions of BF_2 bdks depend on their molecular symmetries.¹ According to TD-SCF calculations, the reddest and strongest

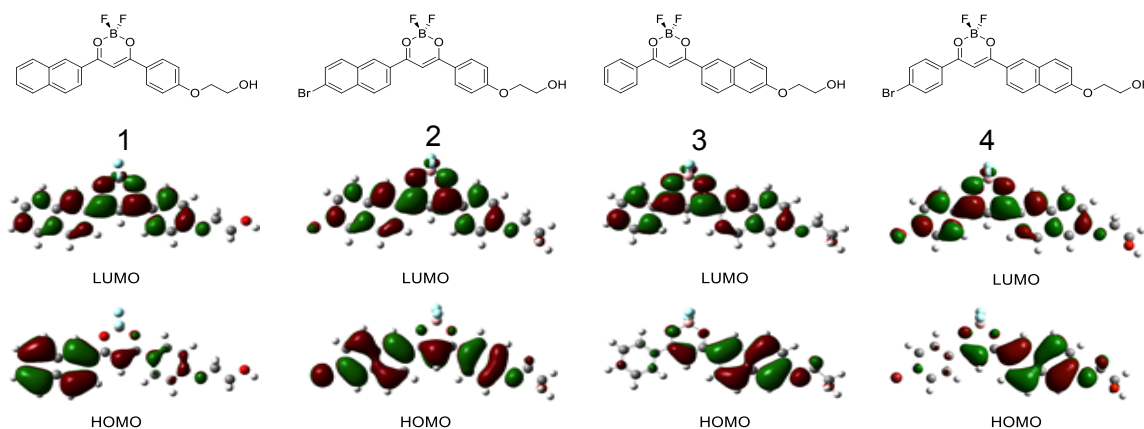


Figure 6.1 Molecular structures and molecular orbital (MO) diagrams for initiators **1-4** depicting the highest occupied molecular orbitals (HOMO) and lowest unoccupied molecular orbitals (LUMO) in CH_2Cl_2 . (Adapted from reference 4).

transitions are dominated by the HOMO to LUMO excitations. An amplitude shift from HOMO to LUMO is observed upon excitation for complexes with unsymmetrical bdk ligands, where there is a disparity in electron donor ability from one arene ring (e.g. anthracene) compared to another (e.g. phenyl). This amplitude shift, paired with experimentally observed red-shifted, broad emissions with long radiative lifetimes (τ_{rad}) suggested that these transitions were intramolecular charge transfer (ICT) in character. For example, a BF_2 bdk naphthyl subunit acts as the donor while the phenyl subunit acts as the acceptor. On the other hand, when the bdk arene rings are comparable (i.e. Ph-Ph

in dbm), a delocalized π to π^* model is proposed.¹ Similar trends are noted here for initiator complexes, **1-4**. Molecular orbital diagrams for compounds **1**, **3**, and **4** suggest ICT character (Figure 6.1). Electron density is localized on the stronger naphthyl donor in the HOMOs whereas in the LUMOs amplitude is more uniformly distributed across the molecular structure. For **2** the electron density is distributed throughout the molecular structure in both HOMO and LUMO and the π to π^* transition dominates. The inductively electron withdrawing bromide substituent may diminish electron density on the naphthyl ring. Another possibility is that the lone pair on the Br atom could act as a π donor and mix with the HOMO, making the amplitude in the molecular orbital predominantly focused on Br instead of the ring. Either way, the donor capacities of Br-Np and Ph-OR rings are comparable. Experimental absorption and emission data lend credence to this claim (Table 6.1). Radiative lifetimes (τ_{rad}) increase with increasing ICT character which is consistent with the molecular twisting between donor and acceptor subunits expected to occur in the excited state.⁸ This is a trend that is observed for samples **1**, **3** and **5** (3.88-5.33 ns) compared to **2** (2.89 ns), with **2** showing the shortest τ_{rad} . Additionally, both **3** and **5** have larger Stokes shifts compared to **1** and **2**. This is consistent with a geometry change in the excited state that can be expected for compounds with stronger charge transfer character.¹ As in naphthyl model studies,¹ these systems show no distinct ICT features in absorption or emission spectra.

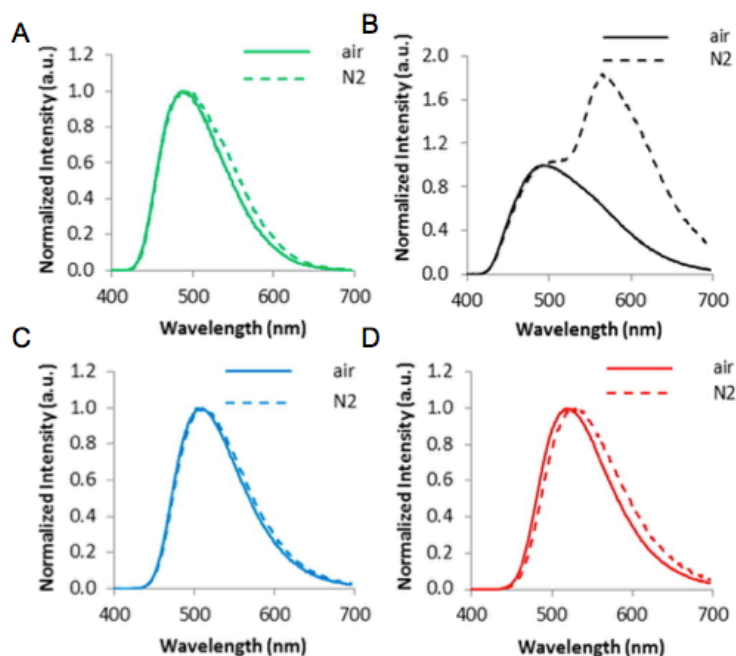
When PLA polymers were grown from the initiators and fabricated as films, we found that polymers grown from initiator **2** exhibited dual emission in a N₂ atmosphere (i.e. oxygen free). In other words, total emission spectra revealed two distinct peaks, a fluorescence peak and a red-shifted phosphorescence peak. This indicates compatibility

for ratiometric oxygen sensing since oxygen should quench the phosphorescence while leaving the fluorescence unaffected. However, polymers grown from the other initiators only exhibited fluorescence whether at room temperature under air or in an oxygen-free environment; no distinct phosphorescence peak or only weak triplet emission was noted under these conditions.⁴ The aforementioned computational results provide a reasonable explanation for this difference in behavior. Molecular twisting in the excited state associated with charge transfer excited states can result in delayed emission dominated by TADF instead of phosphorescence.⁶ This may be true for polymers grown from initiators **1**, **3**, and **4** given computational data indicates that their dominant HOMO to LUMO excitations are largely ICT in character. Also, as a result of ICT in these initiators, there is reduced amplitude on the Br heavy atom in the HOMOs and LUMOs while the π to π^* dominated transition of initiator **2** places considerable amplitude on Br in both the HOMO and LUMO. This would lead to a much stronger heavy atom effect and, thus observable phosphorescence. The presence of a heavy atom (e.g. Br) increases intersystem crossing by enhancing spin-orbit coupling.⁹ The reason for the aforementioned behavior of polymer films under a N_2 atmosphere may be due to a combination of these two factors.

Table 6.1 Absorption and Emission Data for Boron Initiators and Representative Polymer Samples in CH₂Cl₂.⁴

Initiator	λ_{abs}^a (nm)	λ_{abs}^b (nm)	ϵ^c (M ⁻¹ cm ⁻¹)	λ_{em}^d (nm)	τ_{F}^e (ns)	Φ_{F}^f	τ_{rad}^g	Stokes shift (cm ⁻¹)
1	414	482	59,000	452	1.55	0.40	3.88	2,031
2	417	424	65,000	448	0.53	0.19	2.79	1,659
3	418	462	52,000	505	3.41	0.64	5.33	4,121
4	425	471	48,000	521	3.33	0.75	4.44	4,336

^aAbsorption maxima. ^bComputationally generated absorption maxima. ^cExtinction coefficients calculated at the absorption maxima. ^dFluorescence emission maxima. ^eFluorescence lifetime excited with a 369 nm light-emitting diode (LED) monitored at the emission maximum. All fluorescence lifetimes are fitted with single-exponential decay. ^fRelative quantum yield, with anthracene in EtOH as a standard. ^gRadiative lifetime, where $\tau_{\text{rad}} = \tau_{\text{F}} / \Phi_{\text{F}}$.

**Figure 6.2** Total emission spectra for PLA polymers grown from initiators **1** (A), **2** (B), **3** (C), and **4** (D) under both air and nitrogen atmospheres. (Adapted from reference 4).

6.2.2 Computational Investigations into the Solution Optical Properties of Dinaphthoyl β -Diketones and Their Boronated Counterparts

Thorough investigation of BF₂bdk fluorophores has revealed many impressive and unique optical properties both in solution and the solid state, including high quantum yields and mechanochromic luminescence.^{1,10} However, less attention has been paid to the optical properties of their non-boronated bdk precursors. Dibenzoylmethane derivatives containing only phenyl moieties do not display impressive optical properties (i.e. high quantum yields or ML). Easy twisting of the unconstrained bdk moieties creates non-radiative decay pathways in solution and prevents the formation of emissive aggregates in the solid state.¹¹ However, we discovered that a dinaphthoylmethane (dnm) derivative, methoxydinaphthoylmethane (dnmOMe) (Figure 6.3), exhibits rather intriguing optical properties both in solution and the solid state.¹² In solution, the compound exhibited solvatochromism. Also, as non-solvent was added and the molecules were forced to aggregate, enhanced emission was observed (AIE) (Figure 6.3). As a spin-cast film on glass, the dye exhibited unique "turn-on" ML behavior, wherein emission intensity dramatically increased when annealed films were smeared (Figure 6.3).¹²

In solution, the optical properties of dnmOMe were unremarkable by comparison to BF₂bdk. Absorption spectra revealed a peak at 378 nm ($\epsilon = 34,000 \text{ M}^{-1} \text{ cm}^{-1}$) and a weak emission ($\Phi \sim 0.2\%$) with a peak at 443 nm.¹² The weak emission in solution is due to non-radiative decay pathways available in the flexible bdk unrestrained by tetra-coordinate boron. The fluorescence lifetime (τ_f) recorded at the peak emission required a multi-exponential decay model, with a pre-exponential weighted lifetime (τ_{pw0}) of 0.18 ns. The multi-exponential decay suggests multiple emissive species in solution. ¹H NMR

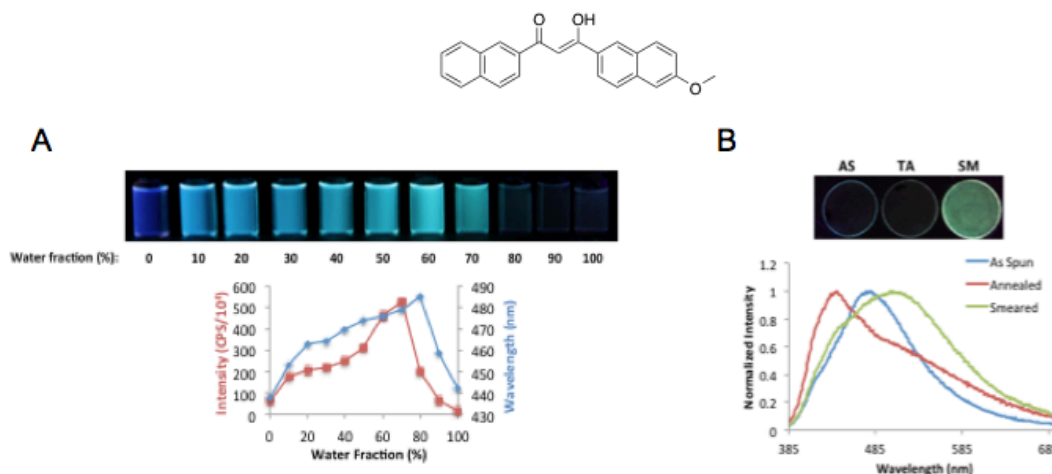


Figure 6.3 A) AIE of dnmOME in increasing water fractions (f_w) with THF as the solvent. B) ML behavior of the dye as a spin-cast film on glass. (Adapted from reference 11).

spectroscopy revealed that both keto and enol forms are present.¹² This tautomerization is common for bdk.¹³ In order to better understand how different forms of the bdk might affect optical properties, DFT calculations were performed on the structures shown in Figure 6.4. According to ground state optimization calculations, **1** was lower in energy compared to **2** (-1151.09786328 a.u. vs. -1151.09782143 a.u.), though the difference was quite small (~ 0.026 kcal/mol) (Table S6.4 Appendix E). This makes the Boltzmann distribution of **1:2** > 0.9 under ambient conditions, making them present in roughly equal parts in solution based purely upon the energies of the computed structures. Compounds **1** and **2** have quite similar MO diagrams, showing amplitude mainly on the major donor (the methoxynaphthyl ring) in the HOMO and more evenly distributed throughout the molecule in the LUMO (Figure 6.5). Interestingly, DFT calculations revealed that the

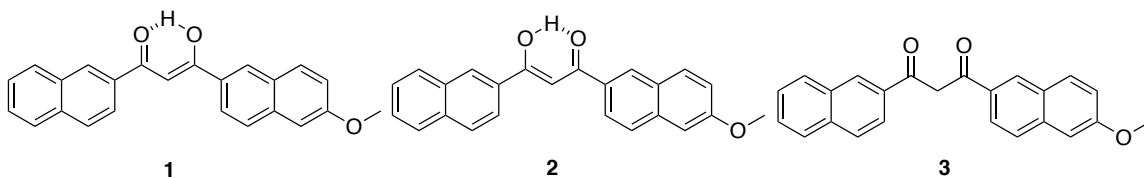


Figure 6.4 Possible structures of dnm(OMe) examined using DFT calculations.

diketone form (**3**) had the lowest energy of all studied structures (-1151.09821786 a.u.), though the structure was highly twisted. The energy difference is still relatively small when compared to the averaged energies of **1** and **2** (~0.236 kcal/mol more stable). This makes the Boltzmann distribution of enol:ketone ~0.7 under ambient conditions based purely on the computed energies of the structures. Just as in the MO diagrams of the enol variants, amplitude goes from being mainly concentrated on the major donor in the HOMO to being more evenly distributed throughout the molecule in the LUMO. The dominance of the twisted ketone form and contributions from non-radiative decay pathways could explain why this dye shows such weak emissions in dilute solution but becomes emissive when aggregates are formed.

In order to further probe the properties of dinaphthyl bdk systems and see what perturbations boron coordination may yield, a full series of dinaphthyl bdks and their boronated counterparts were synthesized (Figure 6.6).¹⁴ Just as was observed for dnmOMe, the dnm bdks had weak emission in dilute CH₂Cl₂ solution despite substitutions (Table 6.1). However, the methoxy-substituted dnm derivatives did exhibit

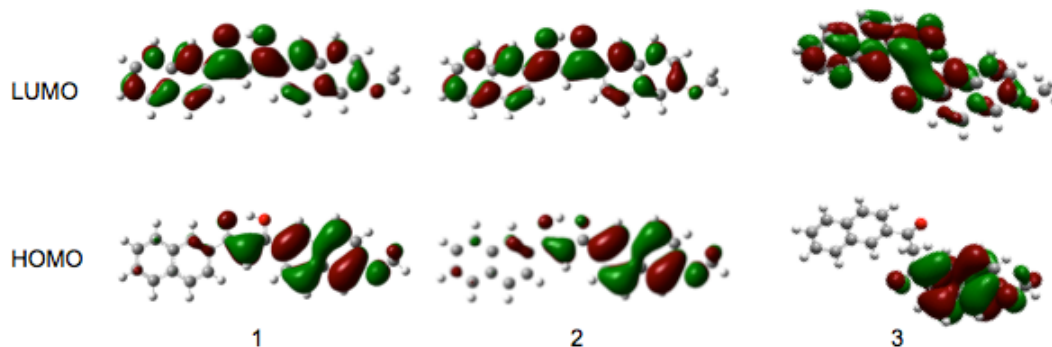


Figure 6.5 Molecular orbital (MO) diagrams of the enol and keto tautomers of dnm(OMe) showing their respective HOMOs and LUMOs.

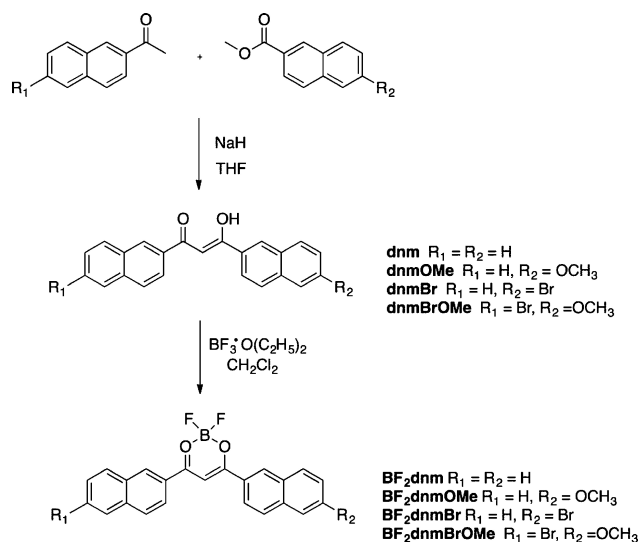


Figure 6.6 Synthesis and molecular structures of dinaphthylmethane (dnm) β -diketones and their boronated counterparts. (Adapted from reference 14).

moderate solvatochromism in addition to AIE. As would be expected, the boronated BF_2dnm compounds exhibited much brighter emissions in solution and the solid-state. Both the dnm-derived ligands and boronated compounds also exhibited high contrast, tunable ML behavior, though we were not able to model these phenomena *via* computational methods.¹⁴ DFT calculations with a Tomasi polarized continuum for

Table 6.2 Optical Properties of β -Diketones and Difluoroboron Complexes in CH_2Cl_2 ^{a14}

Compound	λ_{abs}^b (nm)	ϵ ($\text{M}^{-1}\text{cm}^{-1}$)	λ_{em}^c (nm)	Φ	τ (ns)
dnm	371	32,000	430	0.07	0.03
dnmOMe	378	34,000	443	< 0.01	0.18
dnmBr	372	37,000	446	0.09	0.23
dnmBrOMe	382	39,000	447	< 0.01	0.17
BF_2dnm	421	47,000	479	0.68	1.7
BF_2dnmOMe	435	51,000	514	0.70	2.5
BF_2dnmBr	423	61,000	483	0.39	1.8
$\text{BF}_2\text{dnmBrOMe}$	436	61,000	519	0.67	2.1

^aExcited at 369 nm, room temperature, air. ^bAbsorbance maximum.

^cEmission maximum

dichloromethane solvent were utilized to model excitations and generate MO diagrams to better understand the dominant transitions in these compounds (Figure 6.7). As with dnmOMe, all of the bdk ligands show nearly planar configurations when the optimized geometries were computed for their enol forms. However, the non-emissive, highly twisted ketone tautomers may exist in solution and this may be the cause of the observed low quantum yields. With the exception of the symmetrical diketone ligand, dnm, the HOMO of each dnm ligand showed amplitude mostly localized on the major donor (i.e. the methoxy-substituted ring) and then delocalized throughout the molecule in the LUMO. For example, dnmOMe and dnmBrOMe showed amplitude on the methoxy-substituted naphthyl ring in the HOMO, whereas the majority of electron density is located on the unsubstituted naphthyl ring of dnmBr. Except in the case of symmetrical dnm, which undergoes a π to π^* transition, these results suggest that all ligands undergo an ICT transition, regardless of bromo or methoxy substitution. This is consistent with previous reports for symmetrical and unsymmetrical systems¹ and is further supported

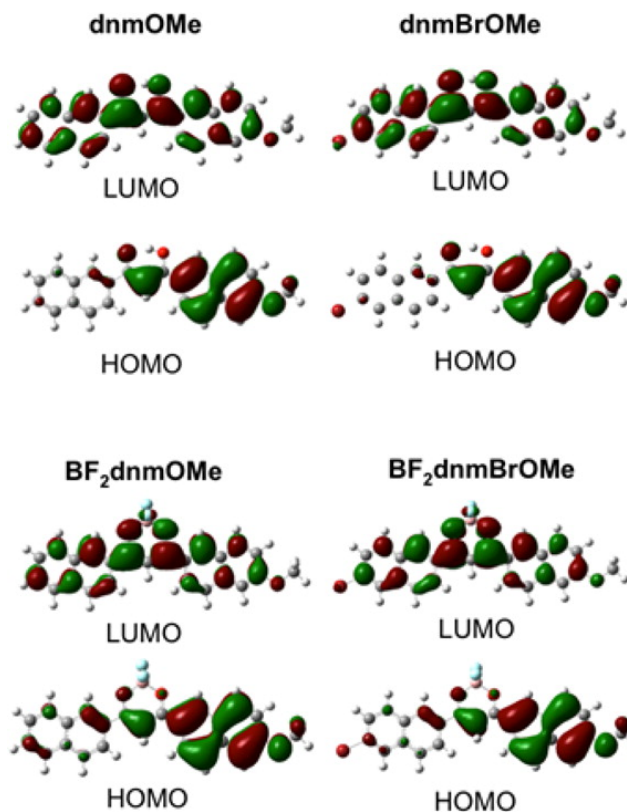


Figure 6.7 Molecular orbital (MO) diagrams of selected dnm ligands and their corresponding boronated complexes showing the HOMOs and LUMOs. (Adapted from reference 14).

experimentally by the relatively large Stokes shifts the ligands experience in dilute CH_2Cl_2 solution ($3,698\text{--}4460\text{ cm}^{-1}$) compared to the boronated complexes ($2,876\text{--}3,668\text{ cm}^{-1}$). For the HOMOs of the boron complexes, some electron density is observed on each naphthyl ring. However, electron density is much more concentrated on the methoxy-substituted naphthyl ring of BF_2dnmOMe and $\text{BF}_2\text{dnmBrOMe}$. For all boron complexes, electron density is distributed throughout the entire LUMO. On the basis of these results, it seems that BF_2dnm and BF_2dnmBr undergo predominantly π to π^*

transitions compared to BF₂dnmOMe and BF₂dnmBrOMe, which show greater ICT character.

6.2.3 Computational Investigations into the Solution Optical Properties of Thienyl Difluoroboron β -Diketonates.

One of the challenges in designing BF₂bdk fluorophores for biological imaging applications is developing a reliable strategy for color tuning. Most current BF₂bdk systems emit in the blue to yellow portion of the visible spectrum.⁵ In particular, redder emissions are desired to provide deeper tissue penetration, less interference from biological autofluorescence, and reduced photo-damage to biological systems.^{15,16} Simply increasing the π conjugation of these materials to achieve this has limitations, including activation of TADF.¹⁷ However, certain heterocycles show promising properties. Yam and coworkers have developed thienyl BF₂bdk with absorption in the near-IR region.¹⁸ Here, we continue our investigation of BF₂bdk structure-property relationships for applications in biological imaging with a series of thienyl-substituted dyes (Figure 6.8). DFT calculations were utilized to model the excitations and MOs of these dyes in CH₂Cl₂ solution and the results were compared to experimental data (Table 6.3).¹⁴

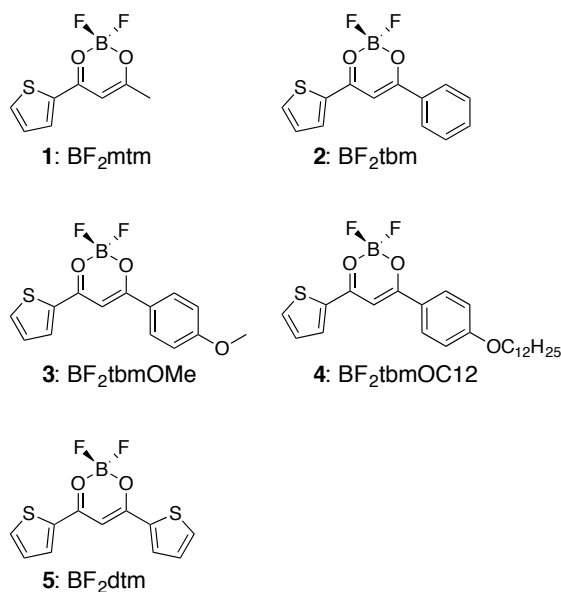


Figure 6.8 Molecular structures of thienyl-substituted dyes.

Table 6.3 Optical Properties of Boron Complexes **1-5** in CH₂Cl₂.¹⁹

Sample	λ_{abs}^a (nm)	λ_{abs}^b (nm)	ϵ^c (M ⁻¹ cm ⁻¹)	λ_{em}^d (nm)	τ_F^e (ns)	Φ_F^f
1	354	341	44,000	392	0.18	0.04
2	401	383	46,400	416	1.83	0.31
3	417	406	56,000	441	2.06	0.38
4	418	-	61,900	445	2.08	0.71
5	420	-	57,200	438	1.02	0.39

^aAbsorption maxima. ^bComputationally generated absorption maxima. ^cExtinction coefficients calculated at the absorption maxima. ^dFluorescence emission maxima excited at 369 nm (except **1**, excited at 350 nm). ^eFluorescence lifetime excited with a 369 nm light-emitting diode (LED) monitored at the emission maximum. All fluorescence lifetimes are fitted with single-exponential decay. ^fRelative quantum yield, with anthracene in EtOH as a standard.

For most compounds, the computed λ_{abs} are in good agreement with the experimental values (Table 6.3 and Table S6.7 Appendix E). The one exception is complex **2**, for which the computed λ_{abs} is blue-shifted ~20 nm compared to the

experimental value. The absorption spectra are almost entirely dominated by HOMO to LUMO transitions. Furthermore, the HOMO to LUMO transitions appeared to be π to π^* corresponding to S_0 to S_1 transitions, with no intramolecular charge transfer (ICT) bands evident from the experimental absorption spectra.¹⁹ Specifically, the absorption spectra of all dyes exhibit blue-shifted λ_{abs} (354-420 nm) with high extinction coefficients (44,000-57,200 $\text{M}^{-1} \text{cm}^{-1}$) typical of π to π^* transitions and no broad, red-shifted bands often observed for ICT transitions.¹ All of the dyes exhibit relatively small Stokes shifts (i.e. 900-2739 cm^{-1}). The molecular orbital diagrams also support this qualitatively. Only a slight transfer of amplitude seems to occur from the aromatic rings to the BF_2bdk moiety when going from the HOMO to the LUMO of these compounds (Figure 6.9). This is an interesting result. In the past, transitions predominantly π to π^* in character have been observed when studying BF_2 complexes with symmetrical diarene ligands. However, when the compound contains an unsymmetrical diarene ligand, the HOMO to LUMO transition typically shows a shifting in electron density. In this case, we observe unsymmetrical compounds with electron density evenly distributed throughout the molecules in both HOMO and LUMO. Perhaps this is due to the thiophene ring being relatively similar in size and electronic character to the phenyl ring, in contrast to a naphthylene or anthracene moiety, as characterized in previous studies.¹ In the case of the thiophene-methyl compound **1**, the reason why no strong ICT is observed may be because the methyl moiety is slightly electron donating and would, therefore, elevate π^* MOs and reduce charge transfer. As a result, we only observe a slight qualitative charge transfer in the MO diagrams from the thiophene ring to the BF_2 moiety. Ono *et al.* have previously performed calculations on compound **5** using methods similar to our own. As

would be expected for the symmetrical di-thienyl BF₂bdk, MO diagrams indicate that the HOMO to LUMO transition of this compound is also π - π^* in character²⁰

In order to better understand and control both luminescence color and oxygen sensitivity, heavy atoms (Br or I) and thiophene subunits were introduced into the dye scaffold (Figure 6.10). MO diagrams for selected Br-substituted dyes are shown in Figure 6.11. These MOs show, qualitatively, that substitution of a heavy atom at the 2 position of the thiophene subunit in these dyes does not fundamentally alter the π to π^* nature of the HOMO to LUMO transition. However, adding a phenyl to the opposing side of the dye scaffold seems to decrease amplitude concentrated on the heavy atom, particularly in the HOMO. A consequence of this may be the increase in quantum yield we see for these dyes in solution as a result of decreasing influence of the heavy atom effect. Understanding the influence different substituents have on the heavy atom effect in these dyes could be important to tuning fluorescence to phosphorescence (F/P) ratios for ratiometric oxygen sensing.

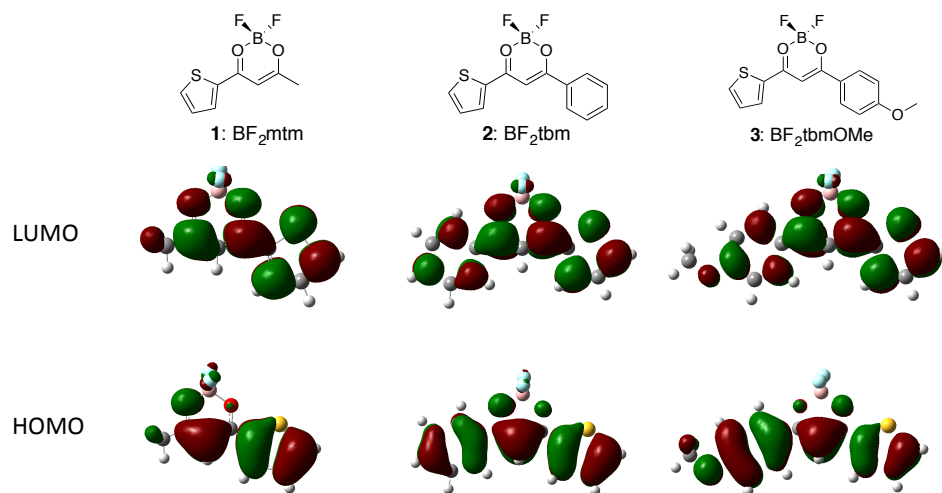


Figure 6.9 Calculated HOMO and LUMO molecular orbitals for **1-3** indicating π to π^* character with minimal charge transfer evident when going from HOMO to LUMO.

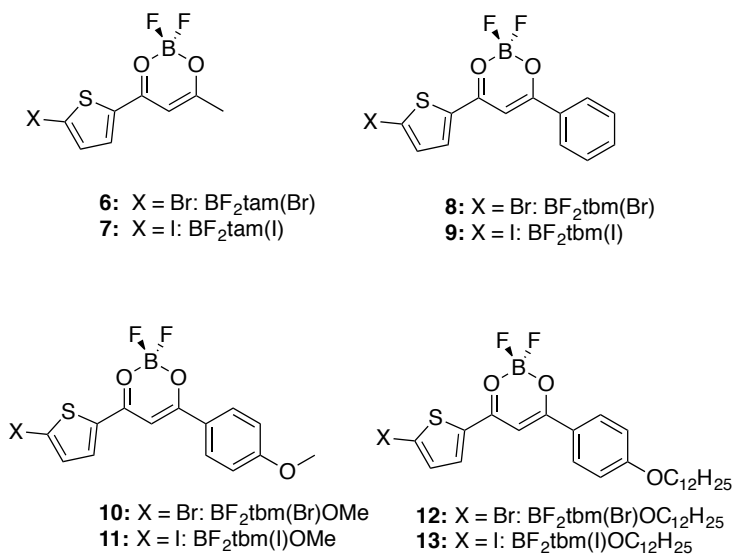
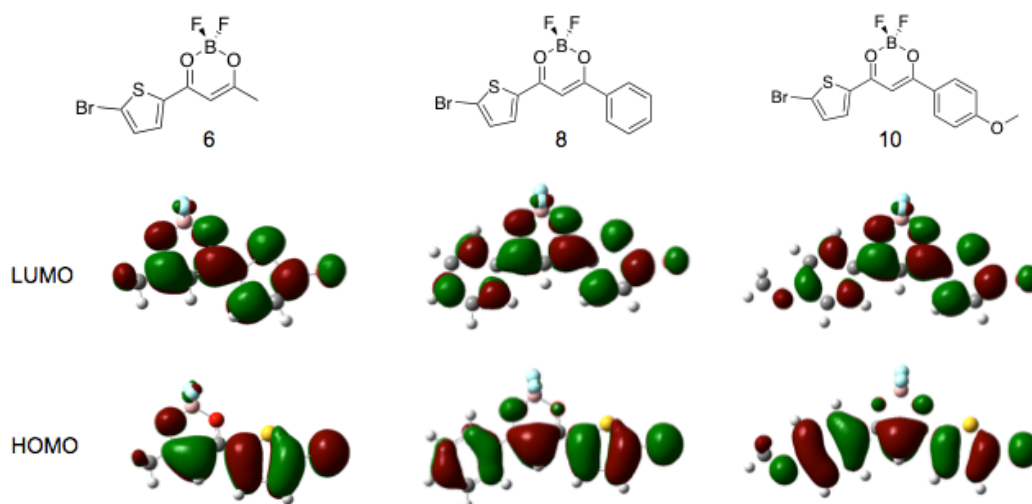


Figure 6.10 Molecular structures of heavy atom-substituted thienyl BF_2bdk derivatives.

Table 6.4 Optical Properties of Heavy Atom-Substituted Thienyl Boron Dyes in CH₂Cl₂

Sample	λ_{abs}^a (nm)	λ_{abs}^b (nm)	ϵ^c (M ⁻¹ cm ⁻¹)	λ_{em}^d (nm)	τ_{F}^e (ns)	Φ_{F}^f
6	365	362	36,600	407	0.50	0.18
7	371	371	32,100	412	0.55	0.25
8	411	401	42,500	432	1.28	0.31
9	419	407	48,400	442	0.87	0.30
10	426	420	69,100	452	1.44	0.50
11	431	423	55,300	458	0.94	0.35
12	429	-	69,400	459	1.51	0.58
13	434	-	65,400	461	0.92	0.37

^aAbsorption maxima. ^bComputationally generated absorption maxima. ^cExtinction coefficients calculated at the absorption maxima. ^dFluorescence emission maxima excited at 369 nm. ^eFluorescence lifetime excited with a 369 nm light-emitting diode (LED) monitored at the emission maximum. All fluorescence lifetimes are fitted with single-exponential decay. ^fRelative quantum yield, versus anthracene in EtOH as a standard.

**Figure 6.11** Calculated HOMO and LUMO molecular orbitals for **6**, **8**, and **10** indicating π - π^* character.

6.2.4 *Toward Computational Modeling of the Solid State Emission Properties of Difluoroboron β -Diketonates*

Calculations discussed so far deal with single dye molecules in solution. However, it is well known that the emission properties of solid-state organic luminophores arise from aggregate species.^{21,22} Aggregation state changes are believed to be responsible for ML behavior.²¹

In order to begin to model aggregate effects on the emissions of BF₂bdks using computational methods, at least, two molecules must be involved. Previous experiments and results of X-ray crystallography studies have suggested that dimers of these molecules tend to arrange themselves in either face-to-face H-aggregate or offset J-aggregate configurations.^{21,23} Therefore, probing the excitation properties of dimeric species in similar orientations may lend insight into ML phenomena. BF₂dbm(OMe)₂ is a relatively simple, symmetric BF₂bdk known to exhibit both bright emission and ML in the solid state.²¹ Therefore, it was selected as a starting point for these studies.

The face-to-face H-aggregate was investigated first, given that it is symmetric and optimization of this form should be simpler. Only single-point energy calculations utilizing ω B97XD/6-31+G(d) were performed to determine energies of dimer configurations. To generate coordinates of the second member of a dimer, rigid rotation and translation operations were applied to the coordinates of a reference monomer. The first dimer generated has monomers in parallel planes, with dipole moments oriented antiparallel, as shown in Figure 6.12. The optimum (i.e. lowest energy) dimer configuration of this H-type has a separation of 3.50 Å between monomer planes. Mirochnik and coworkers have previously reported that, in crystals, these molecules are

separated by 3.52 Å; however the observed structure is the offset J-aggregate-type, packing.²³ Beginning with the optimized H-dimer, TD-DFT calculations using ω B97XD/6-311+G(d) were performed to model excitations of the species and ω B97XD/6-31G(d) calculations were used to generate MOs. Calculations were also performed at other separations between the monomer planes to probe what effect intermolecular distance has on excitations.

The absorption spectrum computed for the optimum H-aggregate with an intermolecular distance of 3.50 Å revealed that the strong red transition at 328.84 nm was comprised of a strong HOMO to LUMO+1 transition and a slightly weaker HOMO-1 to LUMO transition (Table S6.11 Appendix E). MO pictures showed considerable overlap between the orbitals of the two monomers for both the HOMO-1 and the LUMO (Figure 6.13) For the dimer with $X = 4.00$ Å, the strongest transition in the absorption trace was only slightly blue-shifted, to 326.10 nm and is composed of almost equal weights of the single electron excitations HOMO-1 to LUMO and HOMO to LUMO+1. However, in this case, there is no overlap apparent between the MOs of the two monomers. At 6.00 Å separation, the MOs show π to π^* transitions localized on each individual monomer.

All of the dimers had a strong singlet excited state near 326 nm for intramolecular distances in X ranging from 3.50 to 6.00 Å (Table S6.11 Appendix E). The dimer with an intermolecular distance of 3.00 Å (which is strongly destabilized, and energetically inaccessible) had a drastically red-shifted excitation at ~346 nm. All of the dimers had a dark singlet (i.e. oscillator strength of zero) excited state. The energy of this excitation varies with dimer separation as shown in (Figure 6.14). As the separation between dimers increases, the energies of this dark state and the bright state converge; these states are

essentially the two combinations (symmetric and antisymmetric) of the two excitations HOMO-1 to LUMO and HOMO to LUMO+1 . It is difficult to say how this behavior may be expressed in solid state emission, but the presence of a lower-lying singlet state at closer intermolecular distances in H-aggregates may contribute to the shift seen in emission when these aggregates are formed. Perhaps energy transfer to this low-lying state can occur once the molecule is excited, leading to red-shifted emission. In fact, Cornil *et al.* have computationally observed a similar convergence of a "bright" and "dark" singlet state as interchain distances between two cofacial stilbene monomers increased. They attributed the higher energy "bright" singlet state to constructive interactions between intrachain transition dipole moments and the lower energy "dark" singlet state to destructive interactions between intrachain transition dipole moments.²⁴ Further study into how these states may affect the solid-state and ML emissive properties of BF₂bdk's, specifically, is required. In particular, calculations that simulate both emission and energy transfer in the excited state will need to be explored. It may well be that more than two monomers need to be considered, in order to represent configurations other than the optimum H-aggregate.

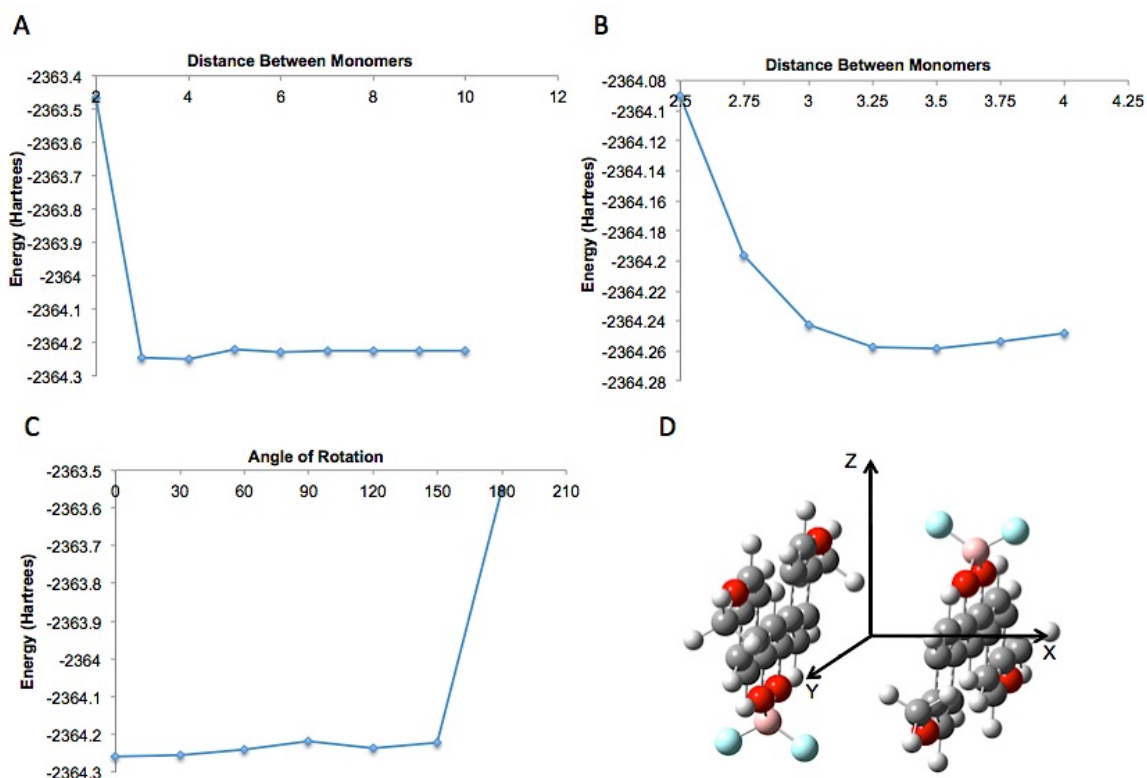


Figure 6.12 A) Plot of the distance between monomers in the X-axis (defined in D) vs. the computed energy of the system. B) Plot of the distance between monomers in the X-axis between 2.5 Å and 4 Å. The minimum energy was determined to be at an intermolecular distance of ~3.5 Å. C) Plot of rotations of one monomer vs. the computed energy of the system with 0° being a configuration wherein the monomers are oriented in an anti-parallel fashion with the BF₂ moieties opposite one-another. The original antiparallel configuration was found to be optimal. In these calculations the monomers were kept at the optimum distance in the X-axis of 3.5 Å. D) A side view of the dimer with the Cartesian axis defined.

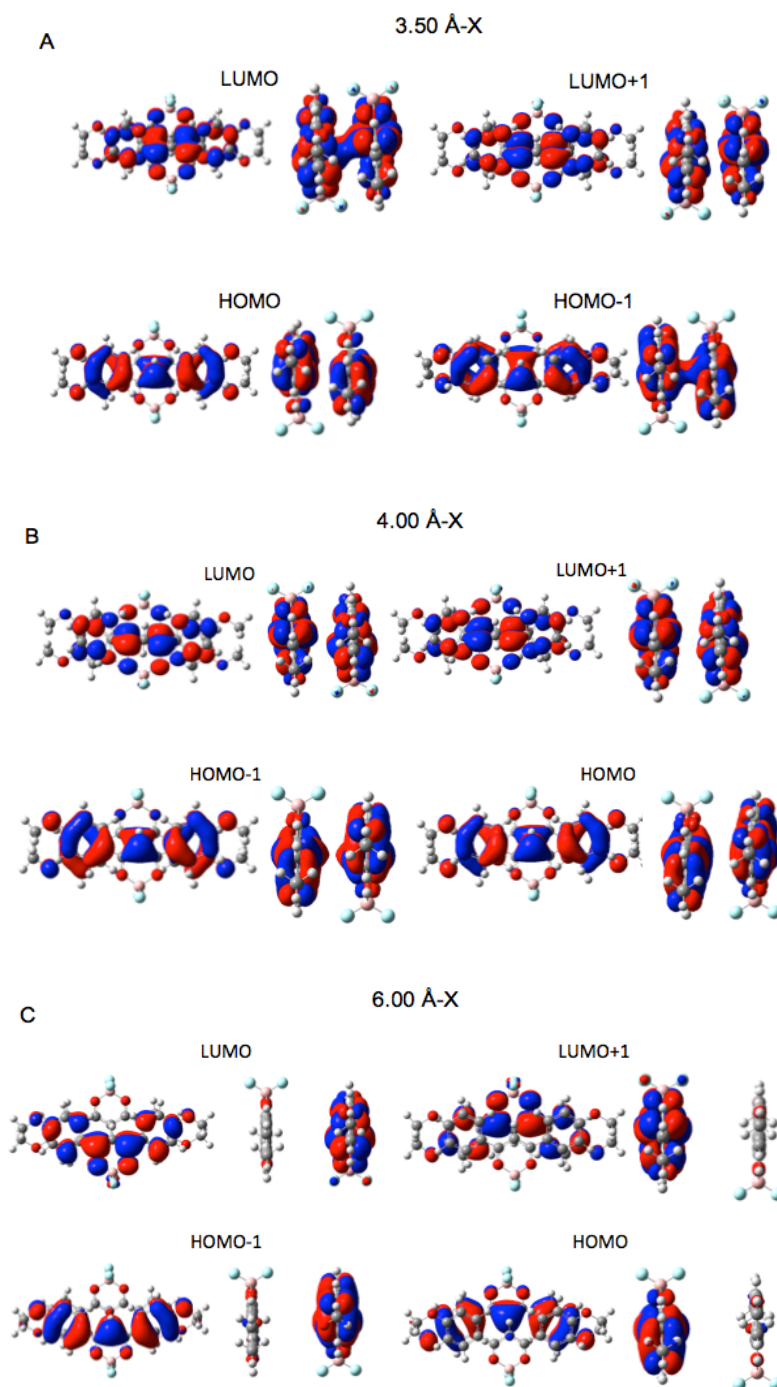


Figure 6.13 Molecular orbitals visualized for the dimer in various configurations. A) Selected molecular orbitals (MOs) for the H-aggregate with a distance of 3.50 Å between the monomers in the X-axis. B) Selected MOs for the H-aggregate with a distance of 4.00 Å between the monomers in the X-axis. C) Selected MOs for the H-aggregate with a distance of 6.00 Å between the monomers in the X-axis.

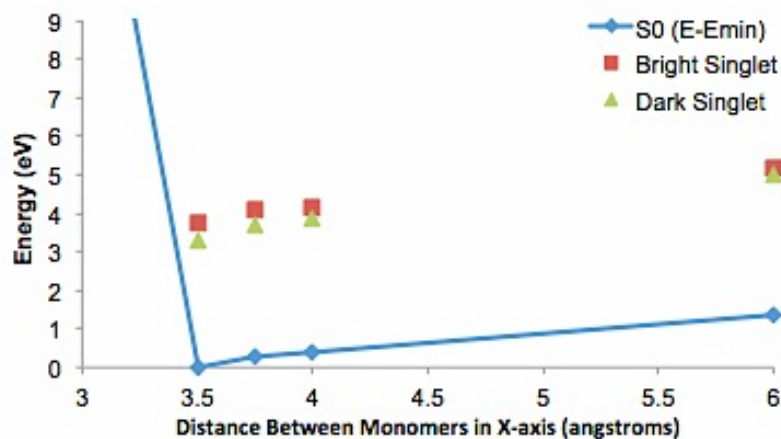


Figure 6.14 A plot showing the relative energies of the bright and dark singlet excited states as they compare to the ground state (S_0) energy. The energies of the ground states are normalized to be energy of the state minus the minimum energy in electron volts (eV).

6.3 Conclusions

DFT methods were utilized to predict and explain the emission properties of BF_2bdk dyes in solution with varying heavy atom and heterocycle substituents. It was found that relatively simple and accessible DFT calculations can be used to model and successfully predict behavior and explain experimental results of BF_2bdk dyes and their ligand counterparts in dilute solution and polymeric materials. Specifically, it is shown that for naphthyl and heavy atom-substituted BF_2bdks covalently linked to PLA, π to π^* , non-ICT transitions from HOMO to LUMO are preferred for ratiometric oxygen sensing. Also, having significant amplitude on the Br heavy atom in both HOMO and LUMO is preferred for these purposes.

It was also shown that the methoxy-substituted dinaphthyl ligand, dnmOMe , most likely shows AIE due to the presence of a dominate, non-emissive twisted ketone species in dilute solution. Also, boronated dinaphthyl bdks (BF_2dnm) showed π to π^* HOMO to

LUMO transitions, whereas simple substitution of a methoxy group on one of the naphthyl rings induced significant charge transfer character. Substitution on the opposing naphthyl ring with Br did little to alter these properties.

Unsymmetrical thiophene heterocycle-substituted BF₂bdk's showed primarily π to π^* transitions from HOMO to LUMO despite being unsymmetrical. Substitutions with Br and I heavy atoms at the 2 position of the thiophene rings did not induce charge transfer character. However, having phenyl substituents on the opposing side of the dye seemed to reduce amplitude on the heavy atom when compared to dyes bearing only a thiophene ring.

Preliminary modeling of the optical properties of BF₂bdk dyes in the solid state suggests that aggregation does have significant effects on electronic states. To be more specific, intermolecular distance between two monomers alters the relative positions of a “bright” singlet with a large oscillator strength and a “dark” singlet with an oscillator strength of zero. To better capture aggregation effects and achieve predictive modeling of solid-state emission properties, more sophisticated models taking into account energy transfer and a range of geometries for larger clusters will be required for further progress.

6.4 Acknowledgements

Jelena Samonina-Kosicka and Christopher DeRosa are acknowledged for carrying out the syntheses and collecting experimental data for the compounds and polymers in 6.2.1. The work in 6.2.1 is published in *Macromolecules*.⁴ Tristan Butler and Jelena Samonina-Kosicka are acknowledged for carrying out the syntheses and collecting experimental data for the compounds in 6.2.2. Much of the work in 6.2.2 is published in *Chemical Communications*¹² and *ACS Applied Materials and Interfaces*.¹⁴ Milena

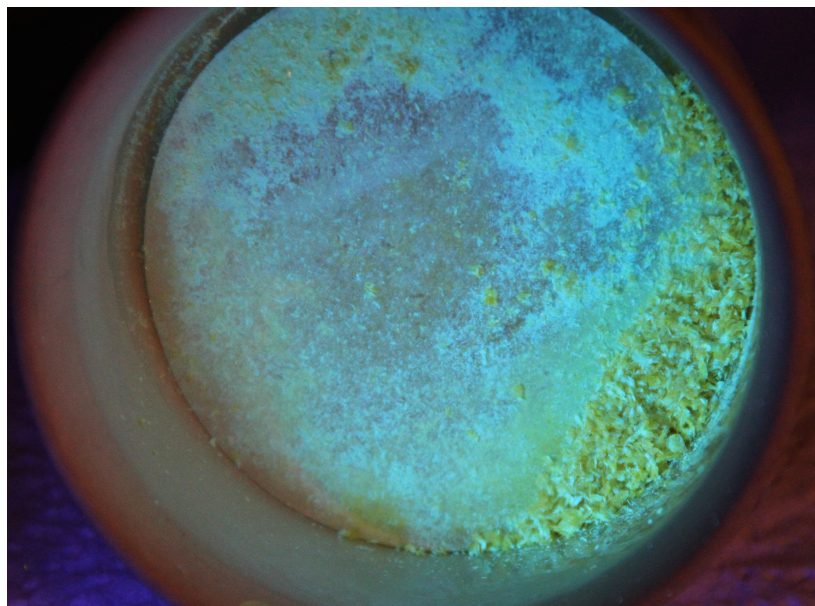
Kolpaczynska and Christopher Derosa are acknowledged for carrying out the syntheses and collecting experimental data for the compounds in 6.2.3. The work in 6.2.3 concerning non heavy atom-substituted thienyl compounds is published in the *Australian Journal of Chemistry*.¹⁹ Professor Carl O. Trindle is acknowledged for guidance and helpful discussions concerning the studies carried out in 6.2.4.

6.5 References

- (1) Xu, S.; Evans, R. E.; Liu, T.; Zhang, G.; Demas, J. N.; Trindle, C. O.; Fraser, C. L. *Inorg. Chem.* **2013**, *52*, 3597.
- (2) Chibani, S.; Charaf-Eddin, A.; Mennucci, B.; Le Guennic, B.; Jacquemin, D. *J. Chem. Theory Comput.* **2014**, *10*, 805.
- (3) Meier, R. J.; Schreml, S.; Wang, X.-d.; Landthaler, M.; Babilas, P.; Wolfbeis, O. S. *Angew. Chem. Int. Ed.* **2011**, *50*, 10893.
- (4) Samonina-Kosicka, J.; DeRosa, C. A.; Morris, W. A.; Fan, Z.; Fraser, C. L. *Macromolecules* **2014**, *47*, 3736.
- (5) Zhang, G.; Palmer, G. M.; Dewhirst, M. W.; Fraser, C. L. *Nat. Mater.* **2009**, *8*, 747.
- (6) Uoyama, H.; Goushi, K.; Shizu, K.; Nomura, H.; Adachi, C. *Nature* **2012**, *492*, 234.
- (7) Zhang, Q.; Li, J.; Shizu, K.; Huang, S.; Hirata, S.; Miyazaki, H.; Adachi, C. *J. Am. Chem. Soc.* **2012**, *134*, 14706.
- (8) Grabowski, Z. R.; Rotkiewicz, K.; Rettig, W. *Chem. Rev.* **2003**, *103*, 3899.
- (9) Lower, S. K. E.-S., M.A. *Chem. Rev.* **1966**, 199.
- (10) Morris, W. A.; Liu, T.; Fraser, C. L. *J. Mater. Chem. C* **2015**, *3*, 352.
- (11) Yoshii, R.; Nagai, A.; Tanaka, K.; Chujo, Y. *Chem. Eur. J.* **2013**, *19*, 4506.
- (12) Butler, T.; Morris, W. A.; Samonina-Kosicka, J.; Fraser, C. L. *Chem. Commun.* **2015**, *51*, 3359.
- (13) Belova, N. V.; Sliznev, V. V.; Oberhammer, H.; Girichev, G. V. *J. Mol. Struct.* **2010**, *978*, 282.

- (14) Butler, T.; Morris, W. A.; Samonina-Kosicka, J.; Fraser, C. L. *ACS Appl. Mat. Interfaces* **2016**, *8*, 1242.
- (15) Wang, X.-d.; Wolfbeis, O. S. *Chem. Soc. Rev.* **2014**, *43*, 3666.
- (16) Weissleder, R. *Nat. Biotech.* **2001**, *19*, 316.
- (17) DeRosa, C. A.; Samonina-Kosicka, J.; Fan, Z.; Hendargo, H. C.; Weitzel, D. H.; Palmer, G. M.; Fraser, C. L. *Macromolecules* **2015**, *48*, 2967.
- (18) Poon, C.-T.; Lam, W. H.; Wong, H.-L.; Yam, V. W.-W. *J. Am. Chem. Soc.* **2010**, *132*, 13992.
- (19) Kolpaczynska, M.; DeRosa, C. A.; Morris, W. A.; Fraser, C. L. *Aust. J. Chem.* **2016**.
- (20) Ono, K.; Yoshikawa, K.; Tsuji, Y.; Yamaguchi, H.; Uozumi, R.; Tomura, M.; Taga, K.; Saito, K. *Tetrahedron* **2007**, *63*, 9354.
- (21) Sun, X.; Zhang, X.; Li, X.; Liu, S.; Zhang, G. *J. Mater. Chem.* **2012**, *22*, 17332.
- (22) Hong, Y.; Lam, J. W. Y.; Tang, B. Z. *Chem. Soc. Rev.* **2011**, *40*, 5361.
- (23) Mirochnik, A. G.; Bukvetskii, B. V.; Fedorenko, E. V.; Karasev, V. E. *Russ. Chem. Bull.* **2004**, *53*, 291.
- (24) Cornil, J.; Dos Santos, D.; Crispin, X.; Silbey, R.; Bredas, J. *J. Am. Chem. Soc.* **1998**, *120*, 1289.

Chapter 7: Conclusions and Future Directions



7.1 Conclusion

These investigations detail how the solution and solid-state optical properties of difluoroboron β -diketonates (BF_2bdk) and, in some cases, even their corresponding non-boronated ligands may be tuned *via* substituents. In particular, these groups can have subtle to dramatic effects on solid-state mechanochromic luminescent (ML) and mechanochromic luminescent quenching (MLQ). Halides (F, Cl, Br, and I), alkoxy chains of varying length (OCH_3 , OC_5H_{11} , OC_6H_{13} , $\text{OC}_{12}\text{H}_{25}$, $\text{OC}_{18}\text{H}_{37}$), arenes and heterocycles (phenyl, naphthyl, furan, and thiophene), as well as α carbon substitution (methyl, methoxyphenyl, and β -tetralone) were all probed. Density functional theory (DFT) calculations were also utilized to aid in understanding how substituents affect the properties of both BF_2bdks and their ligand counterparts in solution. In particular, these calculations were useful in determining the nature of excitations (i.e. π to π^* or intramolecular charge transfer (ICT)) and their relative strengths. They also provided important information on ground-state molecular structure in solution and how different substitutions could distort these geometries. Attempts were also made to model ML behavior by simulating the excitations and emissions of face-to-face H-aggregated species of a relatively simple BF_2bdk , $\text{BF}_2\text{dbm}(\text{OMe})_2$, known to have ML properties.

Both halide and long alkoxy chain substitutions have significant effects on both ML and MLQ solid state properties. With these simple substitutions, emission color, recovery times after smearing, the extent of MLQ, sample morphology, and even the excited triplet state can all be altered. Substitutions with thiophene heterocycles brought high contrast and reversible ML properties while the presence of a furan heterocycle afforded unique, reversible, thermally responsive emissive properties. Substitutions at the

α position of the dioxaborine core affect not only emission color in solution and the solid state, but also change the nature of excitations and emission. Introduction of a methyl group at the α position resulted in a dye that went from being only very weakly emissive in solution to quite emissive in the solid state and when aggregates were formed in high water fractions (AIE). Meanwhile, introduction of an electron-donating methoxyphenyl substituent at this position resulted in a compound whose absorption and emission profiles are dominated by a charge transfer species. This species showed very unique aggregation caused emission properties with dilute solutions exhibiting reasonably strong ($\Phi = 16\%$) red emission, aggregates in moderate water fractions exhibiting very weak emissions, and aggregates in high water fractions showing strong yellow/green emissions similar to what is observed in bulk powders or films. Furthermore, introduction of this methoxyphenyl substituent gave the dye rapidly recovering (i.e. in one day) ML behavior. What is more, a strapped tetralone derivative exhibited a reduced quantum yield and larger Stokes shift compared to the parent dye and only an attenuation of emission intensity in increasing water fractions in either DMSO or THF.

Density functional theory (DFT) calculations were also employed to both predict and explain the excitation and emission properties of BF_2bdks in solution, polymeric materials, and as molecular solids. For BF_2bdk dyes substituted unsymmetrically with a bromine heavy atom and naphthyl and phenyl substituents, calculations coupled with experimental data¹ showed that dyes with π to π^* HOMO to LUMO transitions that place amplitude on the Br heavy atom in both orbitals are optimal for ratiometric oxygen sensing. It was also shown that unsymmetrical dinaphthyl-substituted BF_2bdks with one of the naphthyl rings bearing a methoxy moiety at the six position showed primarily ICT

HOMO to LUMO excitations despite Br-substitution at the six position of the opposite naphthyl ring. Interestingly, it was also discovered that thienyl BF₂bdks showed HOMO to LUMO transitions predominantly π to π^* in character despite being unsymmetrical.² Similar computational studies were also carried out on a dinaphthyl, methoxy-substituted β -diketonate exhibiting high contrast ML behavior in the absence of boron coordination. Furthermore, this compound exhibited stark AIE behavior as well as a fluorescence lifetime fit to multi-exponential decay in dilute CH₂Cl₂ solution.³ DFT calculations simulating solvation in CH₂Cl₂ revealed that this behavior is likely due to the presence of a highly twisted ketone form in addition to the enol form of the dye.

Finally, studies were begun toward computationally modeling the solid-state luminescent behavior of BF₂bdk dyes by attempting to model the excitation features and MOs of BF₂dbm(OMe)₂ dimers. The face-to-face, H-aggregate with the dipole moments of the monomers oriented anti-parallel to one-another was extensively modeled and it was discovered that intermolecular distance between the two monomers had a strong effect on the energy of a weak singlet excited state.

Structure/property relationships of BF₂bdks are well understood. The next step is to find ways to implement these materials into applications. Many applications for ML materials have been proposed but none have achieved wide-spread implementation. However, there is creative and groundbreaking progress toward this end. Kato *et al.* have developed mechanoresponsive micelles that can be covalently linked to glass and respond to mechanical stimuli. When linked to glass beads in an aqueous environment, the pyrene-based dyes showed a switching of emission from yellow to green when the beads were vortexed. If the micelles could be incorporated into living cell membranes, perhaps

they could be used as mechanical sensors for biological processes. However, the dyes did not show any changes in emission when cells were vortexed, presumably due to insufficient mechanical perturbation caused by the cells.⁴ Although the materials were not immediately useful for this application, this still represents an important step in designing ML materials with an application in mind.

In another attempt at making mechanically responsive membrane probes, Molin and coworkers developed mechanosensitive push-pull dithienothiophene derivatives to act as "fluorescent flippers" and probe changes in membranes. The dye molecules would either twist or planarize with corresponding changes in excitation in response to mechanical changes in unilamellar vesicles involving switching between ordered and disordered phases at different temperatures. These changes in excitation could then be translated into even larger changes in emission when paired with a Förster resonance energy transfer (FRET) donor, thus proving their potential for tracking such changes in cellular membranes.⁵ This is an important step forward in using mechanoresponsive emissive materials for biological imaging.

As was mentioned in Chapter 4, Kim *et al.* have demonstrated diketopyrrolopyrrol (DPP) derivatives with both mechanical and thermally responsive emissive behavior derived from a switching between a stable supercooled liquid state (red) and a crystalline state (yellow). Furthermore, they were able to use this unique property to label living cells. When cells were placed on a film of the material in the supercooled liquid state, traction force exerted by the living cells caused localized crystallization and allowed for visualization of the cells against the background.⁶

All of these examples represent progress toward using mechanically responsive luminescent materials for cellular imaging. However, applying these materials to applications outside of biological imaging still remains a challenge. One reason for this is due to the kind of force that needs to be applied in order to cause changes in emission, particularly for BF₂bdks. Shear force is necessary to cause a change in the emission of these materials.⁷⁻⁹ Many force-sensing applications would require the dyes to be responsive to compression instead of only shear force. Since the process of shearing dye films can remove some of the material, even if the materials, themselves, undergo these changes completely reversibly the wearing away of material with each shearing event will limit the number of uses and present potential problems for intensity-based imaging and sensing. This could be addressed with suitable coatings to protect and stabilize the surface, while maintaining its active quality. Of course, for many applications, such as security inks, response specifically to shear force is desirable and perhaps a limited number of uses for the materials are acceptable for these purposes. Also, if a way to quantify the force required to elicit a color change could be developed, these materials could specifically be used as sensors for shear force. Given that these materials show a high contrast in color and/or brightness between different emissive states, the potential for applications in art and design are vast. The fact that these materials are photoluminescent materials responding in this way could provide artists with unique displays and forms of expression. In a similar vein, the fact that these materials change luminescence color in response to heat means they could potentially be a substrate for thermal printing if heat were applied in a more controlled way such as with the metal star example provided in Chapter 4.

Finally, given changes in emission for these materials are caused by energy transfer in the excited state, these changes are, by nature, difficult to predict and model.¹⁰ Here, theoretical computational modeling toward this end has been presented. However, there is still much to be accomplished in this endeavor. Although we had some success modeling face-to-face H-dimers and changes in excitation properties associated with intermolecular distance in one dimension, our attempts at modeling offset dimeric species did not prove enlightening. No drastic changes in excitation properties were observed and finding minimum energy conformations aside from the face-face species proved problematic. Although studying a dimer is a logical starting point to modeling aggregation effects in solid-state emitting fluorophores, incorporating more dye molecules seems necessary to completely model what is experimentally observed, though clearly this requires more demanding calculations. Perhaps periodic boundary conditions, which may be applied when one unit cell for the system is described,¹¹ could be used to simulate larger groups of molecules in future DFT calculations.

Mechanochromic luminescent dyes, and BF₂bdks in particular, will remain at the forefront of materials science research. Advances in applications and theoretical understanding of these dyes will yield functional next generation materials for numerous purposes.

7.2 References

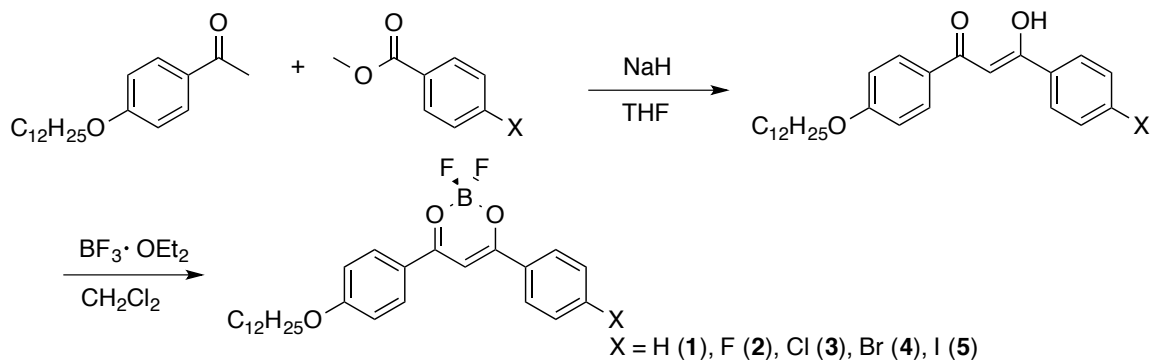
- (1) Samonina-Kosicka, J.; DeRosa, C. A.; Morris, W. A.; Fan, Z.; Fraser, C. L. *Macromolecules* **2014**, *47*, 3736.
- (2) Butler, T.; Morris, W. A.; Samonina-Kosicka, J.; Fraser, C. L. *ACS Appl. Mater. Interfaces* **2016**, *8*, 1242.

- (3) Butler, T.; Morris, W. A.; Samonina-Kosicka, J.; Fraser, C. L. *Chem. Commun.* **2015**, *51*, 3359.
- (4) Sagara, Y.; Komatsu, T.; Ueno, T.; Hanaoka, K.; Kato, T.; Nagano, T. *J. Am. Chem. Soc.* **2014**, *136*, 4273.
- (5) Dal Molin, M.; Verolet, Q.; Colom, A.; Letrun, R.; Derivery, E.; Gonzalez-Gaitan, M.; Vauthey, E.; Roux, A.; Sakai, N.; Matile, S. *J. Am. Chem. Soc.* **2015**, *137*, 568.
- (6) Chung, K.; Kwon, M. S.; Leung, B. M.; Wong-Foy, A. G.; Kim, M. S.; Kim, J.; Takayama, S.; Gierschner, J.; Matzger, A. J.; Kim, J. *ACS Cent. Sci.* **2015**, *1*, 94.
- (7) Morris, W. A.; Liu, T.; Fraser, C. L. *J. Mater. Chem. C* **2015**, *3*, 352.
- (8) Zhang, G.; Lu, J.; Sabat, M.; Fraser, C. L. *J. Am. Chem. Soc.* **2010**, *132*, 2160.
- (9) Nguyen, N. D.; Zhang, G.; Lu, J.; Sherman, A. E.; Fraser, C. L. *J. Mater. Chem.* **2011**, *21*, 8409.
- (10) Sun, X.; Zhang, X.; Li, X.; Liu, S.; Zhang, G. *J. Mater. Chem.* **2012**, *22*, 17332.
- (11) Schwarz, K.; Blaha, P. *Comput. Mater. Sci.* **2003**, *28*, 259.

Supporting Information

Appendix A

Supporting Information for Chapter 2

Scheme S2.1 Synthesis of Halide Substituted $\text{BF}_2\text{dbm}(\text{X})\text{OC}_{12}\text{H}_{25}$ Dyes.

Synthesis of β -Diketones. The β -diketone ligands were prepared by Claisen condensation in the presence of NaH as previously described.¹ A representative synthesis is as follows. **Dbm(F)OC₁₂H₂₅**. 4-Acetophenone (500 mg, 4.16 mmol), ethyl 4-fluorobenzoate (841 mg, 4.99 mmol) and THF (20 mL) were added sequentially to a 50 mL round bottom flask. After stirring the mixture for 10 min, a suspension containing NaH (157 mg, 6.24 mmol) in THF (10 mL) was added dropwise at room temperature under N₂. The mixture was stirred and refluxed at 60 °C for 20 h. After cooling to room temperature, saturated aqueous NH₄Cl (1 mL) was added to quench the reaction. The aqueous phase was extracted with CH₂Cl₂ (3 × 20 mL). The combined organic layers were washed with distilled water (2×10 mL) and brine (10 mL), and dried over Na₂SO₄ before concentration *in vacuo*. The residue was purified by column chromatography on silica gel eluting with hexanes/ethyl acetate (6:1) to give crude 4-fluorobenzoyl 4'-dodecyloxybenzoylmethane as a white solid. The crude product was used for the next step without further purification.

Difluoroboron Diketonate Complex Synthesis. A representative synthesis is as follows. **BF₂dbm(F)OC₁₂H₂₅ (2)**. Boron trifluoride diethyl etherate (627 μ L, 4.99 mmol) was added to a solution of the fluoro ligand in 20 mL CH₂Cl₂ at room temperature under N₂. The mixture was stirred for 12 h. The solvent was removed *in vacuo*. The residue was recrystallized from hexanes/acetone (4:1) to give **2** (418 mg, 71%) as a yellow solid. ¹H NMR (300 MHz, CDCl₃) δ 8.18 - 8.12 (m, 4H, 2, 6-ArH, 2', 6'-ArH), 7.26 - 7.19 (m, 2H, 3, 5-ArH), 7.03 (s, 1H, COCHCO), 7.01 (d, 2H, *J* = 9.0 Hz, 3', 5'-ArH), 4.08 (t, 2H, *J* = 6.3 Hz, OCH₂C₁₁H₂₃), 1.88 - 1.78 (m, 2H, OCH₂CH₂C₁₀H₂₁), 1.49 - 1.27 (m, 18H, OCH₂CH₂C₉H₁₈CH₃), 0.88 (t, 3H, *J* = 6.3 Hz, CH₂CH₃); MS (MALDI): *m/z* calculated for C₁₆H₁₂BF₃O₃ 474.26; found 497.15 [M+Na].

BF₂dbmOC₁₂H₂₅ (1). This compound has been previously synthesized and characterized.² This compound was synthesized as previously described.² ¹H NMR (300 MHz, CDCl₃) δ 8.16 - 8.12 (m, 4H, 2, 6-ArH, 2', 6'-ArH), 7.68 (t, 1H, *J* = 6.0 Hz, 4-ArH), 7.55 (t, 2H, *J* = 7.8 Hz, 3, 5-ArH), 7.10 (s, 1H, COCHCO), 7.02 (d, 2H, *J* = 9.0 Hz, 3', 5'-ArH), 4.08 (t, 2H, *J* = 6.0 Hz, OCH₂C₁₁H₂₃), 1.88 - 1.78 (m, 2H, *J* = 6.0 Hz, OCH₂CH₂C₁₀H₂₁), 1.50-1.27 (m, 18H, OCH₂CH₂C₉H₁₈CH₃), 0.88 (t, 3H, *J* = 6.0 Hz, OC₂₄H₂₂CH₃).

BF₂dbm(Cl)OC₁₂H₂₅ (3). The same method for **2** was used with the ligand for **3**. Recrystallization over hexanes/acetone (3:1) to give **3** (361 mg, 74%) as a yellow solid. ¹H NMR (300 MHz, CDCl₃) δ 8.14 (d, 2H, *J* = 9.0 Hz, 2', 6'-ArH), 8.06 (d, 2H, *J* = 8.7 Hz, 2, 6-ArH), 7.52 (d, 2H, *J* = 8.7 Hz, 3, 5-ArH), 7.05 (s, 1H, COCHCO), 7.01 (d, 2H, *J* = 9.0 Hz, 3', 5'-ArH), 4.08 (t, 2H, *J* = 6.3 Hz, OCH₂C₁₁H₂₃), 1.88 - 1.79 (m, 2H,

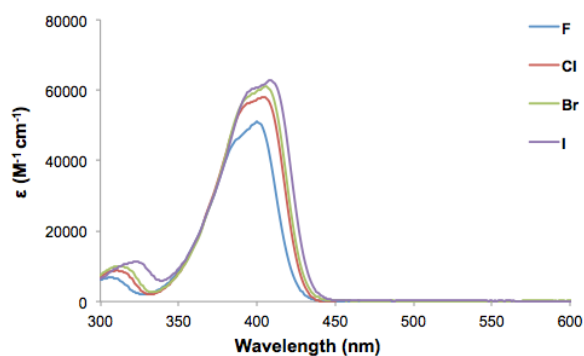
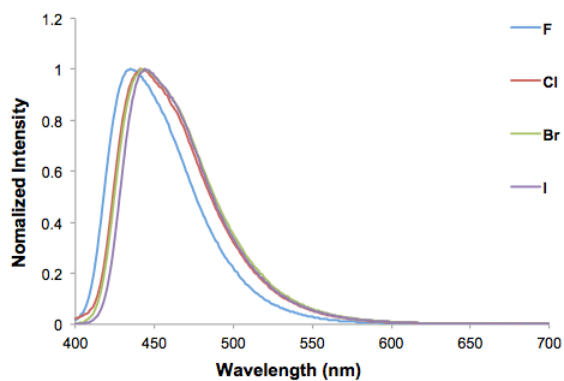
OCH₂CH₂C₁₀H₂₁), 1.49 - 1.27 (m, 18H, OCH₂CH₂C₉H₁₈CH₃), 0.88 (t, 3H, *J* = 6.3 Hz, CH₂CH₃); MS (MALDI): *m/z* calculated for C₂₇H₃₄BClF₂O₃ 490.23; found 513.14 [M+Na].

BF₂dbm(Br)OC₁₂H₂₅ (4). The same method for **2** was used with the ligand for **4**. Recrystallization over hexanes/acetone (3:1) to give **4** (524 mg, 67%) as a yellow solid. ¹H NMR (300 MHz, CDCl₃) δ 8.13 (d, 2H, *J* = 9.3 Hz, 2', 6'-ArH), 7.96 (d, 2H, *J* = 8.7 Hz, 2, 6-ArH), 7.67 (d, 2H, *J* = 8.7 Hz, 3, 5-ArH), 7.05 (s, 1H, COCHCO), 7.00 (d, 2H, *J* = 9.0 Hz, 3', 5'-ArH), 4.08 (t, 2H, *J* = 6.3 Hz, OCH₂C₁₁H₂₃), 1.88 - 1.79 (m, 2H, OCH₂CH₂C₁₀H₂₁), 1.50 - 1.27 (m, 18H, OCH₂CH₂C₉H₁₈CH₃), 0.88 (t, 3H, *J* = 6.3 Hz, CH₂CH₃); MS (MALDI): *m/z* calculated for C₂₇H₃₄BBrF₂O₃ 534.18; found 557.08 [M+Na].

BF₂dbm(I)OC₁₂H₂₅ (5). This compound has been previously synthesized.³ The same method for **2** was used with the ligand for **5**. Recrystallization over hexanes/acetone (2:1) to give **5** (620 mg, 68%) as a yellow solid. ¹H NMR (300 MHz, CDCl₃) δ 8.14 (d, 2H, *J* = 9.0 Hz, 2', 6'-ArH), 7.91 (d, 2H, *J* = 8.7 Hz, 2, 6-ArH), 7.81 (d, 2H, *J* = 8.7 Hz, 3, 5-ArH), 7.05 (s, 1H, COCHCO), 7.01 (d, 2H, *J* = 9.0 Hz, 3', 5'-ArH), 4.08 (t, 2H, *J* = 6.6 Hz, OCH₂C₁₁H₂₃), 1.88 - 1.79 (m, 2H, OCH₂CH₂C₁₀H₂₁), 1.50 - 1.27 (m, 18H, OCH₂CH₂C₉H₁₈CH₃), 0.88 (t, 3H, *J* = 6.0 Hz, CH₂CH₃); MS (MALDI): *m/z* calculated for C₂₇H₃₄BI F₂O₃ 582.16; found 605.07 [M+Na].

Table S2.1 Melting Points of Difluoroboron β -Diketonate Dyes **1-5**.

Compound	Melting Point ($^{\circ}\text{C}$)
1	133-135
2	140-142
3	148-150
4	151-154
5	145-148

**Figure S2.1** UV/vis absorption spectra of $\text{BF}_2\text{dbm}(\text{X})\text{OC}_{12}\text{H}_{25}$ (X = F, Cl, Br, I) dyes in CH_2Cl_2 solution.**Figure S2.2** Steady-state fluorescence spectra of $\text{BF}_2\text{dbm}(\text{X})\text{OC}_{12}\text{H}_{25}$ (X = F, Cl, Br, I) dyes in CH_2Cl_2 solution.

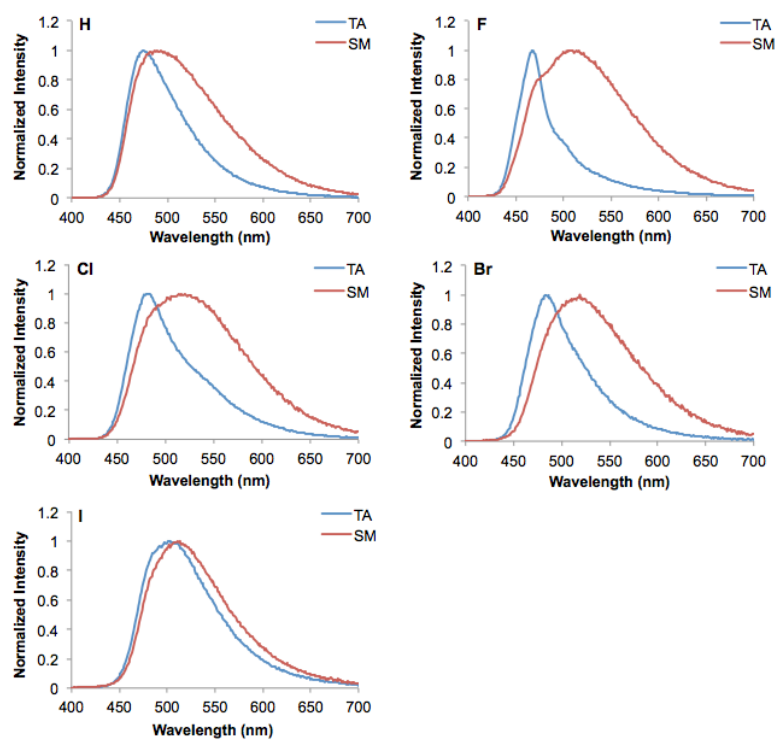


Figure S2.3 Normalized emission spectra of BF₂dbm(X)OC₁₂H₂₅ dyes as films on weighing paper comparing thermally annealed (TA) and smeared (SM) states ($\lambda_{\text{ex}} = 369$ nm) (room temperature, air).

Table S2.2 Emission Maxima and Lifetimes with % Weighting Factors for the Dyes as Films on Weighing Paper at Room Temperature under Air.^a

Dye BF ₂ dbm(X) OC ₁₂ H ₂₅ [X=]	Thermally Annealed λ_{em}^b [nm]	Thermally Annealed τ^c [ns]	Smeared λ_{em}^b [nm]	Smeared τ [ns]	$\Delta\tau_{PW0}^d$ [ns]
H	475	0.42 (7.30%) 5.30 (59.50%) 12.7 (33.20%) 7.40 (τ_{pw0})	487	7.36 (45.76%) 0.89 (8.20%) 27.2 (46.05%) 16.0 (τ_{pw0})	8.60
F	467	0.35 (16.98%) 2.54 (75.44%) 11.24 (7.58%) 2.83 (τ_{pw0})	507	9.58 (39.13%) 1.23 (7.75%) 30.4 (53.11%) 20.0 (τ_{pw0})	17.2
Cl	483	0.39 (9.18%) 4.35 (67.77%) 9.31 (23.05%) 5.13 (τ_{pw0})	514	7.25 (53.31%) 0.87 (9.04%) 25.2 (37.65%) 13.4 (τ_{pw0})	8.27
Br	483	0.97 (89.75%) 5.16 (10.25%) 1.40 (τ_{pw0})	519	4.27 (49.87%) 0.56 (15.09%) 12.7 (35.04%) 6.66 (τ_{pw0})	5.26
I	502	0.23 (31.45%) 1.61 (63.60%) 3.99 (4.94%) 1.29 (τ_{pw0})	513	0.36 (52.21%) 1.40 (43.48%) 4.94 (4.31%) 1.01 (τ_{pw0})	-0.28
^a $\lambda_{ex} = 369$ nm.					
^b Emission maximum; fluorescence.					

Note: Emission lifetimes were multi-exponential, and the decay traces of emission intensity at λ_{em} and the % weighting factors (WF) were analyzed using DataStation version 2.6 software from Horiba Jobin Yvon. τ_{pw0} was calculated as follows:

$$\tau_{pw0} = \sum_{i=1}^N WF_i \cdot \tau_i$$

where N is the number of decay components, WF_i is the weighting factor, τ_i is the component of decay lifetimes, and τ_{pw0} is the pre-exponential weighted lifetime.⁴

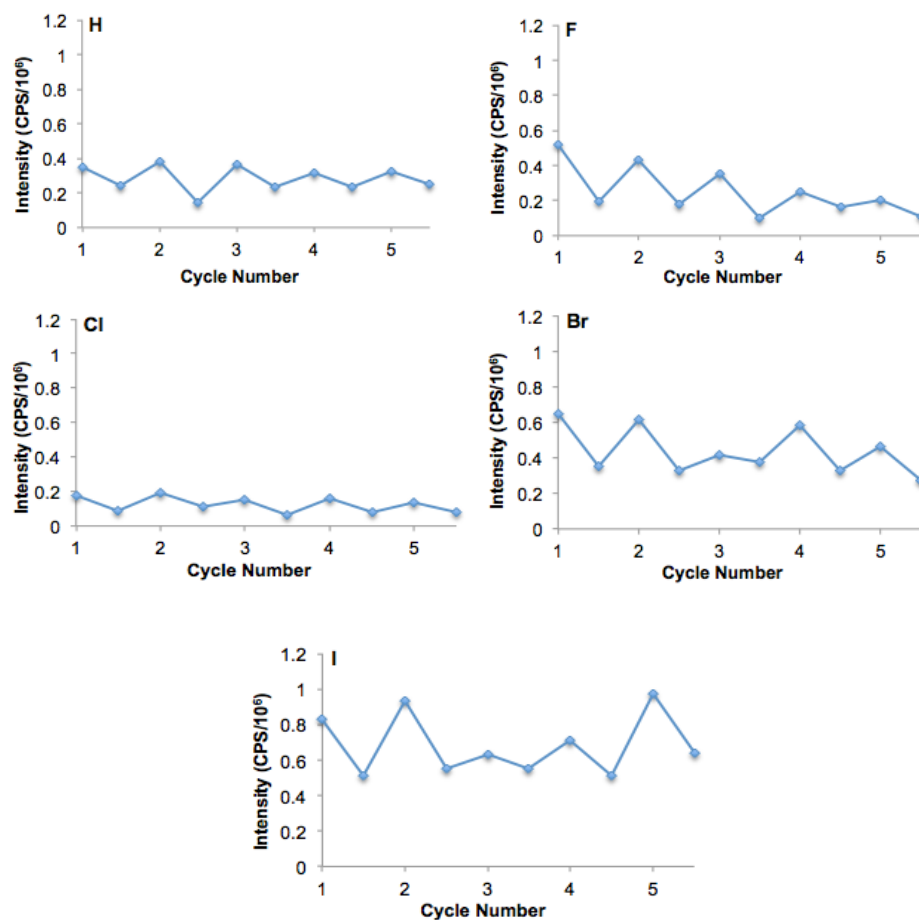


Figure S2.4 Emission intensities of dyes as films on weighing paper monitored through cycles of smearing and annealing at room temperature in air ($\lambda_{\text{ex}} = 369 \text{ nm}$). The intensities were recorded in photon counts per second (CPS) and shown as $\text{CPS}/10^6$.

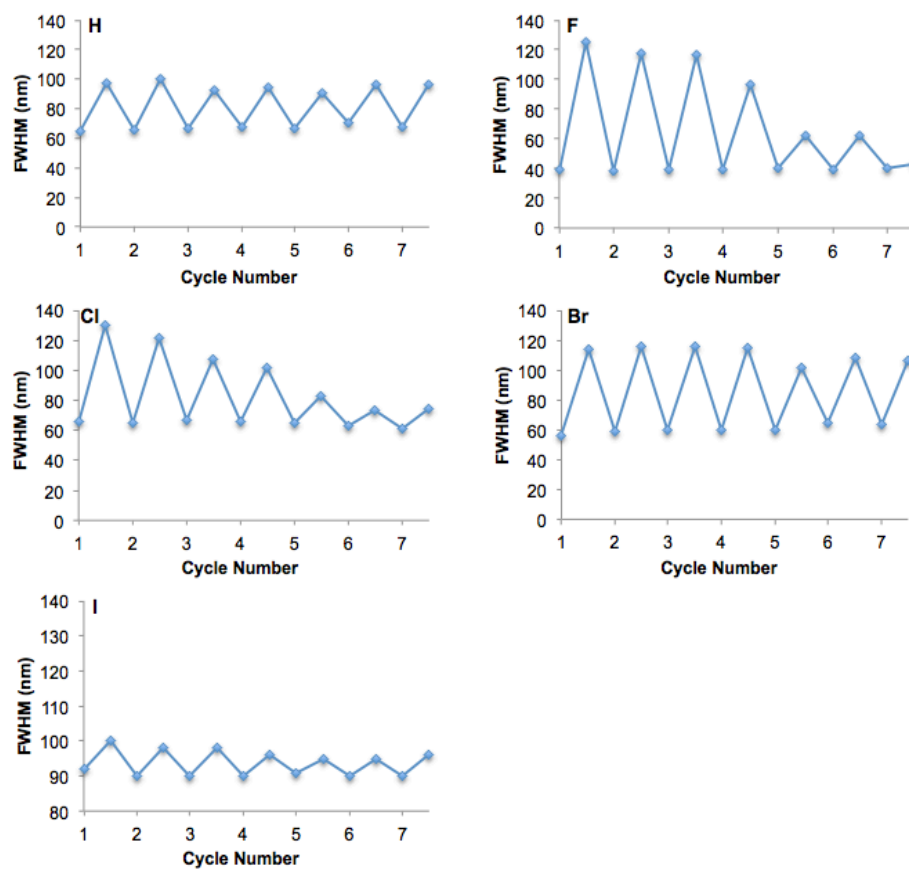


Figure S2.5 Full width at half maximum (FWHM) values for emission peaks monitored through annealing and smearing cycles ($\lambda_{\text{ex}} = 369$ nm) (room temperature, air).

Table S2.3 Total Emission for Boron Dyes as Films on Weighing Paper.^a

Dye	Thermally Annealed		Smeared	
	λ_{em}^b [nm]	FWHM ^c [ns]	λ_{em}^b [nm]	FWHM ^c [nm]
BF ₂ dbm(X)OC ₁₂ H ₂₅ [X=]				
H	504	71	506	79
F	474	49	521	89
Cl	497	67	530	68
Br	497 ^d	67	535 ^f	123
I	489 ^e	84	502 ^g	88

^a $\lambda_{ex} = 369$ nm; 77K, liquid N₂.
^b Emission maximum; fluorescence.
^c Full Width at Half Maximum.
^d Phosphorescence evident; $\lambda_{phos} = 564$ nm.
^e Phosphorescence evident; $\lambda_{phos} = 570$ nm.
^f Phosphorescence evident; $\lambda_{phos} = 561$ nm.
^g Phosphorescence evident; $\lambda_{phos} = 579$ nm.

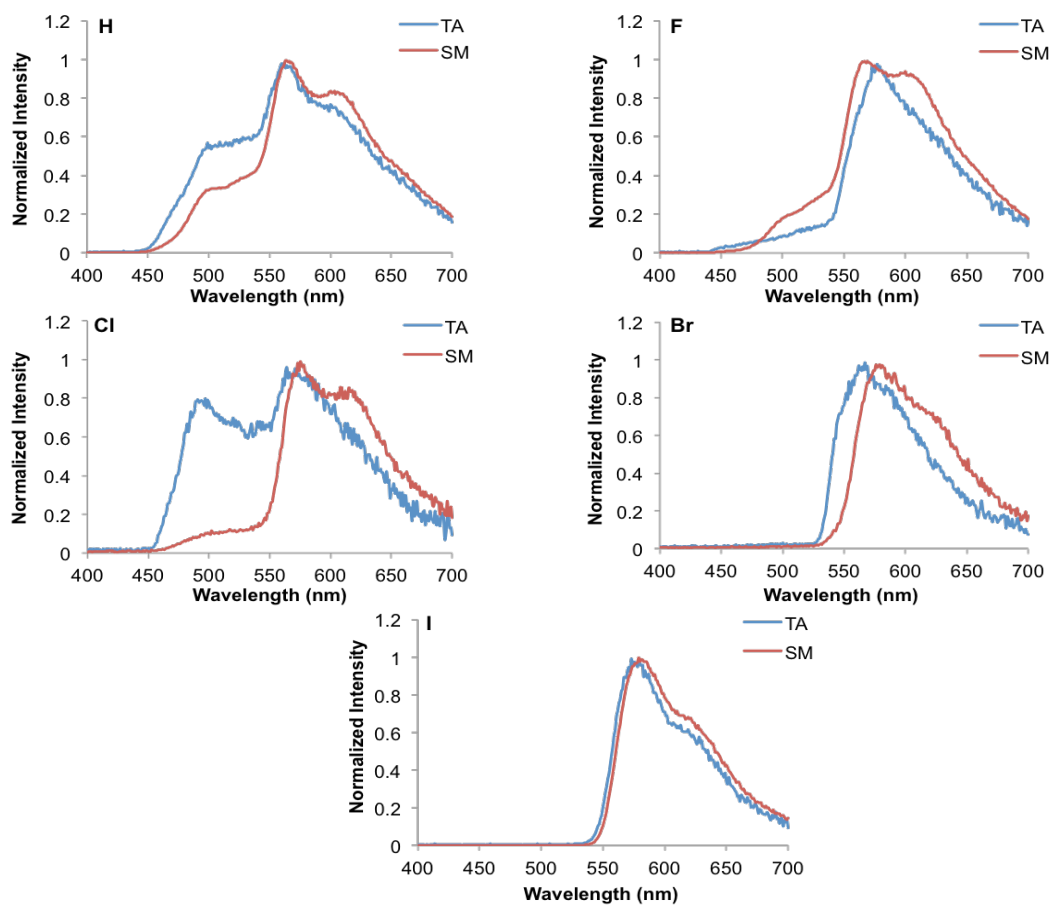


Figure S2.6. Normalized delayed emission spectra of BF₂dbm(X)OC₁₂H₂₅ dyes on weighing paper in both thermally annealed (TA) and smeared (SM) states at 77K in liquid N₂ ($\lambda_{\text{ex}} = 369$ nm).

Table S2.4. Delayed Emission Maxima and Lifetimes with % Weighting Factors for the Dyes as Films on Weighing Paper at 77K in liquid N₂.^a

Dye BF ₂ dbm(X)OC ₁₂ H ₂₅ [X=]	Thermally Annealed λ_{phos}^b [nm]	Thermally Annealed τ_{phos}^c [ms]	Smeared λ_{phos}^b [nm]	Smeared τ_{phos}^c [ms]	$\Delta\tau_{\text{pw0}}$ [ms]
H	562	107 (18.43%) 10.3 (11.47%) 748 (59.16%) 1.25 (10.93%) 463 (τ_{pw0})	563	194 (13.04%) 1010 (81.68%) 17.1 (3.37%) 1.47 (1.92%) 851 (τ_{pw0})	388
F	577	44.1 (47.05%) 545 (40.90%) 3.80 (12.05%) 244 (τ_{pw0})	569	143 (10.22%) 18.7 (4.19%) 1050 (83.93%) 1.28 (1.66%) 897 (τ_{pw0})	653
Cl	564	8.80 (26.49%) 65.1 (20.71%) 553 (34.62%) 1.40 (18.18%) 208 (τ_{pw0})	578	83.2 (9.15%) 581 (81.75%) 8.50 (5.05%) 1.98 (4.05%) 483 (τ_{pw0})	275
Br	567	3.94 (6.61%) 22.7 (50.02%) 218 (3.56%) 58.4 (39.80%) 42.6 (τ_{pw0})	580	44.5 (33.33%) 4.62 (3.28%) 106 (63.39%) 82.0 (τ_{pw0})	39.4
I	573	1.57 (14.20%) 17.6 (31.85%) 233 (1.87%) 8.10 (52.08%) 14.4 (τ_{pw0})	580	96.1 (0.52%) 1480 (1.37%) 14.7 (98.11%) 35.2 (τ_{pw0})	20.8
^a $\lambda_{\text{ex}} = 369$ nm. ^b emission maximum; phosphorescence. ^c Phosphorescence lifetime.					

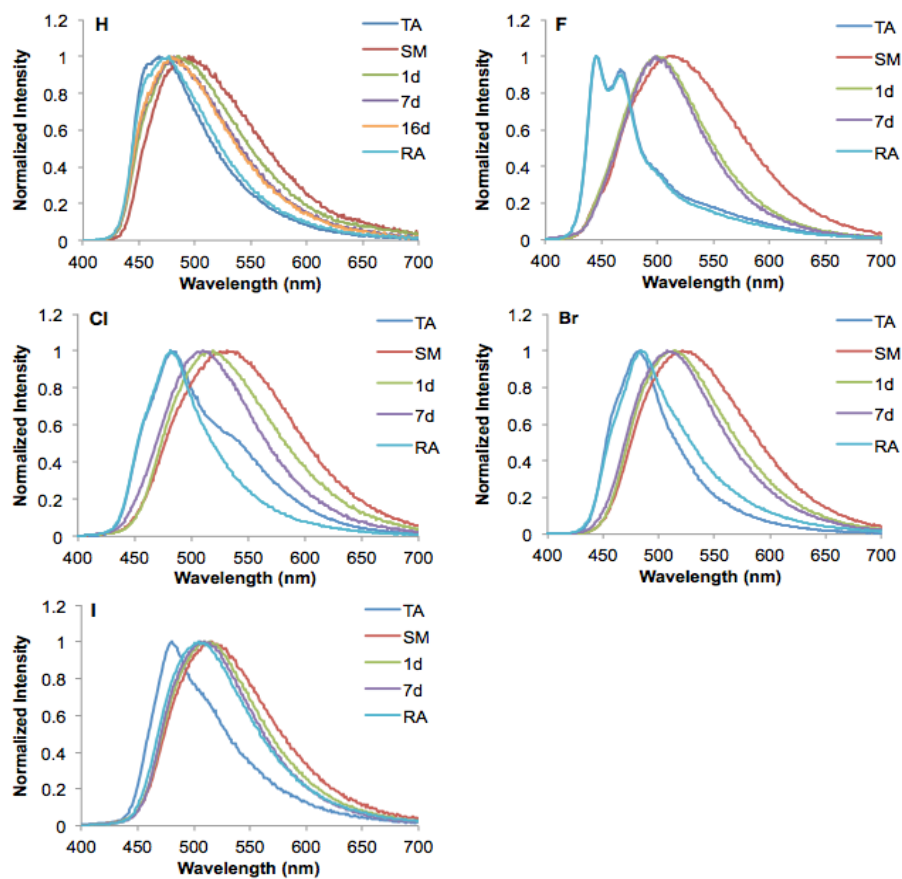


Figure S2.7 Emission spectra of boron dyes as spin-cast films on glass ($\lambda_{\text{ex}} = 369 \text{ nm}$) (room temperature, air). The dyes were thermally annealed (TA), smeared (SM), and then the emission spectra were monitored over time. After three weeks, the films were re-annealed (RA). Note: d = days.

Table S2.5 Emission Maxima and Lifetimes with % Weighting Factors for the Dyes as Spin-cast Films on Glass at Room Temperature under Air.^a

Dye BF ₂ dbm(X)OC ₁₂ H ₂₅ [X=]	As-spun λ_{em}^b [nm]	As-spun τ^c [ns]	Thermally Annealed λ_{em}^b [nm]	Thermally Annealed τ^c [ns]	$\Delta\tau_{pw0}$ (ns)
H	524	16.6 (29.75%) 2.83 (3.51%) 40.9 (66.74%) 32.3 (τ_{pw0})	468	2.12 (16.07%) 6.54 (54.42%) 16.4 (29.50%) 8.74 (τ_{pw0})	-23.6
F	517	13.3 (38.23%) 37.7 (61.77%) 28.4 (τ_{pw0})	445	1.52 (90.99%) 8.77 (9.01%) 2.17 (τ_{pw0})	-26.2
Cl	538	11.3 (62.35%) 34.8 (37.65%) 20.1 (τ_{pw0})	484	5.20 (56.21%) 8.70 (43.79%) 6.73 (τ_{pw0})	-13.4
Br	520	1.25 (13.76%) 5.60 (60.48%) 14.3 (25.76%) 7.24 (τ_{pw0})	483	1.05 (95.70%) 5.43 (5.30%) 1.28 (τ_{pw0})	-5.96
I	515	0.74 (87.99%) 2.89 (12.01%) 1.00 (τ_{pw0})	480	1.66 (54.02%) 3.05 (45.98%) 2.30 (τ_{pw0})	1.30
^a $\lambda_{ex} = 369$ nm. ^b Emission maximum; fluorescence. ^c Fluorescence lifetime.					

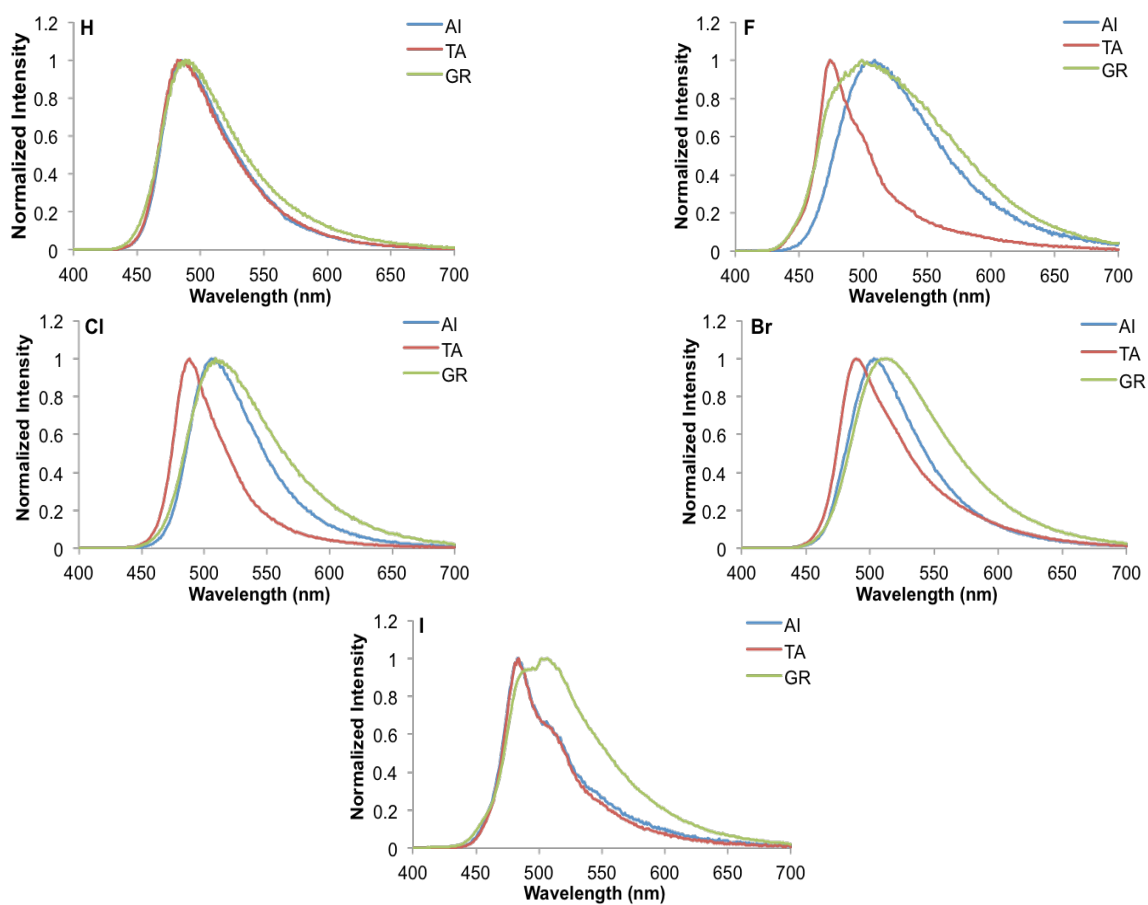


Figure S2.8 Emission spectra of boron dyes as bulk powders ($\lambda_{\text{ex}} = 369$ nm) (room temperature, air). As-isolated (AI), thermally annealed (TA), and ground (GR) powders are compared.

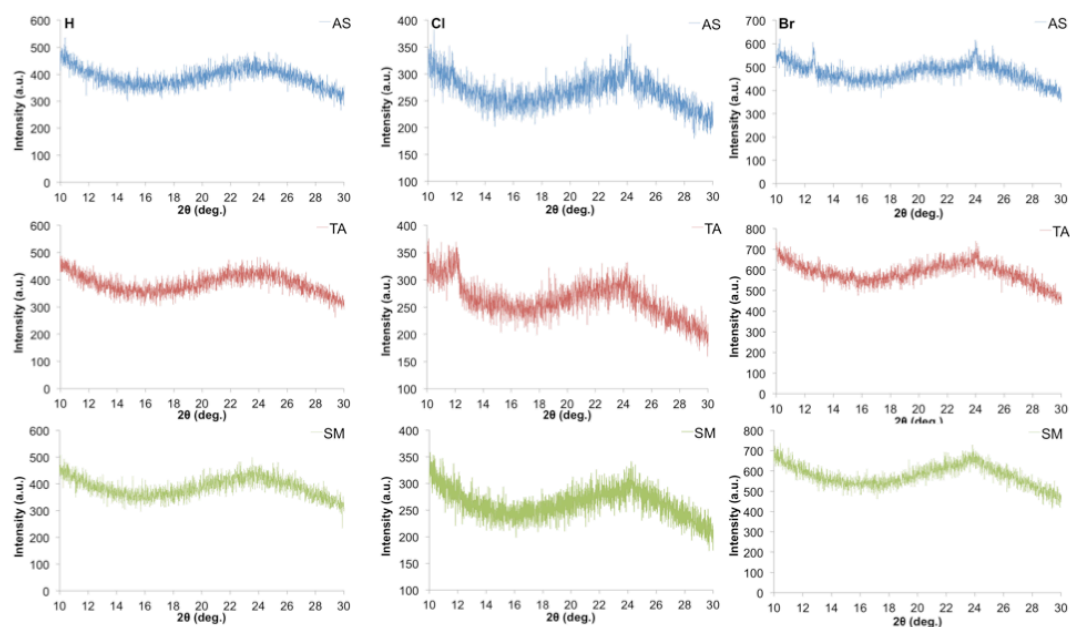


Figure S2.9 X-ray diffraction patterns of the H, Cl, and Br dyes as-spun (AS), thermally annealed (TA), and smeared (SM).

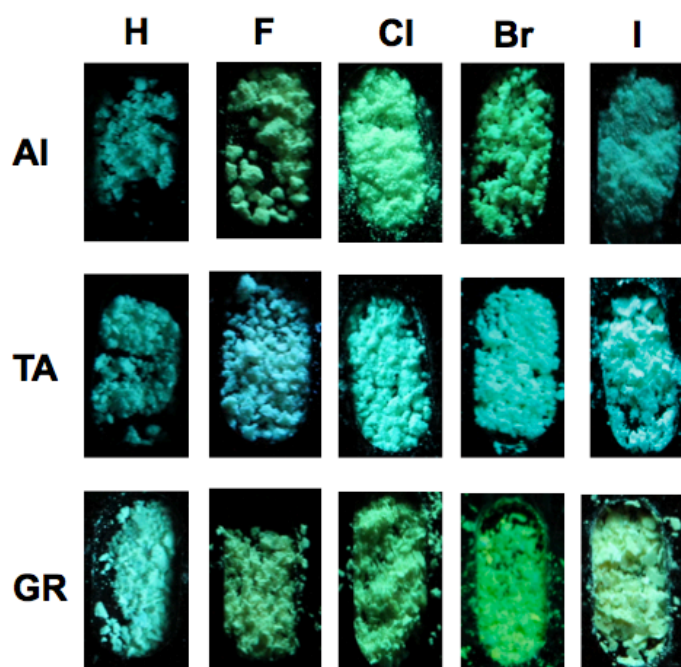
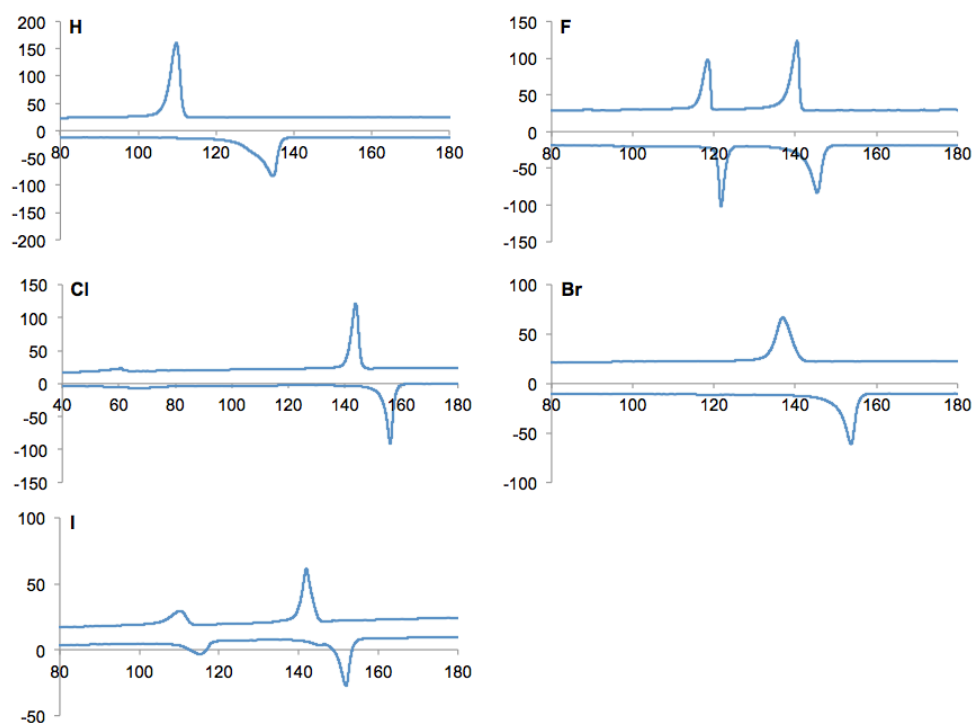


Figure S2.10 The $\text{BF}_2\text{dbm}(\text{X})\text{OC}_{12}\text{H}_{25}$ dyes as bulk powders. As-isolated powders (AI) from acetone/hexanes were thermally annealed (TA) at their respective optimum annealing temperatures for three hours. AI powders were also ground (GR) vigorously for ~30 minutes using a mortar and pestle.

Table S2.6 Fluorescence Properties of the Boron Dyes as Bulk Powders.^a

Dye	As-Isolated		Thermally Annealed		Ground	
	λ_{em}^b [nm]	FWHM ^c [nm]	λ_{em}^b [nm]	FWHM ^c [nm]	λ_{em}^b [nm]	FWHM ^c [nm]
BF ₂ dbm(X)OC ₁ 2H ₂₅ [X=]						
H	485	62	482	61	488	69
F	509	89	474	43	503	79
Cl	506	63	488	45	509	81
Br	504	66	489	56	511	85
I	483	52	484	50	506	82

^a $\lambda_{ex} = 369$ nm.
^b emission maximum; fluorescence.
^c Full Width at Half Maximum.

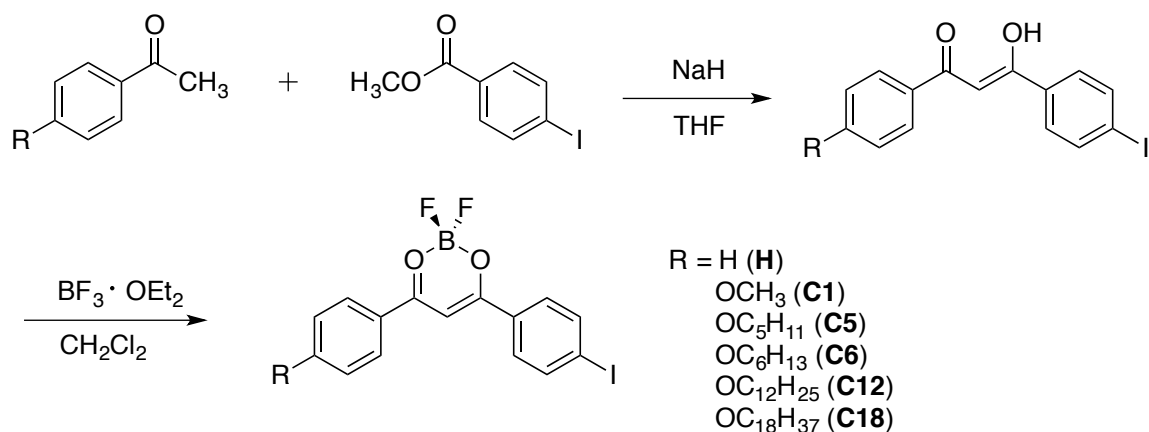
**Figure S2.11** Differential scanning calorimetry (DSC) thermograms of all dyes. The 2nd cycle is shown for all samples.

References

- (1) Zhang, G.; Fiore, G. L.; St. Clair, T. L.; Fraser, C. L. *Macromolecules* **2009**, *42*, 3162.
- (2) Nguyen, N. D.; Zhang, G.; Lu, J.; Sherman, A. E.; Fraser, C. L. *J. Mater. Chem.* **2011**, *21*, 8409.
- (3) Zhang, G.; Lu, J.; Fraser, C. L. *Inorg. Chem.* **2010**, *49*, 10747.
- (4) Carraway, E. R.; Demas, J. N.; DeGraff, B. A.; Bacon, J. R. *Anal. Chem.* **1991**, *63*, 337.

Appendix B

Supporting Information for Chapter 3

Scheme S3.1 Synthesis of Alkoxy-Substituted BF₂dbm(I)OR Dyes.

Synthesis of β -Diketones. The β -diketone ligands were prepared by Claisen condensation in the presence of NaH as previously described and were boronation without further purification.¹

Difluoroboron β -Diketonate Synthesis. A representative synthesis is as follows.

BF₂dbm(I)OCH₃ (C1). Boron trifluoride diethyl etherate (480 μ L, 3.89 mmol) was added to a solution of dbm(I)OCH₃ in CH₂Cl₂ (30 mL) at room temperature under a stream of N₂. The mixture was stirred for 12 h. The solvent was removed *in vacuo*. The residue was recrystallized from THF/hexanes (3:1) to give **2** as a yellow powder: 740 mg, (69%). ¹H NMR (300 MHz, CDCl₃) δ 8.16 (d, 2H, J = 9.0 Hz, 3', 5'-ArH), 7.91 (d, 2H, J = 9.0 Hz, 2, 6-ArH), 7.82 (d, 2H, J = 9.0 Hz, 2', 6'-ArH), 7.06 (s, 1H, COCHCO), 7.04 (d, 2H, J = 9.0 Hz, 3, 5-ArH), 3.94 (s, 3H, OCH₃) MS (MALDI) m/z calcd for C₁₆H₁₂BF₂IO₃ 427.99; found 450.91 [M+Na]. m.p.: 242-245 °C.

BF₂dbm(I) (H). The complex was prepared by the method described for **C1** with the following exceptions. Recrystallization from hexanes/acetone (4:1) gave **H** as a light yellow powder: 310 mg (58%). ¹H NMR (300 MHz, CDCl₃, ppm): δ 8.16 (d, 2H, *J* = 6.0 Hz, 3', 5'-Ar*H*), 7.94 (d, 2H, *J* = 9.0 Hz, 2, 6-Ar*H*), 7.85 (d, 2H, *J* = 9.0 Hz 2', 6'-Ar*H*), 7.72 (t, 1H, *J* = 9.0 Hz, 4-Ar*H*), 7.57 (t, 2H, *J* = 9.0 Hz, 3, 5-Ar*H*), 7.16 (s, 1H, COCHCO). ; MS (MALDI): *m/z* calculated for C₁₅H₁₀BIF₂O₂ 397.98; found 420.91 [M+Na]. m.p.: 229-232 °C.

BF₂dbm(I)OC₅H₁₁ (C5). The complex was prepared by the method described for **C1** with the following exceptions. Recrystallization from hexanes/acetone (4:1) gave **C5** as a yellow powder: 400 mg (80%). ¹H NMR (600 MHz, CDCl₃, ppm): δ 8.15 (d, 2H, *J* = 6.0 Hz, 3', 5'-Ar*H*), 7.91 (d, 2H, *J* = 12.0 Hz, 2, 6-Ar*H*), 7.82 (d, 2H, *J* = 6.0 Hz, 2', 6'-Ar*H*), 7.05 (s, 1H, COCHCO), 7.02 (d, 2H, *J* = 12.0 Hz, 3, 5-Ar*H*), 4.09 (t, 2H, *J* = 6.0 Hz, OCH₂C₄H₈), 1.84 (m, 2H, OCH₂CH₂C₃H₇), 1.47 (m, 2H, OC₂H₄CH₂C₂H₅), 1.41 (m, 2H, OC₃H₆CH₂CH₃), 0.95 (t, 3H, *J* = 6.0 Hz, OC₄H₈CH₃); MS (MALDI): *m/z* calculated for C₂₀H₂₀BIF₂O₃ 484.05; found 506.96 [M+Na]. m.p.: 194-196 °C.

BF₂dbm(I)OC₆H₁₃ (C6). The complex was prepared by the method described for **C1** with the following exceptions. Passage through a silica plug eluting with hexanes/ethyl acetate (1:1) and recrystallization from hexanes/ethyl acetate (3:1) to give **C6** as a yellow powder: 321 mg (58%) as a yellow powder. ¹H NMR (600 MHz, CDCl₃) δ 8.13 (d, 2H, *J* = 12.0 Hz, 3', 5'-Ar*H*), 7.90 (d, 2H, *J* = 6.0 Hz, 2, 6 Ar*H*), 7.81 (d, 2H, *J* = 6.0 Hz, 2', 5'-Ar*H*), 7.04 (s, 1H, COCHCO), 7.01 (d, 2H, *J* = 6.0 Hz, 3, 5-Ar*H*), 4.08 (t, 2H, *J* = 12.0

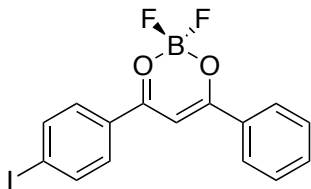
Hz, $\text{OCH}_2\text{C}_5\text{H}_{11}$), 1.82 (m, 2H, $\text{OCH}_2\text{CH}_2\text{C}_4\text{H}_9$), 1.47 (m, 2H, $\text{OCH}_2\text{CH}_2\text{CH}_2\text{C}_3\text{H}_7$), 1.35 (m, 4H, $\text{OCH}_2\text{CH}_2\text{CH}_2\text{C}_2\text{H}_4\text{CH}_3$), 0.91 (t, 3H, $J = 6.0$ Hz, $\text{OC}_5\text{H}_{10}\text{CH}_3$); MS [ESI/TOF HRMS] m/z calculated for $\text{C}_{21}\text{H}_{22}\text{BIF}_2\text{O}_3$ 498.07; found 521.06 [M+Na]. m.p.: 190-192 °C.

$\text{BF}_2\text{dbm}(\text{I})\text{OC}_{12}\text{H}_{25}$ (C12). The complex was prepared by the method described for **C1** with the following exceptions. Recrystallization from hexanes/acetone (2:1) to give **C12** as a yellow powder: 620 mg (68%). ^1H NMR (300 MHz, CDCl_3) δ 8.14 (d, 2H, $J = 9.0$ Hz, 2', 6'-ArH), 7.91 (d, 2H, $J = 8.7$ Hz, 2, 6-ArH), 7.81 (d, 2H, $J = 8.7$ Hz, 3, 5-ArH), 7.05 (s, 1H, COCHCO), 7.01 (d, 2H, $J = 9.0$ Hz, 3', 5'-ArH), 4.08 (t, 2H, $J = 6.6$ Hz, $\text{OCH}_2\text{C}_{11}\text{H}_{23}$), 1.88 - 1.79 (m, 2H, $\text{OCH}_2\text{CH}_2\text{C}_{10}\text{H}_{21}$), 1.50 - 1.27 (m, 18H, $\text{OCH}_2\text{CH}_2\text{C}_9\text{H}_{18}\text{CH}_3$), 0.88 (t, 3H, $J = 6.0$ Hz, CH_2CH_3); MS (MALDI): m/z calculated for $\text{C}_{27}\text{H}_{34}\text{BIF}_2\text{O}_3$ 582.16; found 605.07 [M+Na]. m.p.: 145-148 °C.

$\text{BF}_2\text{dbm}(\text{I})\text{OC}_{18}\text{H}_{37}$ (C18). The complex was prepared by the method described for **C1** with the following exceptions. Recrystallization from hexanes/acetone (5:1) to give **C18** as a yellow powder: 16 mg (30%). ^1H NMR (600 MHz, CDCl_3) δ 8.13 (d, 2H, $J = 12.0$ Hz, 3', 5'-ArH), 7.90 (d, 2H, $J = 6.0$ Hz, 2, 6-ArH), 7.80 (d, 2H, $J = 12.0$ Hz, 2', 6'-ArH), 7.03 (s, 1H, COCHCO), 7.01 (d, 2H, $J = 6.0$ Hz, 3, 5 Ar-H), 4.07 (t, 2H, $J = 6.0$ Hz, $\text{OCH}_2\text{C}_{17}\text{H}_{35}$), 1.82 (m, 2H, $\text{OCH}_2\text{CH}_2\text{C}_{16}\text{H}_{33}$), 1.46 (m, 2H, $\text{OC}_2\text{H}_4\text{CH}_2\text{C}_{15}\text{H}_{31}$), 1.24 (m, 28H, $\text{OC}_3\text{H}_6\text{C}_{14}\text{H}_{28}\text{CH}_3$), 0.86 (t, 3H, $J = 6.0$ Hz, $\text{OC}_{17}\text{H}_{34}\text{CH}_3$); MS [ESI/TOF HRMS] m/z calculated for $\text{C}_{33}\text{H}_{46}\text{BIF}_2\text{O}_3$ 666.26; found 689.24 [M+Na]. m.p.: 137-140 °C.

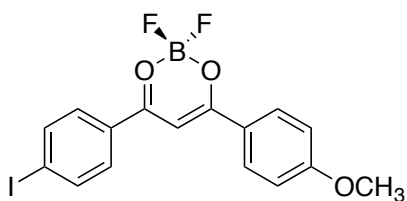
Full Computational Details

All compounds were modeled using the Gaussian 09 suite of programs² utilizing density functional theory (DFT). We chose B3LYP/6-311+G(d) to simulate the B, O, C, and F atoms and B3LYP/SDD to simulate the I heavy atom in ground state and S_1 excited state geometry optimizations of the dyes with the exception of the S_1 geometry optimization of the C5 dye, for which B3LYP/6-311G was used to simulate the I atom. All vibrational frequencies were positive, assuring that the geometries are at least a local minimum. Single point energy calculations were used to generate the molecular orbital diagrams utilizing B3LYP/6-31G(d) for B, O, C, and F atoms and B3LYP/SDD for the I heavy atom. Time-dependent density functional theory, TD-B3LYP/6-311+G(d) for B, O, C, and F atoms and B3LYP/SDD for the I atom, was employed for estimates of the absorption spectra at the respective optimized ground state geometries and emission at the respective optimized S_1 excited state geometries.^{3,4} The emission spectra were computed by calculating the ground state (S_0) energy on the optimized geometry of the S_1 surface. In all calculations, a Tomasi polarized continuum for dichloromethane solvent was used.⁴ Molecular orbital diagrams were depicted using GaussView 5 software.⁶ Coordinates below are given in Cartesian, in Angstroms.

Table S3.1 Optimized Ground State Structures of Boron Compounds.

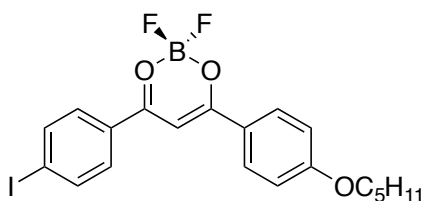
E (HF) = -964.23583231. μ (Debye) = 4.0879

B, -2.56989200, 2.46196400, -0.04769300
 F, -2.69878000, 3.03256800, 1.21706600
 F, -2.80959400, 3.38382900, -1.05211300
 O, -3.55428100, 1.34916800, -0.17481800
 C, -3.22789700, 0.09682200, -0.02116600
 C, -1.88799000, -0.27986500, 0.10008900
 H, -1.63075600, -1.30960700, 0.27939300
 O, -1.18180000, 1.93875800, -0.19873900
 C, -0.88561700, 0.67863400, -0.04087100
 C, 0.55189200, 0.36672900, -0.03474400
 C, 1.02900000, -0.95009700, -0.13371500
 C, 1.47961400, 1.41558800, 0.07112800
 C, 2.39315000, -1.21597800, -0.12041900
 H, 0.34690900, -1.78425100, -0.24100300
 C, 2.84526900, 1.15996600, 0.09027900
 H, 1.12664300, 2.43586600, 0.14782600
 C, 3.29175000, -0.15651700, -0.00536500
 H, 2.74325100, -2.23708600, -0.20349400
 H, 3.54576800, 1.98039100, 0.17997100
 C, -4.34994500, -0.85261200, 0.00002000
 C, -4.14837300, -2.24076900, -0.09454600
 C, -5.66175300, -0.35957100, 0.11410700
 C, -5.23194900, -3.11045000, -0.06992500
 H, -3.15202800, -2.64998300, -0.20642900
 C, -6.74123400, -1.23395400, 0.14354900
 H, -5.82303100, 0.70818200, 0.18703200
 C, -6.52962600, -2.61048400, 0.05180500
 H, -5.06520300, -4.17887000, -0.14975400
 H, -7.74817200, -0.84287900, 0.23863500
 H, -7.37317200, -3.29219500, 0.07268900
 I, 5.39218000, -0.55537700, 0.02143600



E (HF) = -1079.03039437. μ = 10.1638

B, -1.62698300, 2.89925100, -0.01960600
 F, -1.70096400, 3.47669000, 1.24896400
 F, -1.76526100, 3.85207000, -1.01757200
 O, -2.72378100, 1.90194600, -0.15726100
 C, -2.53812200, 0.61613400, -0.02285700
 C, -1.23895300, 0.09948600, 0.08320300
 H, -1.08852000, -0.95625700, 0.22886900
 O, -0.30216600, 2.23806300, -0.16978300
 C, -0.14436900, 0.94735700, -0.03738100
 C, 1.25450500, 0.48622800, -0.03565800
 C, 1.59312600, -0.87185500, -0.14486600
 C, 2.28638600, 1.43151000, 0.07680900
 C, 2.92240700, -1.27793400, -0.13365200
 H, 0.82825300, -1.63012400, -0.25687000
 C, 3.61878500, 1.03598300, 0.09324000
 H, 2.04136600, 2.48238200, 0.15990500
 C, 3.92624200, -0.31872000, -0.01103600
 H, 3.16483800, -2.32911900, -0.22479700
 H, 4.40058900, 1.77886600, 0.18766900
 C, -3.74486100, -0.20244600, -0.01186900
 C, -3.70218300, -1.61340700, -0.00164500
 C, -5.00506800, 0.42068200, -0.01145000
 C, -4.86296500, -2.35808800, 0.01114600
 H, -2.75671500, -2.14100500, -0.01349400
 C, -6.17890400, -0.31751100, 0.00389800
 H, -5.06051300, 1.50157500, -0.01735100
 C, -6.11593500, -1.71894300, 0.01553200
 H, -4.82960100, -3.44138200, 0.01497900
 H, -7.12912300, 0.19964200, 0.00898900
 I, 5.97395700, -0.93712600, 0.01511700
 O, -7.19106300, -2.53242800, 0.02979800
 C, -8.50387300, -1.95885400, 0.02929400
 H, -9.18997600, -2.80192600, 0.03720700
 H, -8.66292300, -1.34789700, 0.92069600
 H, -8.66770200, -1.36055000, -0.86976900



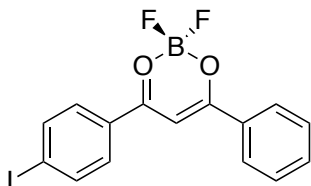
E (HF) = -1236.3239664. μ (Debye) = 10.7401

B, -0.38760100, 3.32780600, 0.02364900
 F, -0.39743400, 3.91434400, -1.24315000
 F, -0.37789000, 4.28684500, 1.02482300
 O, 0.83631900, 2.48950900, 0.15441900
 C, 0.82987000, 1.19357600, -0.00985400
 C, -0.38726900, 0.50718200, -0.12998800
 H, -0.39444300, -0.55596100, -0.29727100
 O, -1.60917700, 2.49026300, 0.17461900
 C, -1.58667300, 1.19277700, 0.01716400
 C, -2.90577500, 0.53771700, 0.02124400
 C, -3.04310600, -0.85301300, 0.15260800
 C, -4.06386700, 1.32128300, -0.10384000
 C, -4.29889800, -1.44833400, 0.15162500
 H, -2.17568500, -1.48894600, 0.27808600
 C, -5.32489900, 0.73544500, -0.11097300
 H, -3.97428700, 2.39537600, -0.20370500
 C, -5.43171300, -0.64772800, 0.01695800
 H, -4.38501600, -2.52189900, 0.26044100
 H, -6.20669000, 1.35500300, -0.21567000
 C, 2.13594300, 0.54668900, -0.02970400
 C, 2.28482800, -0.85375600, -0.13041300
 C, 3.30081000, 1.32972900, 0.05454400
 C, 3.53512400, -1.43492100, -0.14949200
 H, 1.41975100, -1.50195000, -0.19104400
 C, 4.56327700, 0.75662400, 0.03850400
 H, 3.21004400, 2.40562200, 0.13045900
 C, 4.69181300, -0.63763000, -0.06525600
 H, 3.64782900, -2.51017300, -0.22594000
 H, 5.43429500, 1.39458100, 0.10424200
 I, -7.36567200, -1.56216200, 0.01257400
 O, 5.86454600, -1.29889600, -0.09143400
 C, 7.10349000, -0.56425700, 0.00128400
 H, 7.16343300, 0.14095600, -0.83397800
 H, 7.11217200, 0.00244400, 0.93785900
 C, 8.24284400, -1.56643900, -0.04437500
 H, 8.17575000, -2.13726100, -0.97695900
 H, 8.11861000, -2.28228700, 0.77551500
 C, 9.61329600, -0.88755000, 0.05703100

H, 9.72533900, -0.16108800, -0.75804900
 H, 9.66943600, -0.31043800, 0.98893300
 C, 10.77880700, -1.88141700, 0.00978600
 H, 10.72564800, -2.45702000, -0.92241400
 H, 10.66598500, -2.60978800, 0.82219000
 C, 12.14823700, -1.20709600, 0.11583000
 H, 12.95816300, -1.94127700, 0.07941000
 H, 12.30815700, -0.49864400, -0.70333800
 H, 12.24771000, -0.65267800, 1.05459700

Table S3.2 Characterizations of Absorption Spectra Computed in Dichloromethane Solvent.

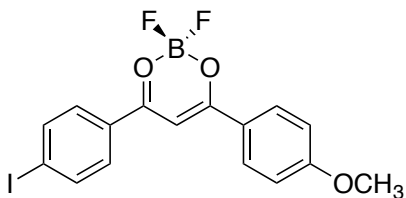
Note: Max amplitude is 0.70714 for a pure one-electron excitation. The highest occupied molecular orbital (HOMO) to the lowest unoccupied molecular orbital (LUMO) transitions are in bold.



Excited State 1: Singlet-A 3.2418 eV 382.45 nm f=1.0383 <S2>=0.000**
73 -> 74 0.70376

Excited State 2: Singlet-A 3.7591 eV 329.82 nm f=0.0180 <S**2>=0.000
 71 -> 74 0.68005
 72 -> 74 -0.16452

Excited State 3: Singlet-A 3.8318 eV 323.57 nm f=0.1242 <S**2>=0.000
 69 -> 74 -0.11448
 71 -> 74 0.16387
 72 -> 74 0.67177



Excited State 1: Singlet-A 3.1003 eV 399.91 nm f=1.2541 <S2>=0.000**
81 -> 82 0.70254

Excited State 2: Singlet-A 3.6699 eV 337.84 nm f=0.0819 <S**2>=0.000

80 -> 82 0.69486

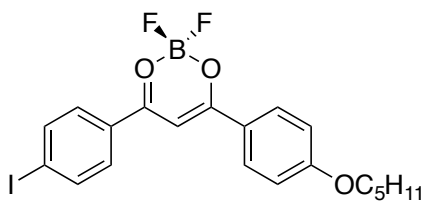
Excited State 3: Singlet-A 3.9495 eV 313.92 nm $f=0.0114$ $\langle S^{**2} \rangle = 0.000$

76 -> 82 -0.16005

77 -> 82 -0.11035

78 -> 82 -0.28097

79 -> 82 0.60412



Excited State 1: Singlet-A 3.0926 eV 400.90 nm $f=1.3073$ $\langle S^{2} \rangle = 0.000$**

97 -> 98 0.70208

Excited State 2: Singlet-A 3.6705 eV 337.79 nm $f=0.0848$ $\langle S^{**2} \rangle = 0.000$

96 -> 98 0.69411

Excited State 3: Singlet-A 3.9470 eV 314.12 nm $f=0.0130$ $\langle S^{**2} \rangle = 0.000$

92 -> 98 -0.15440

93 -> 98 0.10480

95 -> 98 0.66152

Table S3.3 GaussView Traces of Computed TD-B3LYP/6-311+G(d) Absorption Spectra of the Boron Dyes **H**, **C1**, and **C5**.

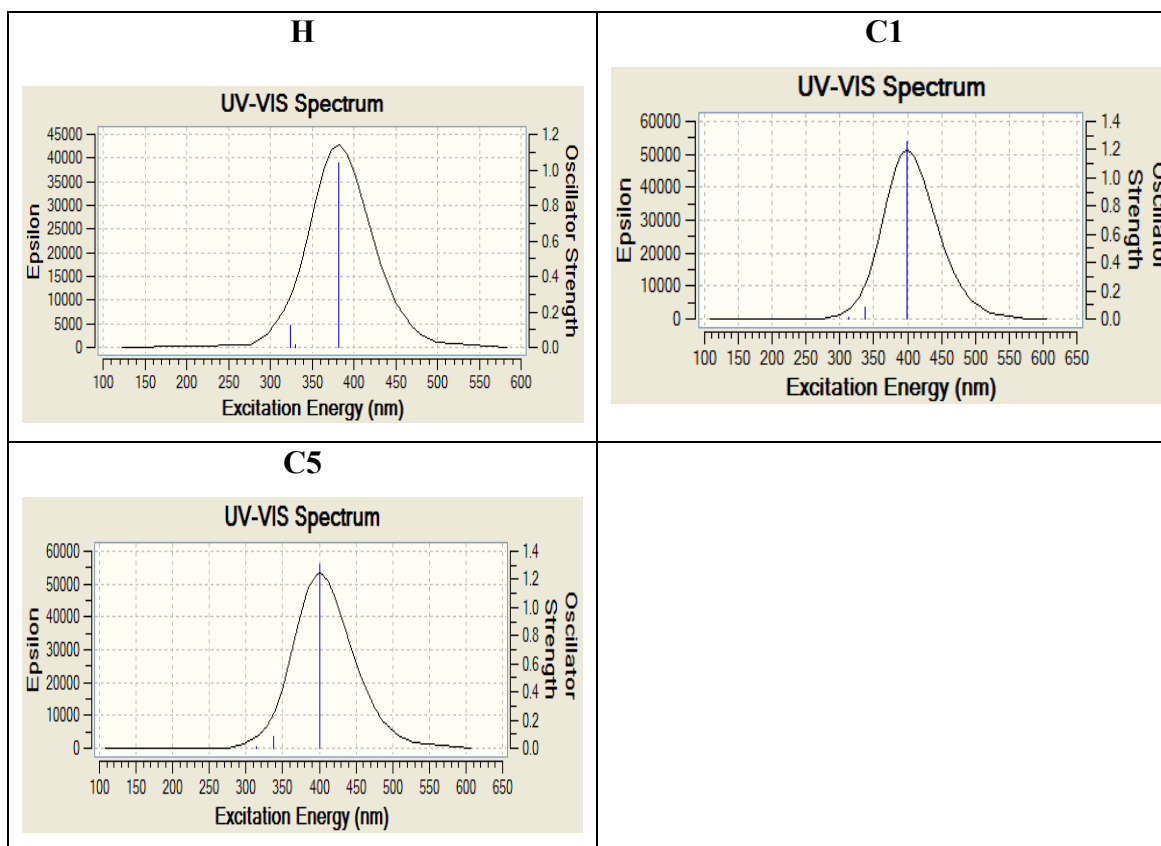
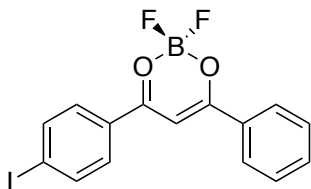
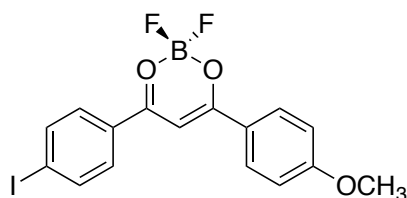


Table S3.4 Optimized S_1 Excited State Structures of Boron Compounds.



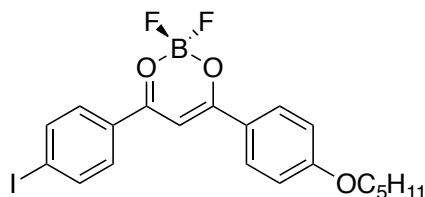
B, -2.55047500, 2.44678300, 0.06585300
 F, -2.64559700, 2.82349200, 1.41982000
 F, -2.82280900, 3.53135700, -0.76397300
 O, -3.54896900, 1.38398700, -0.20602700
 C, -3.24315400, 0.10212500, -0.04779000
 C, -1.88227400, -0.26841300, 0.06781400
 H, -1.62648000, -1.30377000, 0.21926800
 O, -1.17554300, 1.97481600, -0.21028900
 C, -0.86025400, 0.69250500, -0.04393800
 C, 0.54804700, 0.37265900, -0.02961000

C, 1.03785600, -0.95892900, 0.10970300
 C, 1.50071000, 1.42156100, -0.16547200
 C, 2.39104800, -1.22500600, 0.11764400
 H, 0.35401400, -1.79115700, 0.21345000
 C, 2.85516600, 1.16088900, -0.15977600
 H, 1.14861500, 2.43862000, -0.27269000
 C, 3.30372600, -0.16469700, -0.01687900
 H, 2.74041600, -2.24407300, 0.22623000
 H, 3.56333700, 1.97324200, -0.26359600
 C, -4.33899800, -0.83619500, -0.04077500
 C, -4.14419600, -2.24298900, 0.05648100
 C, -5.67171900, -0.35398700, -0.14117100
 C, -5.22402900, -3.10814700, 0.05822900
 H, -3.14646000, -2.65736700, 0.12752500
 C, -6.74279300, -1.23007200, -0.13989500
 H, -5.83733000, 0.71270500, -0.21506700
 C, -6.53092600, -2.61298600, -0.03964500
 H, -5.05404500, -4.17669100, 0.13391000
 H, -7.75336800, -0.84293100, -0.21508800
 H, -7.37398300, -3.29536000, -0.03819400
 I, 5.37283300, -0.55851200, -0.00616300



B, -1.63563200, 2.87876200, 0.05752900
 F, -1.69937300, 3.25805700, 1.41462100
 F, -1.78436600, 3.99412000, -0.76499100
 O, -2.73005000, 1.92745900, -0.23101700
 C, -2.53153600, 0.62113100, -0.05742400
 C, -1.24435400, 0.11350500, 0.07260200
 H, -1.09767900, -0.94194600, 0.23184100
 O, -0.31020300, 2.27109000, -0.20859300
 C, -0.10878500, 0.96860300, -0.03654500
 C, 1.24717000, 0.50995400, -0.02272800
 C, 1.59721200, -0.86570000, 0.10636500
 C, 2.31040300, 1.44952800, -0.14905900
 C, 2.91786000, -1.27215400, 0.11222600
 H, 0.83149400, -1.62494600, 0.20348600
 C, 3.63093900, 1.04429300, -0.14477900
 H, 2.07314000, 2.50065100, -0.24719000
 C, 3.93679700, -0.31829500, -0.01434000
 H, 3.15542600, -2.32392300, 0.21397200

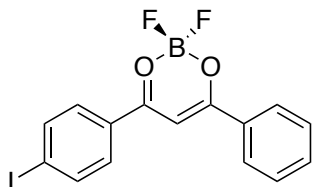
H, 4.42033800, 1.77971100, -0.24054800
 C, -3.73706900, -0.20349000, -0.03877000
 C, -3.70003900, -1.62147300, 0.05642900
 C, -5.00834000, 0.42323500, -0.12302100
 C, -4.85758900, -2.36015100, 0.07364800
 H, -2.75474100, -2.14529200, 0.11348200
 C, -6.17856000, -0.30861600, -0.10854800
 H, -5.05183100, 1.50145300, -0.19687000
 C, -6.11794000, -1.71620700, -0.00756200
 H, -4.83277400 -3.44100200, 0.14630300
 H, -7.12966000, 0.20324200, -0.17255000
 I, 5.96849100, -0.94206100, -0.00985400
 O, -7.18178900, -2.52262000, 0.01699000
 C, -8.50879400 -1.97513700 -0.06009500
 H, -9.17541600, -2.83167900, -0.02262900
 H, -8.69942600, -1.31587400, 0.78863100
 H, -8.64501300, -1.43612300, -0.99937800



B, 0.38333000, 3.32333000, 0.06138700
 F, 0.34410700, 3.68401100, 1.40441300
 F, 0.41525000, 4.42932500, -0.76582400
 O, -0.83304900, 2.52914600, -0.26636200
 C, -0.81598600, 1.20573300, -0.12991800
 C, 0.37847200, 0.51202600, 0.00933100
 H, 0.36671600, -0.55756600, 0.15035000
 O, 1.61784300, 2.52315500, -0.18926200
 C, 1.63060300, 1.20281100, -0.05829200
 C, 2.90595600, 0.55175900, -0.03479500
 C, 3.05215200, -0.86498500, 0.04815200
 C, 4.09935500, 1.33037400, -0.10110300
 C, 4.30312300, -1.45559300, 0.06977900
 H, 2.18130600, -1.50895000, 0.09353700
 C, 5.34696000, 0.73464400, -0.07957600
 H, 4.01661700, 2.40883100, -0.16446500
 C, 5.45876200, -0.66290500, 0.00641800
 H, 4.38329500, -2.53527900, 0.13397400
 H, 6.23798900, 1.35155500, -0.12823500
 C, -2.13199700, 0.55457600, -0.12583500
 C, -2.29314700, -0.85702500, -0.18924000
 C, -3.30227400, 1.35909200, -0.06468400

C, -3.54594300, -1.42741600, -0.17641900
 H, -1.42750900, -1.50495500, -0.26146800
 C, -4.56635500, 0.80030500, -0.05394600
 H, -3.18655300, 2.43514800, -0.02223300
 C, -4.70542400, -0.60851300, -0.10591400
 H, -3.67817300, -2.50292900, -0.22497800
 H, -5.43781700, 1.44162100, -0.00455800
 I, 7.35950700, -1.56952200, 0.03698700
 O, -5.86970600, -1.26079200, -0.09679900
 C, -7.12222400, -0.53784700, -0.01699000
 H, -7.12031300, 0.06529400, 0.89856600
 H, -7.19478800, 0.13329600, -0.88105700
 C, -8.24469600, -1.56280500, -0.00904700
 H, -8.09938500, -2.24065700, 0.84146300
 H, -8.17670400, -2.16998600, -0.92044000
 C, -9.62533900, -0.89744400, 0.07861500
 H, -9.67934300, -0.28218500, 0.98831200
 H, -9.75541500, -0.20830100, -0.76826200
 C, -10.77575900, -1.91298900, 0.08580300
 H, -10.64294200, -2.60332900, 0.93048800
 H, -10.72096700, -2.52715800, -0.82381600
 C, -12.15545000, -1.25295100, 0.17595400
 H, -12.95473100, -2.00273900, 0.17802300
 H, -12.25172200, -0.65960300, 1.09361000
 H, -12.32971400, -0.58128500, -0.67370900

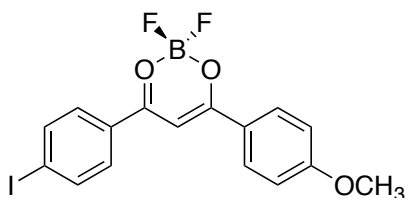
Table S3.5 Characterizations of Spectra Emission Computed in Dichloromethane Solvent
 Note: Max amplitude is 0.70714 for a pure one-electron excitation. The highest occupied molecular orbital (HOMO) to the lowest unoccupied molecular orbital (LUMO) transitions are in bold.



Excited State 1: Singlet-A 3.0048 eV 412.63 nm f=1.1415 <S2>=0.000**
73 -> 74 0.70535

Excited State 2: Singlet-A 3.6581 eV 338.93 nm f=0.0351 <S**2>=0.000
 71 -> 74 0.60240
 72 -> 74 0.35527

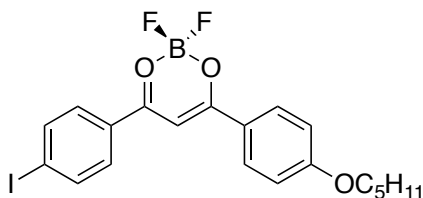
Excited State 3: Singlet-A 3.6903 eV 335.97 nm $f=0.0905$ $\langle S^{**2} \rangle = 0.000$
 71 -> 74 -0.35569
 72 -> 74 0.59781



Excited State 1: Singlet-A 2.8589 eV 433.67 nm $f=1.2553$ $\langle S^{2} \rangle = 0.000$**
81 -> 82 0.70462

Excited State 2: Singlet-A 3.5251 eV 351.72 nm $f=0.1504$ $\langle S^{**2} \rangle = 0.000$
 80 -> 82 0.69305

Excited State 3: Singlet-A 3.8746 eV 319.99 nm $f=0.0000$ $\langle S^{**2} \rangle = 0.000$
 78 -> 82 0.70218

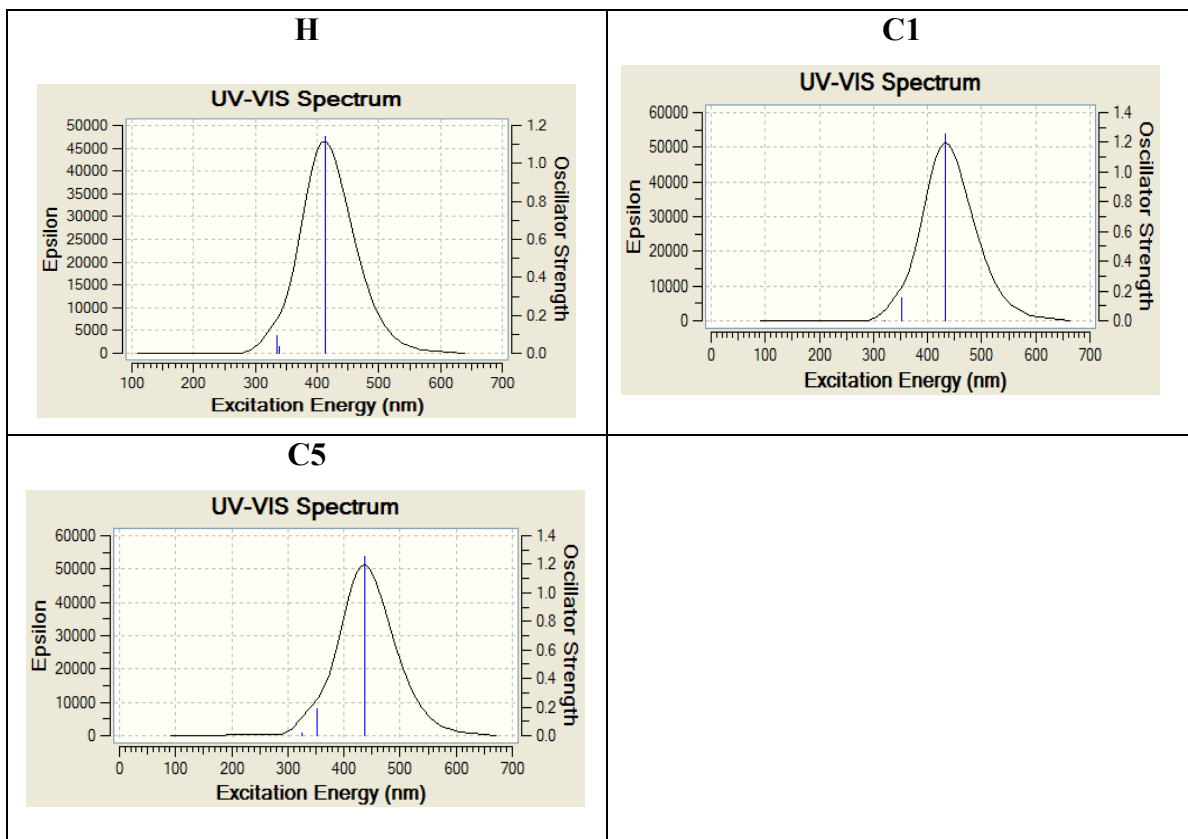


Excited State 1: Singlet-A 2.8394 eV 436.66 nm $f=1.2557$ $\langle S^{2} \rangle = 0.000$**
97 -> 98 0.70477

Excited State 2: Singlet-A 3.5234 eV 351.89 nm $f=0.1868$ $\langle S^{**2} \rangle = 0.000$
 96 -> 98 0.69249

Excited State 3: Singlet-A 3.8188 eV 324.66 nm $f=0.0157$ $\langle S^{**2} \rangle = 0.000$
 93 -> 98 -0.14159
 95 -> 98 0.67498

Table S3.6 GaussView Traces of Computed TD-B3LYP/6-311+G(d) Emission Spectra of the Boron Dyes **H**, **C1**, and **C5**.



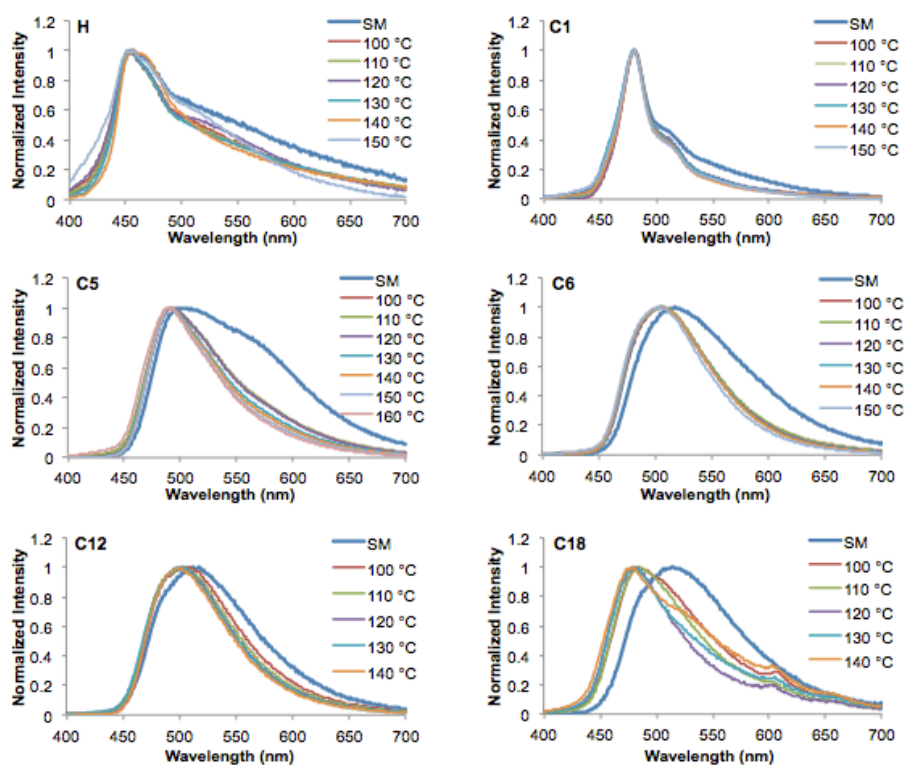


Figure S3.1. Emission spectra of BF₂dbm(I)R dyes as films on weighing paper after annealing for ten minutes at the indicated temperatures ($\lambda_{\text{ex}} = 369$ nm) (room temperature, air). Note: SM = an exemplary spectrum of the smeared dye film.

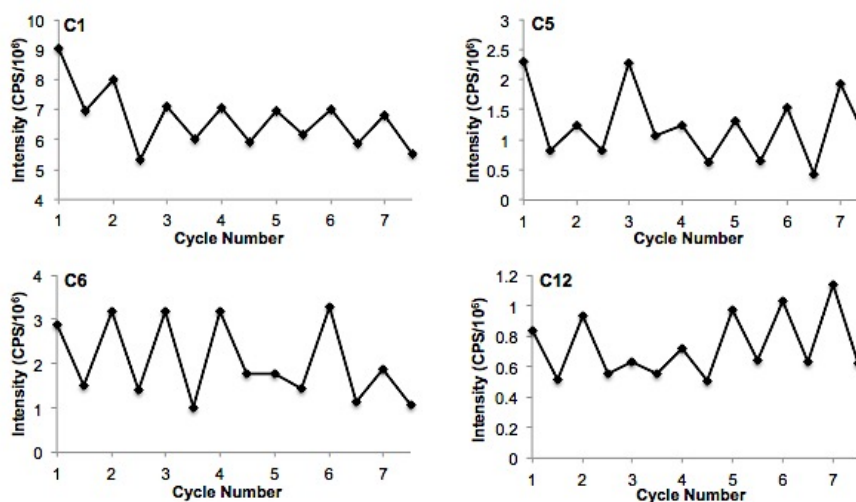


Figure S3.2. Emission intensities of the C1, C5, C6, and C12 dyes as films on weighing paper monitored through seven cycles of smearing and annealing ($\lambda_{\text{ex}} = 369$ nm) (room temperature, air). The intensities were recorded in photon counts per second (CPS) and shown as $\text{CPS}/10^6$.

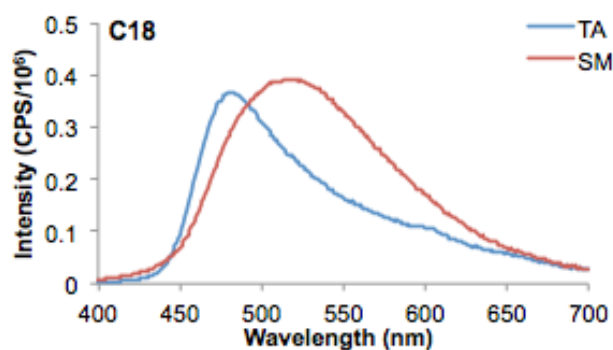


Figure S3.3 Emission spectra of the C18 dye as a film on weighing paper in both thermally annealed (TA) and smeared (SM) states showing an increase in emission intensity after smearing ($\lambda_{\text{ex}} = 369$ nm) (room temperature, air). The intensities were recorded in photon counts per second (CPS) and shown as $\text{CPS}/10^6$.

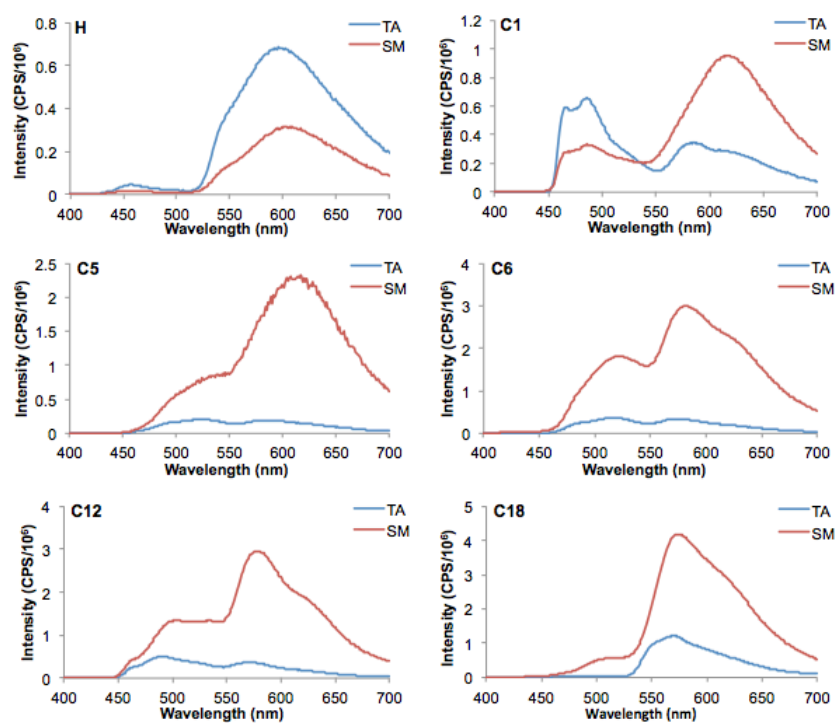


Figure S3.4 Total emission spectra of boron dyes on weighing paper in both thermally annealed (TA) and smeared (SM) states ($\lambda_{\text{ex}} = 369 \text{ nm}$) (77 K, liquid N₂). The intensities were recorded in photon counts per second (CPS) and shown as CPS/10⁶.

Table S3.7 Emission Maxima and Lifetimes with % Weighting Factors for the Dyes as Films on Weighing Paper at Room Temperature under Air.^a

Dye BF ₂ dbm(I)R [R=]	Thermally Annealed λ_{em}^b [nm]	Thermally Annealed τ^c [ns]	Smeared λ_{em}^b [nm]	Smeared τ^c [ns]	$\Delta\tau_{pw0}^d$ [ns]
H	451	0.1 (92.96%) 3.95 (7.04%) 0.37 (τ_{pw0})	457	0.20 (85.13%) 4.45 (14.87%) 0.83 (τ_{pw0})	0.54
C1	481	0.03 (99.43%) 1.32 (0.57%) 0.04 (τ_{pw0})	480	0.04 (98.76%) 1.76 (1.24%) 0.06 (τ_{pw0})	0.02
C5	493	0.14 (34.37%) 1.54 (65.63%) 1.05 (τ_{pw0})	497	0.08 (54.36%) 1.21 (40.91%) 3.21 (4.73%) 0.69 (τ_{pw0})	0.36
C6	504	0.84 (23.80%) 2.92 (76.20%) 2.42 (τ_{pw0})	511	0.03 (80.65%) 1.69 (13.62%) 3.46 (5.72%) 0.45 (τ_{pw0})	1.97
C12	502	0.23 (31.45%) 1.61 (63.60%) 3.99 (4.94%) 1.29 (τ_{pw0})	513	0.36 (52.21%) 1.40 (43.48%) 4.94 (4.31%) 1.01 (τ_{pw0})	0.28
C18	480	0.06 (96.06%) 1.37 (3.05%) 6.39 (0.89%) 0.16 (τ_{pw0})	518	0.50 (82.83%) 3.32 (17.17%) 0.98 (τ_{pw0})	0.82

^a $\lambda_{ex} = 369$ nm.^b Emission maximum; fluorescence.^c Fluorescence lifetime.^d Pre-exponential weighted lifetime.

Note: Emission lifetimes were multi-exponential, and the decay traces of emission intensity at λ_{em} and the % weighting factors (WF) were analyzed using DataStation version 2.6 software from Horiba Jobin Yvon. τ_{pw0} was calculated as follows:

$$\tau_{pw0} = \sum_{i=1}^N WF_i \cdot \tau_i$$

where N is the number of decay components, WF_i is the weighting factor, τ_i is the component of decay lifetimes, and τ_{pw0} is the pre-exponential weighted lifetime.⁷

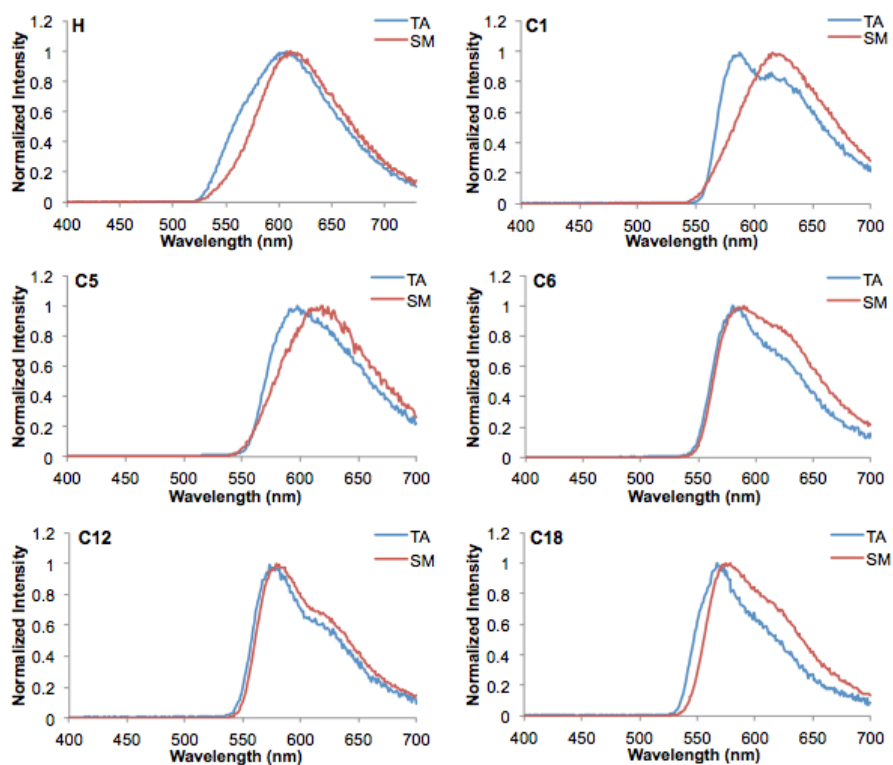


Figure S3.5 Normalized delayed emission spectra of the boron dyes as films on weighing paper in both thermally annealed (TA) and smeared (SM) states ($\lambda_{\text{ex}} = 369$ nm) (77 K, liquid N₂).

Table S3.8 Delayed Emission Maxima and Lifetimes with % Weighting Factors for the Dyes as Films on Weighing Paper at 77K in Liquid N₂.^a

Dye BF ₂ dbm(I)R [R=]	Thermally Annealed λ_{phos}^b [nm]	Thermally Annealed τ_{phos}^c [ms]	Smeared λ_{phos}^b [nm]	Smeared τ_{phos}^c [ms]	$\Delta\tau_{\text{pw0}}^d$ [ms]
H	607	0.06 (τ_{pw0})	611	0.05 (τ_{pw0})	0.01
C1	581	6.29 (40.48%) 23.97 (35.11%) 105.54 (5.11%) 0.98 (19.30%) 16.6 (τ_{pw0})	621	5.98 (61.88%) 15.02 (21.64%) 100.23 (2.69%) 1.27 (13.80%) 9.8 (τ_{pw0})	6.8
C5	598	2.61 (27.22%) 10.92 (68.34%) 48.41 (4.43%) 10.3 (τ_{pw0})	618	7.48 (62.48%) 15.49 (24.18%) 1.69 (13.34%) 8.6 (τ_{pw0})	1.7
C6	580	4.97 (29.75%) 13.50 (63.55%) 81.85 (1.58%) 0.87 (5.13%) 11.4 (τ_{pw0})	590	1.21 (4.30%) 6.52 (36.74%) 103.94 (0.37%) 14.74 (58.59%) 11.5 (τ_{pw0})	0.1
C12	573	1.57 (14.20%) 17.6 (31.85%) 233 (1.87%) 8.10 (52.08%) 14.4 (τ_{pw0})	580	96.1 (0.52%) 1480 (1.37%) 14.7 (98.11%) 35.2 (τ_{pw0})	20.8
C18	567	29.15 (2.39%) 5.46 (30.74%) 1.88 (66.88%) 3.6 (τ_{pw0})	578	36.80 (3.65%) 10.49 (57.45%) 2.22 (38.90%) 8.2 (τ_{pw0})	4.6
^a $\lambda_{\text{ex}} = 369$ nm.					
^b Emission maximum; phosphorescence.					
^c Phosphorescence lifetime.					
^d Pre-exponential weighted lifetime.					

Table S3.9. Emission Maxima and Lifetimes with % Weighting Factors for the Dyes as Spin-cast Films on Glass at Room Temperature under Air.^a

Dye BF ₂ dbm(I)R [R=]	As-spun λ_{em}^b [nm]	As-spun τ^c [ns]	Thermally Annealed λ_{em}^b [nm]	Thermally Annealed τ^c [ns]	Smeared λ_{em}^b [nm]	Smeared τ^c [ns]
H	561	0.42 (30.46%) 1.69 (67.96%) 59.32 (1.58%) 2.21 (τ_{pw0}^d)	565	1.43 (70.02%) 2.21 (29.98%) 1.66 (τ_{pw0})	541	0.48 (44.27%) 1.61 (51.91%) 5.03 (3.82%) 1.24 (τ_{pw0})
C1	481	.21 (τ_{pw0})	480	0.03 (98.96%) 0.80 (1.04%) 0.04 (τ_{pw0})	550	0.56 (50.69%) 1.71 (41.76%) 4.70 (7.55%) 1.35 (τ_{pw0})
C5	549	0.33 (41.69%) 1.58 (44.94%) 5.21 (13.37%) 1.54 (τ_{pw0})	488	0.82 (57.67%) 2.05 (42.33%) 1.34 (τ_{pw0})	557	0.33 (27.29%) 1.55 (52.76%) 4.69 (19.95%) 1.84 (τ_{pw0})
C6	527	0.04 (76.05%) 1.05 (19.18%) 3.81 (4.77%) 0.41 (τ_{pw0})	490	1.26 (16.50%) 3.64 (83.50%) 3.25 (τ_{pw0})	536	0.33 (39.24%) 1.37 (46.31%) 4.39 (14.45%) 1.40 (τ_{pw0})
C12	513	0.30 (51.36%) 0.98 (44.16%) 3.69 (4.48%) 0.75 (τ_{pw0})	479	0.79 (45.96%) 2.00 (54.04%) 1.44 (τ_{pw0})	513	0.03 (88.10%) 0.80 (10.71%) 3.21 (1.19%) 0.15 (τ_{pw0})
C18	484	0.13 (90.22%) 1.54 (9.78%) 0.27 (τ_{pw0})	478	0.09 (98.21%) 1.38 (1.79%) 0.11 (τ_{pw0})	522	0.13 (44.98%) 0.95 (47.80%) 3.79 (7.22%) 0.79 (τ_{pw0})
^a $\lambda_{ex} = 369$ nm. ^b Emission maximum; fluorescence. ^c Fluorescence lifetime. ^d Pre-exponential weighted lifetime.						

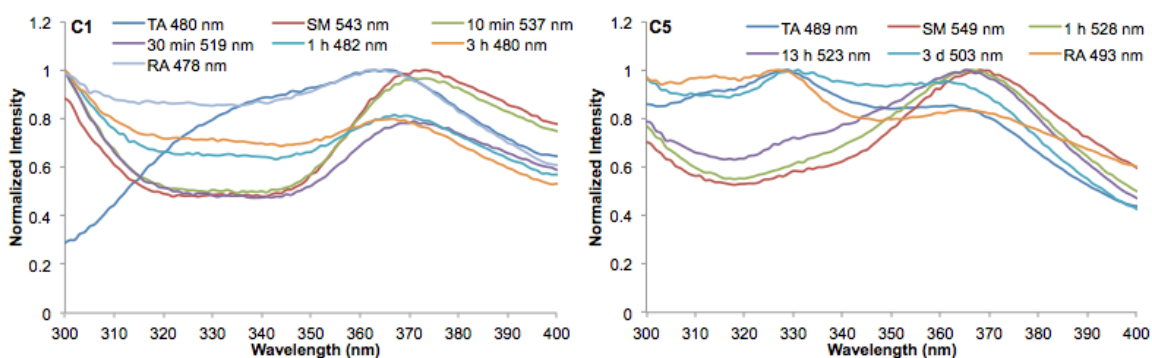


Figure S3.6. Excitation spectra of the C1 and C5 dyes as spin-cast films recorded for the thermally annealed (TA), smeared (SM), and re-annealed (RA) states as well as at various points during the spontaneous recovery processes under ambient conditions. Note: The peak emission wavelength is indicated next to the time interval in the legend.

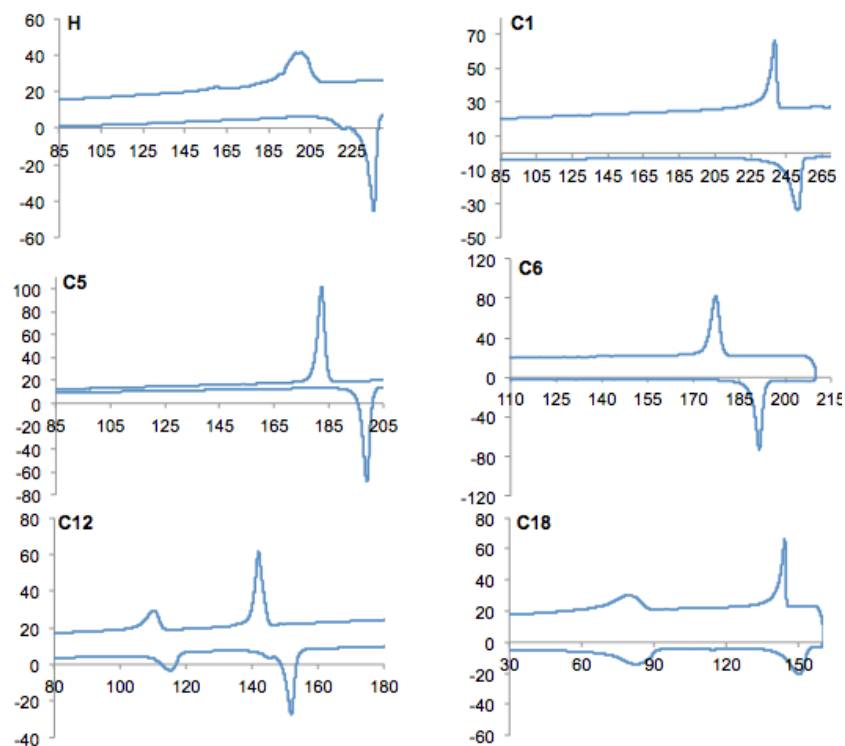


Figure S3.7 Differential scanning calorimetry (DSC) thermograms of the dyes. The second cycle is shown for all samples.

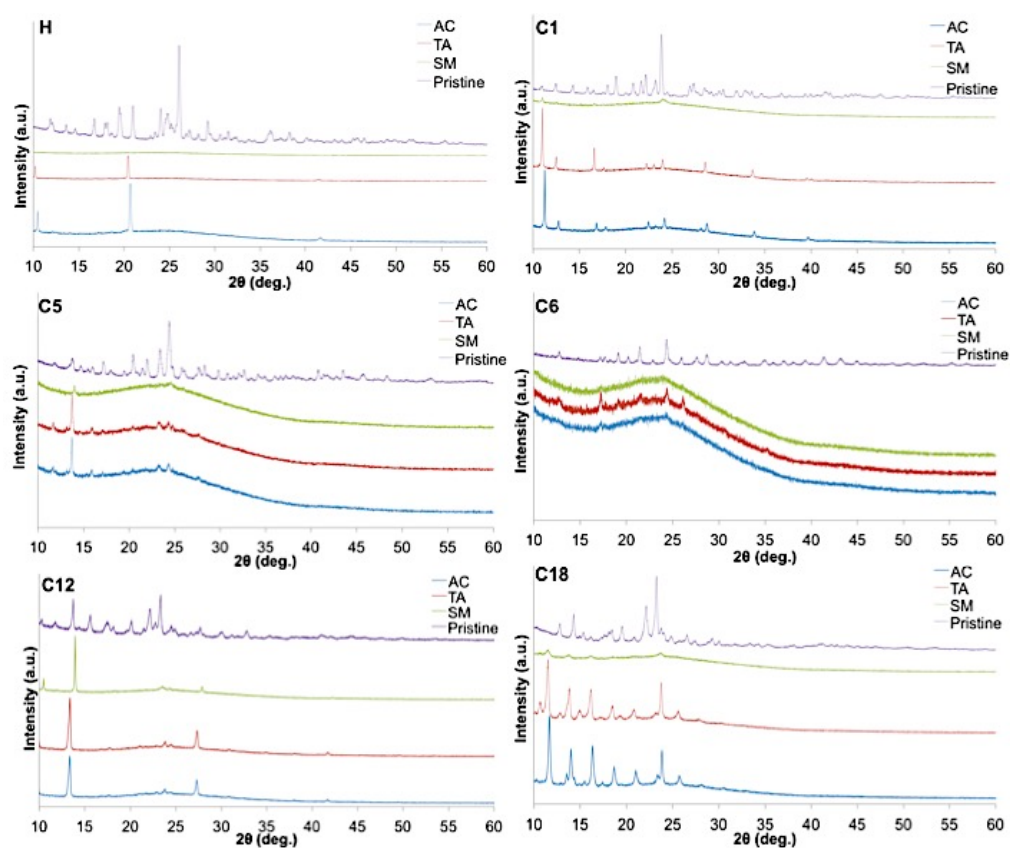


Figure S3.8 Powder X-ray diffraction patterns of the dyes as pristine powders and drop-cast films on glass in their as-cast (AC), thermally annealed (TA), and smeared (SM) states.

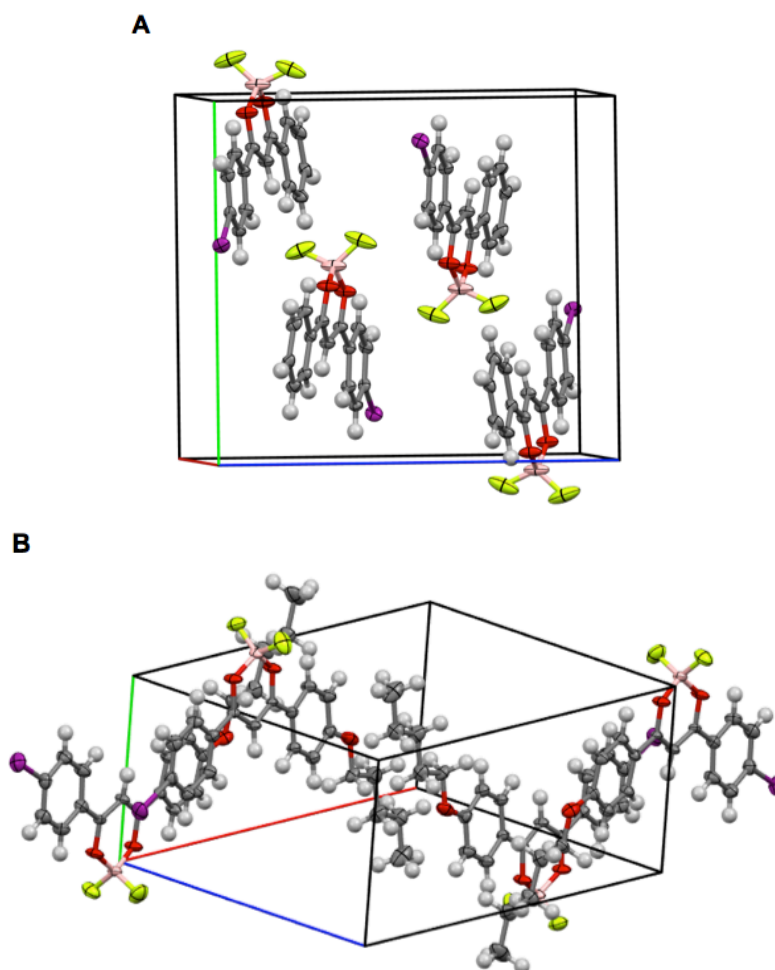


Figure S3.9 Crystal packing of H (A) and C5 (B) dyes showing the unit cells.

References

- (1) Nguyen, N. D.; Zhang, G.; Lu, J.; Sherman, A. E.; Fraser, C. L. *J. Mater. Chem.* **2011**, *21*, 8409.
- (2) Frisch, M. J.; Trucks, G. W.; Schlegel, H. B.; Scuseria, G. E.; Robb, M. A.; Cheeseman, J. R.; Scalmani, G.; Barone, V.; Mennucci, B.; Petersson, G. A.; Nakatsuji, H.; Caricato, M.; Li, X.; Hratchian, H. P.; Izmaylov, A. F.; Bloino, J.; Zheng, G.; Sonnenberg, J. L.; Hada, M.; Ehara, M.; Toyota, K.; Fukuda, R.; Hasegawa, J.; Ishida, M.; Nakajima, T.; Honda, Y.; Kitao, O.; Nakai, H.; Vreven, T.; Montgomery, J. A.; Peralta, J. E.; Ogliaro, F.; Bearpark, M.; Heyd, J. J.; Brothers, E.; Kudin, K. N.; Staroverov, V. N.; Kobayashi, R.; Normand, J.; Raghavachari, K.; Rendell, A.; Burant, J. C.; Iyengar, S. S.; Tomasi, J.; Cossi, M.; Rega, N.; Millam, J. M.; Klene, M.; Knox, J. E.; Cross, J. B.; Bakken, V.; Adamo, C.; Jaramillo, J.; Gomperts, R.; Stratmann, R. E.; Yazyev, O.; Austin, A. J.; Cammi, R.; Pomelli, C.; Ochterski, J. W.; Martin, R. L.;

Morokuma, K.; Zakrzewski, V. G.; Voth, G. A.; Salvador, P.; Dannenberg, J. J.; Dapprich, S.; Daniels, A. D.; Farkas; Foresman, J. B.; Ortiz, J. V.; Cioslowski, J.; Fox, D. J. Wallingford CT, 2009.

(3) Becke, A. D. *J. Chem. Phys.* **1993**, *98*, 5648.

(4) Lee, C.; Yang, W.; Parr, R. G. *Phys. Rev. B: Condens. Matter* **1988**, *37*, 785.

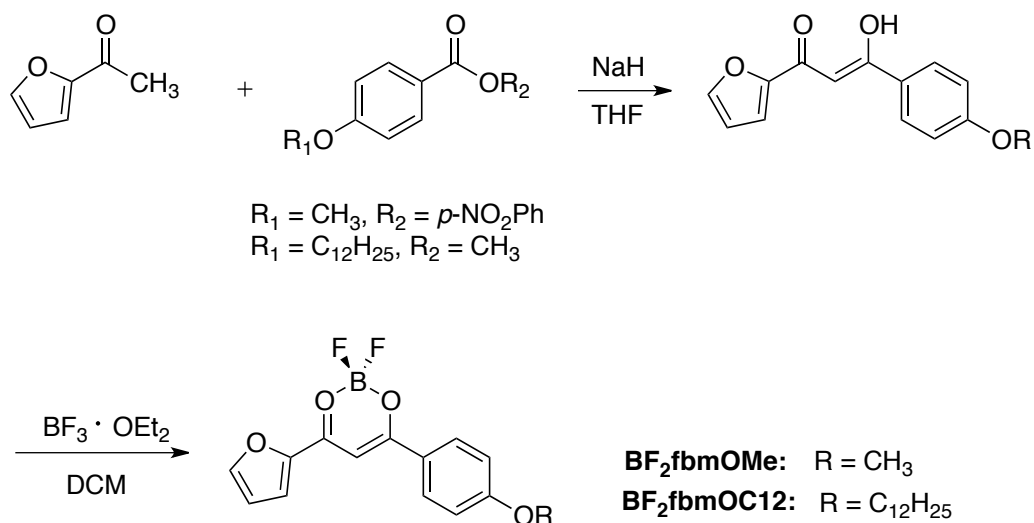
(5) Tomasi, J.; Mennucci, B.; Cammi, R. *Chem. Rev.* **2005**, *105*, 2999.

(6) Dennington, R. In *Version 5*; Keith, T., Ed.; Semichem Inc.: Shawnee Mission, KS, 2009.

(7) Carraway, E. R.; Demas, J. N.; DeGraff, B. A.; Bacon, J. R. *Anal. Chem.* **1991**, *63*, 337.

Appendix C

Supporting Information for Chapter 4

Scheme S4.1 Synthesis of Furan-Substituted Difluoroboron β -Diketonate Dyes


BF₂fbmOMe. The ligand fbmOMe¹ was prepared by Claisen condensation of the 2-furyl methyl ketone (0.360 g, 3.27 mmol) and 4-nitrophenyl-4-methoxybenzoate (0.890 g, 3.26 mmol) in THF in the presence of NaH (0.136 g, 5.67 mmol) under a nitrogen atmosphere. The reaction mixture was refluxed for 22 h, allowed to cool to RT, quenched with 1 M HCl, then THF was removed *via* rotary evaporation. The organic layer was extracted with CH₂Cl₂ (2 × 20 mL), washed with H₂O (2 × 20 mL) and brine (10 mL) then dried over Na₂SO₄. After filtration, and concentration *in vacuo*, the residue was purified by column chromatography on silica gel eluting with hexanes/EtOAc (4:1) to give the ligand as a yellow solid: 377 mg (47%) . The fbmOMe ligand (200 mg, 0.82 mmol) was dissolved in THF (25 mL), and boron trifluoride diethyl etherate (152 μ L, 1.23 mmol) was added at room temperature under a nitrogen atmosphere. The reaction mixture was heated at 60° C and monitored by TLC until consumption of ligand substrate was complete (20 h). The reaction mixture was filtered and the solvent was removed *via* rotary evaporation. The product was purified by column chromatography with hexanes:EtOAc (3:1) and an

orange powder was obtained: 63 mg (47%). ^1H NMR (600 MHz, CDCl_3 , ppm) δ 8.14 (d, 2H, $J = 12.0$ Hz, 2, 6-PhenH), 7.75 (broad s, 1H, 2-FurH), 7.55 (d, 1H, $J = 3.6$ Hz, 4-FurH), 7.03 (d, 2H, $J = 6.0$ Hz, 3, 5-PhenH), 6.71 (m, 1H, 3-FurH), 6.98 (s, 1H, COCHCO), 3.93 (s, 3H, OCH_3). HRMS (ESI, TOF) m/z calcd for $\text{C}_{14}\text{H}_{11}\text{BF}_2\text{O}_4$ 292.07, found 315.0620 $[\text{M} + \text{Na}]^+$.

BF₂fbmOC12. The ligand fbmOC12 was prepared by Claisen condensation of the 2-furyl methyl ketone (1.00 g, 9.08 mmol) and methyl-4-(dodecyloxy)benzoate (2.33 g, 7.28 mmol) in THF in the presence of NaH (0.436 g, 18.17 mmol) under a nitrogen atmosphere. The reaction mixture was heated at 60 °C under a nitrogen atmosphere and monitored by TLC. After 22 h the reaction mixture was removed from the heat and allowed to cool to RT and quenched with 1 M HCl. The THF was removed *via* rotary evaporation. Organics were extracted with CH_2Cl_2 (20 mL \times 2), washed with H_2O (20 mL \times 2) and brine (10 mL) then dried over Na_2SO_4 . After a filtration, and concentration *in vacuo*, the residue run through silica gel column eluting with hexanes/EtOAc (4:1) to give the ligand as a yellow solid. The boron dye, BF₂fbmOC12 was made as described for BF₂fbmOMe but with the fbmOC12 ligand. The product was purified by recrystallization from hexanes to give a yellow solid: 204 mg (37%). ^1H NMR (600 MHz, CDCl_3 , ppm): 8.11 (d, 2H, $J = 12.0$ Hz, 2, 6-PhenH), 7.73 (broad s, 1H, 2-FurH), 7.53 (d, 1H, $J = 3.6$ Hz, 4-FurH), 6.98 (m, 3H, 3-FurH, 3, 5-PhenH), 6.69 (s, 1H, COCHCO), 4.06 (t, 2H, $J = 6.0$ Hz, $\text{OCH}_2\text{C}_{11}\text{H}_{23}$), 1.83-1.81 (m, 2H, $\text{OCH}_2\text{CH}_2\text{C}_{10}\text{H}_{21}$), 1.46-1.25 (m, 18H, $\text{OCH}_2\text{CH}_2\text{C}_9\text{H}_{18}\text{CH}_3$), 0.87 (t, 3H, $J = 6.0$ Hz, CH_2CH_3). HRMS (ESI, TOF) m/z calcd for $\text{C}_{25}\text{H}_{33}\text{BF}_2\text{O}_4$ 446.24, found 447.2519 $[\text{M} + \text{H}]^+$ and 469.2337 $[\text{M} + \text{Na}]^+$.

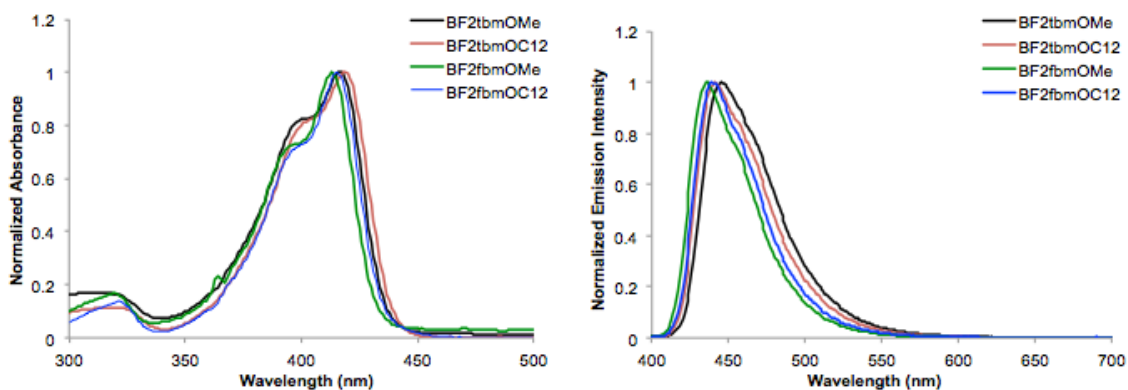


Figure S4.1 Absorption (left) and fluorescence emission (right) spectra of thiophene and furan-substituted dyes in CH_2Cl_2 solution.

Table S4.1 Solid State Emission Properties of Boron Dyes as Pristine Powders.

Dye	$\lambda_{\text{em}}^{\text{a}}$ (nm)	$\tau_{\text{F}}^{\text{b}}$ (ns)	FWHM (nm)
BF ₂ tbmOMe	593	5.0	105
BF ₂ tbmOC12	485	3.6	83
BF ₂ fbmOMe	601	10.7	108
BF ₂ fbmOC12	594	4.1	N/A

^a Peak emission wavelength ($\lambda_{\text{ex}} = 369$ nm), ^b Pre-exponential weighted fluorescence lifetimes excited with a 369 nm light-emitting diode (LED) monitored at the emission maximum. All fluorescence lifetimes are fitted with double-exponential decay.

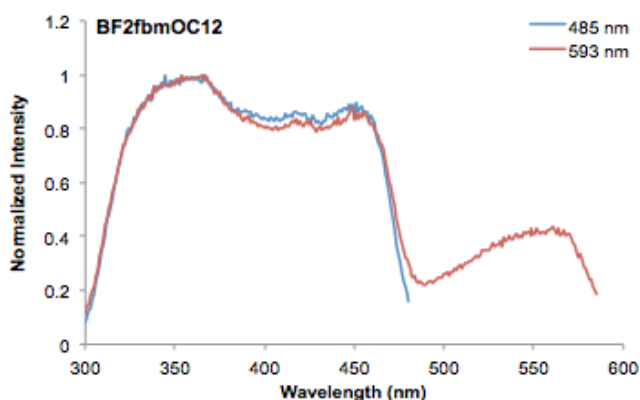


Figure S4.2 Excitation spectra of the BF₂fbmOC12 dye recorded at the indicated emission wavelengths.

Table S4.2 Optical Properties of Boron Dyes as Films on Both Weighing Paper and Glass Substrates.

Dye	As-Spun			Thermally Annealed			Smeared		
	λ_{em}^b [nm]	τ_{pw0}^c [ns]	FWH ^d M ^d [nm]	λ_{em}^b [nm]	τ_{pw0}^c [ns]	FWH ^d M ^d [nm]	λ_{em}^b [nm]	τ_{pw0}^c [ns]	FWH ^d M ^d [nm]
BF ₂ fbm OC12 (Glass)	525	4.06 (40.57%) 0.81 (17.39%) 13.95 (42.05%) 7.65 (τ_{pw0})	135	486	2.32 (11.57%) 7.65 (88.43%) 7.03 (τ_{pw0})	68	570	6.76 (31.02%) 9.62 (4.08%) 15.39 (64.90%) 12.12 (τ_{pw0})	119
	Heated Green			Heated Orange			TA (125 °C, 10 min)		
BF ₂ fbm OC12 (Paper)	517	0.26 (74.06%) 2.44 (20.61%) 17.48 (29.89%) 0.80 (τ_{pw0})	127	553	4.34 (51.06%) 0.88 (19.11%) 17.48 (29.89%) 7.61 (τ_{pw0})		155	3.77 (1.48 %) 0.02 (96.66 %) 10.44 (4.86 %) 0.58 (τ_{pw0})	84
	As-Spun								
	λ_{em}^b [nm]	τ_{pw0}^c [ns]		FWHM ^d [nm]					
BF ₂ fbm OC12 (Glass)	597	8.47 (9.09%) 29.44 (90.91%) 27.53 (τ_{pw0})		114					
^a λ_{ex} = 369 nm; room temperature, air. ^b Emission maximum; fluorescence. ^c Pre-exponential weighted fluorescence lifetime. ^d Full Width at Half Maximum.									

Note: Emission lifetimes were multi-exponential, and the decay traces of emission intensity at λ_{em} and the % weighting factors (WF) were analyzed using DataStation version 2.6 software from Horiba Jobin Yvon. τ_{pw0} was calculated as follows:

$$\tau_{pw0} = \sum_{i=1}^N WF_i \cdot \tau_i$$

where N is the number of decay components, WF_i is the weighting factor, τ_i is the component of decay lifetimes, and τ_{pw0} is the pre-exponential weighted lifetime.²

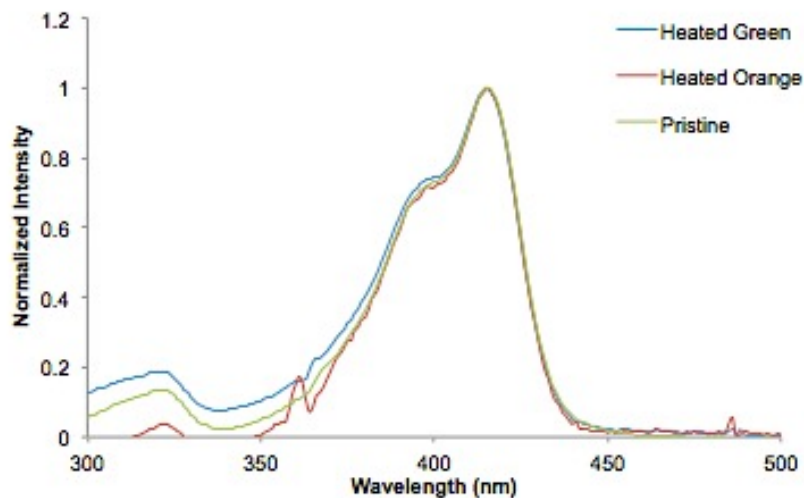


Figure S4.3 Absorption spectra of $\text{BF}_2\text{fbmOC12}$ in CH_2Cl_2 solution. The original spectrum of the pristine powder dissolved in CH_2Cl_2 is compared to the heated green and heated orange forms after they were redissolved and their absorption spectra recorded.

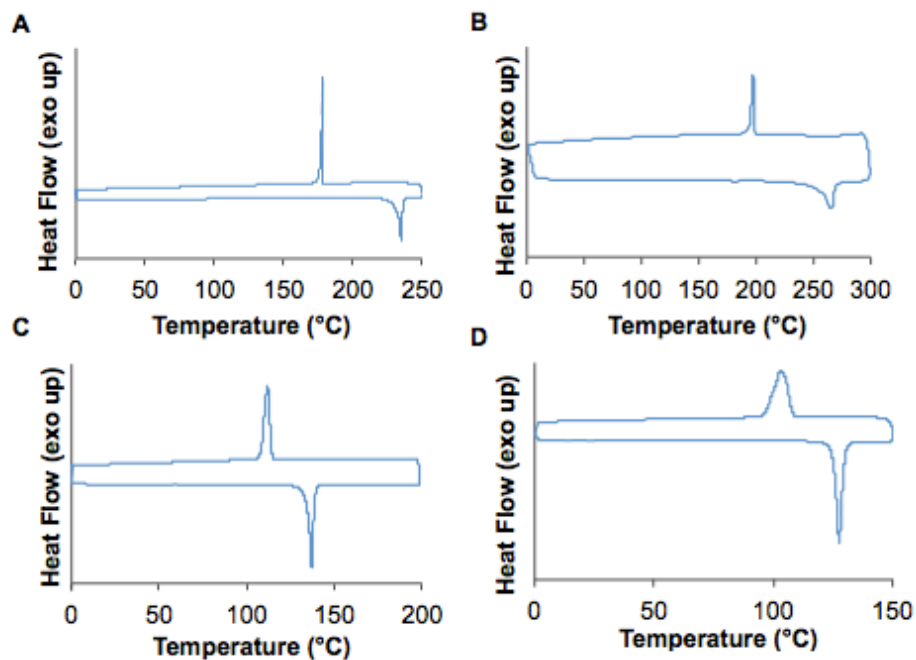


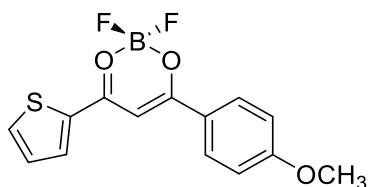
Figure S4.4 DSC thermograms (ramp rate: $5\text{ }^\circ\text{C}/\text{min}$; second heating cycles, after a conditioning cycle) (A = BF_2fbmOMe , B = BF_2tbmOMe , C = $\text{BF}_2\text{tbmOC12}$, D = $\text{BF}_2\text{fbmOC12}$).

Full Computational Details

All compounds were modeled using the Gaussian 09 suite of programs using density functional theory (DFT).³ We chose B3LYP/6-31+G(d) for ground state geometry optimization with a Tomasi polarized continuum for dichloromethane solvent.⁴ The vibrational frequencies for the optimized geometries were all positive, assuring that the geometries are at least a local minimum. Single point energy calculations were used to generate the molecular orbital diagrams utilizing B3LYP/6-31G(d). We used time-dependent density functional theory, TD-B3LYP/6-311+G(d) for estimates of the absorption spectra, at the respective optimized geometries.^{5,6} The first three excited states were computed for each compound. Molecular orbitals were depicted by GaussView 5 software.⁷

Table S4.3 B3LYP/6-31+G(d) optimized structures for future TD-DFT calculations in dichloromethane. Coordinates given in Cartesian, in Angstroms.

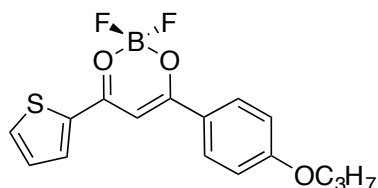
BF₂tbmOMe: E (HF) = -1388.75052444



B, 1.047254, 2.282697, 0.017732
 F, 1.124661, 2.799166, 1.314774
 F, 1.202579, 3.281518, -0.933151
 O, -0.282447, 1.645663, -0.170185
 C, -0.477890, 0.355937, -0.011772
 C, 0.614466, -0.508141, 0.126683
 H, 0.464047, -1.565011, 0.283980
 O, 2.133345, 1.278315, -0.164933
 C, 1.912630, -0.006943, -0.004006
 C, -1.873414, -0.079247, -0.015357
 C, -2.238571, -1.445633, -0.016885
 C, -2.902205, 0.882420, -0.018435
 C, -3.568597, -1.826026, -0.016137
 H, -1.481940, -2.222520, -0.030323
 C, -4.243255, 0.512697, -0.016228

H, -2.642530, 1.935050, -0.016399
 C, -4.585634, -0.850540, -0.014354
 H, -3.849070, -2.874685, -0.021573
 H, -5.006502, 1.281865, -0.013362
 C, 3.091296, -0.843875, -0.001247
 C, 3.181961, -2.226904, 0.061146
 S, 4.682528, -0.116946, -0.087821
 C, 4.518001, -2.694602, 0.042766
 H, 2.320618, -2.883097, 0.113641
 C, 5.432617, -1.666741, -0.036005
 H, 4.795000, -3.741984, 0.083380
 H, 6.512350, -1.742242, -0.066260
 O, -5.853525, -1.322099, -0.012439
 C, -6.944920, -0.391965, -0.016536
 H, -7.847203, -1.003413, -0.016865
 H, -6.924005, 0.236891, 0.880039
 H, -6.920553, 0.232992, -0.915734

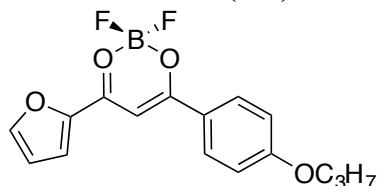
BF₂tbmOC3: E(HF) = -1467.38517722



B, 1.953805, 2.290010, 0.018338
 F, 2.049312, 2.798353, 1.317567
 F, 2.140271, 3.287382, -0.928444
 O, 0.604035, 1.697146, -0.170659
 C, 0.366378, 0.414672, -0.009728
 C, 1.430839, -0.483972, 0.128836
 H, 1.247355, -1.535148, 0.288446
 O, 3.006392, 1.251532, -0.169862
 C, 2.744037, -0.025641, -0.005775
 C, -1.041980, 0.024947, -0.010705
 C, -1.451350, -1.328971, -0.005690
 C, -2.039915, 1.018834, -0.016502
 C, -2.792797, -1.666170, -0.002540
 H, -0.720538, -2.130276, -0.015904
 C, -3.392012, 0.692602, -0.011495
 H, -1.746763, 2.062685, -0.018794
 C, -3.779662, -0.659266, -0.004123
 H, -3.106577, -2.705409, -0.003466
 H, -4.129490, 1.486399, -0.011121
 C, 3.894415, -0.901321, -0.004132

C, 3.938393, -2.286599, 0.057276
 S, 5.508989, -0.228339, -0.092033
 C, 5.257998, -2.799077, 0.037356
 H, 3.055298, -2.913313, 0.109799
 C, 6.206714, -1.802630, -0.041747
 H, 5.499531, -3.855247, 0.077023
 H, 7.283295, -1.914268, -0.073019
 O, -5.060415, -1.090053, -0.000753
 C, -6.136614, -0.128928, -0.013580
 H, -6.055001, 0.512366, 0.873262
 H, -6.047389, 0.496887, -0.910680
 C, -7.449455, -0.897649, -0.011962
 H, -7.481793, -1.542765, 0.875065
 H, -7.476940, -1.555444, -0.889782
 C, -8.658672, 0.045737, -0.021916
 H, -8.660410, 0.685270, -0.913268
 H, -9.592725, -0.526316, -0.020253
 H, -8.664938, 0.697935, 0.860175

BF₂fbmOMe: E (HF) = -1065.77175714



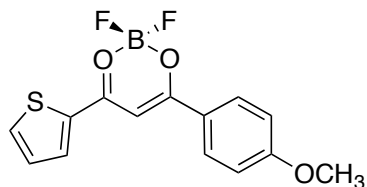
B, -1.358574, 2.226738, 0.012859
 F, -1.529753, 3.221209, -0.939848
 F, -1.445086, 2.743624, 1.309147
 O, -0.017365, 1.612934, -0.173240
 C, 0.201948, 0.326534, -0.015932
 C, -0.875329, -0.555596, 0.119118
 H, -0.711798, -1.611715, 0.270693
 O, -2.430252, 1.205581, -0.167665
 C, -2.180008, -0.070616, -0.010586
 C, 1.605045, -0.083523, -0.017739
 C, 1.994301, -1.443174, -0.016333
 C, 2.616587, 0.896183, -0.020631
 C, 3.330866, -1.799990, -0.013306
 H, 1.251679, -2.233531, -0.028886
 C, 3.964050, 0.550189, -0.015911
 H, 2.338299, 1.944061, -0.020571
 C, 4.330515, -0.806704, -0.011548
 H, 3.629892, -2.843520, -0.016515
 H, 4.713434, 1.332933, -0.013033
 C, -3.325855, -0.946011, -0.008985

C, -3.465932, -2.317200, 0.067186
 O, -4.566794, -0.366235, -0.098147
 C, -4.859809, -2.586287, 0.024174
 H, -2.668745, -3.043737, 0.141668
 C, -5.477374, -1.366615, -0.076452
 H, -5.343678, -3.552179, 0.061361
 H, -6.511731, -1.062234, -0.138998
 O, 5.606594, -1.255843, -0.007143
 C, 6.681325, -0.306603, -0.010065
 H, 6.647465, 0.322728, 0.885765
 H, 7.594334, -0.901924, -0.007891
 H, 6.647818, 0.316911, -0.909961

Table S4.4 Characterizations of Spectra Computed in Solvent Dichloromethane (PCM-Tomasi as implemented in Gaussian).

Note: Max amplitude is 0.70714 for a pure one-electron excitation. The highest occupied molecular orbital (HOMO) to the lowest unoccupied molecular orbital (LUMO) transitions are in bold.

BF₂tbmOMe

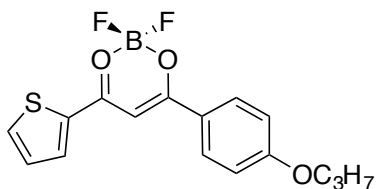


Excited State 1: Singlet-A 3.6394 eV 340.67 nm f=0.7020 <S2>=0.000**
55 -> 56 0.69791

Excited State 2: Singlet-A 4.0132 eV 308.94 nm f=0.0269 <S**2>=0.000
 54 -> 56 0.69496
 55 -> 56 -0.10029

Excited State 3: Singlet-A 4.6387 eV 267.28 nm f=0.0516 <S**2>=0.000
 53 -> 56 0.69228
 55 -> 57 0.10465

BF₂tbmOC3

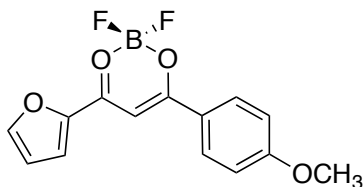


Excited State 1: Singlet-A 3.0430 eV 407.44 nm f=1.1477 <S2>=0.000**
87 -> 88 0.70565

Excited State 2: Singlet-A 3.7549 eV 330.19 nm f=0.0695 <S**2>=0.000
 84 -> 88 -0.19039
 86 -> 88 0.66326

Excited State 3: Singlet-A 3.9128 eV 316.87 nm f=0.0035 <S**2>=0.000
 84 -> 88 -0.19986
 85 -> 88 0.66978

BF₂fbmOMe

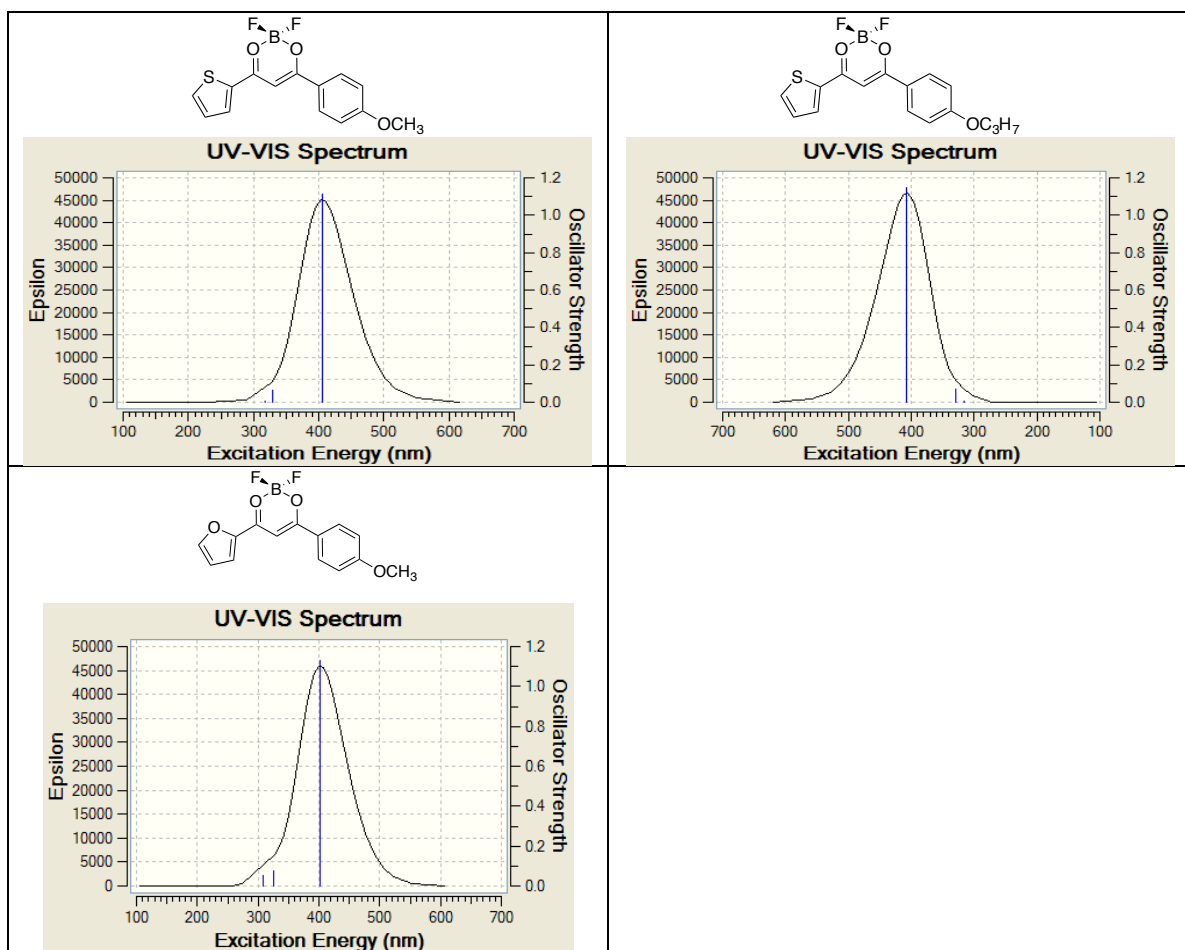


Excited State 1: Singlet-A 3.0808 eV 402.45 nm f=1.1330 <S2>=0.000**
75 -> 76 0.70675

Excited State 2: Singlet-A 3.8072 eV 325.66 nm f=0.0738 <S**2>=0.000
 73 -> 76 0.21864
 74 -> 76 0.66300

Excited State 3: Singlet-A 4.0112 eV 309.09 nm f=0.0539 <S**2>=0.000
 73 -> 76 0.65321
 74 -> 76 -0.21043

Table S4.5 Gaussview traces of computed TD-B3LYP/6-311+G(d) absorption spectra for compounds **1-3** in CH₂Cl₂ represented by Tomasi's Polarizable Continuum Model.

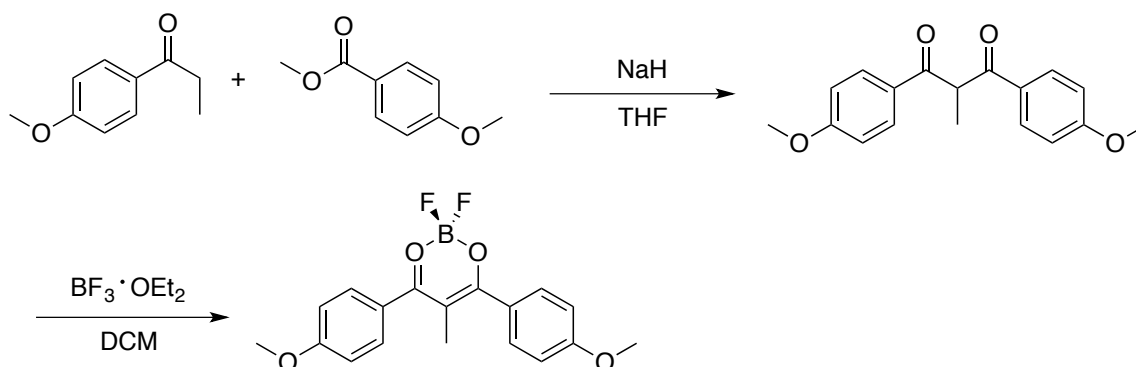


References

- (1) Li, X.; Zou, Y. Q. In *Z. Krist.-New Cryst. St.* **2004**, *219*, 301.
- (2) Carraway, E. R.; Demas, J. N.; DeGraff, B. A.; Bacon, J. R. *Anal. Chem.* **1991**, *63*, 337.
- (3) Frisch, M. J.; Trucks, G. W.; Schlegel, H. B.; Scuseria, G. E.; Robb, M. A.; Cheeseman, J. R.; Scalmani, G.; Barone, V.; Mennucci, B.; Petersson, G. A.; Nakatsuji, H.; Caricato, M.; Li, X.; Hratchian, H. P.; Izmaylov, A. F.; Bloino, J.; Zheng, G.; Sonnenberg, J. L.; Hada, M.; Ehara, M.; Toyota, K.; Fukuda, R.; Hasegawa, J.; Ishida, M.; Nakajima, T.; Honda, Y.; Kitao, O.; Nakai, H.; Vreven, T.; Montgomery, J. A.; Peralta, J. E.; Ogliaro, F.; Bearpark, M.; Heyd, J. J.; Brothers, E.; Kudin, K. N.; Staroverov, V. N.; Kobayashi, R.; Normand, J.; Raghavachari, K.; Rendell, A.; Burant, J. C.; Iyengar, S. S.; Tomasi, J.; Cossi, M.; Rega, N.; Millam, J. M.; Klene, M.; Knox, J. E.; Cross, J. B.; Bakken, V.; Adamo, C.; Jaramillo, J.; Gomperts, R.; Stratmann, R. E.; Yazyev, O.; Austin, A. J.; Cammi, R.; Pomelli, C.; Ochterski, J. W.; Martin, R. L.; Morokuma, K.; Zakrzewski, V. G.; Voth, G. A.; Salvador, P.; Dannenberg, J. J.; Dapprich, S.; Daniels, A. D.; Farkas; Foresman, J. B.; Ortiz, J. V.; Cioslowski, J.; Fox, D. J. Wallingford CT, 2009.
- (4) Tomasi, J.; Mennucci, B.; Cammi, R. *Chem. Rev.* **2005**, *105*, 2999.
- (5) Becke, A. D. *J. Chem. Phys.* **1993**, *98*, 5648.
- (6) Lee, C.; Yang, W.; Parr, R. G. *Phys. Rev. B: Condens. Matter* **1988**, *37*, 785.
- (7) Dennington, R. In *Version 5*; Keith, T., Ed.; Semichem Inc.: Shawnee Mission, KS, 2009.

Appendix D

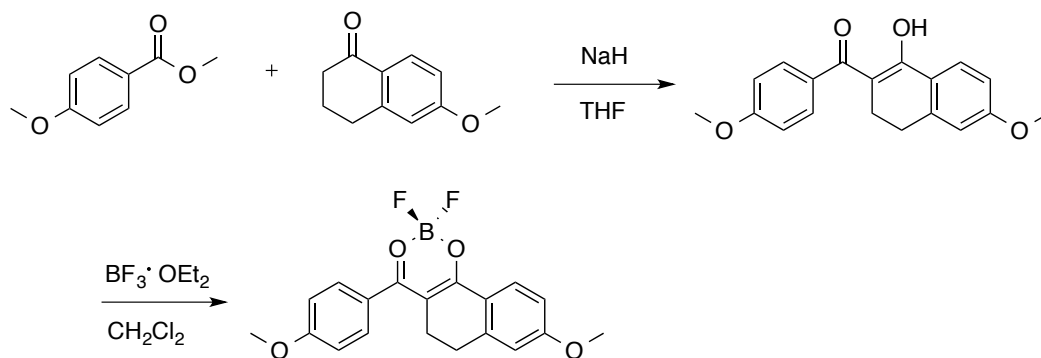
Supporting Information for Chapter 5

Scheme S5.1 Synthesis of $\text{BF}_2\text{dbe}(\text{OMe})_2$.

$\text{BF}_2\text{dbe}(\text{OMe})_2$. The $\text{dbe}(\text{OMe})_2$ ligand was prepared by a Claisen condensation in the presence of NaH as previously described.¹ This compound has been previously synthesized and data are in accord with the literature values. In the literature, Ohtsuka *et al.* synthesized this compound by Claisen condensation of the corresponding ester and ketone followed by treating the sodium enolate with the appropriate RX.² Here, it was synthesized in a one-step reaction between the appropriate ketone/ester pair. The synthesis is as follows. 4'-methoxypropiophenone (502mg, 3.06 mmol), methyl 4-methoxybenzoate (616mg, 3.71 mmol) and anhydrous THF (30 mL) were added sequentially to a clean, dry 100 mL round bottom flask. After stirring the mixture for 10 min, a suspension containing NaH (120 mg, 5.00 mmol) in anhydrous THF (10 mL) was added dropwise at room temperature under N_2 . The mixture was stirred and refluxed for 20 h then saturated aqueous NH_4Cl (5 mL) was added to quench the reaction. The aqueous phase was extracted with CH_2Cl_2 (3 x 35 mL). The combined organic layers were washed with distilled water (3 x 35 mL) and 35 mL of brine, and dried over MgSO_4 before concentration *in vacuo*. The residue was purified by column chromatography eluting with

hexanes/ethyl acetate (3:1) to give 4-methoxy-benzoyl 4'-methoxy-benzoyl ethane as an amber, viscous, liquid (233 mg, 26% yield). The $\text{BF}_2\text{d}(\text{OMe})_2$ dye was synthesized by adding boron trifluoride diethyl etherate (220 μL , 1.79 mmol) to a solution of $\text{d}(\text{OMe})_2$ (196 mg, 0.66 mmol) in CH_2Cl_2 (10 mL) at room temperature under N_2 . The mixture was allowed to stir at room temperature for 12 h. The solvent was removed *in vacuo* and the residue was passed through a silica plug eluting with hexanes/ethyl acetate (1:1). The resulting residue was recrystallized in hexanes/ethyl acetate (1:1). The yellow, crystalline solid was filtered and washed with cold hexanes/ethyl acetate (1:1): 72 mg (32%). ^1H NMR (300 MHz, CDCl_3) δ 7.91 (d, 4H, $J = 9.0$ Hz 2, 6, 2', 6'-ArH), 7.00 (d, 4H, $J = 9.0$ Hz, 3, 5, 3', 5'-ArH), 3.91 (s, 6H, Ph-OCH₃, Ph'-OCH₃), δ 2.30 (s, 3H, COCCH₃CO). [ESI/TOF HRMS] m/z calculated $\text{C}_{18}\text{H}_{18}\text{BF}_2\text{O}_4$ 347.1266 [$\text{M}+\text{H}^+$], found 347.1263. M.P.: 199-202 °C.

Scheme S5.2 Synthesis of $\text{BF}_2\text{bt}(\text{OMe})_2$.

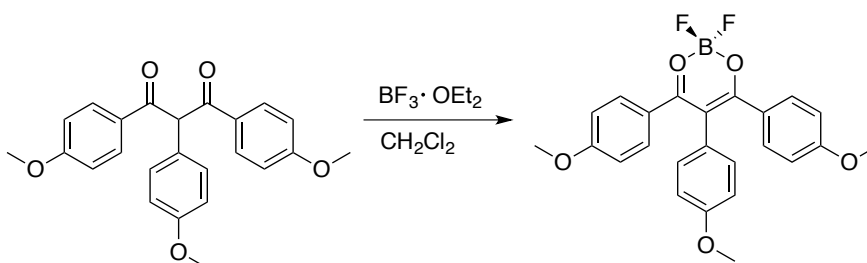


$\text{BF}_2\text{bt}(\text{OMe})_2$. The tetralone ligand ($\text{bt}(\text{OMe})_2$) was prepared by a Claisen condensation in the presence of NaH as previously described.¹ This ligand has been reported previously

in a patent but no synthesis or characterization data are provided.³ The synthesis and ¹H NMR data are as follows. 6-Methoxy-1-tetralone (1.071g, 6.08 mmol), methyl *p*-anisate (1.221g, 7.35 mmol), and anhydrous THF (~50 mL) were added sequentially to a dry 100 mL round bottom flask. After stirring the mixture for 10 min, a suspension containing NaH (0.23g, 9.58 mmol) in anhydrous THF (~10 mL) was added dropwise at room temperature under N₂. The reaction mixture heated at 60 °C with a reflux condenser attached under stream of N₂ for 24 h, after which the reaction was quenched by addition of a saturated NH₄Cl solution (4 mL). The solvent was removed by rotary evaporation. The resulting residue was dissolved in DCM (3 x 20 mL), the aqueous layer was extracted with 1 M HCl (3 x 20 mL), and washed with brine (20 mL). The combined organic layers were dried over Na₂SO₄, filtered, and the solvent was removed *via* rotary evaporation. The final product was purified by recrystallization from hexanes/EtOAc to produce a yellow, crystalline solid: 582 mg (33%) ¹H NMR (600 MHz, CDCl₃) δ 8.00 (s, 1H, 5'-ArH), 7.98 (d, 2H, *J* = 6 Hz, 2, 6-ArH), 7.97 (d, 1H, *J* = 6 Hz, 3'-ArH), 7.57 (d, 1H, *J* = 6 Hz, 2'-ArH), 6.94 (d, 2H, *J* = 12 Hz, 3, 5-ArH), 3.86 (s, 3H, Ph-OCH₃), 3.85 (s, 3H, Ph'-OCH₃), 3.12 and 2.97 (m, 2H, COCCH₂CH₂), 2.58 and 2.33 (m, 2H, COCCH₂CH₂). Boron trifluoride diethyletherate (320 μL, 2.60 mmol) was added to a solution of bt(OMe)₂ (583 mg, 1.70 mmol) in CH₂Cl₂ (30 mL) of bt(OMe)₂ (0.538 g, 1.70 mmol) at room temperature under N₂. The mixture was allowed to stir at room temperature for 12 h, after which the solvent was removed *via* rotary evaporation. The product was purified by recrystallization from hexanes/EtOAc as an emissive yellow, crystalline solid: 0.455g (73%). ¹H NMR (600 MHz, CDCl₃) δ 8.15 (d, 1H, *J* = 12 Hz, 2'-ArH), δ 7.77 (d, 2H, *J* = 6 Hz, 2, 6-ArH), 6.98 (d, 2H, *J* = 6 Hz, 3, 5-ArH), δ 6.90 (d, 1H,

$J = 12$ Hz, 3'-ArH) 6.75 (s, 1H, 5'-ArH), 3.90 (s, 3H, Phen-OCH₃), 3.88 (s, 3H, Phen'-OCH₃), 2.93 (d, 2H, $J = 6$ Hz, COCCH₂CH₂), 2.89 (d, 2H, $J = 6$ Hz, COCCH₂CH₂). [ESI/TOF HRMS] m/z calculated C₁₉H₁₇BF₂O₄ 358.12, found 381.1086 [M + Na⁺] m.p.: 230-232 °C.

Scheme S5.3 Synthesis of BF₂dbmp(OMe)₂.



BF₂dbmp(OMe)₂. The ligand dbmp(OMe)₂ (250 mg, 0.64 mmol) was placed in an oven dried 100 mL round bottom flask and dissolved in anhydrous CH₂Cl₂ (50 mL). Boron trifluoride diethyl etherate (118 μL, 0.96 mmol) was added *via* syringe, whereupon the solution turned red. The reaction mixture was stirred at RT and monitored by TLC until ligand was consumed (20 h). The reaction mixture was filtered and the solvent was removed *via* rotary evaporation to yield a dark yellow solid. The product was purified by column chromatography (CHCl₃) to yield an emissive yellow powder: 219 mg (78 %). ¹H NMR (600 MHz, DMSO): δ 7.31 (d, $J = 12$, 4H, 2, 6, 2', 6'-ArH) 7.09 (d, $J = 12$, 2H, 2'', 6''-ArH) 6.89 (d, $J = 12$, 2H, 3'', 5''-ArH) 6.85 (d, $J = 12$, 4H, 3, 5, 3', 5'-ArH) 3.75 (s, 6H, PhOCH₃, Ph'OCH₃) 3.73 (s, 3H, Ph''OCH₃). [ESI/TOF HRMS] m/z calculated C₂₄H₂₁BF₂O₅ 438.23, found 461.1348 [M + Na⁺] m.p.: 222-224 °C.

Table S5.1 Absorption and Emission Properties of Boron Dyes in Dilute DMSO Solution.^a

Dye	ϵ [M ⁻¹ cm ⁻¹]	λ_{abs}^b [nm]	λ_{em}^c [nm]	Φ_F [%]	Stokes Shift [cm ⁻¹]	τ_F [ns]	τ_{rad} [ns]
BF ₂ dbm(OMe) ₂	61,000	420	440	3.7	1,604	0.03	0.81
BF ₂ dbe(OMe) ₂	39,000	403	445	0.2	2,342	0.23 (38.40%) 1.51 (58.83%) 8.23 (2.78%) $\tau_{\text{pw0}} = 1.21$	N/A
BF ₂ dbmp(OMe) ₂	30,000	428	600	19	6,697	2.56	13.47
BF ₂ bt(OMe) ₂	50,000	427	468	35	2,051	1.44	4.11

^a $\lambda_{\text{ex}} = 369$ nm; room temperature, air. Concentration of dyes = 5×10^{-6} M.
^b Absorbance maximum.
^c Emission maximum; fluorescence.

Note: The Emission lifetime of BF₂dbe(OMe)₂ was multi-exponential, and the decay traces of emission intensity at λ_{em} and the % weighting factors (WF) were analyzed using DataStation version 2.6 software from Horiba Jobin Yvon. τ_{pw0} was calculated as follows:

$$\tau_{\text{pw0}} = \sum_{i=1}^N WF_i \cdot \tau_i$$

where N is the number of decay components, WF_i is the weighting factor, τ_i is the component of decay lifetimes, and τ_{pw0} is the pre-exponential weighted lifetime.⁴

Table S5.2 Absorption and Emission Properties of Boron Dyes in Dilute THF Solution.^a

Dye	ϵ [M ⁻¹ cm ⁻¹]	λ_{abs}^b [nm]	λ_{em}^c [nm]	Φ_F [%]	Stokes Shift [cm ⁻¹]	τ_F [ns]	τ_{rad} [ns]
BF ₂ dbm(OMe) ₂	76,000	409	426	100	976	1.73	1.73
BF ₂ dbe(OMe) ₂	43,000	391	426	<0.1	2,101	1.66	N/A
BF ₂ dbmp(OMe) ₂	33,000	419	566	8.0	6,198	1.18	14.75
BF ₂ bt(OMe) ₂	44,000	417	448	79	1,660	1.62	2.05

^a $\lambda_{\text{ex}} = 369$ nm; room temperature, air. Concentration of dyes = 5×10^{-6} M.
^b Absorbance maximum.
^c Emission maximum; fluorescence.

Full Computational Details

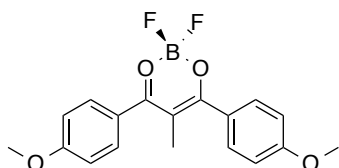
All compounds were modeled using the Gaussian 09 suite of programs⁵ using density functional theory (DFT). We chose B3LYP/6-311+G(d) for ground state geometry optimization with a Tomasi polarized continuum for dichloromethane solvent.⁶ The vibrational frequencies for the optimized geometries were all positive, assuring that the geometries are at least a local minimum. Single point energy calculations were used to generate the molecular orbital (MO) diagrams utilizing B3LYP/6-31G(d). We used time-dependent density functional theory, TD-B3LYP/6-311+G(d) for estimates of the absorption spectra, at the respective optimized geometries.^{7,8} The first three excited states

were computed for each compound. Molecular orbitals were depicted by Gaussview 5 software.⁹

Table S5.3 B3LYP/6-311+G(d) optimized structures for future TD-DFT calculation in dichloromethane. Coordinates given in Cartesian, in Angstroms.

BF₂dbe(OMe)₂ Ground State Optimized Geometry in DCM

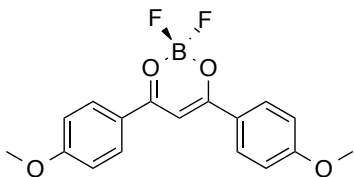
E (HF) = -1222.09262858 μ (Debye) = 8.5779



B, 0.000001, 2.617177, -0.177313
 F, 0.000001, 3.144273, 1.120881
 F, 0.000001, 3.626152, -1.128247
 O, -1.202304, 1.774802, -0.366835
 C, -1.200128, 0.502244, -0.049511
 C, -0.000001, -0.180409, 0.237359
 O, 1.202304, 1.774801, -0.366835
 C, 1.200128, 0.502243, -0.04951
 C, 2.539941, -0.096662, -0.042173
 C, 2.788139, -1.427159, -0.432531
 C, 3.638481, 0.705053, 0.308787
 C, 4.074744, -1.930592, -0.460347
 H, 1.975953, -2.06345, -0.757718
 C, 4.933117, 0.202872, 0.309176
 H, 3.471936, 1.734449, 0.601105
 C, 5.160079, -1.124725, -0.079124
 H, 4.266491, -2.947984, -0.781694
 H, 5.749965, 0.84686, 0.606721
 C, -2.539942, -0.096661, -0.042176
 C, -2.788139, -1.427155, -0.43254
 C, -3.638482, 0.705053, 0.308787
 C, -4.074745, -1.930588, -0.46036
 H, -1.975953, -2.063445, -0.75773
 C, -4.933118, 0.202873, 0.309174
 H, -3.471937, 1.734448, 0.60111
 C, -5.160079, -1.124723, -0.079132
 H, -4.266492, -2.947979, -0.781711

H, -5.749966, 0.846864, 0.606721
 O, 6.377209, -1.712565, -0.124039
 C, 7.532725, -0.949626, 0.237574
 C, 7.47249, -0.615589, 1.276193
 C, 8.377056, -1.624533, 0.120629
 C, 7.657109, -0.089568, -0.424632
 O, -6.377211, -1.712561, -0.124053
 C, -7.532721, -0.949631, 0.237595
 H, -8.377052, -1.624541, 0.120663
 H, -7.472463, -0.615605, 1.276216
 H, -7.657126, -0.089567, -0.424599
 C, -0.000002, -1.547154, 0.892206
 H, -0.878288, -1.661828, 1.528305
 H, -0.000002, -2.383741, 0.189551
 H, 0.878282, -1.661829, 1.528307

BF₂dbm(OMe)₂ Ground State Optimized Geometry in DCM
E (HF) = -1182.78178267 μ (Debye) = 8.7422



B, 0.000000, 2.661799, -0.011379
 F, 0.000000, 3.234829, 1.264355
 F, 0.000000, 3.63944, -0.997961
 O, -1.22189, 1.830039, -0.164296
 C, -1.209864, 0.528203, -0.024399
 C, 0.000000, -0.158849, 0.094219
 O, 1.22189, 1.830039, -0.164296
 C, 1.209864, 0.528203, -0.024399
 C, 2.521276, -0.117244, -0.020375
 C, 2.673984, -1.51963, -0.040317
 C, 3.682852, 0.672354, 0.003912
 C, 3.926838, -2.098097, -0.031507
 H, 1.809887, -2.171221, -0.07635
 C, 4.948255, 0.102242, 0.016083
 H, 3.589194, 1.750561, 0.020048
 C, 5.07945, -1.293546, -0.000753
 H, 4.042446, -3.17564, -0.051649

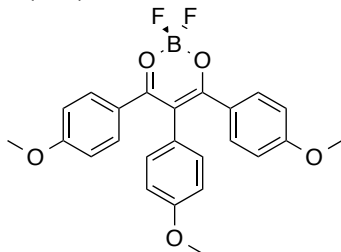
H, 5.817478, 0.745909, 0.040633
 C, -2.521276, -0.117244, -0.020375
 C, -2.673984, -1.51963, -0.040317
 C, -3.682852, 0.672354, 0.003912
 C, -3.926838, -2.098097, -0.031507
 H, -1.809887, -2.171221, -0.07635
 C, -4.948255, 0.102242, 0.016083
 H, -3.589194, 1.750561, 0.020047
 C, -5.07945, -1.293546, -0.000753
 H, -4.042446, -3.17564, -0.051648
 H, -5.817478, 0.745909, 0.040633
 O, 6.258208, -1.952348, 0.008395
 C, 7.477612, -1.202255, 0.033857
 H, 7.542549, -0.592184, 0.937781
 H, 8.274744, -1.941472, 0.034956
 H, 7.565995, -0.56944, -0.852264
 O, -6.258208, -1.952348, 0.008395
 C, -7.477612, -1.202255, 0.033858
 H, -8.274744, -1.941472, 0.034956
 H, -7.542549, -0.592184, 0.937782
 H, -7.565995, -0.56944, -0.852264
 H, 0.000000, -1.224732, 0.24412

BF₂dbm(OMe)₂ Singlet Excited State Optimized Geometry in DCM
E (HF) = -1182.77866677 μ (Debye) = 9.6716

B, -2.639482, 0.076556, 0.000000
 F, -2.975379, 1.44982, 0.000000
 F, -3.798022, -0.701626, 0.000000
 O, -1.865118, -0.230127, 1.221455
 C, -0.540893, -0.06077, 1.225633
 C, 0.143297, 0.053033, 0.000000
 O, -1.865118, -0.230127, -1.221455
 C, -0.540893, -0.06077, -1.225633
 C, 0.104964, -0.042593, -2.516586
 C, 1.515075, 0.092031, -2.67754
 C, -0.678837, -0.165037, -3.69643
 C, 2.09018, 0.111533, -3.925392
 H, 2.161249, 0.184613, -1.813979
 C, -0.106501, -0.148634, -4.953763
 H, -1.751298, -0.269277, -3.599366
 C, 1.290322, -0.006739, -5.08516

H, 3.162457, 0.217646, -4.043918
 H, -0.739752, -0.242699, -5.826283
 C, 0.104964, -0.042593, 2.516586
 C, 1.515075, 0.092031, 2.67754
 C, -0.678837, -0.165037, 3.69643
 C, 2.09018, 0.111533, 3.925392
 H, 2.161249, 0.184613, 1.813979
 C, -0.106501, -0.148634, 4.953763
 H, -1.751298, -0.269277, 3.599366
 C, 1.290322, -0.006739, 5.08516
 H, 3.162457, 0.217646, 4.043918
 H, -0.739752, -0.242699, 5.826283
 O, 1.94839, 0.026831, -6.255828
 C, 1.220327, -0.076696, -7.487085
 H, 0.517633, 0.75298, -7.591048
 H, 1.969945, -0.025319, -8.27207
 H, 0.689795, -1.029563, -7.543588
 O, 1.94839, 0.026831, 6.255828
 C, 1.220327, -0.076696, 7.487085
 H, 1.969945, -0.025319, 8.27207
 H, 0.517633, 0.75298, 7.591048
 H, 0.689795, -1.029563, 7.543588
 H, 1.21019, 0.2041, 0.000000

BF₂dbmp(OMe)₂ Ground State Optimized Geometry in DCM
E (HF) = -1528.42206584 μ (Debye) = 10.4493



B, 0.000066, -3.531802, 0.037671
 F, 0.000072, -4.091919, -1.243395
 F, 0.000032, -4.525737, 1.011801
 O, -1.2079, -2.697982, 0.198392
 C, -1.207619, -1.391606, 0.274819
 C, 0.000014, -0.658888, 0.333548
 O, 1.207954, -2.69797, 0.198461
 C, 1.207644, -1.391575, 0.274808
 C, 2.569333, -0.831943, 0.21294

C, 2.997747, 0.313628, 0.911323
C, 3.519356, -1.519148, -0.563192
C, 4.307264, 0.749105, 0.828135
H, 2.317398, 0.852709, 1.552558
C, 4.8296, -1.074106, -0.67753
H, 3.220179, -2.409477, -1.101715
C, 5.235037, 0.068773, 0.024455
H, 4.636707, 1.618428, 1.385883
H, 5.520044, -1.621705, -1.305301
C, -2.569335, -0.832016, 0.213005
C, -2.99777, 0.31352, 0.911424
C, -3.519325, -1.519211, -0.56317
C, -4.307288, 0.748985, 0.828227
H, -2.317434, 0.852581, 1.552686
C, -4.829576, -1.074175, -0.67752
H, -3.22013, -2.409513, -1.101724
C, -5.235029, 0.068678, 0.024483
H, -4.636764, 1.618278, 1.386002
H, -5.520002, -1.621776, -1.305308
O, 6.48602, 0.583603, -0.003385
C, 7.488811, -0.067208, -0.789448
H, 7.218672, -0.067204, -1.848311
H, 8.396272, 0.514234, -0.64581
H, 7.652352, -1.091537, -0.44624
O, -6.486012, 0.583532, -0.003403
C, -7.488779, -0.067278, -0.789489
H, -8.396218, 0.514226, -0.64596
H, -7.218582, -0.067377, -1.848336
H, -7.652403, -1.091575, -0.446215
C, 0.000031, 0.838596, 0.278447
C, 0.000019, 1.625325, 1.440638
C, -0.000007, 1.496017, -0.95227
C, 0.000015, 3.010242, 1.374198
H, 0.000032, 1.145006, 2.414654
C, -0.000009, 2.889812, -1.039925
H, -0.000049, 0.915712, -1.869411
C, 0.000023, 3.655323, 0.129243
H, -0.000006, 3.61087, 2.277203
H, -0.000047, 3.356091, -2.016673
O, 0.000074, 5.016917, 0.162878
C, -0.000334, 5.731959, -1.072475
H, -0.894717, 5.505924, -1.659601

H, -0.000519, 6.786038, -0.804012
H, 0.893918, 5.506334, -1.659956

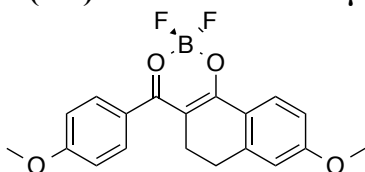
BF₂dbmp(OMe)₂ Ground State Optimized Geometry in DMSO

E (HF) = -1528.42565286 μ (Debye) = 10.9202

B, -0.000027, -3.536703, 0.065956
F, -0.00004, -4.154514, -1.189728
F, -0.00002, -4.496503, 1.079095
O, -1.208005, -2.701851, 0.192875
C, -1.207325, -1.39419, 0.272828
C, -0.000009, -0.662722, 0.338035
O, 1.207967, -2.701863, 0.192849
C, 1.207301, -1.394205, 0.272817
C, 2.567306, -0.833285, 0.204579
C, 2.998904, 0.305738, 0.911976
C, 3.51251, -1.510751, -0.586236
C, 4.307149, 0.744088, 0.823314
H, 2.322952, 0.83586, 1.565353
C, 4.821032, -1.062319, -0.706134
H, 3.210989, -2.394744, -1.133913
C, 5.229972, 0.07395, 0.004991
H, 4.638972, 1.607685, 1.388526
H, 5.50718, -1.601399, -1.345725
C, -2.567325, -0.833259, 0.204586
C, -2.99891, 0.305784, 0.91196
C, -3.512538, -1.51073, -0.586214
C, -4.307151, 0.744147, 0.823291
H, -2.322952, 0.835912, 1.565326
C, -4.821056, -1.062286, -0.706119
H, -3.211028, -2.394737, -1.133873
C, -5.229982, 0.074001, 0.004983
H, -4.638963, 1.607759, 1.388486
H, -5.50721, -1.601372, -1.345698
O, 6.479479, 0.590942, -0.027196
C, 7.478303, -0.049793, -0.828705
H, 7.199027, -0.039796, -1.884877
H, 8.385124, 0.53282, -0.686496
H, 7.646808, -1.076748, -0.496613
O, -6.479483, 0.591007, -0.027213
C, -7.478315, -0.049733, -0.828707
H, -8.385131, 0.532892, -0.686508
H, -7.199041, -0.039761, -1.88488

H, -7.64683, -1.07668, -0.496594
 C, 0.000002, 0.834979, 0.288425
 C, 0.000008, 1.616449, 1.454001
 C, 0.000007, 1.496911, -0.940119
 C, 0.00002, 3.001713, 1.392799
 H, 0.000004, 1.132511, 2.426063
 C, 0.000016, 2.891103, -1.022207
 H, 0, 0.920531, -1.859729
 C, 0.000024, 3.651785, 0.150367
 H, 0.000026, 3.597924, 2.298741
 H, 0.000016, 3.361358, -1.99698
 O, 0.000025, 5.013326, 0.189036
 C, 0.000128, 5.73345, -1.044623
 H, -0.894093, 5.509454, -1.632376
 H, 0.000186, 6.786435, -0.772157
 H, 0.89437, 5.509333, -1.632296

BF₂bt(OMe)₂ Ground State Optimized Geometry in DCM
E (HF) = -1260.22259489 μ (Debye) = 9.5703



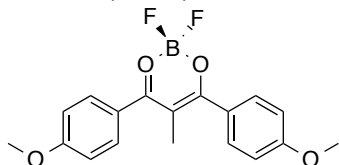
C, 5.127418, -1.157135, -0.249535
 C, 4.034862, -1.820259, -0.830345
 C, 2.766417, -1.27431, -0.757339
 C, 2.546494, -0.038226, -0.119528
 C, 3.654313, 0.628066, 0.42842
 C, 4.928463, 0.077203, 0.383859
 H, 4.205021, -2.761236, -1.341062
 H, 1.95118, -1.79682, -1.239578
 H, 3.511404, 1.587156, 0.910743
 H, 5.751525, 0.613979, 0.836705
 O, 6.324371, -1.779994, -0.357003
 C, 7.484621, -1.156405, 0.201285
 H, 7.379068, -1.027248, 1.281269
 H, 8.309333, -1.834141, -0.005361
 H, 7.677262, -0.19086, -0.272707
 O, 1.229108, 0.60959, -0.05006
 B, 0.113447, 2.802384, 0.040505

O, 1.291924, 1.919866, -0.117798
 O, -1.131043, 2.030458, -0.187376
 F, 0.186506, 3.825132, -0.897347
 F, 0.098768, 3.31822, 1.342396
 C, -0.002412, -0.047523, 0.079862
 C, -1.16958, 0.732858, -0.030589
 C, -0.163646, -1.546241, 0.253912
 C, -2.489123, 0.123434, -0.02249
 C, -1.43211, -1.890712, 1.039705
 H, -0.213626, -2.039547, -0.724902
 C, -2.641482, -1.194425, 0.470531
 C, -3.615484, 0.827405, -0.473949
 H, -1.309086, -1.578899, 2.085131
 C, -3.898985, -1.771652, 0.480888
 C, -4.872824, 0.243283, -0.473355
 H, -3.496542, 1.839361, -0.841213
 C, -5.018449, -1.06804, 0.006543
 H, -4.044085, -2.776914, 0.862141
 H, -5.721603, 0.804054, -0.841191
 H, -1.582784, -2.972424, 1.052271
 H, 0.701899, -1.962263, 0.770851
 O, -6.192739, -1.735527, 0.054951
 C, -7.385267, -1.086345, -0.398347
 H, -8.183287, -1.811397, -0.258796
 H, -7.594174, -0.193072, 0.194908
 H, -7.310306, -0.823634, -1.456163

Table S5.4 Characterization of Spectra Computed in Solvent Dichloromethane (PCM-Tomasi as implemented by Gaussian) using B3LYP/6-311+G(d).

Note: Max amplitude is 0.70714 for a pure one-electron excitation. The highest occupied molecular orbital (HOMO) to the lowest unoccupied molecular orbital (LUMO) transitions are in bold. The HOMO-1 to LUMO transition is also in bold for BF₂dbmp(OMe)₂

BF₂dbe(OMe)₂

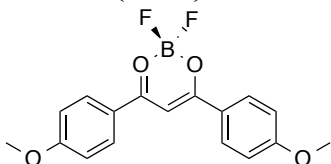


Excited State 1: Singlet-A 3.1518 eV 393.38 nm f=1.0806 <S2>=0.000**
90 -> 91 0.70547

Excited State 2: Singlet-A 3.6600 eV 338.76 nm f=0.0509 <S**2>=0.000
89 -> 91 0.70007

Excited State 3: Singlet-A 4.0928 eV 302.94 nm f=0.0150 <S**2>=0.000
87 -> 91 0.69160
90 -> 93 0.10682

BF₂dbm(OMe)₂

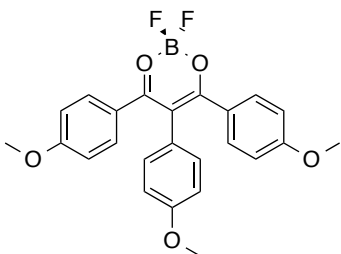


Excited State 1: Singlet-A 3.0971 eV 400.32 nm f=1.3036 <S2>=0.000
86 -> 87 0.70597**

Excited State 2: Singlet-A 3.7410 eV 331.42 nm f=0.0650 <S**2>=0.000
85 -> 87 0.69392

Excited State 3: Singlet-A 4.0470 eV 306.36 nm f=0.0001 <S**2>=0.000
82 -> 87 0.14119
84 -> 87 0.67890
86 -> 90 0.11048

BF₂dbmp(OMe)₂

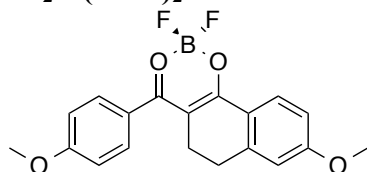


Excited State 1: Singlet-A 2.9192 eV 424.72 nm f=0.0014 <S2>=0.000
114 ->115 0.70022 (HOMO → LUMO)**

Excited State 2: Singlet-A 3.1227 eV 397.04 nm f=1.0507 <S2>=0.000
113 ->115 0.70518 (HOMO-1 → LUMO)**

Excited State 3: Singlet-A 3.5974 eV 344.65 nm f=0.0166 <S**2>=0.000
111 ->115 0.10114
112 ->115 0.68878

BF₂bt(OMe)₂



Excited State 1: Singlet-A 3.0362 eV 408.35 nm f=1.0537 <S2>=0.000**
93 -> 94 0.70383

Excited State 2: Singlet-A 3.6902 eV 335.98 nm f=0.0699 <S**2>=0.000
 92 -> 94 0.69758

Excited State 3: Singlet-A 3.8563 eV 321.51 nm f=0.0244 <S**2>=0.000
 89 -> 94 -0.16988
 91 -> 94 0.67439

Table S5.5 GaussView traces of computed TD-B3LYP/6-311+G(d) absorption spectra for the boron dyes in DCM.

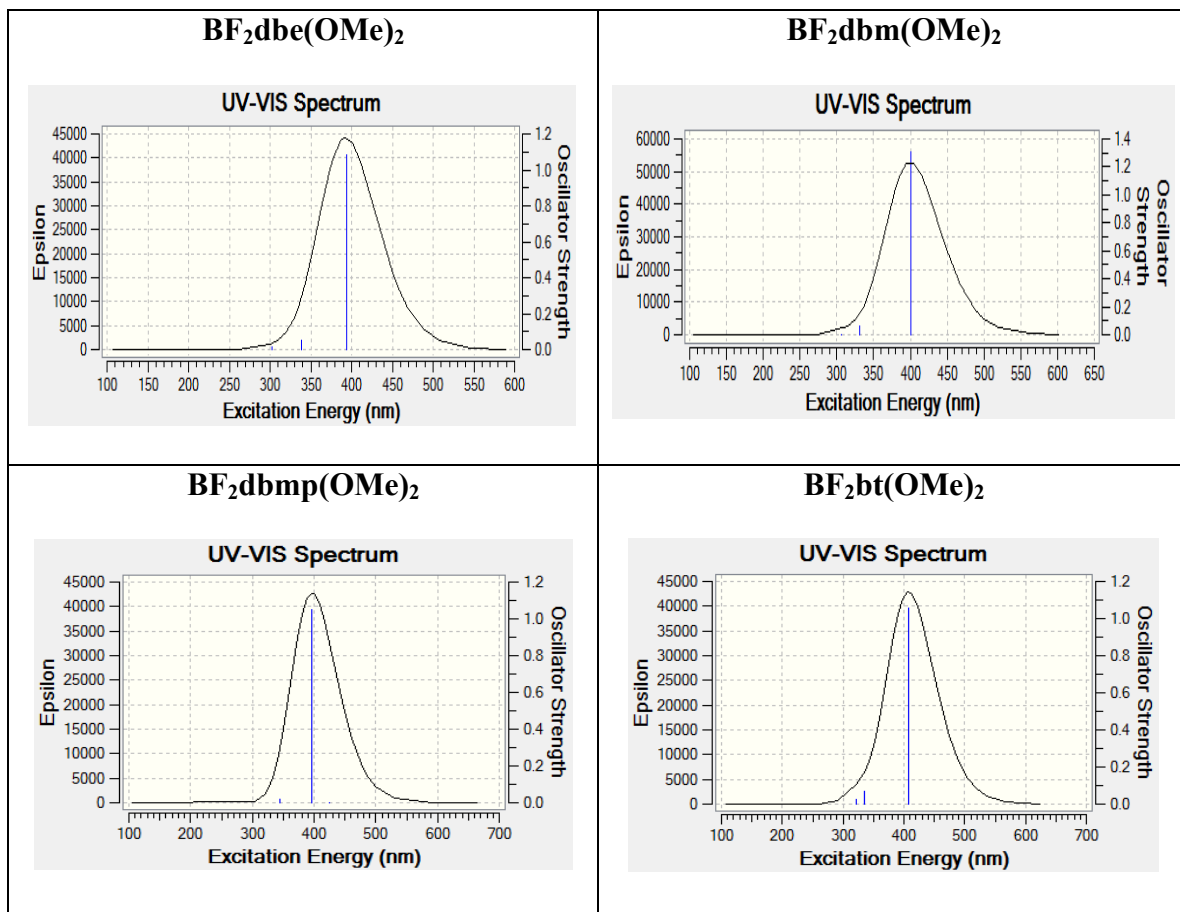
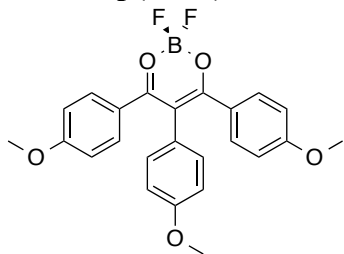


Table S5.6 Characterization of Spectra Computed in Solvent Dichloromethane (PCM-Tomasi as implemented by Gaussian) for BF₂dbmp(OMe)₂ using ωB97XD/6-311+G(d). Note: 22 excited states were calculated, but only 3 are shown here. Note: Max amplitude is 0.70714 for a pure one-electron excitation. The highest occupied molecular orbital (HOMO) to the lowest unoccupied molecular orbital (LUMO) transitions are in bold. The HOMO-1 to LUMO transition is also in bold.

BF₂dbmp(OMe)₂



Excited State 1: Singlet-A 3.5702 eV 347.28 nm f=1.2090 $\langle S^2 \rangle = 0.000$
 108 ->115 -0.15535
 112 ->116 -0.11260
 114 ->115 0.66637 (HOMO \rightarrow LUMO)

Excited State 2: Singlet-A 3.8708 eV 320.30 nm f=0.0070 $\langle S^2 \rangle = 0.000$
 107 ->115 -0.17827
 113 ->115 0.67430 (HOMO-1 \rightarrow LUMO)

Excited State 3: Singlet-A 4.3950 eV 282.10 nm f=0.0205 $\langle S^2 \rangle = 0.000$
 105 ->115 0.10261
 112 ->115 0.66197
 114 ->116 -0.14839

Table S5.7 GaussView trace of computed TD- ω B97XD/6-311+G(d) absorption spectrum for BF₂dbmp(OMe)₂ in DMSO.

BF₂dbmp(OMe)₂

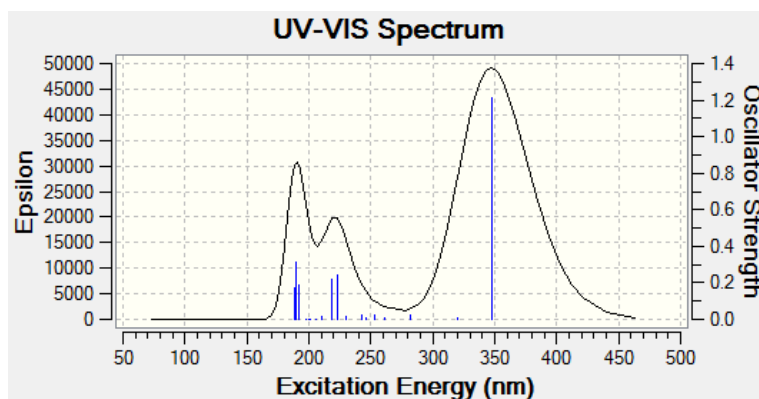


Table S5.8 Emission Maxima and Lifetimes with % Weighting Factors for the Dyes as Films on Weighing Paper at Room Temperature under Air.^a

Dye	Thermally Annealed λ_{em}^b [nm]	Thermally Annealed τ^c [ns]	Smeared λ_{em}^b [nm]	Smeared τ^c [ns]	$\Delta\tau_{pw0}^d$ [ns]
BF ₂ dbm(OMe) ₂	492	2.36 (27.00%) 5.28 (56.96%) 9.76 (16.04%) 5.21 (τ_{pw0})	535	11.34 (33.61%) 4.94 (20.08%) 36.25 (46.32%) 21.59 (τ_{pw0})	16.38
BF ₂ dbe(OMe) ₂	N/A	N/A	463	0.09 (76.46%) 0.93 (21.21%) 4.95 (2.33%) 0.38 (τ_{pw0})	N/A
BF ₂ dbmp(OMe) ₂	536	3.14 (15.55%) 5.62 (84.45%) 5.23 (τ_{pw0})	560	2.12 (45.14%) 5.10 (54.86%) 3.75 (τ_{pw0})	1.48
BF ₂ bt(OMe) ₂	N/A	N/A	505	2.68 (76.34%) 6.20 (23.66%) 3.51 (τ_{pw0})	N/A
^a $\lambda_{ex} = 369$ nm.					
^b Emission maximum; fluorescence.					
^c Fluorescence lifetime.					

Table S5.9 Emission Maxima and Lifetimes with % Weighting Factors for the Dyes as Spin-cast Films on Glass at Room Temperature under Air.^a

Dye	Thermally Annealed λ_{em}^b [nm]	Thermally Annealed τ^c [ns]	Smeared λ_{em}^b [nm]	Smeared τ^c [ns]	$\Delta\tau_{pw0}^d$ [ns]
BF ₂ dbm(OMe) ₂	489	2.42 (11.38%) 7.13 (80.94%) 21.65 (7.68%) 7.75 (τ_{pw0})	551	8.07 (33.28%) 34.52 (66.72%) 25.72 (τ_{pw0})	17.97
BF ₂ dbe(OMe) ₂	463	1.47 (65.74%) 2.47 (34.26%) 1.81 (τ_{pw0})	499	2.82 (47.22%) 0.57 (14.05%) 11.46 (38.73%) 5.85 (τ_{pw0})	4.04
BF ₂ dbmp(OMe) ₂	536	3.13 (52.33%) 5.99 (47.67%) 4.49 (τ_{pw0})	582	1.15 (14.17%) 4.19 (75.37%) 8.44 (10.46%) 4.25 (τ_{pw0})	0.24
^a $\lambda_{ex} = 369$ nm.					
^b Emission maximum; fluorescence.					
^c Fluorescence lifetime.					

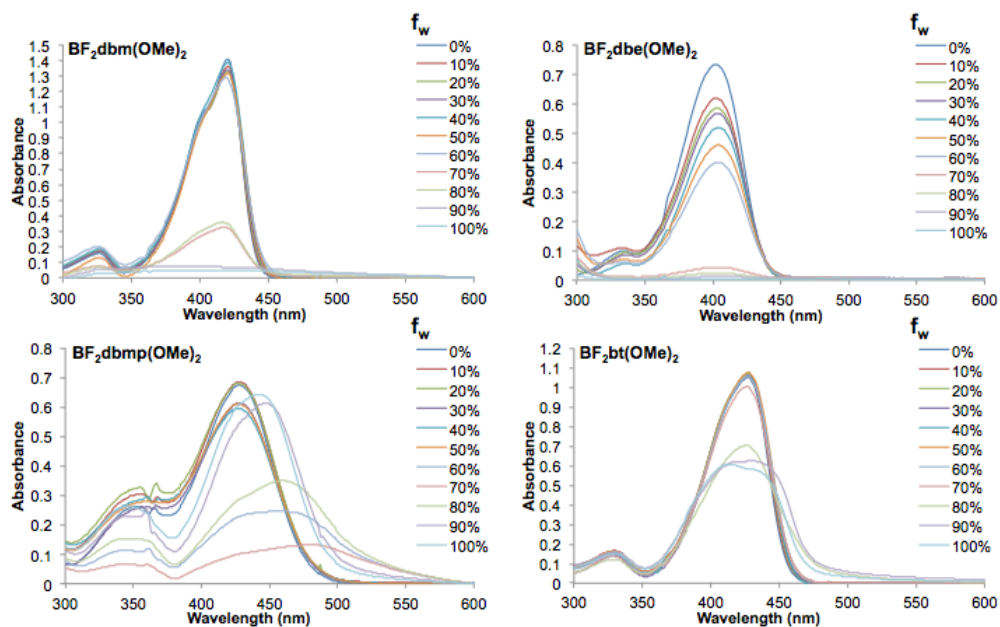


Figure S5.1 UV-vis spectra of boron dyes in differing water fractions (f_w) with DMSO as the solvent.

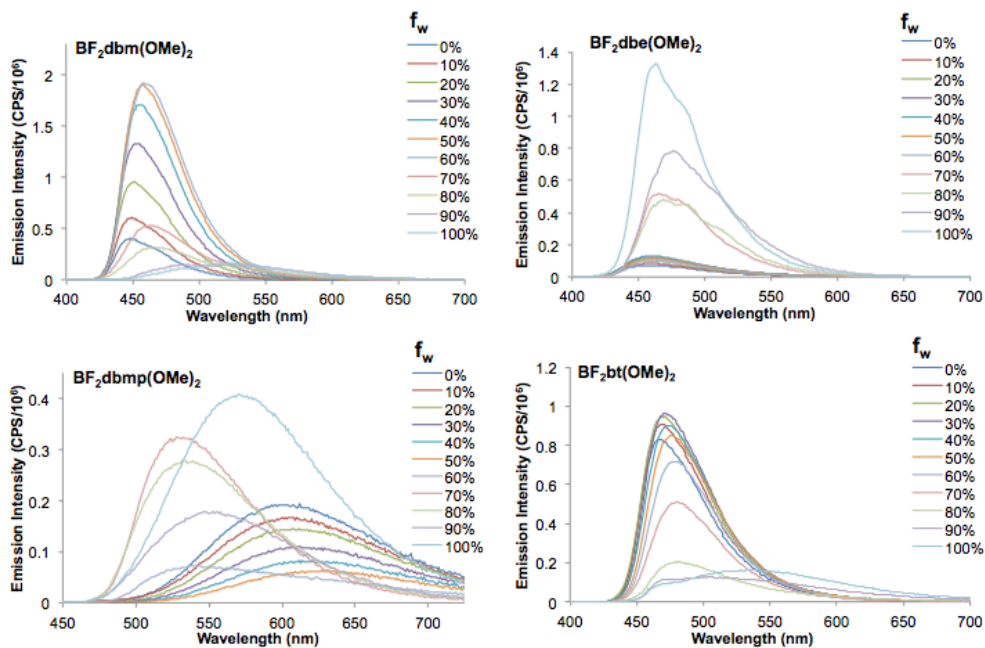


Figure S5.2 Emission spectra of boron dyes in differing water fractions (f_w) with DMSO as the solvent.

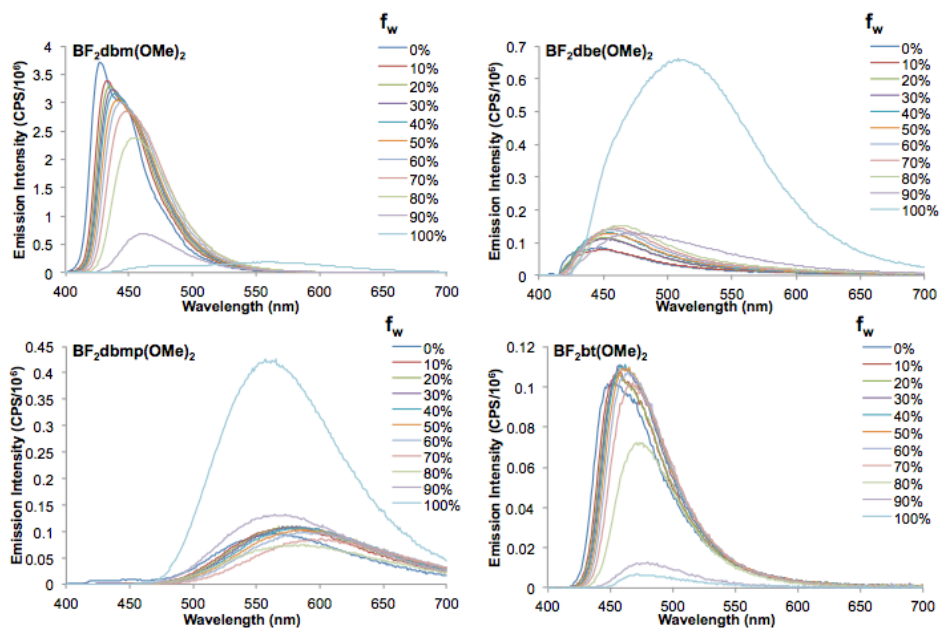


Figure S5.3 Emission spectra of boron dyes in differing water fractions (f_w) with THF as the solvent.

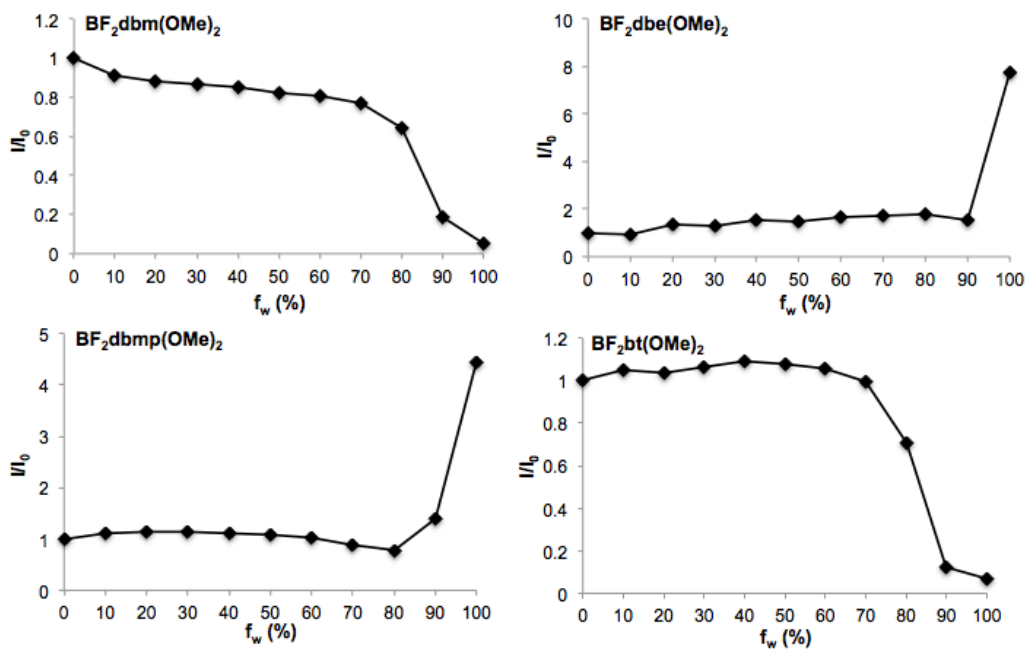


Figure S5.4 I/I_0 values for boron dyes in solutions of increasing water fraction (f_w) using THF as the solvent.

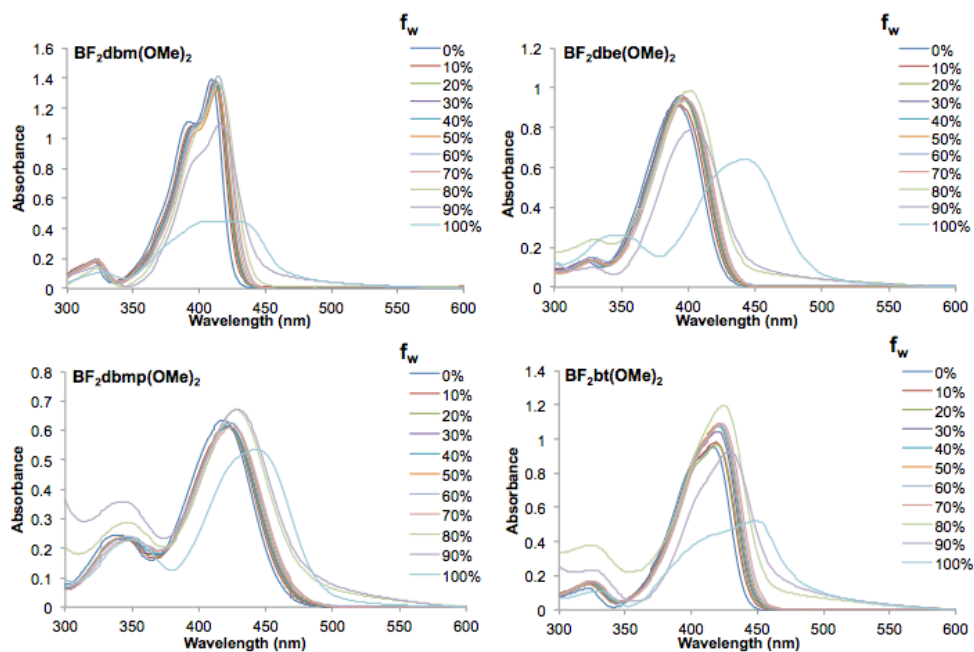


Figure S5.5 UV-vis spectra of boron dyes in differing water fractions (f_w) using THF as the solvent.

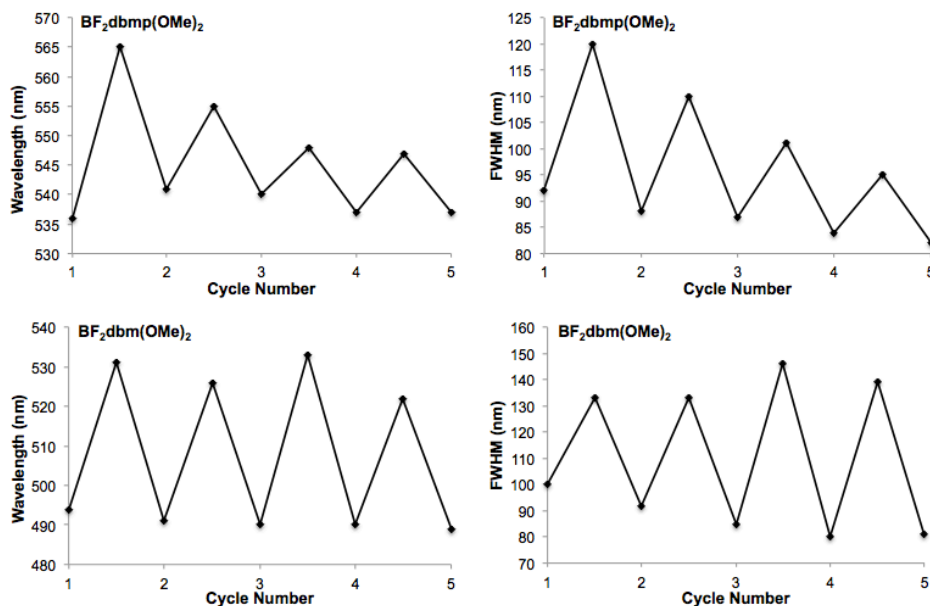


Figure S5.6 Emission intensities of dyes as films on weighing paper monitored through cycles of smearing and annealing at room temperature in air ($\lambda_{\text{ex}} = 369 \text{ nm}$). The intensities were recorded in photon counts per second (CPS) and shown as $\text{CPS}/10^6$.

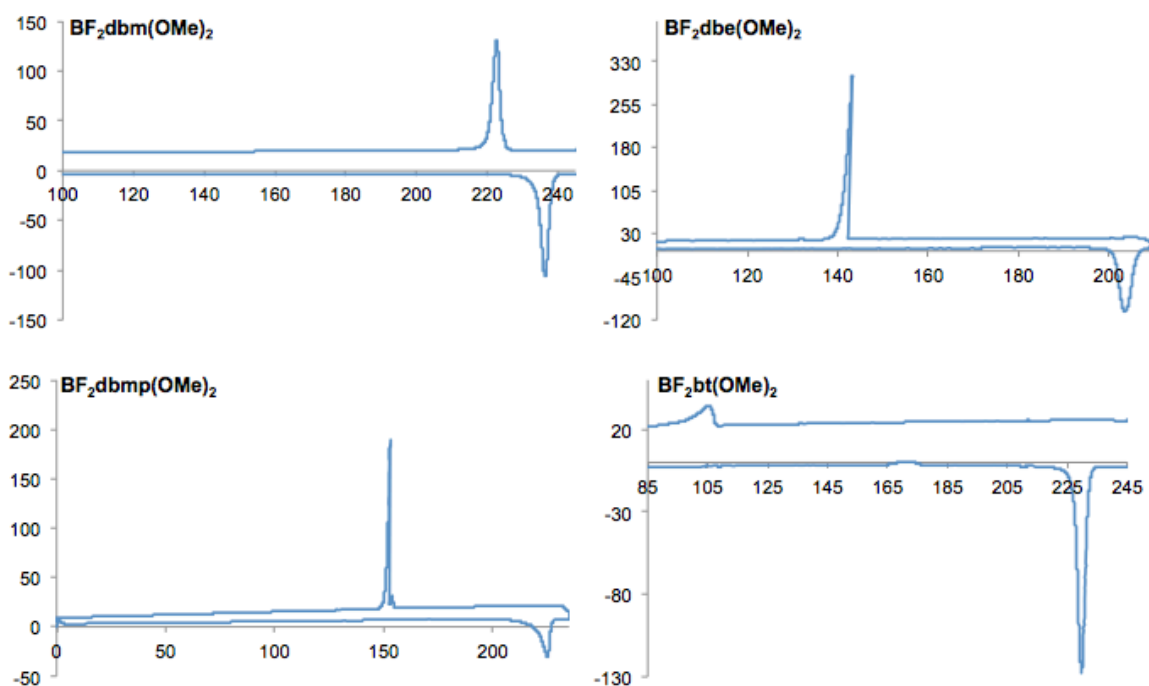


Figure S5.7 Differential scanning calorimetry (DSC) thermograms of the boron dyes. The 2nd cycle is shown for all samples.

References

- (1) Zhang, G.; Fiore, G. L.; St. Clair, T. L.; Fraser, C. L. *Macromolecules* **2009**, *42*, 3162.
- (2) Ohtsuka, Y.; Koyasu, K.; Ikeno, T.; Yamada, T. *Org. Lett.* **2001**, *3*, 2543.
- (3) Cullinan, G. J.; Eacho, P. I.; Foxworthy-Mason, P. S.; Schelm, J. A.; Eli Lilly and Company, USA . 1999, p 42 pp.
- (4) Carraway, E. R.; Demas, J. N.; DeGraff, B. A.; Bacon, J. R. *Anal. Chem.* **1991**, *63*, 337.
- (5) Frisch, M. J.; Trucks, G. W.; Schlegel, H. B.; Scuseria, G. E.; Robb, M. A.; Cheeseman, J. R.; Scalmani, G.; Barone, V.; Mennucci, B.; Petersson, G. A.; Nakatsuji, H.; Caricato, M.; Li, X.; Hratchian, H. P.; Izmaylov, A. F.; Bloino, J.; Zheng, G.; Sonnenberg, J. L.; Hada, M.; Ehara, M.; Toyota, K.; Fukuda, R.; Hasegawa, J.; Ishida, M.; Nakajima, T.; Honda, Y.; Kitao, O.; Nakai, H.; Vreven, T.; Montgomery, J. A.; Peralta, J. E.; Ogliaro, F.; Bearpark, M.; Heyd, J. J.; Brothers, E.; Kudin, K. N.; Staroverov, V. N.; Kobayashi, R.; Normand, J.; Raghavachari, K.; Rendell, A.; Burant, J. C.; Iyengar, S. S.; Tomasi, J.; Cossi, M.; Rega, N.; Millam, J. M.; Klene, M.; Knox, J. E.; Cross, J. B.; Bakken, V.; Adamo, C.; Jaramillo, J.; Gomperts, R.; Stratmann, R. E.;

Yazyev, O.; Austin, A. J.; Cammi, R.; Pomelli, C.; Ochterski, J. W.; Martin, R. L.; Morokuma, K.; Zakrzewski, V. G.; Voth, G. A.; Salvador, P.; Dannenberg, J. J.; Dapprich, S.; Daniels, A. D.; Farkas; Foresman, J. B.; Ortiz, J. V.; Cioslowski, J.; Fox, D. J. Wallingford CT, 2009.

(6) Tomasi, J.; Mennucci, B.; Cammi, R. *Chem. Rev.* **2005**, *105*, 2999.

(7) Becke, A. D. *J. Chem. Phys.* **1993**, *98*, 5648.

(8) Lee, C.; Yang, W.; Parr, R. G. *Phys. Rev. B: Condens. Matter* **1988**, *37*, 785.

(9) Dennington, R. In *Version 5*; Keith, T., Ed.; Semichem Inc.: Shawnee Mission, KS, 2009.

Appendix E

Supporting Information for Chapter 6

Supporting Information for Section 6.3.1: Modeling Molecular Orbitals and Absorption Spectra of Naphthyl-Phenyl β -Diketonate Polymer Initiators

Full Computational Details

All compounds were modeled using the Gaussian 09 suite of programs¹ using density functional theory. We chose B3LYP/6-31+G(d) for ground state geometry optimization with a Tomasi polarized continuum for dichloromethane solvent.² The vibrational frequencies for the optimized geometries were all positive, assuring that the geometries are at least a local minimum. Single point energy calculations were used to generate the molecular orbital diagrams utilizing B3LYP/6-31G(d). We used time-dependent density functional theory, TD-B3LYP/6-311+G(d) for estimates of the absorption spectra, at the respective optimized geometries.^{3,4} The first three excited states were computed for each compound. Molecular orbitals were depicted by GaussView 5 software.⁵

Gaussian 09 Specifications for Initiators 1-4 in CH₂Cl₂ Solvent.

Table S6.1 B3LYP/6-31+G(d) optimized structures for future TD-DFT calculation in dichloromethane. Coordinates given in Cartesian, in Angstroms.

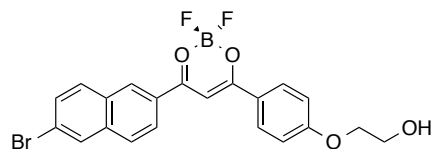
1. BF₂nbmC₂H₄OH: E (HF) = -1336.17162124



B, -0.637245, 2.650393, 0.070921
 F, -0.663738, 3.013377, 1.441615
 F, -0.743982, 3.800648, -0.722173
 O, -1.789629, 1.773891, -0.217257
 C, -1.654766, 0.447202, -0.049804
 C, -0.391883, -0.125942, 0.054211
 H, -0.295970, -1.190816, 0.208234
 O, 0.642511, 1.985830, -0.230515
 C, 0.768851, 0.659690, -0.062786

C, -2.920522, -0.292115, -0.018560
 C, -2.983700, -1.697248, 0.083273
 C, -4.146740, 0.416500, -0.099304
 C, -4.204993, -2.371942, 0.113244
 H, -2.074699, -2.285259, 0.138525
 C, -5.391197, -0.244210, -0.074313
 H, -4.117547, 1.497420, -0.180395
 C, -5.434336, -1.671061, 0.035901
 H, -4.214112, -3.455103, 0.195334
 C, -6.617959, 0.466091, -0.152452
 C, -6.685130, -2.329233, 0.063048
 C, -7.846586, -0.209347, -0.122328
 H, -6.598347, 1.549068, -0.236135
 C, -7.884248, -1.602604, -0.014995
 H, -6.713278, -3.412147, 0.145506
 H, -8.769915, 0.357854, -0.183414
 H, -8.834829, -2.125289, 0.008020
 C, 2.125621, 0.143911, -0.048020
 C, 3.222272, 1.036000, -0.096713
 C, 2.421034, -1.244468, 0.010808
 C, 4.539665, 0.583127, -0.080836
 H, 3.029091, 2.101802, -0.141342
 C, 3.726847, -1.702547, 0.028079
 H, 1.621061, -1.977062, 0.038705
 C, 4.802524, -0.794141, -0.016746
 H, 5.347256, 1.305630, -0.115638
 H, 3.941329, -2.766349, 0.073060
 O, 6.048829, -1.346718, 0.004774
 C, 7.191899, -0.487490, -0.035670
 H, 7.187350, 0.108512, -0.956906
 H, 7.188924, 0.189688, 0.827587
 C, 8.417252, -1.388658, 0.004449
 H, 8.406918, -2.069392, -0.857112
 H, 8.408663, -1.987405, 0.924878
 O, 9.555948, -0.52550, -0.036401
 H, 10.359134, -1.068058, -0.006203

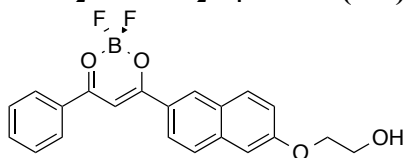
2. BF₂n(Br)bmC₂H₄OH: E(HF) = -3907.30673415



B,1.067747,3.057564,-0.065497

F,1.050160,3.618824,1.215305
F,1.093300,4.039382,-1.045949
O,-0.153543,2.230608,-0.247094
C,-0.152054,0.934120,-0.040788
C,1.046640,0.243978,0.134670
H,1.036101,-0.814045,0.340678
O,2.286915,2.214651,-0.202898
C,2.270496,0.919466,-0.000988
C,3.575922,0.267213,0.050473
C,3.717601,-1.139645,0.093980
C,4.745530,1.052464,0.062978
C,4.968435,-1.726684,0.152866
H,2.847341,-1.786172,0.068150
C,6.008503,0.474323,0.124356
H,4.658569,2.132782,0.032371
C,6.128546,-0.926125,0.171380
H,5.077678,-2.806279,0.180071
H,6.883290,1.113229,0.138362
C,-1.477357,0.294092,-0.031104
C,-1.626175,-1.126522,-0.015352
C,-2.614755,1.092473,-0.043939
C,-2.873327,-1.701752,-0.008590
H,-0.753646,-1.769790,-0.024708
C,-3.911304,0.525434,-0.034737
H,-2.511297,2.172285,-0.055170
C,-4.050714,-0.900685,-0.015393
H,-2.972553,-2.783906,-0.002432
C,-5.082858,1.333528,-0.038455
C,-5.349542,-1.473070,-0.004721
C,-6.336114,0.763085,-0.025235
H,-4.979568,2.415331,-0.051571
C,-6.451413,-0.648011,-0.008482
H,-5.460070,-2.552597,0.008258
H,-7.227331,1.381046,-0.027716
Br,-8.201137,-1.414043,0.009793
O,7.301762,-1.593429,0.236540
C,8.536569,-0.855954,0.241637
H,8.600269,-0.237107,-0.661109
H,8.575687,-0.211341,1.128168
C,9.681818,-1.842447,0.280971
H,10.605287,-1.279920,0.477940
H,9.528141,-2.557993,1.099712
O,9.755470,-2.514555,-0.978124
H,10.450526,-3.189586,-0.931009

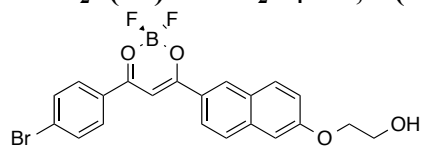
3. BF₂bnmOC₂H₄OH: E (HF) = -1336.17516942



B, 2.984043, 2.358484, 0.047310
 F, 3.034083, 2.852428, 1.354130
 F, 3.159119, 3.373069, -0.883282
 O, 1.657598, 1.726235, -0.179877
 C, 1.462154, 0.436080, -0.043696
 C, 2.556220, -0.429127, 0.098668
 H, 2.396069, -1.484238, 0.251195
 O, 4.070950, 1.356495, -0.129587
 C, 3.856136, 0.069905, -0.002061
 C, 0.068021, -0.007176, -0.076275
 C, -0.286237, -1.394533, -0.097518
 C, -0.948106, 0.945016, -0.085980
 C, -1.600925, -1.784337, -0.124042
 H, 0.484576, -2.157031, -0.105540
 C, -2.309208, 0.569959, -0.111106
 H, -0.691793, 1.999260, -0.067493
 C, -2.658242, -0.823899, -0.129883
 H, -1.852553, -2.841513, -0.144676
 C, -3.355734, 1.532112, -0.115953
 C, -4.017402, -1.196553, -0.154747
 C, -4.679776, 1.151453, -0.140547
 H, -3.100283, 2.588580, -0.100467
 C, -5.017247, -0.231458, -0.160736
 H, -4.297638, -2.246132, -0.168562
 H, -5.453735, 1.909837, -0.144799
 O, -6.295956, -0.690947, -0.190849
 C, -7.388423, 0.240114, -0.178168
 H, -7.337669, 0.864407, 0.722233
 H, -7.341523, 0.881429, -1.067081
 C, -8.682300, -0.543422, -0.194339
 H, -9.503933, 0.162764, -0.379829
 H, -8.660921, -1.276241, -1.011883
 O, -8.847605, -1.192211, 1.068710
 H, -9.640355, -1.749950, 1.030692
 C, 5.062947, -0.774590, 0.010723
 C, 6.322585, -0.172250, 0.197134
 C, 4.991286, -2.171009, -0.161398
 C, 7.478923, -0.949666, 0.222461
 H, 6.383441, 0.902155, 0.330008
 C, 6.150827, -2.943423, -0.140058

H, 4.037725, -2.658696, -0.334035
 C, 7.396738, -2.336314, 0.054661
 H, 8.443935, -0.474619, 0.374544
 H, 6.083240, -4.018334, -0.280949
 H, 8.299081, -2.941419, 0.072454

4. BF₂b(Br)nmOC₂H₄OH; E(HF) = -3907.30337535



B,1.268271,3.056378,0.042504
 F,1.250971,3.565001,1.343566
 F,1.306860,4.075295,-0.898639
 O,0.037720,2.249976,-0.176763
 C,0.016469,0.943626,-0.068921
 C,1.217688,0.228947,0.053728
 H,1.200207,-0.840977,0.184947
 O,2.480546,2.207033,-0.124574
 C,2.436605,0.901394,-0.023038
 C,3.746451,0.228242,-0.005991
 C,3.869864,-1.159917,-0.201931
 C,4.910132,0.992705,0.199166
 C,5.119472,-1.772733,-0.185966
 H,2.996643,-1.775270,-0.388760
 C,6.164728,0.389752,0.215882
 H,4.827289,2.063097,0.349714
 C,6.256679,-0.989977,0.024690
 H,5.205785,-2.842204,-0.342868
 H,7.056349,0.984979,0.379568
 C,-1.304847,0.318417,-0.106379
 C,-1.468966,-1.102287,-0.179460
 C,-2.440040,1.124480,-0.069683
 C,-2.719143,-1.665093,-0.212444
 H,-0.602129,-1.751910,-0.225595
 C,-3.737851,0.569679,-0.098406
 H,-2.328486,2.202322,-0.011815
 C,-3.896208,-0.856760,-0.171709
 H,-2.826561,-2.744905,-0.274048
 C,-4.904402,1.380939,-0.055269
 C,-5.192701,-1.408644,-0.201188
 C,-6.165021,0.825676,-0.084101
 H,-4.793481,2.460822,0.000869
 C,-6.313667,-0.588167,-0.158595
 H,-5.328551,-2.485137,-0.255160

H,-7.033744,1.472199,-0.050242
 Br,7.968431,-1.824337,0.051619
 O,-7.518950,-1.214622,-0.195670
 C,-8.727064,-0.441594,-0.132746
 H,-8.741778,0.155349,0.787193
 H,-8.786568,0.227680,-1.000226
 C,-9.903086,-1.392712,-0.152264
 H,-10.816397,-0.798909,-0.298550
 H,-9.802044,-2.090456,-0.994246
 O,-9.950421,-2.096640,1.091018
 H,-10.665166,-2.751250,1.051324

Table S6.2 Characterizations of Spectra Computed in Solvent Dichloromethane (PCM-Tomasi as implemented in Gaussian).

Note: Max amplitude is 0.70714 for a pure one-electron excitation. The highest occupied molecular orbital (HOMO) to the lowest unoccupied molecular orbital (LUMO) transitions are in bold.

BF₂nbmC₂H₄OH

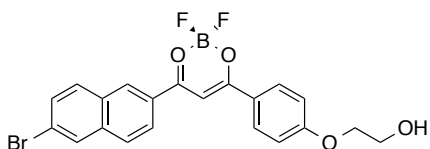


Excited State 1: Singlet-A 2.5736 eV 481.76 nm f=0.6333 <S2>=0.000**
99 ->100 0.70358

Excited State 2: Singlet-A 2.9728 eV 417.06 nm f=1.0186 <S**2>=0.000
 97 ->100 0.10141
 98 ->100 0.69630

Excited State 3: Singlet-A 3.6424 eV 340.39 nm f=0.0725 <S**2>=0.000
 96 ->100 0.11216
 97 ->100 0.67779

BF₂n(Br)bmC₂H₄OH

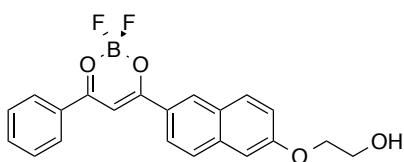


Excited State 1: Singlet-A 2.9230 eV 424.17 nm f=1.1826 <S2>=0.000**
116 ->117 0.70224

Excited State 2: Singlet-A 3.1889 eV 388.80 nm f=0.3501 <S**2>=0.000
 114 ->117 0.17290
 115 ->117 0.67634

Excited State 3: Singlet-A 3.6507 eV 339.62 nm f=0.0734 <S**2>=0.000
 114 ->117 0.66024
 115 ->117 -0.17869
 116 ->119 0.11843

BF₂bnmOC₂H₄OH

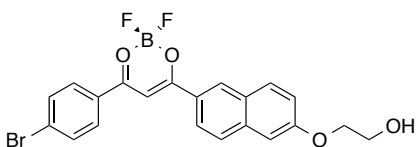


Excited State 1: Singlet-A 2.6838 eV 461.98 nm f=0.6974 <S2>=0.000**
99 ->100 0.70145

Excited State 2: Singlet-A 3.2668 eV 379.53 nm f=0.5237 <S**2>=0.000
 98 ->100 0.69405

Excited State 3: Singlet-A 3.7571 eV 330.00 nm f=0.2364 <S**2>=0.000
 96 ->100 -0.16456
 97 ->100 0.64930
 99 ->101 0.10222
 99 ->102 0.17709

BF₂b(Br)nmOC₂H₄OH

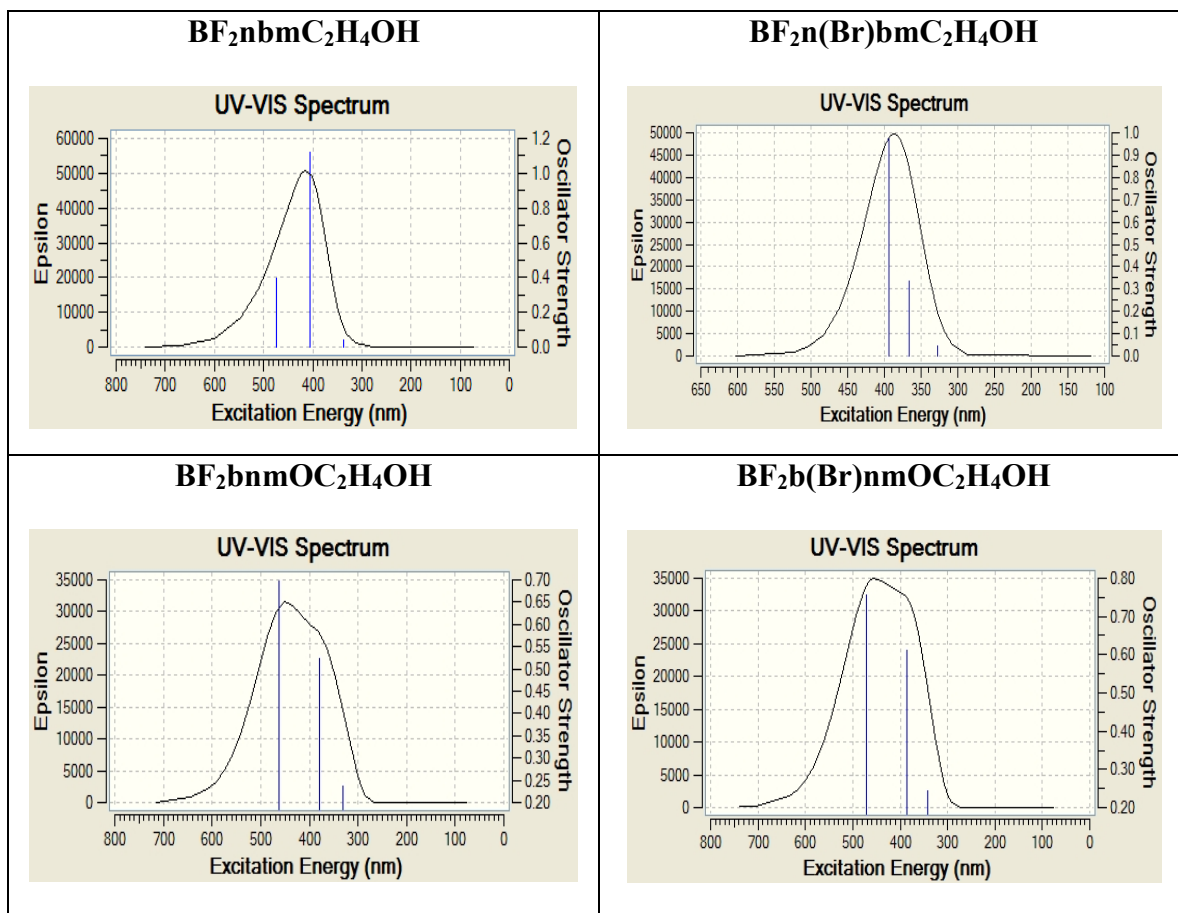


Excited State 1: Singlet-A 2.6327 eV 470.93 nm f=0.7578 <S2>=0.000**
116 ->117 0.70161

Excited State 2: Singlet-A 3.2063 eV 386.69 nm f=0.6128 <S**2>=0.000
 115 ->117 0.69568

Excited State 3: Singlet-A 3.6188 eV 342.61 nm f=0.2426 <S**2>=0.000
 114 ->117 0.67741
 116 ->119 -0.15970

Table S6.3 Gaussview traces of computed TD-B3LYP/6-311+G(d) absorption spectra for initiators in CH₂Cl₂ represented by Tomasi's Polarizable Continuum Model.



Supporting Information for Section 6.3.2: Computational Investigations into the Solution Optical Properties of Dinaphthoyl β -Diketones and Their Boronated Counterparts

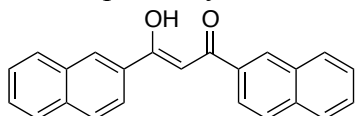
Full Computational Details

All compounds were modeled using the Gaussian 09 suite of programs¹ utilizing density functional theory (DFT). We chose B3LYP/6-31G(d) for ground state geometry optimization of the ligands with a Tomasi polarized continuum for dichloromethane

solvent.² The vibrational frequencies for the optimized geometries were calculated in an additional calculation also utilizing B3LYP/6-31G(d). The same calculations were used for the boronated complexes except that the more flexible B3LYP/6-31+G(d) was used. Calculations performed on the ligands using B3LYP/6-31+G(d) tended to crash, possibly due to the greater degree of rotational freedom available to the ligands compared to the complexes. All vibrational frequencies were positive, assuring that the geometries were at least a local minimum. Single point energy calculations were used to generate the molecular orbital diagrams utilizing B3LYP/6-31G(d) for both the ligands and the boronated complexes. Molecular orbitals were depicted by GaussView 5 software.⁵

Gaussian 09 Specifications for all ligands and compounds in CH₂Cl₂ Solvent.

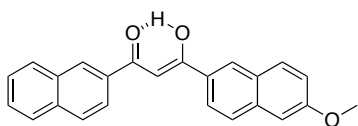
Table S6.4 B3LYP/6-31G(d) optimized structure for ligands and B3LYP/6-31+G(d) for boron compounds. Coordinates are given in Cartesian, in Angstroms. Molecular Orbitals were depicted by GaussView 5 software.⁴



E (HF) = -1036.57373317. μ (Debye) = 4.0879

O, -2.125439, 2.230985, -0.305982
 C, -2.078267, 0.96992, -0.222565
 C, -0.822312, 0.273779, -0.17245
 H, -0.806001, -0.79652, -0.038154
 O, 0.388785, 2.292695, -0.343117
 C, 0.375192, 0.965014, -0.235274
 C, 1.705332, 0.337839, -0.181029
 C, 2.831691, 1.136928, -0.045294
 C, 1.875408, -1.078695, -0.263699
 C, 4.130421, 0.579899, 0.022269
 H, 2.717742, 2.21407, 0.016984
 C, 3.12234, -1.645668, -0.204027
 H, 1.011621, -1.721128, -0.394871
 C, 4.292272, -0.843686, -0.056243

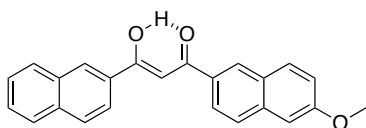
C, 5.290796, 1.384475, 0.166672
 H, 3.232936, -2.72449, -0.275264
 C, 5.587337, -1.398444, 0.009933
 C, 6.548503, 0.826772, 0.229892
 H, 5.17753, 2.463774, 0.227388
 C, 6.701895, -0.584399, 0.150567
 H, 5.725583, -2.474133, -0.048806
 H, 7.414073, 1.469085, 0.339711
 C, -3.365226, 0.213919, -0.156686
 C, -3.443425, -1.197926, -0.337421
 C, -4.529999, 0.924715, 0.084255
 C, -4.651904, -1.849134, -0.269154
 H, -2.548627, -1.770284, -0.556228
 C, -5.788717, 0.282051, 0.169203
 H, -4.468905, 2.000649, 0.214549
 C, -5.856305, -1.139099, -0.010272
 H, -4.699815, -2.924919, -0.418142
 C, -6.988291, 1.003036, 0.426083
 C, -7.119384, -1.783029, 0.072911
 C, -8.197612, 0.34936, 0.50099
 H, -6.93224, 2.080227, 0.561604
 C, -8.263043, -1.056008, 0.322788
 H, -7.169528, -2.860388, -0.063985
 H, -9.10844, 0.907974, 0.697052
 H, -9.224034, -1.559109, 0.384582
 O, 7.906078, -1.215808, 0.204614
 C, 9.091175, -0.434278, 0.348152
 H, 9.914491, -1.149553, 0.366187
 H, 9.224349, 0.25108, -0.497098
 H, 9.084744, 0.135346, 1.284818
 H, -0.588134, 2.571294, -0.342049



E (HF) = -1151.09785731. μ (Debye) = 4.1695

O, -2.125551, 2.231039, -0.307715
 C, -2.078278, 0.969788, -0.227301
 C, -0.822289, 0.273422, -0.181031

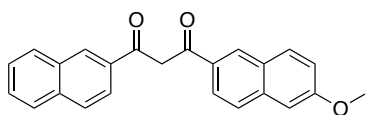
H, -0.80603, -0.797212, -0.049477
O, 0.388522, 2.292804, -0.348158
C, 0.375145, 0.96487, -0.242961
C, 1.705366, 0.337825, -0.189373
C, 2.831532, 1.136841, -0.051671
C, 1.875804, -1.078568, -0.272825
C, 4.130109, 0.579746, 0.018256
H, 2.717495, 2.213959, 0.010872
C, 3.122604, -1.645634, -0.210785
H, 1.01232, -1.720987, -0.406059
C, 4.292271, -0.843776, -0.05982
C, 5.290142, 1.384323, 0.16554
H, 3.233143, -2.724474, -0.281961
C, 5.587084, -1.398723, 0.010639
C, 6.547531, 0.82644, 0.233076
H, 5.176936, 2.463694, 0.225198
C, 6.701195, -0.584757, 0.155224
H, 5.725302, -2.474482, -0.046904
H, 7.412808, 1.468721, 0.345437
C, -3.365184, 0.213848, -0.159742
C, -3.444299, -1.197315, -0.34519
C, -4.528853, 0.924225, 0.087611
C, -4.652919, -1.848195, -0.275747
H, -2.550267, -1.769108, -0.568502
C, -5.787562, 0.281768, 0.174415
H, -4.466777, 1.99972, 0.221047
C, -5.856222, -1.138587, -0.010511
H, -4.701732, -2.923453, -0.428249
C, -6.98596, 1.00229, 0.437989
C, -7.119398, -1.782231, 0.07417
C, -8.195369, 0.348919, 0.5142
H, -6.929011, 2.07897, 0.577222
C, -8.261914, -1.055684, 0.330634
H, -7.170591, -2.859063, -0.066489
H, -9.105335, 0.907175, 0.715199
H, -9.222879, -1.55869, 0.393657
O, 7.90526, -1.215968, 0.215054
C, 9.089428, -0.433821, 0.363179
H, 9.912687, -1.148932, 0.388712
H, 9.22762, 0.248675, -0.483594
H, 9.077036, 0.139079, 1.297787
H, -0.588361, 2.571325, -0.345208



E (HF) = -1151.09782143. μ (Debye) = 3.2524

O, -2.158955, 2.218211, -0.325343
 C, -2.060752, 0.893992, -0.218992
 C, -0.82739, 0.274118, -0.166916
 H, -0.783844, -0.795263, -0.031345
 O, 0.353862, 2.304623, -0.317258
 C, 0.388812, 1.043192, -0.230958
 C, 1.716132, 0.368657, -0.181835
 C, 2.846644, 1.156367, -0.027214
 C, 1.877251, -1.045472, -0.292785
 C, 4.141896, 0.592965, 0.033682
 H, 2.727119, 2.232511, 0.051947
 C, 3.122331, -1.621976, -0.244259
 H, 1.012122, -1.682795, -0.439192
 C, 4.295297, -0.8303, -0.075889
 C, 5.307014, 1.387391, 0.199182
 H, 3.227503, -2.699691, -0.338617
 C, 5.588014, -1.393564, -0.017849
 C, 6.560933, 0.821235, 0.253507
 H, 5.199416, 2.465722, 0.283301
 C, 6.706141, -0.589313, 0.143405
 H, 5.720636, -2.468465, -0.099848
 H, 7.430126, 1.455595, 0.379935
 C, -3.352794, 0.185267, -0.148997
 C, -3.439212, -1.231396, -0.29732
 C, -4.515327, 0.910052, 0.066918
 C, -4.650354, -1.87264, -0.219144
 H, -2.54485, -1.811327, -0.497031
 C, -5.77848, 0.274579, 0.155666
 H, -4.45964, 1.98773, 0.178339
 C, -5.853657, -1.149456, 0.01206
 H, -4.702827, -2.951446, -0.341473
 C, -6.975146, 1.009003, 0.383867
 C, -7.120334, -1.783819, 0.10012
 C, -8.189356, 0.364384, 0.46507

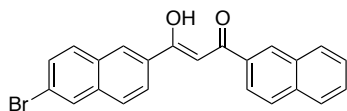
H, -6.913986, 2.088926, 0.492571
 C, -8.262171, -1.044033, 0.321874
 H, -7.175561, -2.863938, -0.010143
 H, -9.098069, 0.933527, 0.639288
 H, -9.226566, -1.539883, 0.388147
 O, 7.907134, -1.228403, 0.186603
 C, 9.096227, -0.456611, 0.347278
 H, 9.91567, -1.176585, 0.350936
 H, 9.234026, 0.24559, -0.483318
 H, 9.092462, 0.093389, 1.29563
 H, -1.20039, 2.555225, -0.33396



E (HF) = -1151.09821786. μ (Debye) = 2.5439

C, -1.267768, -0.631767, 1.420665
 O, -0.447774, -1.596324, 1.521392
 C, -0.861894, 0.726285, 2.040484
 H, -1.713287, 1.252131, 2.482475
 H, -0.127707, 0.51602, 2.82567
 C, -0.280649, 1.619607, 0.972935
 O, -0.915083, 2.54921, 0.47575
 C, 1.119338, 1.346284, 0.46147
 C, 1.856673, 0.196627, 0.823434
 C, 1.698134, 2.303558, -0.390838
 C, 3.160542, 0.009438, 0.349252
 H, 1.381729, -0.571925, 1.428148
 C, 2.99053, 2.14384, -0.865386
 H, 1.1097, 3.171419, -0.664755
 C, 3.753567, 0.995774, -0.504636
 C, 3.926558, -1.149221, 0.688971
 H, 3.434285, 2.890098, -1.516939
 C, 5.057856, 0.801553, -0.97058
 C, 5.21205, -1.341166, 0.228674
 H, 3.472464, -1.897613, 1.330729
 C, 5.793199, -0.36202, -0.607419
 H, 5.536566, 1.526719, -1.619553
 C, -2.530661, -0.736274, 0.727003
 C, -3.438362, 0.32775, 0.53012

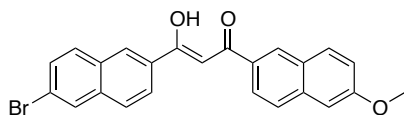
C, -2.914926, -2.029221, 0.221744
 C, -4.676682, 0.141322, -0.125073
 H, -3.183771, 1.331233, 0.854466
 C, -4.106858, -2.233163, -0.413483
 H, -2.218167, -2.848153, 0.370276
 C, -5.039206, -1.162848, -0.613707
 C, -5.600138, 1.209651, -0.331557
 H, -4.368211, -3.223838, -0.781803
 C, -6.277588, -1.341763, -1.266701
 C, -6.803861, 1.001821, -0.974915
 H, -5.337169, 2.201285, 0.031162
 C, -7.154407, -0.282957, -1.449503
 H, -6.536701, -2.335125, -1.629059
 H, -7.489927, 1.833436, -1.118592
 H, -8.104201, -0.436823, -1.954219
 H, 5.760628, -2.231524, 0.506726
 O, 7.018532, -0.421096, -1.117263
 C, 7.865485, -1.550946, -0.829209
 H, 7.408516, -2.470614, -1.203887
 H, 8.796199, -1.351062, -1.356627
 H, 8.048057, -1.622959, 0.246278



E (HF) = -3607.67847359 μ (Debye) = 4.4272

O, 0.48297, 2.459215, -0.320527
 C, 0.396929, 1.2005, -0.25493
 C, 1.572894, 0.375799, -0.192347
 H, 1.47742, -0.692209, -0.073903
 O, 2.992545, 2.259062, -0.30482
 C, 2.835041, 0.940131, -0.220447
 C, 4.092398, 0.173341, -0.147343
 C, 5.285179, 0.84395, 0.079874
 C, 4.115206, -1.245057, -0.303222
 C, 6.517507, 0.151556, 0.172125
 H, 5.277802, 1.922384, 0.197336
 C, 5.295704, -1.940547, -0.22198
 H, 3.196902, -1.783335, -0.510265

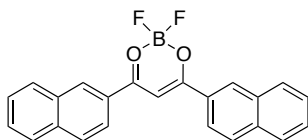
C, 6.528982, -1.273622, 0.020302
 C, 7.744529, 0.830189, 0.41156
 H, 5.30028, -3.019943, -0.349698
 C, 7.765103, -1.965001, 0.112137
 C, 8.92782, 0.130958, 0.495899
 H, 7.731214, 1.911127, 0.526036
 C, 8.93765, -1.278509, 0.344884
 H, 7.772354, -3.045895, -0.003776
 H, 9.860321, 0.657307, 0.678534
 H, 9.878243, -1.817755, 0.414042
 C, -0.964015, 0.583186, -0.224506
 C, -1.185948, -0.812544, -0.407453
 C, -2.052957, 1.414215, -0.01601
 C, -2.456786, -1.334975, -0.373802
 H, -0.351216, -1.477538, -0.599291
 C, -3.372655, 0.906415, 0.032913
 H, -1.882736, 2.478004, 0.115308
 C, -3.584293, -0.499189, -0.14847
 H, -2.613826, -2.399696, -0.523681
 C, -4.497467, 1.748247, 0.255773
 C, -4.906822, -1.0141, -0.101167
 C, -5.772331, 1.233245, 0.298187
 H, -4.338708, 2.81435, 0.39331
 C, -5.959537, -0.157926, 0.117371
 H, -5.074213, -2.077473, -0.237105
 H, -6.628971, 1.875947, 0.467392
 H, 2.052568, 2.641699, -0.318648
 Br, -7.743838, -0.851279, 0.184318



E (HF) = -3722.20263194 μ (Debye) = 5.9022

O, -0.397265, 2.575267, -0.209719
 C, -0.440887, 1.311881, -0.185114
 C, 0.757663, 0.523148, -0.140004
 H, 0.690572, -0.550961, -0.070407
 O, 2.116099, 2.451574, -0.189863
 C, 2.004764, 1.125286, -0.142191

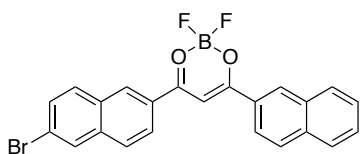
C, 3.284361, 0.400644, -0.092401
C, 4.471484, 1.117267, -0.03013
C, 3.346603, -1.027383, -0.106141
C, 5.726943, 0.467741, 0.022763
H, 4.440453, 2.201552, -0.019603
C, 4.549355, -1.683249, -0.055566
H, 2.434777, -1.611203, -0.165179
C, 5.780172, -0.966042, 0.011696
C, 6.948026, 1.188641, 0.086984
H, 4.576756, -2.769626, -0.068991
C, 7.031958, -1.613173, 0.064806
C, 8.162607, 0.541325, 0.137761
H, 6.916854, 2.275085, 0.095514
C, 8.20806, -0.879715, 0.127048
H, 7.088309, -2.697773, 0.057348
H, 9.076699, 1.121127, 0.185541
C, -1.781947, 0.650286, -0.185549
C, -1.958508, -0.741183, -0.43712
C, -2.897441, 1.434172, 0.060855
C, -3.211768, -1.305485, -0.433287
H, -1.102421, -1.368416, -0.659736
C, -4.200276, 0.882093, 0.081528
H, -2.761873, 2.495323, 0.244067
C, -4.366066, -0.518734, -0.170536
H, -3.333844, -2.365999, -0.636254
C, -5.352295, 1.674496, 0.34297
C, -5.671363, -1.077713, -0.154103
C, -6.609988, 1.117112, 0.355399
H, -5.228807, 2.736995, 0.534293
C, -6.751737, -0.268296, 0.103684
H, -5.804115, -2.137574, -0.344571
H, -7.487104, 1.722546, 0.554269
O, 9.362948, -1.597237, 0.175252
C, 10.607239, -0.901893, 0.240104
H, 11.375191, -1.675922, 0.269841
H, 10.760757, -0.272035, -0.64388
H, 10.676055, -0.287242, 1.145215
H, 1.163116, 2.801769, -0.202278
Br, -8.513068, -1.021766, 0.128535



E (HF) = -1260.76184420 μ (Debye) = 10.0981

B, 0, 2.546808, -0.073425
 F, -0.000001, 3.079375, 1.218378
 F, 0.000001, 3.54673, -1.034357
 O, -1.221052, 1.713689, -0.250755
 C, -1.210912, 0.415247, -0.075817
 C, 0, -0.270903, 0.067373
 H, -0.000001, -1.331879, 0.257678
 O, 1.221052, 1.713689, -0.250753
 C, 1.210912, 0.415247, -0.075815
 C, 2.526461, -0.238269, -0.060815
 C, 3.67185, 0.546378, 0.018423
 C, 2.658937, -1.660099, -0.121625
 C, 4.962494, -0.034524, 0.049271
 H, 3.578212, 1.626382, 0.066388
 C, 3.900352, -2.247158, -0.097797
 H, 1.780504, -2.289749, -0.208019
 C, 5.086169, -1.462751, -0.008786
 C, 6.140638, 0.761044, 0.137792
 H, 3.989602, -3.329172, -0.152382
 C, 6.382206, -2.041967, 0.021229
 C, 7.385063, 0.168657, 0.165398
 H, 6.041782, 1.842838, 0.181937
 C, 7.505722, -1.244042, 0.106692
 H, 6.477245, -3.124164, -0.023346
 H, 8.279627, 0.781507, 0.232463
 H, 8.49272, -1.698097, 0.12974
 C, -2.526461, -0.238269, -0.060818
 C, -2.658937, -1.660099, -0.121633
 C, -3.67185, 0.546378, 0.018425
 C, -3.900352, -2.247157, -0.097806
 H, -1.780505, -2.289748, -0.208032
 C, -4.962494, -0.034524, 0.049273
 H, -3.578212, 1.626382, 0.066394
 C, -5.086169, -1.46275, -0.008791
 H, -3.989603, -3.329171, -0.152396

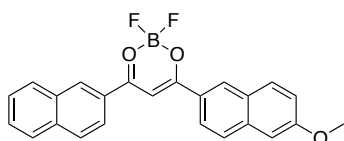
C, -6.140638, 0.761044, 0.137799
 C, -6.382206, -2.041967, 0.021224
 C, -7.385062, 0.168657, 0.165405
 H, -6.041781, 1.842837, 0.181949
 C, -7.505722, -1.244042, 0.106692
 H, -6.477246, -3.124164, -0.023355
 H, -8.279626, 0.781506, 0.232474
 H, -8.49272, -1.698098, 0.12974



E (HF) = -3831.873676 μ (Debye) = 7.0147

Br, 1.64632, 2.709036, -0.022461
 F, 1.684702, 3.130526, 1.293987
 F, 1.738115, 3.723693, -0.936822
 O, 0.351359, 1.968845, -0.246191
 C, 0.248982, 0.685067, -0.06135
 C, 1.390746, -0.110835, 0.088917
 H, 1.29642, -1.166815, 0.285386
 O, 2.787051, 1.748233, -0.246849
 C, 2.658948, 0.467037, -0.064868
 C, 3.913651, -0.305645, -0.055538
 C, 5.120593, 0.37864, 0.008168
 C, 3.926215, -1.732369, -0.106422
 C, 6.358157, -0.308605, 0.031449
 H, 5.112368, 1.463218, 0.046519
 C, 5.113408, -2.422988, -0.088296
 H, 2.995788, -2.285142, -0.180491
 C, 6.361598, -1.741833, -0.016731
 C, 7.599295, 0.384826, 0.101374
 H, 5.110923, -3.509435, -0.134915
 C, 7.604956, -2.426512, 0.005156
 C, 8.789927, -0.308408, 0.120895
 H, 7.590832, 1.4715, 0.137824
 C, 8.791739, -1.725864, 0.072469
 H, 7.608842, -3.513481, -0.03174
 H, 9.733062, 0.228586, 0.173785

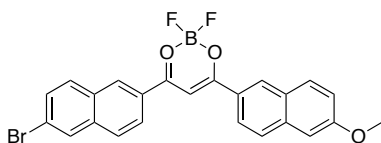
H, 9.737501, -2.261159, 0.089
 C, -1.126645, 0.152924, -0.048977
 C, -1.399847, -1.247812, -0.06308
 C, -2.189114, 1.046629, -0.027284
 C, -2.692559, -1.712148, -0.051226
 H, -0.585373, -1.963192, -0.100155
 C, -3.529973, 0.595763, -0.012464
 H, -1.984141, 2.112185, -0.017368
 H, -3.795473, -0.812337, -0.02382
 H, -2.887004, -2.781641, -0.068228
 C, -4.625993, 1.502423, 0.016773
 C, -5.139693, -1.266633, -0.010379
 C, -5.924049, 1.045037, 0.032264
 H, -4.426056, 2.570916, 0.026743
 C, -6.166761, -0.350205, 0.018019
 H, -5.347675, -2.332133, -0.020803
 H, -6.758675, 1.737599, 0.054724
 Br, -7.97342, -0.955934, 0.039759



E (HF) = -1335.98816861 μ (Debye) = 8.6087

B, -0.840039, 2.617801, -0.049926
 F, -0.865428, 3.142242, 1.246334
 F, -0.879185, 3.626502, -1.002642
 O, -2.024505, 1.738081, -0.237257
 C, -1.958583, 0.438653, -0.069276
 C, -0.72273, -0.196831, 0.072502
 H, -0.681145, -1.258719, 0.252927
 O, 0.41458, 1.839701, -0.23019
 C, 0.462622, 0.539535, -0.061949
 C, 1.800021, -0.05477, -0.049855
 C, 2.914512, 0.779459, -0.02033
 C, 1.999874, -1.47254, -0.065938
 C, 4.225994, 0.256179, 0.000022
 H, 2.776252, 1.855659, -0.005408
 C, 3.263695, -2.00533, -0.04956
 H, 1.149952, -2.14458, -0.108189
 C, 4.42, -1.167545, -0.013497

C, 5.371644, 1.097017, 0.035693
 H, 3.397993, -3.083757, -0.068451
 C, 5.729927, -1.688133, 0.006151
 C, 6.645611, 0.57216, 0.054692
 H, 5.233718, 2.175196, 0.046763
 C, 6.829295, -0.83895, 0.03978
 H, 5.891999, -2.762362, -0.004516
 H, 7.498593, 1.239742, 0.08082
 C, -3.247726, -0.267886, -0.060583
 C, -3.324294, -1.693036, -0.136204
 C, -4.423037, 0.46967, 0.026223
 C, -4.541753, -2.328867, -0.119196
 H, -2.421695, -2.286764, -0.228772
 C, -5.690174, -0.161736, 0.049922
 H, -4.371942, 1.551932, 0.085135
 C, -5.757655, -1.592874, -0.023158
 H, -4.588308, -3.412968, -0.185176
 C, -6.898586, 0.586008, 0.145568
 C, -7.030161, -2.222668, -0.000704
 C, -8.118994, -0.054792, 0.165559
 H, -6.841997, 1.670349, 0.201305
 C, -8.184216, -1.470435, 0.091733
 H, -7.082732, -3.307242, -0.056649
 H, -9.03687, 0.521933, 0.23818
 H, -9.152668, -1.963114, 0.108766
 O, 8.051056, -1.435487, 0.057315
 C, 9.231107, -0.624933, 0.094148
 H, 10.064704, -1.327676, 0.103112
 H, 9.29907, 0.013086, -0.794064
 H, 9.25939, -0.010909, 1.001212



E (HF) = -3946.400079958 μ (Debye) = 7.2218

B, 0.810385, 2.889447, -0.009918
 F, 0.830976, 3.30722, 1.30908
 F, 0.85756, 3.913848, -0.918303
 O, -0.450811, 2.096111, -0.237245
 C, -0.494855, 0.806657, -0.061173

C, 0.679242, 0.061229, 0.08144
H, 0.63111, -0.9994, 0.26905
O, 1.992485, 1.982912, -0.239691
C, 1.923428, 0.694823, -0.066409
C, 3.206747, -0.020394, -0.061319
C, 4.385731, 0.714337, -0.018691
C, 3.285218, -1.447813, -0.094341
C, 5.648897, 0.08058, -0.000637
H, 4.332286, 1.798133, 0.006848
C, 4.49843, -2.088024, -0.080856
H, 2.379451, -2.042328, -0.149387
C, 5.721177, -1.353389, -0.03109
C, 6.860993, 0.81892, 0.04704
H, 4.54094, -3.173937, -0.113571
C, 6.982437, -1.983748, -0.014617
C, 8.086009, 0.1872, 0.061858
H, 6.814096, 1.904925, 0.070761
C, 8.148875, -1.233155, 0.030616
H, 7.05675, -3.067326, -0.037288
H, 8.992874, 0.779907, 0.097529
C, -1.846442, 0.214165, -0.049543
C, -2.05682, -1.197167, -0.071067
C, -2.948023, 1.058631, -0.023068
C, -3.327157, -1.719685, -0.060547
H, -1.211094, -1.874981, -0.113
C, -4.26753, 0.547502, -0.009063
H, -2.791345, 2.132305, -0.008145
C, -4.46945, -0.870865, -0.026916
H, -3.472941, -2.796818, -0.08316
C, -5.403602, 1.403142, 0.025568
C, -5.791798, -1.38569, -0.014986
C, -6.679715, 0.887264, 0.040203
H, -5.252516, 2.479593, 0.040607
C, -6.859372, -0.517221, 0.018882
H, -5.950994, -2.459459, -0.030449
H, -7.544653, 1.541319, 0.067298
Br, -8.637121, -1.204335, 0.040497
O, 9.315992, -1.934574, 0.042865
C, 10.554188, -1.231077, 0.089754
H, 10.637076, -0.630145, 1.003942
H, 11.327005, -2.001108, 0.091055
H, 10.681462, -0.588713, -0.790531

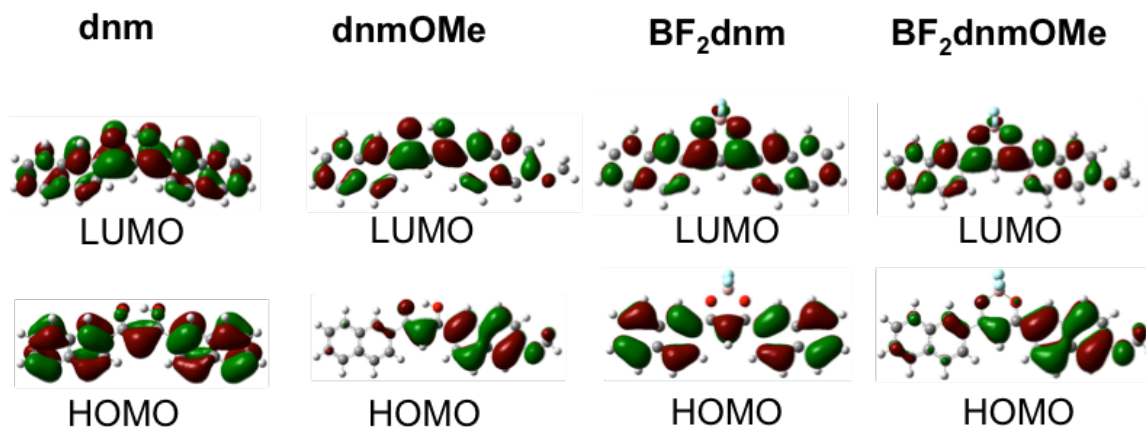
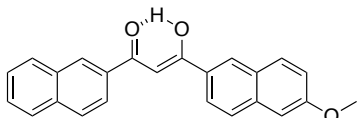


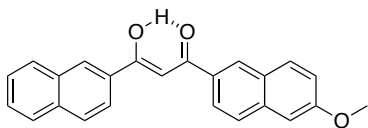
Figure S6.1 Frontier molecular orbitals of dnm, dnmOMe and boron derivatives BF₂dnm and BF₂dnmOMe.

Table S6.5 Characterization of Spectrum Computed in Solvent Dichloromethane (PCM-Tomasi as implemented in Gaussian) for the tautomers of dnm(OMe).

Note: Max amplitude is 0.70714 for a pure one-electron excitation. The highest occupied molecular orbital (HOMO) to the lowest unoccupied molecular orbital (LUMO) transitions are in bold.



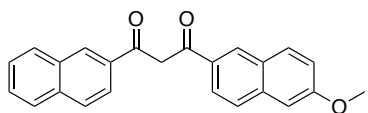
Excited State	1:	Singlet-A	3.0005 eV	413.21 nm	f=0.9707	<S**2>=0.000
	93 -> 94	0.69887				
Excited State	2:	Singlet-A	3.2780 eV	378.23 nm	f=0.0601	<S**2>=0.000
	92 -> 94	0.69187				
Excited State	3:	Singlet-A	3.5607 eV	348.20 nm	f=0.3753	<S**2>=0.000
	91 -> 94	0.67509				
	93 -> 96	0.12882				



Excited State 1: Singlet-A 2.9946 eV 414.02 nm f=0.7639 <S2>=0.000**
93 -> 94 0.70086

Excited State 2: Singlet-A 3.3016 eV 375.53 nm f=0.2585 <S**2>=0.000
 92 -> 94 0.68777

Excited State 3: Singlet-A 3.5527 eV 348.99 nm f=0.4607 <S**2>=0.000
 91 -> 94 0.68116

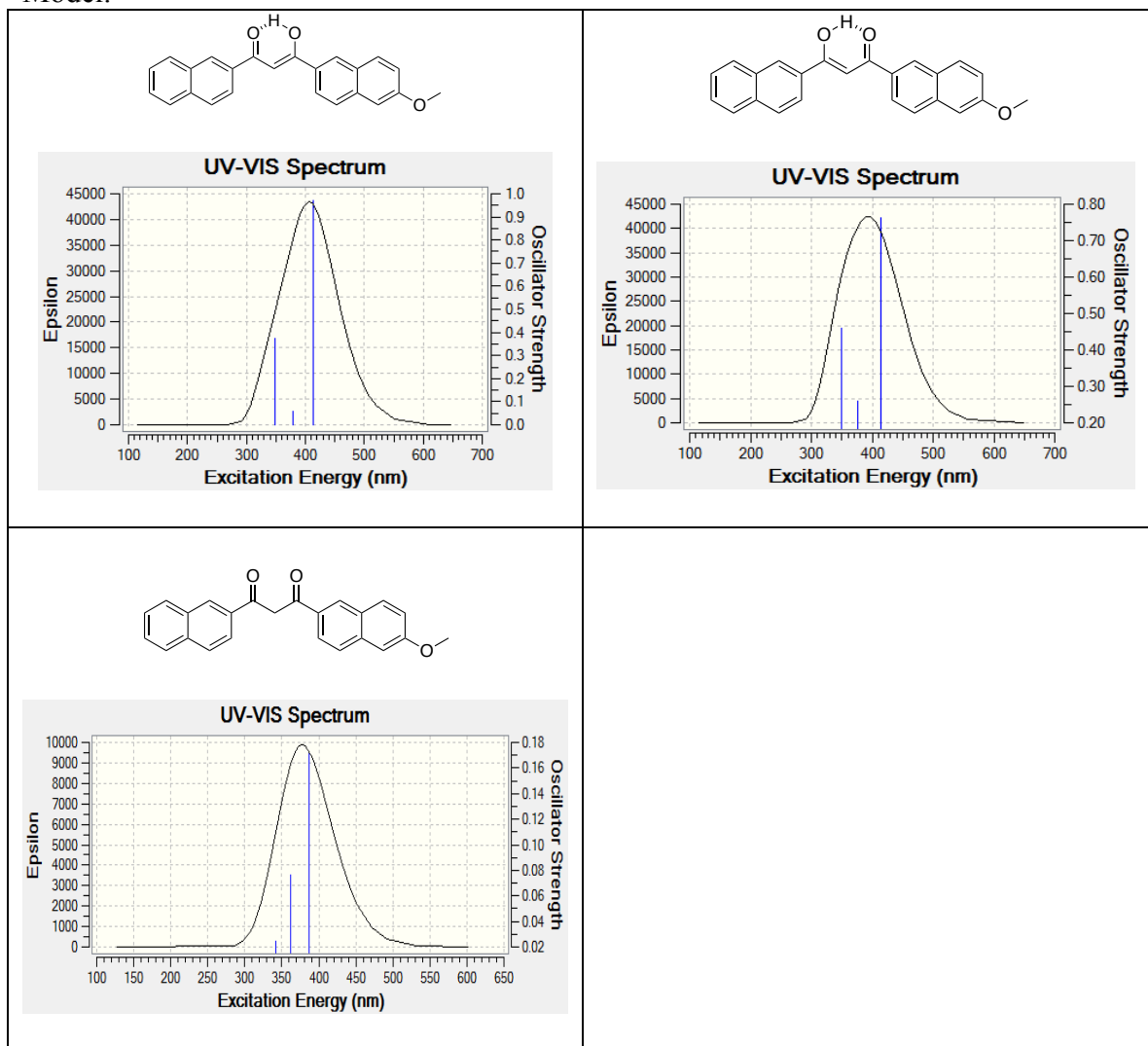


Excited State 1: Singlet-A 3.2012 eV 387.31 nm f=0.1718 <S2>=0.000**
93 -> 94 0.69683

Excited State 2: Singlet-A 3.4234 eV 362.17 nm f=0.0760 <S**2>=0.000
 92 -> 94 0.68555

Excited State 3: Singlet-A 3.6205 eV 342.45 nm f=0.0244 <S**2>=0.000
 88 -> 95 -0.18523
 89 -> 94 0.63275
 93 -> 95 -0.15433

Table S6.6. Gaussview traces of computed TD-B3LYP/6-311+G(d) absorption spectra for dnm(OMe) tautomers in CH₂Cl₂ represented by Tomasi's Polarizable Continuum Model.



Supporting Information for Section 6.3.3: Computational Investigations into the Solution Optical Properties of Thienyl Difluoroboron β -Diketonates

Full Computational Details

All compounds were modeled using the Gaussian 09 suite of programs¹ using density functional theory (DFT). We chose B3LYP/6-31+G(d) to simulate the B, O, C, and F atoms and B3LYP/SDD to simulate the I heavy atom for ground state geometry

optimization with a Tomasi polarized continuum for dichloromethane solvent.² The vibrational frequencies for the optimized geometries were all positive, assuring that the geometries are at least a local minimum. Single point energy calculations were used to generate the molecular orbital diagrams utilizing B3LYP/6-31G(d). We used time-dependent density functional theory, TD-B3LYP/6-311+G(d) for estimates of the absorption spectra, at the respective optimized geometries.^{3,4} In all calculations, B3LYP/SDD was used to simulate the iodine atom. The first three excited states were computed for each compound. Molecular orbitals were depicted by GaussView 5 software.⁵

Table S6.7 B3LYP/6-31+G(d) optimized structures for future TD-DFT calculations in dichloromethane. Coordinates given in Cartesian, in Angstroms.

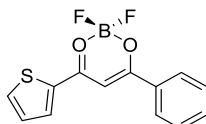
BF₂Thio-CH₃: E (HF) = -1082.47284568



B, 1.91675800, -1.14945100, 0.00984700
 F, 2.17867800, -1.69510000, 1.26548600
 F, 2.29178400, -2.01241400, -1.00926500
 O, 2.67795000, 0.12374600, -0.13083500
 C, 2.11144600, 1.29867800, -0.03184300
 C, 0.73445800, 1.43965600, 0.06838400
 H, 0.29984000, 2.42534300, 0.15464500
 O, 0.44622000, -0.89580600, -0.10129300
 C, -0.08154500, 0.29766700, -0.00409500
 C, -1.52241300, 0.34942500, -0.00167500
 C, -2.35260300, 1.46237100, 0.02215000
 S, -2.45943000, -1.13028100, -0.03333800
 C, -3.72614500, 1.12530300, 0.01739200
 H, -1.98754500, 2.48304600, 0.03763200
 C, -3.93095400, -0.23809800, -0.01115900
 H, -4.53034100, 1.85203000, 0.03293800
 H, -4.87744400, -0.76407900, -0.01997900
 C, 3.05303200, 2.45835600, -0.05559400
 H, 3.63577100, 2.43755400, -0.98418300

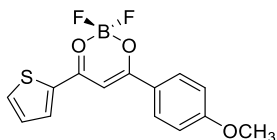
H, 2.52404200, 3.41030000, 0.01786000
 H, 3.76358700, 2.37152400, 0.77492800

BF₂Thio-Ph: E (HF) = -1274.21867029



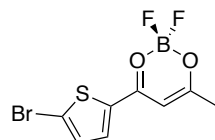
B, 0.10957100, 2.22131500, -0.00827300
 F, 0.13538100, 2.76126200, 1.27895300
 F, 0.17850500, 3.21044400, -0.97685600
 O, -1.15650200, 1.46045100, -0.18780200
 C, -1.22879600, 0.16151500, -0.02043000
 C, -0.06979400, -0.59974300, 0.12999000
 H, -0.12725000, -1.66312400, 0.30432500
 O, 1.28352900, 1.31313900, -0.17110600
 C, 1.18233400, 0.01695000, -0.00146900
 C, -2.58933900, -0.40211300, -0.02158800
 C, -2.81655000, -1.78985000, -0.10783900
 C, -3.69418200, 0.46758800, 0.06422400
 C, -4.11616100, -2.29216000, -0.10160300
 H, -1.98639200, -2.48221800, -0.19833200
 C, -4.99196200, -0.03996600, 0.07330900
 H, -3.52499700, 1.53645300, 0.13044700
 C, -5.20689200, -1.42000200, -0.00874400
 H, -4.27850900, -3.36368400, -0.17417000
 H, -5.83571400, 0.64034600, 0.14586400
 C, 2.42845000, -0.71128200, 0.01055900
 C, 2.63702100, -2.08218900, 0.07532600
 S, 3.95176700, 0.15007400, -0.06840400
 C, 4.00752600, -2.43291600, 0.06528800
 H, 1.83465700, -2.80963400, 0.12205600
 C, 4.83051900, -1.32930800, -0.00952900
 H, 4.37405800, -3.45220700, 0.10882700
 H, 5.91295600, -1.31193400, -0.03278600
 H, -6.21915800, -1.81496200, -0.00297600

BF₂Thio-PhOCH₃: E (HF) = -1388.75052444



B, 1.04725400, 2.28269700, 0.01773200
 F, 1.12466100, 2.79916600, 1.31477400
 F, 1.20257900, 3.28151800, -0.93315100
 O, -0.28244700, 1.64566300, -0.17018500
 C, -0.47789000, 0.35593700, -0.01177200
 C, 0.61446600, -0.50814100, 0.12668300
 H, 0.46404700, -1.56501100, 0.28398000
 O, 2.13334500, 1.27831500, -0.16493300
 C, 1.91263000, -0.00694300, -0.00400600
 C, -1.87341400, -0.07924700, -0.01535700
 C, -2.23857100, -1.44563300, -0.01688500
 C, -2.90220500, 0.88242000, -0.01843500
 C, -3.56859700, -1.82602600, -0.01613700
 H, -1.48194000, -2.22252000, -0.03032300
 C, -4.24325500, 0.51269700, -0.01622800
 H, -2.64253000, 1.93505000, -0.01639900
 C, -4.58563400, -0.85054000, -0.01435400
 H, -3.84907000, -2.87468500 -0.02157300
 H, -5.00650200, 1.28186500, -0.01336200
 C, 3.09129600, -0.84387500, -0.00124700
 C, 3.18196100, -2.22690400, 0.06114600
 S, 4.68252800, -0.11694600, -0.08782100
 C, 4.51800100, -2.69460200, 0.04276600
 H, 2.32061800, -2.88309700, 0.11364100
 C, 5.43261700, -1.66674100, -0.03600500
 H, 4.79500000, -3.74198400, 0.08338000
 H, 6.51235000, -1.74224200, -0.06626000
 O, -5.85352500, -1.32209900, -0.01243900
 C, -6.94492000, -0.39196500, -0.01653600
 H, -7.84720300, -1.00341300, -0.01686500
 H, -6.92400500, 0.23689100, 0.88003900
 H, -6.92055300, 0.23299200, -0.91573400

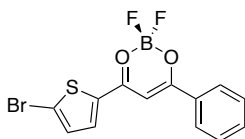
BF₂Thio(Br) E (HF) = -3653.59422354



B, 3.090736, -1.29936, 0.014613
 F, 3.285602, -1.890382, 1.260794
 F, 3.340161, -2.190935, -1.017996
 O, 4.013478, -0.136491, -0.117204
 C, 3.608928, 1.104288, -0.041432

C, 2.261847, 1.429988, 0.046024
 H, 1.962965, 2.466592, 0.110122
 O, 1.665691, -0.850355, -0.080265
 C, 1.303697, 0.404782, -0.002278
 C, -0.118142, 0.642, 0.008721
 C, -0.802465, 1.847439, 0.046736
 S, -1.223902, -0.718871, -0.030583
 C, -2.206245, 1.691019, 0.046666
 H, -0.315101, 2.815336, 0.073738
 C, -2.572318, 0.363024, 0.005144
 H, -2.916268, 2.508702, 0.073526
 C, 4.696932, 2.127144, -0.072862
 H, 5.28456, 2.008507, -0.99085
 H, 4.298651, 3.142374, -0.026194
 H, 5.377623, 1.963859, 0.771105
 Br, -4.333208, -0.283946, -0.012026

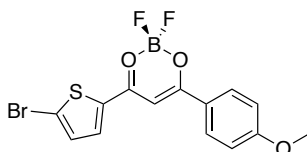
BF₂Thio(Br)-Ph E (HF) = -3845.34035992



B, -1.450599, 2.322327, 0.001919
 F, -1.475355, 2.863038, 1.28809
 F, -1.495999, 3.310467, -0.968312
 O, -2.627764, 1.427301, -0.168335
 C, -2.559262, 0.126974, -0.017439
 C, -1.322864, -0.506985, 0.116146
 H, -1.263502, -1.572537, 0.275179
 O, -0.186006, 1.545559, -0.166805
 C, -0.147958, 0.244528, -0.005859
 C, -3.85069, -0.580073, -0.023135
 C, -3.926813, -1.98507, -0.098263
 C, -5.043414, 0.166645, 0.045248
 C, -5.164974, -2.623798, -0.097696
 H, -3.027091, -2.586051, -0.174614
 C, -6.279161, -0.477168, 0.049187
 H, -4.990828, 1.248006, 0.102706
 C, -6.343753, -1.872977, -0.021777
 H, -5.210827, -3.70713, -0.160924
 H, -7.191559, 0.109279, 0.108467

C, 1.172909, -0.336892, 0.012929
 C, 1.546532, -1.668916, 0.105063
 S, 2.574766, 0.713884, -0.072858
 C, 2.94719, -1.855747, 0.104811
 H, 0.841025, -2.489761, 0.165741
 C, 3.622939, -0.658333, 0.017539
 H, 3.438986, -2.818875, 0.167127
 H, -7.307802, -2.374214, -0.020191
 Br, 5.489046, -0.457716, -0.01785

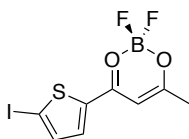
BF₂Thio(Br)-PhOCH₃ E (HF) = -3959.87232970



B, -0.552846, 2.553906, 0.013936
 F, -0.53639, 3.074535, 1.310797
 F, -0.516759, 3.562596, -0.937455
 O, -1.797761, 1.762893, -0.17325
 C, -1.842033, 0.459968, -0.013442
 C, -0.654916, -0.270566, 0.125677
 H, -0.678956, -1.337042, 0.288916
 O, 0.644106, 1.682795, -0.168745
 C, 0.572877, 0.380932, -0.004463
 C, -3.176077, -0.135347, -0.016258
 C, -3.379272, -1.535198, -0.018071
 C, -4.310173, 0.699852, -0.020208
 C, -4.655676, -2.068186, -0.017902
 H, -2.537041, -2.218396, -0.031999
 C, -5.598449, 0.176003, -0.018735
 H, -4.175395, 1.775628, -0.018048
 C, -5.779753, -1.21792, -0.016814
 H, -4.811805, -3.142377, -0.023597
 H, -6.445899, 0.850934, -0.016436
 C, 1.84357, -0.307715, 0.00796
 C, 2.105877, -1.666704, 0.067556
 S, 3.327121, 0.625513, -0.053952
 C, 3.487312, -1.969037, 0.065982
 H, 1.333662, -2.426669, 0.104584
 C, 4.25961, -0.830637, 0.005399

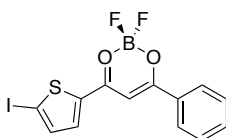
H, 3.897035, -2.971088, 0.105794
 Br, 6.13748, -0.783196, -0.022975
 O, -6.983569, -1.83405, -0.015498
 C, -8.177438, -1.039161, -0.02087
 H, -9.000871, -1.753262, -0.021247
 H, -8.231964, -0.411962, 0.875442
 H, -8.226888, -0.416644, -0.920728

BF₂Thio(I) E (HF) = -1093.26503541



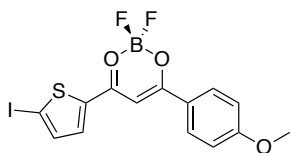
B, 3.614118, -1.328641, 0.019018
 F, 3.79175, -1.895507, 1.280051
 F, 3.844722, -2.249914, -0.991537
 O, 4.564151, -0.191349, -0.137236
 C, 4.191519, 1.058735, -0.050532
 C, 2.85328, 1.416544, 0.054055
 H, 2.579645, 2.459524, 0.127388
 O, 2.201323, -0.847463, -0.090915
 C, 1.869745, 0.415342, -0.001624
 C, 0.453402, 0.688405, 0.010322
 C, -0.201323, 1.910448, 0.060689
 S, -0.691868, -0.637581, -0.038775
 C, -1.610383, 1.791529, 0.061423
 H, 0.310285, 2.865659, 0.095626
 C, -2.014545, 0.473295, 0.010218
 H, -2.290812, 2.633608, 0.097412
 C, 5.303738, 2.05544, -0.093934
 H, 5.873626, 1.927417, -1.021931
 H, 4.93106, 3.079787, -0.036359
 H, 5.993761, 1.871353, 0.738123
 I, -4.006092, -0.211924, -0.010378

BF₂Thio(I)-Ph E (HF) -1285.00735419



B, -2.059035, 2.329061, -0.007861
 F, -2.105078, 2.874573, 1.27649
 F, -2.108543, 3.313654, -0.982162
 O, -3.220856, 1.416857, -0.187198
 C, -3.134865, 0.118797, -0.025458
 C, -1.890656, -0.496885, 0.124286
 H, -1.818197, -1.560379, 0.292086
 O, -0.78175, 1.570706, -0.160504
 C, -0.725237, 0.271239, 0.006487
 C, 0.604469, -0.291805, 0.031606
 C, 0.996396, -1.61925, 0.121735
 S, 1.996321, 0.769642, -0.060006
 C, 2.400663, -1.790862, 0.12019
 H, 0.301576, -2.449242, 0.183724
 C, 3.065064, -0.585681, 0.026755
 H, 2.895638, -2.752536, 0.183089
 I, 5.154845, -0.322439, -0.016455
 C, -4.416506, -0.605914, -0.028931
 C, -4.473816, -2.010255, -0.130736
 C, -5.618137, 0.123215, 0.071195
 C, -5.703374, -2.666221, -0.126825
 H, -3.566344, -2.595726, -0.232296
 C, -6.845052, -0.53795, 0.078511
 H, -5.578949, 1.203798, 0.150373
 C, -6.891355, -1.933209, -0.020033
 H, -5.735616, -3.748521, -0.211983
 H, -7.764585, 0.034133, 0.162588
 H, -7.848389, -2.447668, -0.016055

BF₂Thio-PhOCH₃ E (HF) = -1399.53773264



B, -1.194905, 2.592006, 0.011488
 F, -1.196014, 3.130162, 1.30189
 F, -1.175815, 3.590479, -0.952211
 O, -2.421629, 1.77317, -0.171394
 C, -2.438844, 0.46947, -0.014033
 C, -1.236554, -0.236391, 0.126323

H, -1.237927, -1.30383, 0.284627
 O, 0.021521, 1.745885, -0.154688
 C, -0.022221, 0.442455, 0.005163
 C, 1.264261, -0.218685, 0.019711
 C, 1.557655, -1.571817, 0.080118
 S, 2.729995, 0.739508, -0.046272
 C, 2.946676, -1.846218, 0.077272
 H, 0.802824, -2.349195, 0.120137
 C, 3.697857, -0.692046, 0.012504
 H, 3.368538, -2.843235, 0.118744
 I, 5.802089, -0.579129, -0.01977
 C, -3.760937, -0.152894, -0.018821
 C, -3.935645, -1.556747, -0.026153
 C, -4.912027, 0.659318, -0.016934
 C, -5.201218, -2.115877, -0.026823
 H, -3.079572, -2.222345, -0.044266
 C, -6.189675, 0.109028, -0.015554
 H, -4.799454, 1.737643, -0.009904
 C, -6.342724, -1.288572, -0.019859
 H, -5.33538, -3.193002, -0.037159
 H, -7.050567, 0.766717, -0.008468
 O, -7.533818, -1.928713, -0.019494
 C, -8.743118, -1.158141, -0.019239
 H, -8.806775, -0.532565, -0.916167
 H, -9.552362, -1.888381, -0.021281
 H, -8.808529, -0.535913, 0.879892

Table S6.8 Characterizations of Spectra Computed in Solvent Dichloromethane (PCM-Tomasi as implemented in Gaussian).

Note: Max amplitude is 0.70714 for a pure one-electron excitation. The highest occupied molecular orbital (HOMO) to the lowest unoccupied molecular orbital (LUMO) transitions are in bold.

BF₂Thio-CH₃

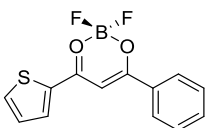


Excited State 1: Singlet-A 3.6394 eV 340.67 nm f=0.7020 <S2>=0.000**
55 -> 56 0.69791

Excited State 2: Singlet-A 4.0132 eV 308.94 nm $f=0.0269$ $\langle S^{**2} \rangle=0.000$
 54 -> 56 0.69496
 55 -> 56 -0.10029

Excited State 3: Singlet-A 4.6387 eV 267.28 nm $f=0.0516$ $\langle S^{**2} \rangle=0.000$
 53 -> 56 0.69228
 55 -> 57 0.10465

BF₂Thio-Ph

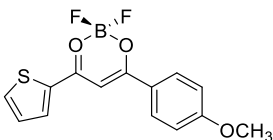


Excited State 1: Singlet-A 3.2410 eV 382.55 nm $f=0.9934$ $\langle S^{2} \rangle=0.000$**
71 -> 72 0.70380

Excited State 2: Singlet-A 3.7572 eV 329.99 nm $f=0.0191$ $\langle S^{**2} \rangle=0.000$
 70 -> 72 0.69768

Excited State 3: Singlet-A 3.8277 eV 323.92 nm $f=0.0015$ $\langle S^{**2} \rangle=0.000$
 68 -> 72 0.19548
 69 -> 72 0.67312

BF₂Thio-PhOCH₃

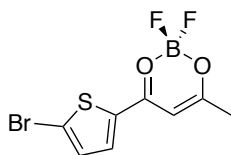


Excited State 1: Singlet-A 3.0542 eV 405.95 nm $f=1.1123$ $\langle S^{2} \rangle=0.000$**
79 -> 80 0.70571

Excited State 2: Singlet-A 3.7605 eV 329.70 nm $f=0.0658$ $\langle S^{**2} \rangle=0.000$
 76 -> 80 -0.18491
 77 -> 80 -0.11983
 78 -> 80 0.66139

Excited State 3: Singlet-A 3.9115 eV 316.97 nm $f=0.0048$ $\langle S^{**2} \rangle=0.000$
 76 -> 80 -0.19736
 77 -> 80 0.66901

BF₂Thio(Br)

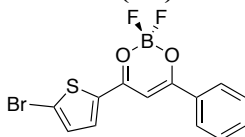


Excited State 1: Singlet-A 3.4235 eV 362.15 nm f=0.8318 <S2>=0.000**
72 -> 73 0.70420

Excited State 2: Singlet-A 4.1132 eV 301.43 nm f=0.0181 <S**2>=0.000
 70 -> 73 -0.17482
 71 -> 73 0.67699

Excited State 3: Singlet-A 4.4050 eV 281.46 nm f=0.0291 <S**2>=0.000
 70 -> 73 0.67510
 71 -> 73 0.17382

BF₂Thio(Br)-Ph

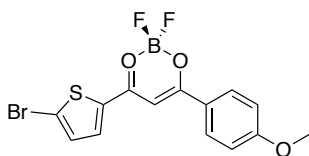


Excited State 1: Singlet-A 3.0913 eV 401.08 nm f=1.1239 <S2>=0.000**
88 -> 89 0.70395

Excited State 2: Singlet-A 3.7002 eV 335.08 nm f=0.0170 <S**2>=0.000
 87 -> 89 0.69587

Excited State 3: Singlet-A 3.8926 eV 318.51 nm f=0.0268 <S**2>=0.000
 85 -> 89 -0.25872
 86 -> 89 0.64390

BF₂Thio(Br)-PhOCH₃

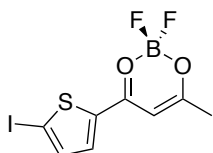


Excited State 1: Singlet-A 2.9516 eV 420.06 nm f=1.2616 <S2>=0.000**
96 -> 97 0.70587

Excited State 2: Singlet-A 3.6239 eV 342.13 nm $f=0.0715$ $\langle S^{**2} \rangle=0.000$
 95 -> 97 0.68926

Excited State 3: Singlet-A 3.9047 eV 317.53 nm $f=0.0165$ $\langle S^{**2} \rangle=0.000$
 94 -> 97 0.68637

BF₂Thio(I)

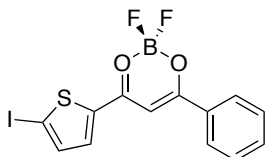


Excited State 1: Singlet-A 3.3404 eV 371.16 nm $f=0.8094$ $\langle S^{**2} \rangle=0.000$
 58 -> 59 0.70422

Excited State 2: Singlet-A 4.0862 eV 303.42 nm $f=0.0193$ $\langle S^{**2} \rangle=0.000$
 56 -> 59 -0.37176
 57 -> 59 0.59249

Excited State 3: Singlet-A 4.1379 eV 299.63 nm $f=0.0001$ $\langle S^{**2} \rangle=0.000$
 55 -> 59 0.70129

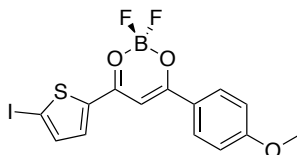
BF₂Thio(I)-Ph



Excited State 1: Singlet-A 3.0444 eV 407.25 nm $f=1.1175$ $\langle S^{**2} \rangle=0.000$
 74 -> 75 0.70377

Excited State 2: Singlet-A 3.7041 eV 334.72 nm $f=0.0146$ $\langle S^{**2} \rangle=0.000$
 72 -> 75 0.68468
 73 -> 75 -0.14635

Excited State 3: Singlet-A 3.8219 eV 324.40 nm $f=0.0714$ $\langle S^{**2} \rangle=0.000$
 71 -> 75 -0.10050
 72 -> 75 0.14593
 73 -> 75 0.67575

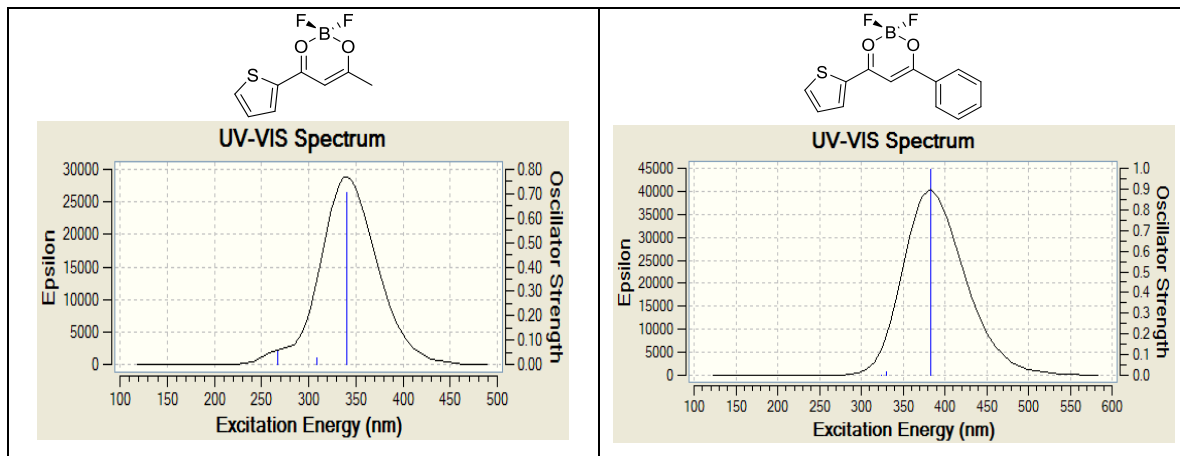
BF₂Thio(I)-PhOCH₃

Excited State 1: Singlet-A 2.9295 eV 423.23 nm f=1.2990 <S**2>=0.000
82 -> 83 0.70549

Excited State 2: Singlet-A 3.5645 eV 347.83 nm f=0.0518 <S**2>=0.000
81 -> 83 0.69534

Excited State 3: Singlet-A 3.8958 eV 318.25 nm f=0.0095 <S**2>=0.000
80 -> 83 0.68460

Table S6.9 Gaussview traces of computed TD-B3LYP/6-311+G(d) absorption spectra for thienyl compounds in CH₂Cl₂ represented by Tomasi's Polarizable Continuum Model.



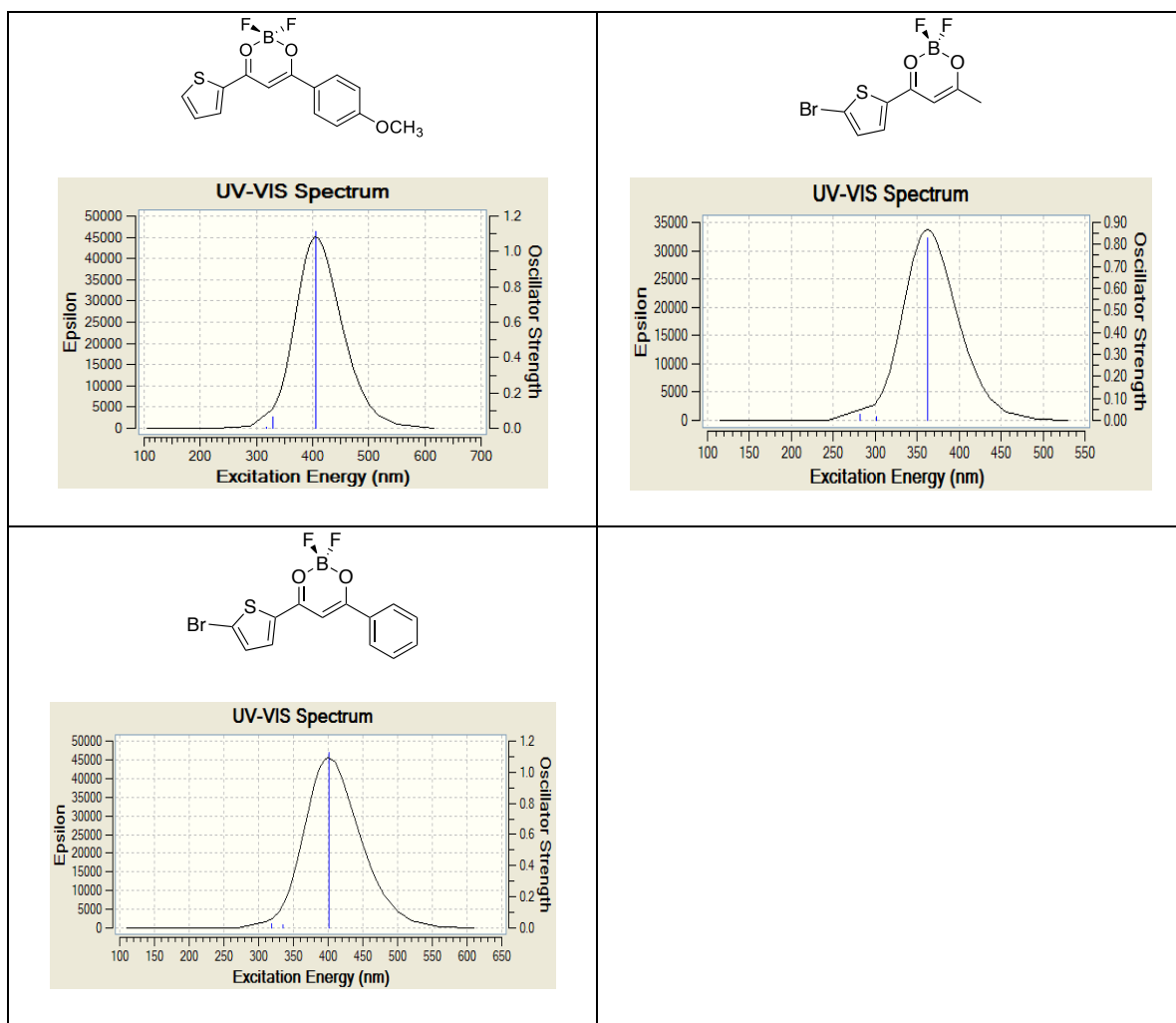


Table S6.9 Computational Data Compared with Experimental Data.⁶

Dye	E^* [a.u.]	μ^* [Debye]	λ_{abs}^* [nm]	$\lambda_{\text{abs}}^\dagger$ [nm]	$\lambda_{\text{em}}^\dagger$ [nm]	Φ_F^\dagger [%]	Stokes Shift [†] [cm ⁻¹]
1	-1082.47	11.11	340.67	354	392	0.04	2739
2	-1274.22	11.36	382.55	401	416	0.31	900
3	-1388.75	10.71	405.95	417	445	0.38	1509

*Values generated computationally.
[†]Values generated from experiments.

Supporting Information for Section 6.3.4: Toward Computational Modeling of the Solid State Emission Properties of Difluoroboron β -Diketonates

All dimers were modeled using the Gaussian 09 suite of programs¹ using density functional theory (DFT). We chose B3LYP/6-31+G(d) for the single point energy calculations used to optimize the configuration of the dimer. Single point energy calculations were used to generate the molecular orbital diagrams utilizing B3LYP/6-31G(d). We used time-dependent density functional theory, TD-B3LYP/6-311+G(d) for estimates of the absorption spectra.^{2,3} Molecular orbitals were depicted by GaussView 5 software.⁴

Table S6.10 Coordinates of the optimum H-dimer whose energy was calculated using B3LYP/6-31+G(d). Coordinates given in Cartesian, in Angstroms.

(BF₂dbm(OMe)₂)₂ E (HF) = -2364.25835002

B, 0.00000000, 0.00000000, 2.67332996
 F, -1.15945362, 0.00000000, 3.37965042
 F, 1.15945362, 0.00000000, 3.37965042
 O, 0.00000000, 1.26909049, 1.84837351
 C, 0.00000000, 1.22059711, 0.54830041
 C, 0.00000000, 0.00000000, -0.13833504
 H, 0.00000000, 0.00000000, -1.22499904
 O, 0.00000000, -1.26909049, 1.84837351
 C, 0.00000000, -1.22059711, 0.54830041
 C, 0.00000000, -2.5406406, -0.09409316
 C, 0.00000000, -2.67077077, -1.50113342
 C, 0.00000000, -3.70008022, 0.7079735
 C, 0.00000000, -3.92138557, -2.09514694
 H, 0.00000000, -1.77418651, -2.12684962
 C, 0.00000000, -4.96840806, 0.13336195
 H, 0.00000000, -3.59102842, 1.80062872
 C, 0.00000000, -5.06911724, -1.26677825
 H, 0.00000000, -4.04484139, -3.17651919
 H, 0.00000000, -5.84980534, 0.76719617
 C, 0.00000000, 2.5406406, -0.09409316

C, 0.00000000, 2.67077077, -1.50113342
C, 0.00000000, 3.70008022, 0.7079735
C, 0.00000000, 3.92138557, -2.09514694
H, 0.00000000, 1.77418651, -2.12684962
C, 0.00000000, 4.96840806, 0.13336195
H, 0.00000000, 3.59102842, 1.80062872
C, 0.00000000, 5.06911724, -1.26677825
H, 0.00000000, 4.04484139, -3.17651919
H, 0.00000000, 5.84980534, 0.76719617
O, 0.00000000, 6.2341992, -1.98118549
C, 0.00000000, 7.48869173, -1.25109496
H, 0.00000000, 8.22110238, -2.06997549
H, -0.90715365, 7.57542183, -0.64649681
H, 0.90715365, 7.57542183, -0.64649681
O, 0.00000000, -6.2341992, -1.98118549
C, 0.00000000, -7.48869173, -1.25109496
H, 0.00000000, -8.22110238, -2.06997549
H, 0.90715365, -7.57542183, -0.64649681
H, -0.90715365, -7.57542183, -0.64649681
B, 3.50000000, 0.00000000, -2.67332996
F, 4.65945362, 0.00000000, -3.37965042
F, 2.34054638, 0.00000000, -3.37965042
O, 3.50000000, -1.26909049, -1.84837351
C, 3.50000000, -1.22059711, -0.54830041
C, 3.50000000, 0.00000000, 0.13833504
H, 3.50000000, 0.00000000, 1.22499904
O, 3.50000000, 1.26909049, -1.84837351
C, 3.50000000, 1.22059711, -0.54830041
C, 3.50000000, 2.5406406, 0.09409316
C, 3.50000000, 2.67077077, 1.50113342
C, 3.50000000, 3.70008022, -0.7079735
C, 3.50000000, 3.92138557, 2.09514694
H, 3.50000000, 1.77418651, 2.12684962
C, 3.50000000, 4.96840806, -0.13336195
H, 3.50000000, 3.59102842, -1.80062872
C, 3.50000000, 5.06911724, 1.26677825
H, 3.50000000, 4.04484139, 3.17651919
H, 3.50000000, 5.84980534, -0.76719617
C, 3.50000000, -2.5406406, 0.09409316
C, 3.50000000, -2.67077077, 1.50113342
C, 3.50000000, -3.70008022, -0.7079735
C, 3.50000000, -3.92138557, 2.09514694

H, 3.50000000, -1.77418651, 2.12684962
 C, 3.50000000, -4.96840806, -0.13336195
 H, 3.50000000, -3.59102842, -1.80062872
 C, 3.50000000, -5.06911724, 1.26677825
 H, 3.50000000, -4.04484139, 3.17651919
 H, 3.50000000, -5.84980534, -0.76719617
 O, 3.50000000, -6.2341992, 1.98118549
 C, 3.50000000, -7.48869173, 1.25109496
 H, 3.50000000, -8.22110238, 2.06997549
 H, 2.59284635, -7.57542183, 0.64649681
 H, 4.40715365, -7.57542183, 0.64649681
 O, 3.50000000, 6.2341992, 1.98118549
 C, 3.50000000, 7.48869173, 1.25109496
 H, 3.50000000, 8.22110238, 2.06997549
 H, 4.40745365, 7.57542183, 0.64649681
 H, 2.59284635, 7.57542183, 0.64649681

Table S6.11 Characterization of the first 13 excited states of selected dimers with varying distances between monomers in the X-axis.

Note: Max amplitude is 0.70714 for a pure one-electron excitation. The strongest singlet transitions for each dimer are in bold.

(BF₂dbm(OMe)₂)₂: 3.00 Å in X

Excited State 1:	Triplet-A	2.1277 eV	582.71 nm	f=0.0000	<S**2>=2.000
167 ->174	-0.11615				
168 ->173	0.20442				
170 ->174	0.18337				
171 ->175	-0.11664				
172 ->173	0.60769				
Excited State 2:	Triplet-A	2.4210 eV	512.12 nm	f=0.0000	<S**2>=2.000
163 ->173	-0.13690				
167 ->173	-0.14154				
168 ->174	0.17194				
169 ->175	0.10499				
170 ->173	0.32051				
171 ->176	0.12275				
172 ->174	0.52614				
Excited State 3:	Singlet-A	2.8060 eV	441.85 nm	f=0.0000	<S**2>=0.000
168 ->173	0.12810				
170 ->174	0.10202				

171 ->175	-0.10479				
172 ->173	0.67034				
Excited State 4:	Triplet-A	2.8789 eV	430.66 nm	f=0.0000	<S**2>=2.000
166 ->174	-0.11392				
169 ->174	-0.20362				
170 ->176	0.12218				
170 ->182	0.11333				
171 ->173	0.50643				
172 ->175	-0.28739				
Excited State 5:	Triplet-A	2.9806 eV	415.97 nm	f=0.0000	<S**2>=2.000
169 ->173	-0.34704				
170 ->175	-0.23963				
171 ->174	0.38306				
172 ->176	0.26806				
Excited State 6:	Triplet-A	3.2609 eV	380.21 nm	f=0.0000	<S**2>=2.000
159 ->173	-0.10394				
163 ->174	-0.22433				
168 ->173	0.49526				
169 ->182	0.10813				
170 ->174	-0.13248				
171 ->175	0.23309				
172 ->194	0.14815				
Excited State 7:	Triplet-A	3.3379 eV	371.45 nm	f=0.0000	<S**2>=2.000
163 ->173	-0.25797				
167 ->173	-0.20574				
168 ->174	0.38999				
169 ->175	-0.21946				
170 ->173	-0.24888				
170 ->194	0.10107				
171 ->176	-0.18529				
172 ->191	-0.11512				
Excited State 8:	Singlet-A	3.5735 eV	346.95 nm	f=1.3350	<S**2>=0.000
168 ->174	0.11337				
170 ->173	0.12485				
171 ->176	0.11220				
172 ->174	0.66752				
Excited State 9:	Triplet-A	3.7510 eV	330.53 nm	f=0.0000	<S**2>=2.000
163 ->173	-0.20168				
164 ->174	0.11896				

168 ->174 0.12928
 169 ->175 0.10432
 170 ->173 0.47296
 171 ->176 -0.17469
 172 ->174 -0.34332

Excited State 10: Singlet-A 3.7975 eV 326.49 nm f=0.0627 <S**2>=0.000
 171 ->173 0.64615
 172 ->175 -0.23149

Excited State 11: Triplet-A 3.9191 eV 316.36 nm f=0.0000 <S**2>=2.000
 164 ->173 0.16833
 165 ->174 -0.14189
 165 ->175 -0.10109
 166 ->173 -0.14990
 167 ->175 0.11714
 169 ->173 0.35793
 170 ->174 0.27043
 170 ->175 0.10626
 171 ->174 0.20018
 172 ->173 -0.16024
 172 ->176 0.20417

Excited State 12: Triplet-A 3.9206 eV 316.24 nm f=0.0000 <S**2>=2.000
 164 ->173 0.20461
 165 ->174 0.11069
 165 ->175 -0.13035
 166 ->173 0.13087
 168 ->173 0.11654
 169 ->173 -0.27836
 169 ->176 -0.10445
 170 ->174 0.35343
 171 ->174 -0.14553
 172 ->173 -0.20512
 172 ->176 -0.15852

Excited State 13: Singlet-A 3.9683 eV 312.43 nm f=0.5915 <S**2>=0.000
 169 ->175 0.14003
 170 ->173 0.66790
 172 ->174 -0.13455

(BF₂dbm(OMe)₂)₂: 3.50 Å in X

Excited State 1: Triplet-A 2.4262 eV 511.02 nm f=0.0000 <S**2>=2.000
 163 -> 174 0.11217
 167 -> 174 0.11892
 168 -> 173 0.17170

170 -> 176	0.11980				
171 -> 174	0.31448				
172 -> 173	0.54281				
Excited State 2:	Triplet-A	2.5096 eV	494.05 nm	f=0.0000	<S**2>=2.000
163 -> 173	0.13414				
167 -> 173	0.12433				
168 -> 174	0.15303				
169 -> 176	0.11092				
170 -> 175	0.10379				
171 -> 173	0.39492				
172 -> 174	0.48074				
Excited State 3:	Triplet-A	3.0648 eV	404.54 nm	f=0.0000	<S**2>=2.000
168 -> 176	-0.10815				
169 -> 174	0.29593				
170 -> 173	0.42804				
171 -> 175	0.17831				
171 -> 182	-0.13664				
172 -> 176	0.27185				
Excited State 4:	Triplet-A	3.0796 eV	402.60 nm	f=0.0000	<S**2>=2.000
169 -> 173	0.35937				
170 -> 174	0.36902				
171 -> 176	0.24694				
172 -> 175	0.24215				
172 -> 182	-0.11572				
Excited State 5:	Singlet-A	3.3010 eV	375.59 nm	f=0.0000	<S**2>=0.000
168 -> 173	0.11611				
170 -> 176	0.10040				
171 -> 174	0.24279				
172 -> 173	0.62883				
Excited State 6:	Triplet-A	3.3862 eV	366.14 nm	f=0.0000	<S**2>=2.000
163 -> 174	0.24259				
167 -> 174	0.19552				
168 -> 173	0.44052				
169 -> 175	-0.14210				
169 -> 182	0.13503				
170 -> 176	-0.22123				
171 -> 174	-0.12376				
172 -> 194	0.12654				
Excited State 7:	Triplet-A	3.4028 eV	364.36 nm	f=0.0000	<S**2>=2.000

163 -> 173	0.26211
167 -> 173	0.26713
168 -> 174	0.38791
169 -> 176	-0.21561
170 -> 175	-0.18800
171 -> 173	-0.12760
171 -> 194	0.10682
172 -> 192	0.10369

Excited State 8: Singlet-A 3.7704 eV 328.84 nm f=1.9770 <S2>=0.000**

171 -> 173	0.35484
172 -> 174	0.57047

Excited State 9: Triplet-A 4.1060 eV 301.96 nm f=0.0000 <S**2>=2.000

163 -> 173	0.19146
164 -> 174	-0.18969
166 -> 176	0.11187
167 -> 173	-0.14012
169 -> 176	0.11111
170 -> 175	-0.16613
171 -> 173	0.38243
171 -> 178	0.11621
172 -> 174	-0.34822
172 -> 179	0.15138

Excited State 10: Triplet-A 4.1686 eV 297.43 nm f=0.0000 <S**2>=2.000

163 -> 174	0.19342
164 -> 173	-0.28059
165 -> 176	0.16156
166 -> 182	-0.11744
169 -> 175	0.11331
171 -> 174	0.37663
172 -> 173	-0.33277
172 -> 178	-0.11751

Excited State 11: Triplet-A 4.1890 eV 295.97 nm f=0.0000 <S**2>=2.000

164 -> 175	-0.11557
164 -> 182	0.10357
165 -> 174	0.25704
166 -> 173	0.30064
167 -> 176	-0.19780
169 -> 173	0.26621
169 -> 178	0.13516
170 -> 174	-0.16928
170 -> 179	0.15246

171 -> 177 0.15706
 172 -> 175 -0.24916

Excited State 12: Triplet-A 4.2475 eV 291.90 nm f=0.0000 <S**2>=2.000

164 -> 176 -0.24269
 165 -> 173 0.39238
 165 -> 178 0.12172
 166 -> 174 0.27672
 166 -> 179 0.11047
 167 -> 182 0.17561
 169 -> 174 0.16503
 170 -> 173 -0.24268

Excited State 13: Singlet-A 4.2851 eV 289.33 nm f=0.1411 <S**2>=0.000

171 -> 173 0.58048
 172 -> 174 -0.36647

(BF₂dbm(OMe)₂)₂: 3.75 Å in X

Excited State 1: Triplet-A 2.4899 eV 497.96 nm f=0.0000 <S**2>=2.000

163 -> 174 -0.11763
 167 -> 174 0.11566
 168 -> 173 0.15512
 170 -> 176 -0.12306
 171 -> 174 0.35704
 172 -> 173 0.51327

Excited State 2: Triplet-A 2.5309 eV 489.87 nm f=0.0000 <S**2>=2.000

163 -> 173 -0.13250
 167 -> 173 0.11766
 168 -> 174 0.14529
 169 -> 176 0.11366
 170 -> 175 0.10238
 171 -> 173 0.41101
 172 -> 174 0.46847

Excited State 3: Triplet-A 3.0932 eV 400.83 nm f=0.0000 <S**2>=2.000

168 -> 176 0.10569
 169 -> 174 -0.32116
 170 -> 173 0.40882
 171 -> 175 0.19875
 171 -> 182 -0.13309
 172 -> 176 -0.27257

Excited State 4: Triplet-A 3.1007 eV 399.86 nm f=0.0000 <S**2>=2.000

169 -> 173 -0.36334
 170 -> 174 0.36950
 171 -> 176 -0.25497
 172 -> 175 0.23912
 172 -> 182 -0.11609

Excited State 5: Triplet-A 3.4096 eV 363.63 nm f=0.0000 <S**2>=2.000

163 -> 174 -0.24333
 167 -> 173 -0.10596
 167 -> 174 0.23315
 168 -> 173 0.40444
 169 -> 175 0.15812
 169 -> 182 -0.13031
 170 -> 176 0.22165
 171 -> 174 -0.10483
 172 -> 194 0.11737

Excited State 6: Triplet-A 3.4194 eV 362.59 nm f=0.0000 <S**2>=2.000

163 -> 173 -0.25353
 167 -> 173 0.26785
 168 -> 174 0.37792
 169 -> 176 -0.21696
 170 -> 175 -0.18805
 171 -> 173 -0.10529
 171 -> 194 0.10477

Excited State 7: Singlet-A 3.4222 eV 362.30 nm f=0.0000 <S**2>=0.000

168 -> 173 0.10633
 171 -> 174 0.31387
 172 -> 173 0.59432

Excited State 8: Singlet-A 3.7934 eV 326.84 nm f=2.0837 <S2>=0.000**

171 -> 173 0.40443
172 -> 174 0.53544

Excited State 9: Triplet-A 4.2113 eV 294.41 nm f=0.0000 <S**2>=2.000

163 -> 173 0.20890
 164 -> 174 0.22030
 165 -> 175 -0.10587
 166 -> 176 -0.14594
 167 -> 173 0.16820
 169 -> 177 0.13576
 170 -> 175 0.16398
 171 -> 173 -0.28957
 171 -> 178 -0.15648

172 -> 174 0.30125
 172 -> 179 -0.17261

Excited State 10: Triplet-A 4.2510 eV 291.66 nm f=0.0000 <S**2>=2.000

164 -> 175 0.10859
 164 -> 182 -0.11266
 165 -> 174 -0.26696
 166 -> 173 0.31181
 167 -> 176 -0.18780
 169 -> 173 0.17374
 169 -> 178 0.16819
 170 -> 174 0.13633
 170 -> 179 -0.16688
 171 -> 177 -0.19178
 172 -> 175 0.22333
 172 -> 182 0.10362

Excited State 11: Triplet-A 4.2665 eV 290.60 nm f=0.0000 <S**2>=2.000

163 -> 174 0.23099
 164 -> 173 0.32184
 165 -> 176 0.18567
 166 -> 182 -0.12466
 167 -> 174 0.15137
 171 -> 174 -0.31024
 172 -> 173 0.31264

Excited State 12: Triplet-A 4.2901 eV 289.00 nm f=0.0000 <S**2>=2.000

164 -> 176 0.19723
 165 -> 173 0.33361
 165 -> 178 0.13746
 166 -> 174 -0.27150
 167 -> 182 0.18457
 169 -> 179 -0.18287
 170 -> 173 -0.14949
 170 -> 178 0.14185
 171 -> 175 -0.10115
 171 -> 182 -0.14550
 172 -> 177 0.15854

Excited State 13: Triplet-A 4.3137 eV 287.42 nm f=0.0000 <S**2>=2.000

164 -> 173 -0.11124
 164 -> 178 -0.13517
 165 -> 173 0.11719
 165 -> 177 0.16270
 166 -> 174 -0.11194

166 -> 182	0.11985
167 -> 175	-0.10699
167 -> 179	-0.17492
168 -> 178	-0.15477
169 -> 174	-0.10984
169 -> 175	0.17904
169 -> 182	0.20913
170 -> 177	0.21477
171 -> 174	-0.13769
171 -> 179	0.24087
172 -> 178	0.21587

(BF₂dbm(OMe)₂)₂: 4.00 Å in X

Excited State 1:	Triplet-A	2.5231 eV	491.40 nm	f=0.0000	<S**2>=2.000
163 -> 174	0.12092				
164 -> 173	-0.10235				
168 -> 173	0.11778				
170 -> 176	-0.12168				
171 -> 174	0.38658				
172 -> 173	0.48960				
Excited State 2:	Triplet-A	2.5430 eV	487.56 nm	f=0.0000	<S**2>=2.000
163 -> 173	0.13076				
168 -> 174	0.11514				
169 -> 176	0.11301				
171 -> 173	0.42248				
172 -> 174	0.45893				
Excited State 3:	Triplet-A	3.1084 eV	398.86 nm	f=0.0000	<S**2>=2.000
169 -> 174	-0.33398				
170 -> 173	0.39072				
171 -> 175	0.20424				
171 -> 182	-0.12602				
172 -> 176	-0.27055				
Excited State 4:	Triplet-A	3.1133 eV	398.24 nm	f=0.0000	<S**2>=2.000
169 -> 173	0.36546				
170 -> 174	-0.36140				
171 -> 176	0.25131				
172 -> 175	-0.23545				
172 -> 182	0.11347				
Excited State 5:	Triplet-A	3.4197 eV	362.56 nm	f=0.0000	<S**2>=2.000
163 -> 174	0.23994				

164 -> 173 -0.11973
 167 -> 173 -0.24529
 167 -> 174 -0.21031
 168 -> 173 0.31207
 168 -> 174 -0.15403
 169 -> 175 0.16926
 169 -> 182 -0.12494
 170 -> 176 0.22267

Excited State 6: Triplet-A 3.4276 eV 361.72 nm f=0.0000 <S**2>=2.000

163 -> 173 0.24488
 164 -> 174 -0.12364
 167 -> 173 -0.23516
 167 -> 174 -0.20775
 168 -> 173 -0.17499
 168 -> 174 0.30684
 169 -> 176 -0.21550
 170 -> 175 -0.18816
 170 -> 182 0.10255
 172 -> 192 0.10091

Excited State 7: Singlet-A 3.4956 eV 354.69 nm f=0.0000 <S**2>=0.000

171 -> 174 0.37085
 172 -> 173 0.55858

Excited State 8: Singlet-A 3.8021 eV 326.10 nm f=2.1348 <S2>=0.000**

171 -> 173 0.43620
172 -> 174 0.50962

Excited State 9: Triplet-A 4.2839 eV 289.42 nm f=0.0000 <S**2>=2.000

163 -> 173 -0.21370
 164 -> 174 0.22329
 165 -> 182 -0.13494
 166 -> 176 0.15430
 167 -> 173 -0.13150
 169 -> 177 0.19634
 170 -> 175 0.15956
 170 -> 182 0.12467
 171 -> 173 -0.14504
 171 -> 178 -0.20108
 172 -> 174 0.21259
 172 -> 179 0.20339

Excited State 10: Triplet-A 4.2860 eV 289.28 nm f=0.0000 <S**2>=2.000

164 -> 182 0.11688

165 -> 174	-0.24731
166 -> 173	0.28660
167 -> 176	-0.12500
168 -> 182	0.10096
169 -> 178	-0.19523
170 -> 174	-0.10952
170 -> 179	-0.18330
171 -> 177	0.21103
172 -> 175	-0.19387
172 -> 182	-0.13109

Excited State 11: Triplet-A 4.3033 eV 288.11 nm f=0.0000 <S**2>=2.000

164 -> 176	-0.14073
164 -> 177	0.11290
165 -> 173	0.26210
165 -> 178	0.15387
166 -> 174	-0.22399
166 -> 179	0.11874
167 -> 182	0.15981
168 -> 177	0.11834
168 -> 182	0.11792
169 -> 179	-0.23218
170 -> 173	0.10882
170 -> 178	-0.20316
171 -> 175	0.14504
171 -> 182	0.18042
172 -> 177	-0.21224

Excited State 12: Triplet-A 4.3174 eV 287.18 nm f=0.0000 <S**2>=2.000

163 -> 174	-0.17901
164 -> 173	0.23976
164 -> 178	0.11980
165 -> 176	-0.13788
165 -> 177	0.16860
166 -> 182	0.16961
167 -> 178	-0.10462
167 -> 179	0.14143
168 -> 178	0.12711
168 -> 179	0.12110
169 -> 175	-0.13792
169 -> 182	-0.21087
170 -> 177	-0.21321
171 -> 179	0.23084
172 -> 173	0.10822
172 -> 178	-0.21061

Excited State 13: Triplet-A 4.3386 eV 285.77 nm f=0.0000 $\langle S^{*2} \rangle = 2.000$

163 -> 175	-0.10098
164 -> 176	-0.12506
164 -> 177	-0.14297
165 -> 173	0.29107
165 -> 178	-0.19018
166 -> 174	-0.28383
166 -> 179	-0.16902
167 -> 175	-0.21405
168 -> 175	-0.13886
168 -> 176	-0.10408
168 -> 177	-0.11106
169 -> 174	0.21607
169 -> 179	0.12669

(BF₂dbm(OMe)₂): 6.00 Å in X.

Excited State 1: Triplet-A 2.5589 eV 484.52 nm f=0.0000 $\langle S^{*2} \rangle = 2.000$

164 -> 174	0.14087
168 -> 174	-0.17235
170 -> 176	-0.13259
171 -> 173	0.12139
171 -> 174	0.17288
172 -> 173	0.21380
172 -> 174	0.54604

Excited State 2: Triplet-A 2.5590 eV 484.51 nm f=0.0000 $\langle S^{*2} \rangle = 2.000$

163 -> 173	0.13913
167 -> 173	0.17279
169 -> 175	-0.13194
171 -> 173	0.53343
171 -> 174	-0.24100
172 -> 173	-0.21013

Excited State 3: Triplet-A 3.1196 eV 397.44 nm f=0.0000 $\langle S^{*2} \rangle = 2.000$

166 -> 180	0.11722
168 -> 179	-0.10476
169 -> 174	0.12951
170 -> 173	0.19502
170 -> 174	0.46175
171 -> 176	-0.10641
172 -> 175	-0.12369
172 -> 176	-0.30265

172 -> 179	-0.10282				
Excited State 4:	Triplet-A	3.1204 eV	397.34 nm	f=0.0000	<S**2>=2.000
165 -> 178	-0.11808				
167 -> 177	0.10205				
169 -> 173	0.46144				
169 -> 174	-0.19412				
170 -> 173	-0.13224				
171 -> 175	-0.30545				
171 -> 176	0.11624				
172 -> 175	0.10929				
Excited State 5:	Triplet-A	3.4276 eV	361.72 nm	f=0.0000	<S**2>=2.000
163 -> 173	0.23206				
167 -> 173	0.44501				
167 -> 174	-0.18653				
169 -> 175	0.25489				
Excited State 6:	Triplet-A	3.4281 eV	361.67 nm	f=0.0000	<S**2>=2.000
164 -> 174	-0.23118				
168 -> 173	0.18828				
168 -> 174	0.44401				
170 -> 175	-0.10442				
170 -> 176	-0.25132				
170 -> 179	-0.10059				
Excited State 7:	Singlet-A	3.6296 eV	341.59 nm	f=0.0000	<S**2>=0.000
171 -> 173	-0.34854				
171 -> 174	0.31668				
172 -> 173	0.32237				
172 -> 174	0.35162				
Excited State 8:	Singlet-A	3.7772 eV	328.24 nm	f=2.2168	<S**2>=0.000
171 -> 173	0.47388				
172 -> 174	0.47202				
Excited State 9:	Triplet-A	4.3041 eV	288.06 nm	f=0.0000	<S**2>=2.000
164 -> 179	0.10851				
166 -> 174	0.18639				
166 -> 180	-0.18240				
168 -> 177	0.14990				
168 -> 179	0.20005				
170 -> 178	0.13431				
170 -> 180	0.31182				
172 -> 176	-0.16631				

172 -> 177 0.17188
 172 -> 179 0.22644
 172 -> 180 -0.12304

Excited State 10: Triplet-A 4.3049 eV 288.01 nm f=0.0000 <S**2>=2.000
 163 -> 177 0.11048
 165 -> 173 -0.18759
 165 -> 178 0.17832
 167 -> 177 -0.21561
 167 -> 179 0.15530
 169 -> 178 0.30408
 169 -> 180 -0.15465
 171 -> 175 -0.15552
 171 -> 177 0.24692
 171 -> 179 -0.17733

Excited State 11: Triplet-A 4.3155 eV 287.30 nm f=0.0000 <S**2>=2.000
 164 -> 174 -0.16601
 166 -> 177 -0.13468
 166 -> 179 -0.19098
 168 -> 178 0.10735
 168 -> 180 0.21529
 170 -> 176 -0.16412
 170 -> 177 0.17107
 170 -> 179 0.27104
 171 -> 178 0.10140
 172 -> 178 0.11971
 172 -> 179 0.10896
 172 -> 180 0.28713

Excited State 12: Triplet-A 4.3158 eV 287.28 nm f=0.0000 <S**2>=2.000
 163 -> 173 -0.16029
 165 -> 177 0.19234
 165 -> 179 -0.12500
 167 -> 178 -0.22936
 167 -> 180 0.12622
 169 -> 175 -0.14863
 169 -> 177 0.25247
 169 -> 179 -0.18138
 170 -> 177 -0.10585
 171 -> 178 0.28413
 171 -> 180 -0.17588
 172 -> 178 -0.12788

Excited State 13: Triplet-A 4.3681 eV 283.84 nm f=0.0000 <S**2>=2.000

164 -> 176	0.20050
166 -> 173	0.17126
166 -> 174	0.41138
166 -> 180	0.21152
168 -> 176	0.26680
170 -> 174	-0.17552
172 -> 176	-0.10929

References

- (1) M. J. Frisch, G. W. T., H. B. Schlegel, G. E. Scuseria, M. A. Robb, J. R. Cheeseman, G. Scalmani, V. Barone, B. Mennucci, G. A. Petersson, H. Nakatsuji, M. Caricato, X. Li, H. P. Hratchian, A. F. Izmaylov, J. Bloino, G. Zheng, J. L. Sonnenberg, M. Hada, M. Ehara, K. Toyota, R. Fukuda, J. Hasegawa, M. Ishida, T. Nakajima, Y. Honda, O. Kitao, H. Nakai, T. Vreven, J. A. Montgomery, Jr., J. E. Peralta, F. Ogliaro, M. Bearpark, J. J. Heyd, E. Brothers, K. N. Kudin, V. N. Staroverov, R. Kobayashi, J. Normand, K. Raghavachari, A. Rendell, J. C. Burant, S. S. Iyengar, J. Tomasi, M. Cossi, N. Rega, J. M. Millam, M. Klene, J. E. Knox, J. B. Cross, V. Bakken, C. Adamo, J. Jaramillo, R. Gomperts, R. E. Stratmann, O. Yazyev, A. J. Austin, R. Cammi, C. Pomelli, J. W. Ochterski, R. L. Martin, K. Morokuma, V. G. Zakrzewski, G. A. Voth, P. Salvador, J. J. Dannenberg, S. Dapprich, A. D. Daniels, Ö. Farkas, J. B. Foresman, J. V. Ortiz, J. Cioslowski, and D. J. Fox, Gaussian, Inc., Wallingford CT, 2009.
- (2) Tomasi, J.; Mennucci, B.; Cammi, R. *Chem. Rev.* **2005**, *105*, 2999.
- (3) Becke, A. D. *J. Chem. Phys.* **1993**, *98*, 5648.
- (4) Lee, C.; Yang, W.; Parr, R. G. *Phys. Rev. B: Condens. Matter* **1988**, *37*, 785.
- (5) Dennington, R. In *Version 5*; Keith, T., Ed.; Semichem Inc.: Shawnee Mission, KS, 2009.
- (6) Kolpaczynska, M.; DeRosa, C. A.; Morris, W. A.; Fraser, C. L. *Aust. J. Chem.* **2016**.